

Abstract

Dynamics and rare events in non-equilibrium systems

Lukas Takaaki Kikuchi

My abstract ...

This thesis is dedicated to...

Acknowledgements

Contents

1	Introduction	11
I	Global methods for sampling rare diffusive events	13
2	Ritz methods for Freidlin-Wentzel-Graham actions	15
2.1	Introduction	15
2.2	Large deviation theory	16
2.3	On-shell action	20
2.4	Ritz method	23
2.5	Numerical results	27
2.5.1	Brownian dynamics in a complex potential	28
2.5.2	Brownian dynamics in a circulatory field	30
2.5.3	Multistability in a genetic switch	31
2.5.4	Transitions between limit cycles	32
2.5.5	Egger model of weather	34
2.6	Numerical convergence	35
2.7	Conclusion	35
3	Monte Carlo methods in Path Spaces	39
3.1	Introduction	39
3.2	Path-space MCMC methods	46
3.2.1	The preconditioned Crank-Nicolson algorithm	46
3.2.2	Kosambi-Karhunen-Lo�eve expansions of stochastic trajectories	51
3.2.3	Numerical algorithm	54
3.2.4	Mode-space band structure	57
3.2.5	Mode-dependent step-sizes	61
3.2.6	Generalised end-point conditions	62
3.3	Sampling multi-modal transition path ensembles	63
3.3.1	Quadratic expansions of the Onsager-Machlup action	63
3.3.2	Calculation of the Gaussian normalisation constants	63

3.3.3	The Teleporter MCMC method	63
3.3.4	Model system	67
3.3.5	Gaussian mixture approximation of the transition path ensemble . .	67
3.3.6	The quadratic expansion of the Onsager-Machlup action	68
3.3.7	The Gaussian mixture approximation	69
3.3.8	Approximations of transition channel probabilities	70
3.3.9	Calculation of the Gaussian normalisation constants	70
3.4	Conclusion	73
4	Diffusivity dependence of transition paths	75
4.1	Introduction	75
4.2	The transition path ensemble	76
4.3	Model system	76
4.4	Transition channel probabilities	77
4.5	Numerical experiments	77
4.6	Results	78
4.7	Conclusion	81
II	Geometric mechanics of soft, slender matter	83
5	Introduction	85
5.1	Classical Cosserat theory	86
5.2	Mathematical preliminaries	91
5.2.1	Differential geometry	91
5.2.2	Exterior calculus	92
5.2.3	Lie groups	94
5.2.4	Homogeneous spaces	97
5.2.5	The Maurer-Cartan form	97
5.2.6	Sub-manifolds of homogeneous spaces	99
6	Cosserat rod models and geometric mechanics	103
6.1	Geometric mechanics of a rigid body	103
6.2	Geometric Cosserat rod mechanics	109
6.2.1	Cosserat rod kinematics	109
6.2.2	Cosserat rod dynamics	117
6.2.3	Summary and discussion	125
6.3	Mechanics of kinematically constrained Cosserat rods	127
6.3.1	Kinematic constraints and gauge freedoms	127
6.3.2	Kinematically constrained dynamics	132

6.4	The hyperelastic Cosserat rod model	136
6.5	Dissipative and overdamped dynamics	139
7	Geometric continuum mechanics on Lie group- and homogeneous configuration spaces	143
7.1	The geometrisation programme	144
7.1.1	Kinematics	145
7.1.2	Dynamics	147
7.1.3	Kinematic constraints	149
7.1.4	Summary and discussion	151
7.2	Derivation of the geometric kinematic and dynamical equations of motion .	155
7.2.1	Kinematics	155
7.2.2	Dynamics	157
7.3	Applications	164
7.3.1	Three-dimensional Cosserat media	164
7.3.2	Cosserat surfaces	168
7.3.3	Cosserat rods on 2-spheres	171
7.3.4	Relativistic Cosserat rods	174
7.3.5	The $O(N)$ non-linear σ model	177
8	Geometric numerical integrators	179
8.1	Geometric numerical integrators for sub-manifolds of Lie groups	179
8.2	Geometric numerical integrators for Cosserat rods	179
8.3	Geometric numerical integrators for Cosserat surfaces	179
8.4	Geometric numerical integrators for Cosserat rods on 2-spheres	179
9	Conclusion	181
References		183
A	Glossary of notation	205
A.1	Part I notation	205
A.2	Part II notation	205
B	MCMC benchmark models	207
B.1	The asymmetric double-well system	207
B.2	The switch system	208
C	Nondimensionalisation of the Cosserat rod	211

D Numerical algorithms for spatio-temporal reconstruction	213
D.1 Reconstructing the Cosserat rod from the Maurer-Cartan form	213
D.2 Reconstructing the spatio-temporal configuration from the Maurer-Cartan form	214

Chapter 1

Introduction

A wide range of structures exhibit properties of softness and slenderness, from biological materials like cilia [97] and cellular membranes [128], to strands of DNA [37] and hydrogels [175]. In this instance ‘soft’ refers to the constitutive properties of the material, like that of rubber or biological tissue, and ‘slender’ refers to its geometrical thinness.

- Also include references to research that have been done using cosserat theory.

We develop a general geometric theory of the kinematics and dynamics of G or G/H -valued systems. We show in particular that the continuum mechanics of all directed media, otherwise known as Cosserat media, can be unified in description using this framework. As a special case, we also recover classical (undirected) continuum mechanics, expressed in Cartan’s theory of moving frames.

Make it clear what is new: The general geometric framework and the Lie group integrators, as well as the presentation of all of the various Cosserat theories through the same framework.

Whilst the connection between Lie groups and mechanics has long been studied [149], here we provide a theory of mechanics Lie group-valued continua.

At a level of abstraction sufficient to describe all Cosserat theories, but also more general systems. For example, the framework is amenable to relativistic systems as well.

A lot of the results have already been shown before (a lot of the stuff in the Cosserat rod section in particular). The main purpose is to show how it all falls out of the a unified framework, and also works as a review article to some extent.

Part I

Global methods for sampling rare diffusive events

Chapter 2

Ritz methods for Freidlin-Wentzel-Graham actions

2.1 Introduction

The theory of Freidlin and Wentzell [214] gives asymptotic probability estimates of rare events in dynamical systems perturbed by small noise [17, 4, 5, 51]. Specifically, Freidlin-Wentzell theory yields estimates of the stationary distributions and mean first-passage times. Both these quantities are determined, in turn, by the asymptotic estimate of the probability of a stochastic trajectory to not deviate from a smooth path by more than a given amount in a given interval of time. The key result of Freidlin and Wentzell is that the limiting form of this probability, for small noise and small deviations, is given by a non-negative functional of the smooth path. This functional is the Freidlin-Wentzell action and its minimum, for fixed initial and terminal states, determines both the stationary distributions and first-passage times. The smooth path minimising the action is often called the Freidlin-Wentzell instanton. The theory is applicable to dynamical systems of both gradient and non-gradient character and can so be used to study a wide variety of equilibrium and non-equilibrium systems modelled by Itô diffusions [165, 110, 20, 141, 218, 156, 143, 73, 44, 154].

Determining the minimum of the Freidlin-Wentzell action is a problem in the calculus of variations. The Euler-Lagrange equations provide the necessary conditions for extrema of variational problems and, unsurprisingly, have been the basis of the large literature devoted to the numerical computation of Freidlin-Wentzell instantons [212, 165, 104, 90]. There exists, however, an alternative “direct” route for the solution of variational problems in which the functional is reduced, through finite-dimensional parametrizations of paths, to a multivariate function and then extremised by appropriate multivariate optimisation methods [80, 120]. To the best of our knowledge, the first use of the direct method for the Freidlin-Wentzell action, discretised by finite-differences, appears in the work of Weinan, Ren and Vanden-Eijnden [213].

Here we combine the direct method with a Ritz discretisation [184, 80, 120] to minimize the Freidlin-Wentzell action. We analyse paths in a spectral basis of Chebyshev polynomials and use spectral quadrature to express the action as a multivariate function of the basis coefficients. Nonlinear optimisation is used to obtain coefficients that give the least action from which the instanton is synthesised in the spectral basis. For minimisation over paths regardless of their duration, this procedure is especially effective when applied to a reparametrisation-invariant on-shell form of the action that follows from the time-translational invariance of the Lagrangian. This generalises the scalar work functional of Olander and Elber (for gradient dynamics) and the geometric action of Heyman and Vanden-Eijnden [208] (for non-gradient dynamics). Our method is efficient enough to robustly sample the logarithm of the asymptotic estimate of the stationary distribution, *i.e.* the quasipotential, avoiding the alternative, but numerically delicate, route of solving the Hamilton-Jacobi equation [25, 220, 40]. Our method is simple to use, converges rapidly, and is applicable to both equilibrium and non-equilibrium problems. Its implementation is freely available on GitHub as the open-source Python library PyRitz.

The remainder of this chapter is organized as follows. In the next section, we recall key results of Freidlin-Wentzell theory from dual perspectives of Itô stochastic differential equations and the corresponding Fokker-Planck equations. Sec. 2.3 we present the derivation of the on-shell form of the Freidlin-Wentzell action in a manner reminiscent of the Routh reduction procedure in classical mechanics and explain its relation to the scalar work and the geometric action. In Sec. 2.4 we describe the direct method for the minimisation of functionals, the Chebyshev spectral basis in which we construct smooth paths, the spectral quadrature rule we use to evaluate the action, and the multivariate non-linear optimisation methods we employ to find the minimum. In Sec. 2.5 we apply the direct method to three well-known diffusion processes and demonstrate convergence in each case.

A particular achievement of our approach is its relatively facile ability to calculate quasipotentials. This can be done with a sufficiently high density of sample points to construct effectively continuous maps of the quasipotential, which we do here for the same set of benchmark problems. We conclude with a discussion on extending the method to degenerate diffusion processes, systems with inertia and to the stochastic dynamics of fields.

2.2 Large deviation theory

We consider the autonomous dynamics of a d -dimensional coordinate $X = (X^1, \dots, X^d)$ in \mathbb{R}^d perturbed by configuration-dependent noise of intensity $\sqrt{\varepsilon}$ described by the Itô

diffusion equation [? ?]

$$dX^\mu = a^\mu(X)dt + \sqrt{\varepsilon}\sigma_\nu^\mu(X)dW^\nu \quad (2.1)$$

governing the stochastic trajectory $X(t)$, where $a^\mu(X)$ is the drift vector, $\sqrt{\varepsilon}\sigma_\nu^\mu(X)$ is the volatility, $W^\nu(t)$ is a d -dimensional Wiener process and repeated indices are summed over. Eq. 2.1 is also often referred to as an *overdamped Langevin equation*.

The transition probability density of the process, $P_{1|1}(x, t|x_0) = P(X(t) = x|X(0) = x_0)$, obeys the Fokker-Planck equation $\partial_t P(x|x_0) = \mathcal{L}P(x|x_0)$ where the Fokker-Planck operator is

$$\mathcal{L}(x) = -\frac{\partial}{\partial x^\mu}a^\mu(x) + \frac{\varepsilon}{2}\frac{\partial^2}{\partial x^\mu\partial x^\nu}b^{\mu\nu}(x) \quad (2.2)$$

and $b^{\mu\nu}(x) = \sigma_\lambda^\mu(x)\sigma_\sigma^\nu(x)\delta^{\lambda\sigma}$ is the diffusion tensor. We assume it to be non-degenerate, positive-definite and invertible. The inverse, $b_{\mu\nu}(x)$, induces a Riemannian structure in \mathbb{R}^d with a norm $|x|_b = \sqrt{b_{\mu\nu}x^\mu x^\nu}$ that is distinct from the Euclidean norm $|x| = \sqrt{(x^1)^2 + \dots + (x^d)^2}$. We use the subscript b to indicate this second “diffusion” norm. The stationary density satisfies the time-independent Fokker-Planck equation $\mathcal{L}P_1(x) = 0$ and, when it exists, is reached asymptotically in time for arbitrary initial distributions, $\lim_{t \rightarrow \infty} P_{1|1}(x, t|x_0) = P_1(x)$. The stationary distribution is unique for ergodic systems [171].

Associated with the Itô process is the Freidlin-Wentzell “action” functional [214, 92, 93]

$$S[x(t)] = \frac{1}{2} \int_0^T |\dot{x} - a(x)|_b^2 dt \quad (2.3)$$

which gives an asymptotic estimate for the logarithm of the probability of trajectories $X(t)$ to remain in the tubular neighbourhood of a smooth path $x(t)$ over the duration $0 \leq t \leq T$. We write this as

$$P_{\text{tube}}[x(t)] \asymp \exp\left(-\frac{1}{\varepsilon} S[x(t)]\right) \quad (2.4)$$

which, in terms of limits, means

$$S[x(t)] = \lim_{\delta \rightarrow 0} \lim_{\varepsilon \rightarrow 0} -\varepsilon \ln P\left[\sup_{0 \leq t \leq T} |X(t) - x(t)|_b < \delta\right].$$

The limits must be taken in the order above as they do not commute. Eq. 2.4 is a large deviation principle for trajectories of Itô processes, due to Wentzell and Freidlin and Graham [203].

For reasons described below, it is of interest to obtain the mode of the tube probability

over the set of continuous paths

$$\gamma_T = \{x(t) \mid x(0) = x_1, x(T) = x_2, 0 \leq t \leq T\}$$

which have fixed termini x_1 and x_2 and are of duration T . This is equivalent to the variational problem of minimising the Freidlin-Wentzell action. The minimum value of the action,

$$V_T(x_2|x_1) = \min_{\gamma_T} S[x(t)], \quad (2.5)$$

is called the quasipotential. The path attaining the minimum,

$$x_T^*(t) = \arg \min_{\gamma_T} S[x(t)], \quad (2.6)$$

is called the instanton. We emphasise that this path describes the smooth centerline of the tube of maximum probability and not a non-differentiable trajectory of the diffusion process. It is the most probable dynamical path connecting two points in configuration space.

The instanton and the quasipotential are central objects in Freidlin-Wentzell-Graham theory and relate to the eikonal approximation of the Fokker-Planck equation [139]. Assuming the JWKB form of the transition density,

$$P_{1|1}(x, t|x_0) \sim \exp \left[\frac{1}{\varepsilon} \sum_{n=0}^{\infty} \varepsilon^n \phi_n(x, x_0; t) \right],$$

with prefactors suppressed, substituting in the Fokker-Planck equation and matching terms gives a Hamilton-Jacobi equation for the lowest order contribution,

$$\partial_t \phi_0 + \frac{1}{2} b^{\mu\nu} \partial_\mu \partial_\nu \phi_0 + a^\mu \partial_\mu \phi_0 = 0. \quad (2.7)$$

This corresponds to the Hamiltonian system

$$\begin{aligned} H(x, p) &= \frac{1}{2} b^{\mu\nu} p_\mu p_\nu + a^\mu p_\mu \\ \dot{x}^\mu &= + \frac{\partial H}{\partial p_\mu} = b^{\mu\nu} p_\nu + a^\mu \\ \dot{p}_\mu &= - \frac{\partial H}{\partial x^\mu} = - \frac{\partial b^{\nu\lambda}}{\partial x^\mu} p_\nu p_\lambda - \frac{\partial a^\nu}{\partial x^\mu} p_\nu \end{aligned} \quad (2.8)$$

whose solutions define an equivalent variational problem of extremising an action with the Lagrangian

$$\begin{aligned}
L(x, \dot{x}) &= p_\mu \dot{x}^\mu - H(x, p) \\
&= \frac{1}{2}(\dot{x}^\mu - a^\mu)b_{\mu\nu}(\dot{x}^\nu - a^\nu). \\
&= \frac{1}{2}|\dot{x} - a(x)|_b^2
\end{aligned} \tag{2.9}$$

Thus, the rays of the Hamilton-Jacobi equation that determine the lowest order contribution to the eikonal are local maxima of the tube probability, or in other words, $\phi_0(x, x_0; T) = V_T(x|x_0)$. The large-deviation principle of Freidlin and Wentzell and the theory of the non-equilibrium potential of Graham [92, 93] thus appear as elegant reformulations of the JWKB approximation [139].

The correspondence with the JWKB approximation yields the asymptotic form of the transition density,

$$P_{1|1}(x, T|x_0) \asymp \exp\left[-\frac{1}{\varepsilon}V_T(x|x_0)\right], \tag{2.10}$$

and, in the $T \rightarrow \infty$ limit of the above, the asymptotic form of the stationary distribution,

$$P_1(x) \asymp \lim_{T \rightarrow \infty} \exp\left[-\frac{1}{\varepsilon}V_T(x|x_0)\right]. \tag{2.11}$$

where x and x_0 belong to the same basin of attraction of an attractor \mathcal{A} . As is indicated by Eq. 2.11, it can be shown that this limit is independent of the initial coordinate,

$$\lim_{T \rightarrow \infty} V_T(x|x_0) = V_\infty^{\mathcal{A}}(x), \tag{2.12}$$

where $V_\infty^{\mathcal{A}}$ is equal, to within a constant, to the stationary quasipotential $V_\infty(x)$ in the basin of attraction of \mathcal{A} . For a system with multiple attractors \mathcal{A}_i , the global quasipotential is

$$V_\infty(x) = \min_i (V_\infty^{\mathcal{A}_i}(x) + C^{\mathcal{A}_i}) \tag{2.13}$$

where $C^{\mathcal{A}_i}$ is an additive constant. The constants are fixed by requiring

$$V_\infty^{\mathcal{A}_i}(x_s^{(i,j)}) + C^{\mathcal{A}_i} = V_\infty^{\mathcal{A}_j}(x_s^{(i,j)}) + C^{\mathcal{A}_j} \tag{2.14}$$

for attractors \mathcal{A}_i and \mathcal{A}_j with adjacent basins of attraction, where $x_s^{(i,j)}$ is the saddle with the lowest value on the separatrix between the basins [93]. The stationary quasipotential determines the mean persistence time of a trajectory in a basin of attraction which generalises the Arrhenius law to systems out of equilibrium.

The $T \rightarrow \infty$ limit involved in the definition of the stationary quasipotential presents considerable numerical difficulties in the minimisation of the Freidlin-Wentzell action. A

more numerically amenable route to determining the stationary quasipotential is by the minimisation of the action over paths that start at an attractor and end at a point in its basin, regardless of the duration. We show in the next section that the solution of this second variational problem does, indeed, yield the stationary quasipotential and derive an alternative form of the Freidlin-Wentzell action that is adapted to computing instantons regardless of their duration.

2.3 On-shell action

We consider the variational problem of minimising the Freidlin-Wentzell action over paths with fixed termini but of arbitrary duration,

$$\min_T \min_{\gamma_T} S[x(t)] = \min_T \min_{\gamma_T} \int_0^T L(x, \dot{x}) dt, \quad (2.15)$$

where both the initial and final points are in the basin of the attraction \mathcal{A} and the Freidlin-Wentzell Lagrangian following from Eq. 2.9 is

$$L(x, \dot{x}) = \frac{1}{2} b_{\mu\nu} \dot{x}^\mu \dot{x}^\nu - b_{\mu\nu} a^\mu \dot{x}^\nu + \frac{1}{2} b_{\mu\nu} a^\mu a^\nu. \quad (2.16)$$

This variational problem can be solved by introducing a parametrisation u for both the coordinate and time,

$$x = x(u), \quad x' = dx/du; \quad t = t(u), \quad t' = dt/du,$$

that allows the shape of the path,

$$\sigma = \{x(u) \mid x(u_1) = x_1, x(u_2) = x_2, u_1 \leq u \leq u_2\},$$

to be varied independently of its duration,

$$T = \int_{u_1}^{u_2} t' du.$$

Coordinates x and time t are dependent variables in the reparametrised action,

$$S[x(u)] = \int_{u_1}^{u_2} L(x, \frac{x'}{t'}) t' du, \quad (2.17)$$

in which the time-dependence appears only through the derivative t' . Therefore, t is a cyclic (or ignorable) coordinate and Noether's theorem implies that the corresponding

conjugate momentum is conserved [215]:

$$-\frac{\partial(Lt')}{\partial t'} = \frac{1}{2}b_{\mu\nu}\frac{x'^\mu x'^\nu}{(t')^2} - \frac{1}{2}b_{\mu\nu}a^\mu a^\nu = E. \quad (2.18)$$

This defines submanifolds of the dynamics labelled by the “energy” E which we shall call shells. The bound $2E + |a|_b^2 \geq 0$ for the energy follows immediately from the positive-definiteness of the diffusion tensor.

Solving the first integral for t' gives

$$t' = \frac{dt}{du} = \frac{|x'|_b}{\sqrt{2E + |a|_b^2}}, \quad (2.19)$$

from which the duration of the path is obtained to be

$$T_E = \int_{u_1}^{u_2} \frac{|x'|_b}{\sqrt{2E + |a|_b^2}} du. \quad (2.20)$$

This shows that paths γ_{T_E} (of duration T_E) are equivalent to shapes σ_E (of energy E), where the latter is the restriction of shapes in σ to the shell of constant energy. Then, minimisation over paths γ_T regardless of their duration is equivalent to minimisation over shapes σ_E regardless of their energy, or

$$\min_T \min_{\gamma_T} S[x(t)] = \min_E \min_{\sigma_E} S[x(u)].$$

The action for shapes restricted to σ_E is obtained by eliminating t' between Eq. 2.17 and Eq. 2.19. This gives the “on-shell” form of the Freidlin-Wentzell action,

$$S_E[x(u)] = \int_{u_1}^{u_2} \left[\frac{E + |a|_b^2}{\sqrt{2E + |a|_b^2}} |x'|_b - b^{\mu\nu} a_\mu x'_\nu \right] du,$$

which is a functional of the shape $x(u)$, a function of the energy E , and allows for independent variations of both. It is straightforward to see that the integrand and, therefore, the action is minimised when $E = 0$. Therefore, most probable paths, regardless of their duration, are obtained by minimising

$$S_0[x(u)] = \int_{u_0}^{u_1} (|a|_b |x'|_b - b^{\mu\nu} a_\mu x'_\nu) du \quad (2.21)$$

over shapes restricted to the zero-energy shell. The duration on the zero-energy shell,

$$T_0 = \int_{u_1}^{u_2} \frac{|x'|_b}{|a|_b} du, \quad (2.22)$$

shows that paths that leave, cross, or terminate at points of vanishing drift, $a^\mu(x) = 0$, are

necessarily of infinite duration. The corresponding shapes σ_0^A can then be taken to start at a fixed point and end at another point x in the basin of attraction. The quasipotential is determined by a minimisation over such shapes σ_0^A ,

$$V_\infty^A(x) = \min_{\sigma_0^A} S_0[x(u)], \quad (2.23)$$

and the shape attaining the minimum,

$$x_\infty^*(u) = \arg \min_{\sigma_0^A} S_0[x(u)], \quad (2.24)$$

is the stationary instanton. The time on the instanton path can be obtained by integrating $t' = |x'|_b / |a|_b$. The utility of the on-shell form of the action is that it provides the shape of the path independently of its duration. The latitude of obtaining the shape from a parametrisation over a finite interval, even for paths of infinite duration, is extremely useful in numerical work.

The on-shell action is related to, but distinct from, the Jacobi action in mechanics [130, 70], which, following a Routh reduction [215], would in this case be

$$\hat{S}[x(u)] = \int_{u_1}^{u_2} \left[\sqrt{2E + |a|_b^2} |x'|_b - a^\mu x'_\mu \right] du.$$

Though both the on-shell and Jacobi action agree on the zero-energy shell, only the former supports the interpretation as least action for non-zero energies. Furthermore, variations of the on-shell action have to respect the on-shell condition Eq. 2.19 (in other words, the solutions of its Euler-Lagrange equations does not coincide with its extrema). On the other hand, the Jacobi action can be varied using the standard Euler-Lagrange approach.

For gradient dynamics, that is $a^\mu = b^{\mu\nu} \partial U / \partial x^\nu$, the on-shell action generalises the “scalar work” functional of Olander and Elber [159] to non-zero energies and configuration-dependent diffusion tensors. For non-gradient dynamics, where the drift cannot be so expressed, the on-shell action generalises the geometric action of Heyman and Vanden-Eijnden [104] to non-zero energies. The non-zero energy shell $|\dot{x}|_b^2 = |a|_b^2 + E$ admits the most general path consistent with time-translation invariance, in contrast to the zero-energy shell where the magnitude of the velocity is always equal to that of the drift, $|\dot{x}|_b^2 = |a|_b^2$. Such general paths determine the quasipotential and the asymptotic form of the transition density for finite times and will be examined in detail in future work. Accordingly, we set $E = 0$ below. The derivation of the on-shell action only requires time-translation invariance of the Lagrangian and not, as in [159, 104], their positive-definiteness. Thus, it can be applied to stochastic actions whose Lagrangians are not necessarily positive-definite, as for example the Onsager-Machlup action [164, 198]. We now describe the Ritz method by which we minimise actions.

2.4 Ritz method

The direct method in the calculus of variations consists of constructing a sequence of extremisation problems for a function of a finite number of variables that, in the passage to the limit of an infinite number of variables, yields the solution to the variational problem. The two main families of direct methods are finite differences and Ritz methods [184, 120, 55, 80]. In the latter, the solution of the variational problem is sought in a sequence of functions

$$\varphi_1(t), \varphi_2(t), \dots, \varphi_n(t), \dots$$

each of which satisfies end point conditions. The path is expressed as a linear combination of these functions

$$x_n(t) = \alpha_1 \varphi_1(t) + \dots + \alpha_n \varphi_n(t) \quad (2.25)$$

which transforms the action from a functional of the path into a function of the expansion coefficients,

$$\begin{aligned} S(\alpha_1, \dots, \alpha_n) &= \int_0^T L(x_n, \dot{x}_n) dt \\ &= \int_0^T L\left(\sum_{i=1}^n \alpha_i \varphi_i, \sum_{i=1}^n \alpha_i \dot{\varphi}_i\right) dt. \end{aligned} \quad (2.26)$$

Action minimisation now becomes a search for a set of coefficients, α_i^* such that $S(\alpha_1^*, \dots, \alpha_n^*) < S(\alpha_1, \dots, \alpha_n)$. The necessary condition for this is the vanishing of the gradient,

$$\frac{\partial S}{\partial \alpha_i} = 0 \quad (i = 1, 2, \dots, n), \quad (2.27)$$

which is the Ritz system of non-linear equations. Coefficients satisfying these conditions can be obtained by non-linear optimisation. The n -th approximation to the minimum action path, $x_T^*(t)$, and the minimum value of the action, $S[x_T^*(t)]$, are obtained from these values of the coefficients. It is generally the case that this sequence of approximations converges to the minimum of the variational problem as $n \rightarrow \infty$ [80, 120].

The method, then, has three parts: first, the choice of basis functions $\varphi_i(t)$; second, the quadrature rule that integrates the Lagrangian to obtain the action as a function of the expansion coefficients; and third, the optimisation that yields the coefficients at the minimum. Since each part is only loosely dependent on the others, Ritz methods come in many varieties [69]. Our choices are centered around Chebyshev polynomials as described below. Approximation by Chebyshev polynomials and their optimality for the purpose are described in [204, 21, 205].

Basis functions: We consider a path $x(u)$ that is a Lipschitz continuous function of the parameter u in the interval $[-1, 1]$. Then, it has an absolutely and uniformly convergent

Chebyshev expansion,

$$x(u) = \sum_{k=0}^{\infty} a_k T_k(u), \quad a_k = \frac{2}{\pi} \int_{-1}^1 \frac{x(u) T_k(u)}{\sqrt{1-u^2}} du$$

where $T_k(u)$ are Chebyshev polynomials of the first kind and the integral must be halved for $k = 0$. A suitable sequence of paths can be constructed from the first n terms of this infinite series. However, it is computationally more convenient, for reasons that will be clear below, to construct the sequence from n -th degree polynomials that interpolate the path at the $n + 1$ Chebyshev points

$$u_j = -\cos(j\pi/n), \quad (j = 0, 1, \dots, n). \quad (2.28)$$

The n -th degree interpolant can be expressed in standard form as a sum of Lagrange cardinal polynomials $\ell_j(u)$ or as a linear combination of Chebyshev polynomials,

$$x_n(u) = \sum_{j=0}^n \alpha_j \ell_j(u) = \sum_{k=0}^n c_k T_k(u). \quad (2.29)$$

The coefficients c_k are aliased versions of the coefficients a_k . Since the cardinal polynomials have the property

$$\ell_j(u_k) = \begin{cases} 1, & j = k \\ 0, & \text{otherwise,} \end{cases} \quad (j, k = 0, \dots, n),$$

$x_n(u_k) = \alpha_k$, that is, the expansion coefficients α_k are path coordinates at the Chebyshev points. Expressing the entire path in terms its discrete coordinates has the advantage that end point conditions can be imposed by setting

$$\alpha_0 = x(u_0) = x_0, \quad \alpha_n = x(u_n) = x_1. \quad (2.30)$$

Admissible paths of degree n are, then, parametrised by the $n - 1$ independent coefficients $\alpha_1, \dots, \alpha_{n-1}$. In contrast, imposing end point conditions in series form leads to a numerically inconvenient linear dependence between the coefficients c_k . The derivative of the path is a polynomial of degree $n - 1$ that can be expressed in terms of the interpolant as

$$x'_n(u) = \sum_{j=0}^n \alpha_j \ell'_j(u) = \sum_{j=0}^n \beta_j \ell_j(u) \quad (2.31)$$

with the two sets of expansion coefficients related by the Chebyshev spectral differentiation matrix

$$\beta_j = D_{jk} \alpha_k, \quad D_{jk} = \ell'_k(u_j). \quad (2.32)$$

We use the barycentric form of the Lagrange polynomials [101]

$$\ell_j(u) = \frac{w_j}{u - u_j} \Bigg/ \sum_{k=0}^n \frac{w_k}{u - u_k}. \quad (2.33)$$

with weights [188]

$$w_j = \begin{cases} \frac{1}{2}, & j = 0 \\ (-1)^j, & j = 1, \dots, n-1 \\ \frac{1}{2} \cdot (-1)^n, & j = n. \end{cases}$$

This form is both numerically stable and, costing no more than $O(n)$ operations, efficient to evaluate. [12].

Chebyshev interpolants converge exponentially for analytic functions and algebraically for functions with a finite number of derivatives. More precisely, for an analytic path, $\|x - x_n\| = O(\rho^{-n})$ for some $\rho > 1$ as $n \rightarrow \infty$. For a path with ν derivatives and ν -th derivative of bounded variation K , $\|x - x_n\| = O(Kn^{-\nu})$ as $n \rightarrow \infty$. These estimates are in the supremum norm $\|a\|$, that is, the maximum of the absolute value of a in the interval $[-1, 1]$. In contrast, finite-difference methods can only achieve polynomial, but never exponential, rates of convergence, even for analytic paths [204, 21].

Quadrature: To reduce the action to a multivariate function of the coefficients it is necessary to evaluate the integral

$$S(\alpha_1, \dots, \alpha_n) = \int_{-1}^1 L(x_n(u), x'_n(u)) du \quad (2.34)$$

using a quadrature rule. For instance, quadrature at the Chebyshev points u_j gives

$$\begin{aligned} S(\alpha_1, \dots, \alpha_n) &= \sum_{j=0}^n \omega_j L(x_n(u_j), x'_n(u_j)) \\ &= \sum_{j=0}^n \omega_j L(\alpha_j, \beta_j) \\ &= \sum_{j=0}^n \omega_j L(\alpha_j, D_{jk} \alpha_k) \end{aligned}$$

where ω_j are the quadrature weights. However, standard quadrature rules at this set of n Chebyshev points, which integrate a polynomial of degree less than or equal to n exactly, will generally be inaccurate. The reason is that the Lagrangian has polynomial degree different from, and usually greater than, the polynomial degree of the path. For instance, when b_{ij} is a constant, the term quadratic in the velocities has twice the polynomial degree of the path. Therefore, if the Lagrangian is to be integrated accurately, the order of the

quadrature must be different from, and in general greater than, the polynomial degree of the path.

Therefore, we define a second set of $n_q > n$ Chebyshev points

$$v_j = -\cos(j\pi/n_q), \quad (j = 0, 1, \dots, n_q) \quad (2.35)$$

and interpolate the path at these points. This is done efficiently by matrix multiplication with a $(n_q + 1) \times (n + 1)$ matrix

$$x_n(v_j) = \sum_{k=0}^{n_q} B_{jk} \alpha_k, \quad (2.36)$$

$$x'_n(v_j) = \sum_{k=0}^{n_q} B_{jk} \beta_k, \quad (2.37)$$

whose elements are derived from the barycentric interpolant

$$B_{jk} = \frac{w_k}{v_j - u_k} \left/ \sum_{l=0}^{n_q} \frac{w_l}{v_l - u_l} \right.. \quad (2.38)$$

The Lagrangian is evaluated at these second set of points after which Clenshaw-Curtis quadrature [204, 21] is used to evaluate the action,

$$\begin{aligned} S(\alpha_1, \dots, \alpha_n) &= \sum_{j=0}^{n_q} \omega_j L(x_n(v_j), x'_n(v_j)) \\ &= \sum_{j=0}^{n_q} \omega_j L(B_{jk} \alpha_k, B_{jk} \beta_k) \\ &= \sum_{j=0}^{n_q} \omega_j L(B_{jk} \alpha_k, B_{jk} D_{kl} \alpha_l) \\ &\equiv \sum_{j=0}^{n_q} \omega_j L(B_{jk} \alpha_k, C_{jk} \alpha_k). \end{aligned} \quad (2.39)$$

As with interpolation, Clenshaw-Curtis quadrature converges exponentially for Lagrangians that are analytic in u and algebraically for Lagrangians with a finite number u derivatives. Precise estimates are given in [205]. For fixed values of n and n_q , the matrices B_{ij} and C_{ij} in the above expression are constant and can be precomputed and stored. The multiplications require $O(nn_q)$ operations, and so there is a linear cost, for fixed n , to increase the order of the quadrature. For Lagrangians of polynomial order n_L , the number of quadrature points must be $n_q > (n + 1)n_L$. For nonpolynomial Lagrangians, n_q has to be chosen to

ensure that the n_q -th Chebyshev coefficient is suitably small. Well-defined procedures exist for the adaptive truncation of Chebyshev series [9] but here we use a simple rule of thumb and set $n_q = 10n$ leaving the implementation of more efficient truncations to future work. We note that in the direct finite-difference method, introduced in [213], the path is interpolated at uniformly spaced points by a quadratic polynomial and the Lagrangian is integrated using the trapezoidal rule. This combination can exactly evaluate the action for Lagrangians that are at most quadratic polynomials.

Optimisation: To minimise the action over the expansion coefficients $\alpha_1, \dots, \alpha_{n-1}$ we use both gradient-free and gradient-based algorithms. For gradient-free algorithms we provide Eq. 2.39 directly. For algorithms that require the gradient, the chain rule gives

$$\begin{aligned}\nabla_{\alpha_i} S &= \frac{\partial}{\partial \alpha_i} \left[\sum_{j=1}^{n_q} \omega_j L(B_{jk} \alpha_k, C_{jk} \alpha_k) \right] \\ &= \sum_{j=1}^{n_q} \left[\frac{\partial L}{\partial x_n(v_j)} B_{ji}^* + \frac{\partial L}{\partial x'_n(v_j)} C_{ji}^* \right]\end{aligned}\tag{2.40}$$

where $B_{ij}^* = \omega_i B_{ij}$ and $C_{ij}^* = \omega_i C_{ij}$. These matrices, too, can be precomputed and stored and only the partial derivatives of the Lagrangian need to be computed for given values of the coefficients. For the examples presented below, we use *NEWUOA* [173] for gradient-free optimisation and *SLSQP* algorithm [?] for gradient-based optimisation, both of which are implemented in the *NLOPT* numerical optimisation package [117]. For non-equilibrium systems, instantons lose smoothness when passing through fixed points. For such paths, convergence is still achieved but at less than spectral rates. Spectral convergence can be recovered if paths are evaluated piecewise, taking care to isolate the points of derivative discontinuities. This is feasible because fixed points are the only locations where Freidlin-Wentzell instantons can lose smoothness [93].

2.5 Numerical results

In this section, we apply the Ritz method to three diffusion processes that are widely used to benchmark rare event algorithms. The first is overdamped Brownian motion in a complex energy landscape, the second is overdamped Brownian motion under the influence of a circulatory force, and the third is a model of the weather. All three models have configuration-independent diffusion tensors for which it is not necessary to distinguish between covariant and contravariant indices. Python codes for each of these examples are freely available on GitHub.

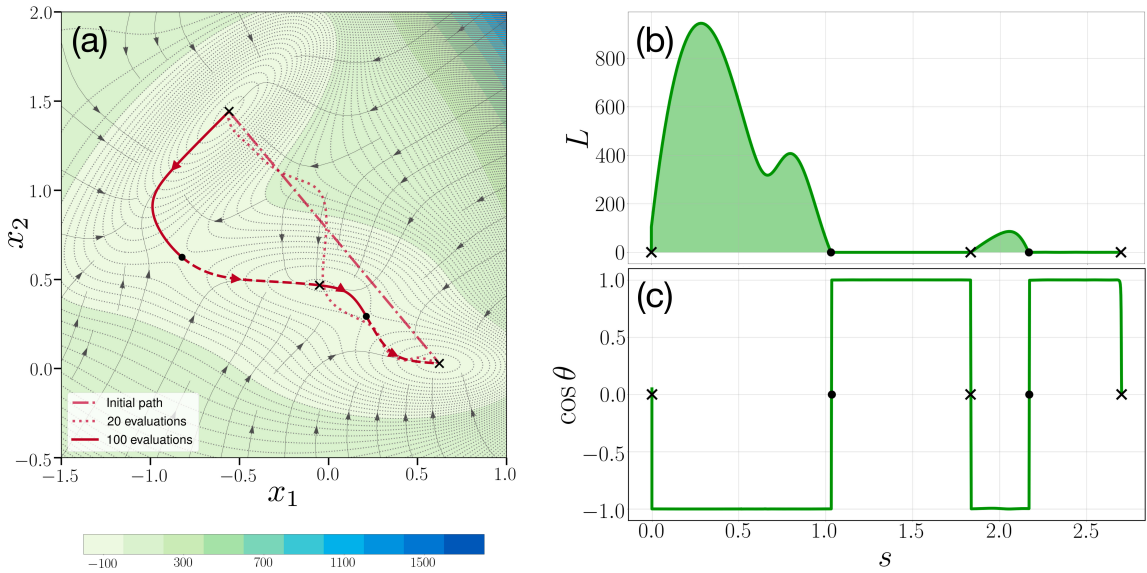


Figure 2.1: Ritz method for overdamped motion in the Müller-Brown potential, which has three minima (crosses) and two saddle points (dots). The initial path is the straight line connecting two minima and the instanton is the solid line, with broken segments showing motion along the force. The instanton automatically locates and passes through both saddles. A typical path before convergence to the minimum is shown as a dotted line. (b) The value of the Lagrangian as a function of Euclidean arc-length of the instanton. The action vanishes to machine precision on segments of the path where motion is along the force. (c) The cosine of the angle θ between the tangent and the force is always ± 1 , i.e. the instanton is a minimum energy path. The instanton is represented by a polynomial of degree $n = 10$.

2.5.1 Brownian dynamics in a complex potential

Our first example considers the overdamped Brownian motion in a two-dimensional potential with a constant friction. The usual equations of Brownian dynamics can be recast into Itô form,

$$\begin{aligned} dX_1 &= -\mu \partial_1 U dt + \sqrt{2\mu\varepsilon} dW_1 \\ dX_2 &= -\mu \partial_2 U dt + \sqrt{2\mu\varepsilon} dW_2, \end{aligned}$$

where μ is the mobility and $\varepsilon = k_B T$ is the temperature. The Freidlin-Wentzell action for a smooth path with two-dimensional coordinate $x = (x_1, x_2)$ is

$$S[x] = \frac{1}{2} \int_0^T \frac{1}{2\mu} |\dot{x} + \mu \nabla U|^2 dt$$

where $\nabla U = (\partial_1 U, \partial_2 U)$. The minimum of the zero-energy action,

$$S_0[x] = \int_{-1}^1 |\nabla U(x)| |x'| du + [U(x)]_{-1}^1,$$

provides the most probable shape and the stationary quasipotential. The second term does not affect the minimisation and can be discarded. The resulting reduced action

$$\tilde{S}[x] = \int_{-1}^1 |\nabla U| |x'| du \quad (2.41)$$

is of the same form as Fermat's principle for optical rays, where $|\nabla U(x)|$ plays the role of the refractive index and $|x'|du = ds$ is the arc-length of the ray. In geometric optics, Fermat's principle is equivalent to Huygen's principle and its “wavelet equation”

$$\partial_i U = |\nabla U| \frac{dx_i}{ds}. \quad (2.42)$$

This can be easily verified by differentiating it with respect to arc-length, to obtain the eikonal equation

$$\partial_i |\nabla U| = \frac{d}{ds} \left[|\nabla U| \frac{dx_i}{ds} \right],$$

which is identical to the Euler-Lagrange equation of the zero-energy action. The wavelet equation implies that the tangent $t = dx/ds$ to the path is parallel to the gradient of the potential, or equivalently, that rays are normal to contours of the potential. This is the well-known condition for a minimum energy path and was first derived variationally from the scalar work functional by Olander and Elber [159]. It provides a stringent test of the fidelity of the paths obtained by minimisation.

Following [159], we choose the Müller-Brown potential of [152] as an example of a complex energy landscape. The potential and its stationary points are shown in Fig. 2.1. The three minima are marked by crosses and two saddle points by dots. The instanton is computed by requiring the path to start at the minimum on the top left and terminate at the minimum on the bottom right. The initial straight line shape, an intermediate shape and the converged instanton are shown in panel (a). The minimisation automatically locates the two saddle points and makes the instanton pass through them. The action cost along the path is shown in panel (b), where the vanishing of the action on segments of the path along the force is clearly seen. The cosine of the angle between the tangent and force is shown in panel (c) and the condition for a minimum energy path is clearly fulfilled. We emphasise that the condition is not imposed separately but is satisfied automatically at the minimum. The Ritz method provides an alternative to chain-of-states methods for finding minimum energy paths. It does not need the Hessian of the potential, which makes it suitable for problems where such evaluations are expensive. Unlike [104], our parametrisation has no unit-speed constraint and the minimisation,

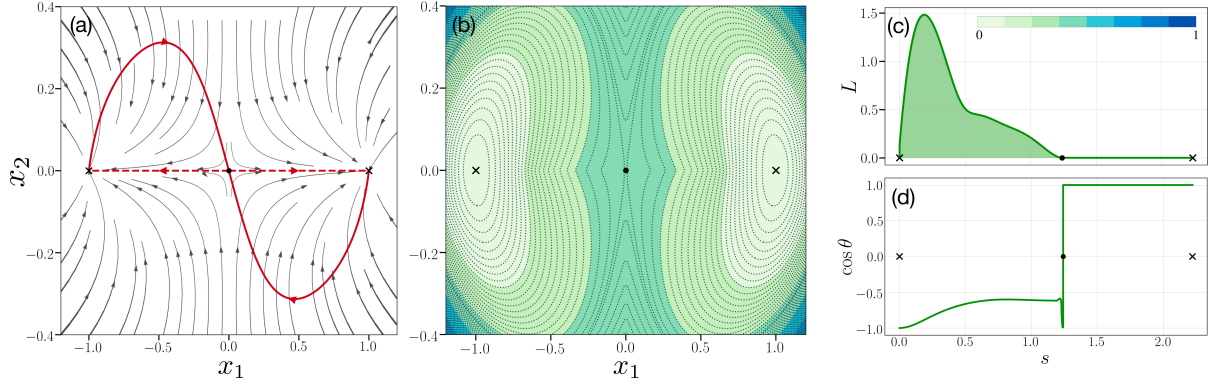


Figure 2.2: Ritz method for overdamped motion in a circulatory (i.e. non-gradient) force field. The instanton is in red with solid (dashed) segments showing motion against (along) the force field. The instanton is reflected about the horizontal axis for motion starting on the right, showing the inequivalence of fluctuational and relaxational paths for non-gradient dynamics. (b) The quasipotential, computed using Eq. 2.13, with a caustic at the unstable fixed point. (c) The value of the Lagrangian as a function of the Euclidean arc-length of the instanton. As in the potential case, the action vanishes to machine precision on segments where motion is along the force. (d) The cosine of the angle θ between the tangent and the force is, unlike in the potential case, not always ± 1 . The instanton is represented by a polynomial of degree $n = 8$.

accordingly, is unconstrained. The method applies without change to dynamics with configuration-dependent friction.

2.5.2 Brownian dynamics in a circulatory field

For our second example we consider, in contrast to the first, Brownian motion in a force field that cannot be derived from a potential and, as such, necessarily has a non-vanishing curl. Choosing the force field of Maier and Stein [141] gives

$$\begin{aligned} dX_1 &= (X_1 - X_1^3 - \beta X_1 X_2^2) dt + \sqrt{\epsilon} dW_1 \\ dX_2 &= -(1 + X_1^2) X_2 dt + \sqrt{\epsilon} dW_2 \end{aligned}$$

for the overdamped motion of the two-dimensional coordinate $X = (X_1, X_2)$, where β is a parameter. The force field $f(x_1, x_2) = (x_1 - x_1^3 - \beta x_1 x_2^2, -(1 + x_1^2)x_2)$ is smooth, and f_1 is odd in x_1 and even in x_2 , while for f_2 the converse holds. There are two stable fixed points at $x_a = (-1, 0)$ and $x_b = (1, 0)$, and a saddle point at $x_s = (0, 0)$. The force field admits a potential only for $\beta = 1$, when it can be written as $f = -\nabla U$, with $U(x_1, x_2) = -\frac{1}{2}x_1^2 + \frac{1}{4}x_1^4 + \frac{1}{2}(1 + x_1^2)x_2^2$. The force field is shown in the first panel of Fig. 2.2 for $\beta = 10$ together with the instanton moving from x_a to x_b . As before, solid (dashed) segments represent motion against (along) the vector field. The instanton moving from x_b to x_a is obtained by reflection about the x_1 -axis showing that that fluctuational and relaxational paths are not identical in a non-gradient field.

The middle panels shows the stationary quasipotential $V_\infty^{\mathcal{A}_i}(x)$ with respect to the attractors at $(-1, 0)$ and $(1, 0)$ respectively. The quasipotential is sampled on a 128×128 grid by computing instantons between a point on the grid and the relevant attractor. The contours of the quasipotential and its heatmap are obtained from these discrete samples. To the best of our knowledge, all prior estimations of the quasipotential for this problem (and more generally, for circulatory forces) have required numerical solutions of the Hamilton-Jacobi equation. Our method of direct sampling provides an alternative to this route of computing the quasipotential. The right panel shows the Lagrangian as a function of arc-length along the instanton. As in the previous example, the Lagrangian vanishes along segments of the path where motion is along the force. For motion against the force, the tangent to the path is no longer parallel to the force, as shown by the variation of the cosine of the angle θ between the tangent and the force. We note that our method is agnostic to the existence, or not, of a potential for the drift and treats both these cases on equal footing.

2.5.3 Multistability in a genetic switch

We continue with the dynamics of a two-dimensional coordinate $x = (x^1, x^2)$ in a non-gradient field, but now of non-mechanical origin and non-polynomial form,

$$\begin{aligned} dx^1 &= \left(\frac{a_1}{1 + \left(\frac{x^2}{K_2}\right)^n} - \frac{x^1}{\tau} \right) dt + \sqrt{\epsilon} dW^1 \\ dx^2 &= \left(\frac{a_2}{1 + \left(\frac{x^1}{K_1}\right)^m} - \frac{x^2}{\tau} \right) dt + \sqrt{\epsilon} dW^2, \end{aligned} \tag{2.43}$$

where $a_1, a_2, \tau, n, m, K_1$ and K_2 are constants. This model is due to Roma *et al* [185] and describes a multistable genetic network. In the region of configuration space we consider, the vector field has two fixed points one of which is stable and the other a saddle. The top panel of Fig. 2.3 shows the instantons moving between these fixed points. Unlike in the previous examples, here the instantons move either entire with (solid line) or entirely against (dashed line) the flow. The bottom panel shows the quasipotential with respect to the stable fixed point. The procedure to evaluate and plot it is as described above. The quasipotential provides a quantification of the dispersion of the coordinate about the stable fixed point and a measure of the non-equilibrium “temperature” of this non-mechanical system.

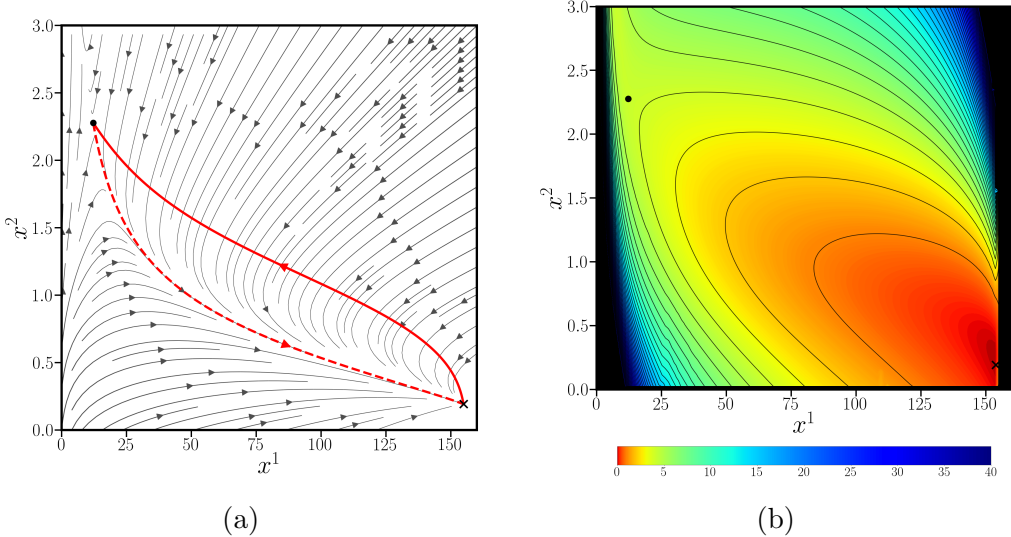


Figure 2.3: Instantons for the genetic switch. (a) shows the instantons in red with solid (dashed) lines representing motion against (along) the vector field. (b) shows the quasipotential with respect to the stable fixed point (cross). Parameter values are $a_1 = 156$, $a_2 = 30$, $\tau = 1$, $n = 3$, $m = 1$ and $K_1 = K_2 = 1$. A polynomial of degree $n = 10$ was used to parametrise the path.

2.5.4 Transitions between limit cycles

To demonstrate that our method is not limited to fixed points, we constructed a simple but non-trivial system:

$$\begin{aligned} dr &= (1 + \cos^2 \theta)f(r)dt + dW^r \\ d\theta &= r(1 + \sin^2 \theta)dt + dW^\theta \end{aligned} \tag{2.44}$$

where $f(r) = -\frac{1}{4}r(r - s_1)(r - s_2)(r - s_3)$, and $s^{(i)} = [1, 3, 5]$. We have an unstable fixed point at $r = 0$, stable limit cycles at $r = s_1$ and $r = s_3$, and an unstable limit cycle at $r = s_2$. The trigonometric factors in the drift breaks the circular symmetry of the system, but preserves the concentric circular limit cycles. We consider instantons moving from the inner stable limit cycle $r = s_1$ to the outer limit cycle $r = s_3$. Let $\Gamma_i = \{(r, \theta) | r = s_i\}$ for $i = 1, 2, 3$, be the set of points comprising the three limit cycles. For a given path $x(t)$, let $x_i \in \Gamma_i$ be the points along the path located along the respective limit cycles. Since $a_r(x_i) = 0$ and $a_\theta(x)$ is positive definite, the system can move to any point within a limit cycle without incurring any action cost. Therefore the starting, intermediate and end points x_1 , x_2 and x_3 should be varied freely within their respective limit cycles during the minimisation. We can split the instanton $x^*(t)$ into an “uphill” path $x_{\uparrow}^*(t)$, moving between Γ_1 and Γ_2 , and a “downhill” path $x_{\downarrow}^*(t)$, moving between Γ_2 and Γ_3 . The downhill path follows deterministic relaxational dynamics, and does not contribute to the action, and therefore the only non-trivial part of the problem is the uphill path $x_{\uparrow}^*(t)$. One issue with limit cycle problems is that instantons in general have infinite arc-lengths. In the

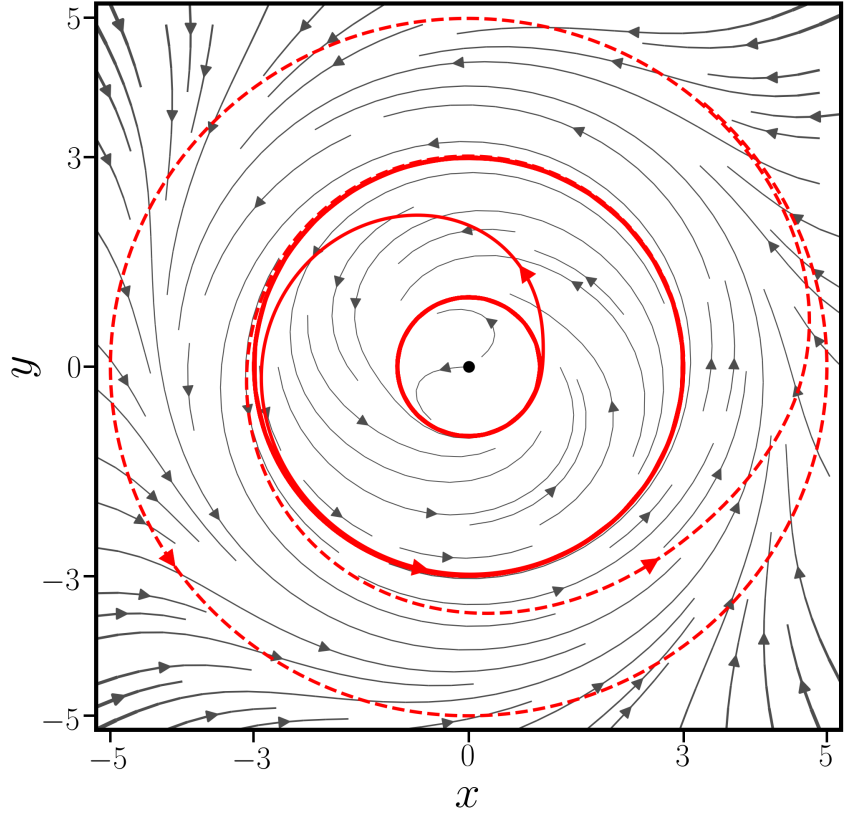


Figure 2.4: An approximate instanton of the concentric limit cycle system with $S \approx 3.65053$. The instanton moves from the inner stable limit cycle at $r = 1$ to the unstable limit cycle at $r = 3$, and then moves hetero-clinically along the drift to the outer stable limit cycle at $r = 4$.

case of the relaxational path $x_{\downarrow}^*(t)$, this can be verified to be the case using an ODE solver. The system will not only relax to the attractor in infinite time, but the system will also undergo an infinite number of cycles before reaching the stable limit cycle Γ_3 . We would expect similar behaviour for diffusive paths leaving stable limit cycles. Paths of infinite Euclidean arc-length are not possible to parametrise exactly in the Chebyshev basis, so only an approximate finite-length instanton can be found, as shown in Fig. 2.4. As we increased the arc-length the action of the candidate instanton converged to a value of $S \approx 3.65053$.

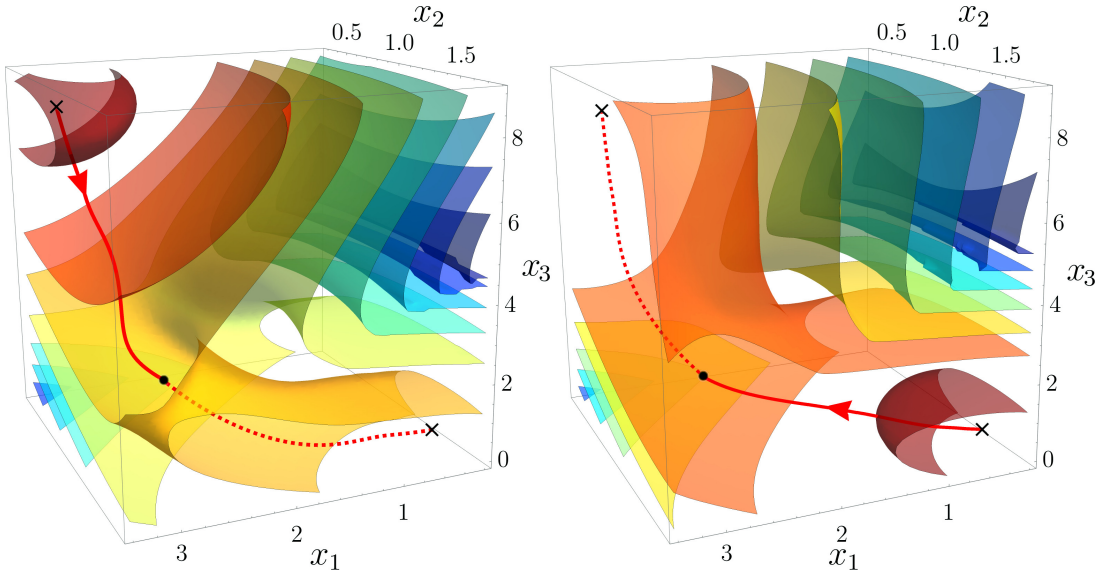


Figure 2.5: Instantons and quasi-potentials of the Egger model. The instantons are shown in red with solid (dashed) lines representing motion against (along) the vector field. The left and right panels are forward and reverse instantons. Isosurfaces of the quasipotential with respect to each attractor is shown in the respective panels. Isovalues increase from light red to blue in the range $\{1, 7, 11, 16, 21, 26, 31, 36\}$. Parameter values are $k = 2$, $\beta = 1.25$, $\gamma = 2$, $U_0 = 10.5$ and $H = 12$. The instanton is represented by a polynomial of degree $n = 10$.

2.5.5 Egger model of weather

Our final example is a reduced model of the weather for a three-dimensional coordinate $X = (X_1, X_2, X_3)$ that has a circulatory drift,

$$\begin{aligned} dX_1 &= \left[kX_2 \left(X_3 - \frac{\beta}{k^2} \right) - \gamma X_1 \right] dt + \sqrt{\epsilon} dW_1 \\ dX_2 &= \left[kX_1 \left(\frac{\beta}{k^2} - X_3 \right) - \gamma X_2 + \frac{HX_3}{k} \right] dt + \sqrt{\epsilon} dW_2 \\ dX_3 &= \left[-\frac{1}{2}HkX_2 - \gamma(X_3 - U_0) \right] dt + \sqrt{\epsilon} dW_3 \end{aligned} \quad (2.45)$$

where k , β , γ , U_0 and H are constants. This model is due to Egger [53]. It is not particularly illuminating to visualise the three-dimensional vector field describing this dynamics but we note that it has two stable fixed points, marked by crosses in Fig. 2.5, and a saddle fixed point marked by a dot. The instanton moving between these points is shown as before in the left and right panels of the figure. Also shown are isosurfaces of the quasipotential with respect to the stable fixed points, with isovalues increasing from red to blue. To the best of our knowledge, this is the first computation of the quasipotential for this model. We provide this example primarily to demonstrate the feasibility of sampling quasipotentials in dimensions greater than two with our method.

Model	$S_1 - S_2$	$S_3 - S_4$	$S_7 - S_8$	$S_{15} - S_{16}$	$S_{31} - S_{32}$
M-B	2	3×10^{-4}	1×10^{-7}	5×10^{-14}	1×10^{-13}
M-S	2×10^{-3}	3×10^{-7}	2×10^{-12}	1×10^{-16}	5×10^{-16}
Egger	8×10^{-3}	1×10^{-3}	6×10^{-7}	4×10^{-9}	8×10^{-13}
Model	$S_2 - S_{50}$	$S_4 - S_{50}$	$S_8 - S_{50}$	$S_{16} - S_{50}$	$S_{32} - S_{50}$
M-B	4×10^{-2}	4×10^{-5}	8×10^{-8}	1×10^{-12}	3×10^{-13}
M-S	2×10^{-4}	7×10^{-11}	2×10^{-13}	1×10^{-16}	2×10^{-16}
Egger	5×10^{-3}	1×10^{-4}	1×10^{-6}	1×10^{-8}	2×10^{-10}

Table 2.1: Convergence of the action S_n for a path of polynomial order n . The abbreviations M-B and M-S refer to Brownian dynamics in the Müller-Brown potential and the Maier-Stein force field respectively. The first table shows the difference $S_n - S_{n+1}$ while the second table shows the difference $S_n - S_{50}$. A tenth-order polynomial typically gives at least six digits of accuracy.

2.6 Numerical convergence

We briefly recall the convergence properties of the Ritz method, comprising that of the basis functions, the quadrature, and the optimisation. The Chebyshev interpolant converges to the most probable path, assuming that it is Lipschitz continuous, at a rate that increases with the number of derivatives the path admits and is exponential for a smooth path. Likewise, the Clenshaw-Curtis quadrature is guaranteed to converge to the minimum of the action, assuming that the Lagrangian is Lipschitz continuous. The optimal number of quadrature points for accuracy to machine precision can be obtained by following the decay of the Chebyshev coefficients of the Lagrangian and truncating at that value beyond which the coefficients vanish to machine precision. The optimisation has lesser theoretical guarantees than the interpolation and quadrature, as is generally the case with search in high-dimensional spaces. However, the residual of the Ritz system provides an empirical measure for how closely the minimum has been located. In all three examples (and in others not presented here) we have found both gradient-free and gradient-based optimization to robustly locate the minima, and gradient-based methods to yield faster convergence. We note that for equilibrium problems, the gradient-free method does not require the Hessian of the energy function, which can be of significant computational advantage. In Table 2.1 we show the spectral convergence of the action with increasing polynomial order of the path for each of our examples.

2.7 Conclusion

We have presented an efficient and accurate numerical method for computing most probable transitions paths and quasipotentials of rare diffusive events. The method directly minimises the Freidlin-Wentzell action and thus provides a unified approach for

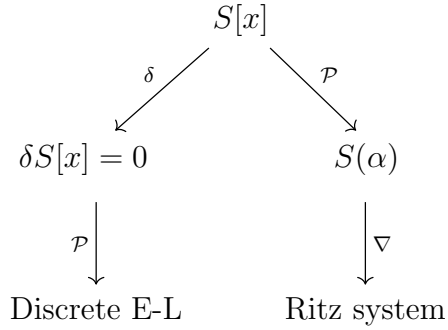


Figure 2.6: Inequivalence of the direct and Euler-Lagrange routes to numerical action minimization. Here, $\delta \rightarrow$ functional variation, $\mathcal{P} \rightarrow$ finite-dimensional projection, and $\nabla \rightarrow$ function minimisation. On the left branch, the action is first varied to obtain the Euler-Lagrange equation and then projected onto a finite-dimensional basis for numerical solution. On the right branch, the action is first projected onto a finite-dimensional basis and then minimised to obtain the Ritz system. The finite-dimensional projection of the Euler-Lagrange equations is, in general, not identical to the Ritz system.

transition paths in both equilibrium and non-equilibrium systems. Our reparametrisation-invariant form of the action, derived using a Noether symmetry, is well-suited for numerical work and is a generalisation of the geometric action. This frees us from the constraints of the commonly used arc-length path parametrisation and offers the maximum flexibility in choosing the space of polynomials in which action is minimised. Thus our method is not limited to the Chebyshev polynomials in $[-1, 1]$ used here but easily admits trigonometric polynomials and, more generally, any global basis. Numerical quadrature reduces the action to a multivariate function of coefficients of the path polynomial whose minimum is obtained by both gradient-free and gradient-based optimisation. This gives, simultaneously, both the minimum value of the action and the most probable path. This efficiency of the method allows us to repeatedly compute minimum action paths between an attractor and a point in its basin of attraction and, thereby, map out the quasipotential. The quasipotential in a non-equilibrium steady state has the same significance as the Gibbs distribution in equilibrium and our method provides a robust way of obtaining it without the need to numerically solve the Hamilton-Jacobi partial differential equation.

The direct method used here consists of a discretisation of the action followed by a search for the minimum in the resulting finite-dimensional space, expressed schematically in Fig. (2.6). In contrast, the majority of methods impose the vanishing variation of the action and then search for the solution of the Euler-Lagrange equation in a finite-dimensional space. The resulting discretised Euler-Lagrange equations is, in general, not identical to the Ritz system; in other words, these two methods of reducing an infinite-dimensional problem to a finite-dimensional one are not equivalent. In contrast to mechanics, where Newton's equations of motion are considered primary and the action derived, here it

is the tube probability and hence the Freidlin-Wentzell action that is primary and the Euler-Lagrange equation for the most probable path that is derived. It appears more natural to us to discretise the primary, rather than the derived, object directly. Our approach is algorithmically simple and the only adjustable parameters are the polynomial order n and the quadrature order n_q . This simplicity does not compromise accuracy or efficiency, as confirmed by our examples.

The rapid convergence of the method holds promise for its application to problems involving the stochastic dynamics of fields, with both scalar and Lie group-valued order parameters. We also expect the method to apply to stochastic dynamics with degenerate diffusion tensors and to stochastic systems with inertia. These will be addressed in forthcoming work.

Chapter 3

Monte Carlo methods in Path Spaces

3.1 Introduction

In a large deviation limit, the dominant transition pathway of an Itô diffusion equation between fixed points of its drift field is given by the minimiser of the associated Freidlin-Wentzell action. Physically, this corresponds to taking a limit of vanishing noise. Although useful for many applications, as discussed in the introduction of the previous chapter, in any real system the zero-noise limit is un-physical. At finite noise, we must instead consider the whole *transition path ensemble* (TPE), the set of all transition paths of a system given fixed end-points. Therefore at finite noise one can have multiple competing transition *channels*, as will be a major topic in Ch. 4.

Due to the fixed end-points, standard simulation methods like the Euler-Maruyama integrator [?] are often inefficient at sampling the transition path ensemble. In this chapter we will apply some recent mathematical developments in the field of infinite-dimensional *Markov-Chain Monte Carlo* (MCMC) methods [39, 13, 98, 99, 100], to sample the *transition path ensemble* (TPE) of Itô diffusion equations. The resulting algorithm, known as the *pCN*-algorithm, is an MCMC procedure which can evaluate probabilistic path-integrals over the space of stochastic paths. Using Kosambi-Karhunen-Loève (KKL) theory [? ? 137], we develop a fast implementation of the pCN using Fast-Fourier Transforms. In Sec. 3.3 we present the *teleporter MCMC* (TMC), an extension of the pCN geared towards effectively sampling TPEs with multiple competing transition channels.

Other well-known techniques of sampling the TPE are the *transition path sampling* (TPS) [42, 43, 41, 16, 18] and *forward flux sampling* (FFS) [? ? ?]. One of the main differences in our proposed method is that it is defined for general Itô diffusions with additive noise, whilst established methods like the TPE and FFS tend to require that the system drift and noise satisfy the detailed balance condition, such that the dynamics is reversible. As our method is defined for arbitrary drift-fields, it can sample the TPEs of both equilibrium and non-equilibrium systems. Another point of difference is that we

parametrise stochastic paths in a global basis, where the TPE and FFS use a uniform discretisation of stochastic paths. Specifically, we expand the stochastic paths of Itô diffusions in the Kosambi-Karhunen-Loève basis of Brownian bridge processes. As will be discussed in Sec. 3.2, we find that the statistics of the TPE separates into distinct low- and high-frequency bands in the KKL basis, where the higher band is completely decorrelated and behave is near that of a Brownian process. We find that the non-trivial statistics of the TPE is wholly contained in the lower band. Furthermore, our choice of basis also allows great freedom in the choice of initial- and final-conditions of the TPE. As for the TPS and FFS, we can choose paths to start and end in open regions in state-space. However, the pCN and TMC also admits fixed start- and end-point configurations. Perhaps one of the main differences. The TMC, which will be discussed in Sec. 3.3, also allows for the simultaneous sampling of multiple transition channels in the TPE simultaneously. Without recourse to techniques such as [? 66], which requires a costly hierarchical sequence of MCMC algorithms running at different temperatures, established methods and traditional MCMC methods will often fail to sample all transition channels. This is referred to as the *slow mixing* [?] of the modes of target probability distribution. Finally, another point of difference is that the the pCN and TMC algorithms are mathematically formulated directly on the infinite-dimensional space of stochastic paths, whilst the TPE and FFS are defined on discretised path-spaces that approximate the true system under mesh-refinement.

We will commence by giving a brief summary of the necessary mathematical theory for path-space MCMC methods. This will simultaneously also serve as an introduction to, and discussion of, the transition path ensemble and path-integral approaches to study this infinite-dimensional space of stochastic paths. In particular we aim to show that path-integrals, which are often described as the ‘symbolic’ limit of a finite-dimensional discretisation [? 199], can be understood without recourse to discretisation. Furthermore, in Sec. 3.2 we will see that this mathematical rigour is the necessary theoretical understanding that enables the construction of path-space MCMC methods. We will also discuss the distinctions between two common expressions for the path-integral approach: the Freidlin-Wentzell and the *Onsager-Machlup* path-probability densities, of which the former was discussed in Ch. 2. The main purpose of the treatment below is to explain the relevant mathematical concepts, and we will therefore eschew rigour whenever it facilitates more didactic explanations. The reader can see the references for more details.

Physically, the broad class of systems we consider are described by *overdamped Langevin equations*, which are often written as [? ?]

$$\dot{\mathbf{X}} = \mu \mathbf{F}(\mathbf{X}) + \sqrt{2D} \boldsymbol{\xi} \quad (3.1)$$

where $\mathbf{X}(t)$ is a vector in \mathbb{R}^d representing the state of the system at time t , d is the dimension of the system, $\mathbf{F} : \mathbb{R}^d \rightarrow \mathbb{R}$ is a force-field on the system, $\mu \in \mathbb{R}^{d \times d}$ is the

mobility, $\xi(t) \in \mathbb{R}^d$ is a white-noise realisation with correlation function

$$\langle \xi_i(t)\xi_j(t') \rangle = 2D\delta_{ij}\delta(t-t') \quad (3.2)$$

and where D is the *diffusion matrix*. The diffusion constant is often written as $D = \mu\theta$, where θ is the temperature, in which case the prefactor of ξ in Eq. 3.1 is a matrix square-root. In general the diffusion matrix can be state-dependent $D(\mathbf{X})$, in which case we call the noise *multiplicative*, and if it is not state-dependent we call the noise *additive*. In the following we will focus on systems with additive noise. We will also D is diagonal with constant entries, as this can always be achieved with coordinate transformations. This is equivalent to assuming that the mobility μ is a scalar constant.

The notation in Eq. 3.1 is highly symbolical, as the time-derivative of a stochastic process \mathbf{X} is not well-defined, and realisations of a white-noise process ξ are not functions, but distributions. However, the Langevin equation is equivalent to the Itô diffusion equation with additive noise

$$d\mathbf{X} = \mathbf{b}(\mathbf{X})dt + \sqrt{2D}d\mathbf{W} \quad (3.3)$$

which represents the stochastic displacement $d\mathbf{X}$ in a time interval dt , subject to a drift-field \mathbf{b} and Brownian displacements $\sigma d\mathbf{W}$, where \mathbf{W} is the Wiener process and $\sigma \in \mathbb{R}^{d \times d}$ is the *volatility matrix*. Equation 3.3 and Eq. 3.1 can be related by setting $\mathbf{b} = \mu\mathbf{F}$ and $\sigma = \sqrt{2D}$. Symbolically, we may relate \mathbf{W} and ξ as $\dot{\mathbf{W}} = \xi$. Equation 3.3 can be understood as a short-hand for an alternative integral representation of the Itô diffusion equation

$$\mathbf{X}(t) = \int_0^t \mathbf{b}(\mathbf{X}(t'))dt' + \sqrt{2D} \int_0^t d\mathbf{W}(t') \quad (3.4)$$

where the second term is an *Itô stochastic integral* [? ?] with respect to the stochastic increment $d\mathbf{W}$.

Let $C^0([0, T])$ be the set of continuous paths $\mathbf{x} : [0, T] \rightarrow \mathbb{R}^d$, and furthermore let $C_{\mathbf{x}_0}^0([0, T]) \subset C^0([0, T])$ be the subset of paths that satisfy $\mathbf{x}(0) = \mathbf{x}_0$, where $\mathbf{x}_0 \in \mathbb{R}^d$ is the star-point of the path. The *transition path ensemble* $E_{\mathbf{x}_0}^{\mathbf{x}_T}([0, T]) \subset C_{\mathbf{x}_0}^0([0, T])$ of Eq. 3.3 is the subset of paths that satisfy $\mathbf{x}(0) = \mathbf{x}_0$ and $\mathbf{x}(T) = \mathbf{x}_T$, where $\mathbf{x}_T \in \mathbb{R}^d$ is the end-point of the path. Realisations of Eq. 3.3 are elements $\mathbf{X} \in C_{\mathbf{x}_0}^0([0, T])$, and we will often refer to these as *stochastic paths*. Given an end-point \mathbf{x}_T , a *transition path* is a stochastic path that is an element $\mathbf{X} \in E_{\mathbf{x}_0}^{\mathbf{x}_T}([0, T])$. Transition paths can thus be considered realisations of a *pinned* Itô diffusion, where we condition on the end-point $\mathbf{X}(T) = \mathbf{x}_T$.

Consider some measurable subset of stochastic paths $U \subset C_{\mathbf{x}_0}^0([0, T])$. The *law* $\mathbb{P}_{\mathbf{X}}$ of a stochastic differential equation like Eq. 3.3 is a *probability measure* over $C_{\mathbf{x}_0}^0([0, T])$. The probability of observing a stochastic trajectory in a measurable subset $U \subset C_{\mathbf{x}_0}^0([0, T])$ is

then $\mathbb{P}_{\mathbf{x}}(U)$. In the physics literature $\mathbb{P}_{\mathbf{x}}(U)$ is often written in a path-integral formulation as [? 3?]

$$\mathbb{P}_{\mathbf{x}}(U) = \int_U P_{\mathbf{x}}[\mathbf{x}] \mathcal{D}\mathbf{x} \quad (3.5)$$

where

$$P_{\mathbf{x}}[\mathbf{x}] \propto \exp(-S[\mathbf{x}]) \quad (3.6)$$

represents a *path-space probability density* over $C_{\mathbf{x}_0}^0([0, T])$, and the exponential scaling-factor of the density $S[\mathbf{x}]$ is called the *stochastic action*. In Eq. 3.5 we expressed the law $\mathbb{P}_{\mathbf{x}}$ in terms of the *path-probability density* $P_{\mathbf{x}}$. $\mathcal{D}\mathbf{x}$ represents what would be a volume measure over the infinite-dimensional space of stochastic paths. Mathematically, one would call $\mathcal{D}\mathbf{x}$ an infinite-dimensional analogue of a *Lebesgue measure* (although as we will discuss below, such an analogue does not exist). Equation 3.5 applies equivalently to subsets $A \subset E_{\mathbf{x}_0}^{\mathbf{x}_T}([0, T])$, by simply conditioning Eq. 3.6 on the end-point. Accordingly, we can compute the expectations of observables as

$$\langle \mathcal{O}[\mathbf{X}] \rangle = \int_{C_{\mathbf{x}_0}^0} \mathcal{O}[\mathbf{x}] P_{\mathbf{x}}[\mathbf{x}] \mathcal{D}\mathbf{x} \quad (3.7)$$

where $\mathcal{O}[\mathbf{x}]$ is a functional of stochastic paths $\mathbf{x} \in C_{\mathbf{x}_0}^0$ representing an observable. Equivalently, we can compute the expectations of observables in TPE by computing the integral over $E_{\mathbf{x}_0}^{\mathbf{x}_T}([0, T])$.

There are two well-known expressions for the action. The *Freidlin-Wentzell* (FW) action functional is [3, 209? ?]

$$S_{\text{FW}}[\mathbf{x}] = \int_0^T \frac{1}{2D} |\dot{\mathbf{x}} - \mathbf{b}(\mathbf{x})|^2 dt \quad (3.8)$$

and the *Onsager-Machlup* (OM) action functional is [3? ? , 68, 163, 10?]

$$S_{\text{OM}}[\mathbf{x}] = \int_0^T \left\{ \frac{1}{2D} |\dot{\mathbf{x}} - \mathbf{b}(\mathbf{x})|^2 + \frac{1}{2} \nabla \cdot \mathbf{b}(\mathbf{x}) \right\} dt. \quad (3.9)$$

Note that Eq. 3.8 is not interpreted here as a large deviation principle in a zero-temperature limit, but rather defines a path-probability density via Eq. 3.6 for arbitrary temperatures. This seeming contradiction, along with the fact that there are two stochastic actions, yielding ostensibly two different path-probability densities, has been a point of confusion [3, 83]. In [3] it is shown that the actions are equivalent for the purposes of sampling the path-probability distribution. In other words, formally Eq. 3.5 yields the same value for the probability $\mathbb{P}_{\mathbf{x}}(A)$ regardless of what action is used. However, in [83] it is shown that if one considers the subset $C_{\mathbf{x}_0}^1([0, T]) \subset C_{\mathbf{x}_0}^0([0, T])$ of paths with at-least one derivative, then the appropriate action functional is the Onsager-Machlup action. Therefore if one wants

to consider *most-probable paths*, which are always piece-wise smooth, the Onsager-Machlup action is to be preferred over the Freidlin-Wentzell action. Note that in the limit of vanishing noise, which is the regime in which we worked in Ch. 2, the Onsager-Machlup action converges to the Freidlin-Wentzell action.

In terms of path-probability densities, there is in fact an infinite family of equally valid stochastic actions [83]. This is due to the right-hand side of Eq. 3.5 being ill-defined unless an explicit discretisation scheme is prescribed

$$\mathbf{x} \longrightarrow \mathbf{x}_i = \mathbf{x}(i\Delta t), \quad (3.10)$$

such that

$$\dot{\mathbf{x}} \longrightarrow \frac{\mathbf{x}_{i+1} - \mathbf{x}_i}{\Delta t}, \quad (3.11)$$

where $i = 0, 1, \dots, N_T$ and δt is the time-step of the discretisation. Under such a discretisation the path-space volume density is replaced with

$$\mathcal{D}\mathbf{x} \longrightarrow \prod_{i=0}^{N_T} d\mathbf{x}_i. \quad (3.12)$$

We thus replace the path-space probability density $P_{\mathbf{X}}[\mathbf{X}]$ with a finite-dimensional probability density $p(\mathbf{x}_1, \mathbf{x}_2, \dots, \mathbf{x}_{N_T})$. The discretised probability distribution approximates the statistics of the true process \mathbf{X} , and this approximation is improved with increasing N_T . However, we should note that the limit $N_T \rightarrow \infty$ does not exist. That Eq. 3.5 is ill-defined for continuous paths can be seen by evaluating any of the actions on an un-differentiable stochastic path, which then diverge due to the $\frac{1}{2D}|\dot{\mathbf{x}}|^2$ term. Eq. 3.5 should therefore only be interpreted as a symbolic expression for the path-probability.

Mathematically, the root of the problem stems from the non-existence of the ‘path-space volume measure’ $\mathcal{D}\mathbf{x}$. Consider some probability measure μ with density p over a finite-dimensional space \mathbb{R}^n . Probabilities can then be computed using integrals $\mu(U) = \int_U p(\mathbf{z})d\mathbf{z}$ for a measurable subset $U \subset \mathbb{R}^n$. Here, $d\mathbf{z}$ is a volume measure on the space \mathbb{R}^d , and is known in the mathematical literature as a *Lebesgue measure*. In particular, Lebesgue measures have the desirable property of translation-invariance. Intuitively we can see that $\mathcal{D}\mathbf{x}$ symbolically plays the role of an infinite-dimensional Lebesgue measure from Eq. 3.12. However, it is a theorem that there exists no infinite-dimensional analogue of a Lebesgue measure [?].

Although not a Lebesgue measure, there is a measure that is well-defined on general infinite dimensional spaces, known as the *abstract Wiener space construction* [96?]. If the sample space is $C_{\mathbf{x}_0}^0([0, T])$, then the corresponding probability measure $\mathbb{P}_{\mathbf{W}}$ is called the *classical Wiener measure* [? ?]. As its name suggests, $\mathbb{P}_{\mathbf{W}}$ is the law of the Wiener process. If we consider the Wiener process as an Itô diffusion with the drift-field set to

zero $\mathbf{b} = 0$, we can write the Wiener measure using Eqs. 3.5, 3.6 and 3.8 (or Eq. 3.9) as

$$\mathbb{P}_{\mathbf{W}}(U) = \int_U P_{\mathbf{W}}[\mathbf{x}] \mathcal{D}\mathbf{x} \quad (3.13)$$

where $A \subset C_{\mathbf{x}_0}^0([0, T])$ and

$$P_{\mathbf{W}}[\mathbf{x}] \propto \exp(-S_0[\mathbf{x}]) \quad (3.14a)$$

$$S_0[\mathbf{x}] = \int_0^T \frac{1}{2D} |\dot{\mathbf{x}}|^2 dt \quad (3.14b)$$

with the understanding that Eq. 3.13 is to be interpreted symbolically in the sense described above. Under any finite-dimensional discretisation, the resulting probability density becomes a multi-variate Gaussian. We thus call $\mathbb{P}_{\mathbf{W}}$ a *Gaussian measure*, and indeed \mathbf{W} is an example of a Gaussian process.

Symbolically, we can now decompose the path-space probability density Eq. 3.6 as

$$\begin{aligned} P_{\mathbf{X}}[\mathbf{x}] &= (P_{\mathbf{X}}/P_{\mathbf{W}})P_{\mathbf{W}} \\ &= \frac{d\mathbb{P}_{\mathbf{X}}}{d\mathbb{P}_{\mathbf{W}}}[\mathbf{x}]P_{\mathbf{W}}[\mathbf{x}] \end{aligned} \quad (3.15)$$

where we have identified $P_{\mathbf{X}}/P_{\mathbf{W}}$ as the *Radon-Nikodym derivative* of $\mathbb{P}_{\mathbf{X}}$ with respect to $\mathbb{P}_{\mathbf{W}}$. We find

$$\frac{d\mathbb{P}_{\mathbf{X}}}{d\mathbb{P}_{\mathbf{W}}}[\mathbf{x}] \propto \exp(-\Phi[\mathbf{x}]) \quad (3.16)$$

and $\Phi[\mathbf{x}] = S_{\mathbf{FW}}[\mathbf{x}] - S_0[\mathbf{x}]$ is the *relative action*, which is equivalently $\Phi[\mathbf{x}] = S_{\text{OM}}[\mathbf{x}] - S_0[\mathbf{x}]$. Intuitively, we can understand $\frac{d\mathbb{P}_{\mathbf{X}}}{d\mathbb{P}_{\mathbf{W}}}$ as the probability density of $\mathbb{P}_{\mathbf{X}}$ with respect to the Wiener measure $\mathbb{P}_{\mathbf{W}}$. Compare this with $P_{\mathbf{X}}$, which we symbolically understand to be a probability density with respect to the fictitious path-space volume measure $\mathcal{D}\mathbf{x}$. In other words, $\frac{d\mathbb{P}_{\mathbf{X}}}{d\mathbb{P}_{\mathbf{W}}}$ can be seen as a re-weighting of the probability distribution over stochastic Wiener realisations \mathbf{W} to the realisations \mathbf{X} of the Itô equation, whilst $P_{\mathbf{X}}$ re-weights the ‘uniform distribution’ over the space of continuous paths.

We now introduce some notation which will be of use in the subsequent section. For any two probability measures \mathbb{P} and \mathbb{P}_0 defined on a sample space C , if the Radon-Nikodym derivative $\frac{d\mathbb{P}}{d\mathbb{P}_0}$ exists, we say that \mathbb{P} has a *density with respect to* \mathbb{P}_0 . Furthermore, the existence of $\frac{d\mathbb{P}}{d\mathbb{P}_0}$ implies that \mathbb{P} is *absolutely continuous* with respect to \mathbb{P}_0 , which means that

$$\mathbb{P}_0(A) = 0 \Rightarrow \mathbb{P}(A) = 0 \quad (3.17)$$

for all measurable subsets $A \subset C$, where \Rightarrow signifies implication. We write this as $\mathbb{P} \ll \mathbb{P}_0$.

As opposed to $P_{\mathbf{X}}$, the density $\frac{d\mathbb{P}_{\mathbf{X}}}{d\mathbb{P}_{\mathbf{W}}}$ can be evaluated on un-differentiable stochastic

paths. To see this, consider

$$\begin{aligned}\Phi[\mathbf{x}] &= S_{\text{FW}}[\mathbf{x}] - S_0[\mathbf{x}] \\ &= \int_0^T \left\{ \frac{1}{2D} |\mathbf{b}(\mathbf{x})|^2 - \frac{1}{D} \mathbf{b}(\mathbf{x}) \cdot \dot{\mathbf{x}} + \right\} dt \\ &= \int_0^T \frac{1}{2D} |\mathbf{b}(\mathbf{x})|^2 dt - \int_{\mathbf{x}_0}^{\mathbf{x}_T} \frac{1}{D} \mathbf{b}(\mathbf{x}) \cdot d\mathbf{x}.\end{aligned}\tag{3.18}$$

The integrals in the third line are well-defined for un-differentiable paths. Therefore, the second term of the relative action becomes a stochastic integral if we evaluate it on a realisation of the Itô process

$$\Phi[\mathbf{X}] = \int_0^T \frac{1}{2D} |\mathbf{b}(\mathbf{X})|^2 dt - \int_{\mathbf{x}_0}^{\mathbf{x}_T} \frac{1}{D} \mathbf{b}(\mathbf{X}) \cdot d\mathbf{X}.\tag{3.19}$$

Like any integral Eq. 3.19 has to be discretised in order to be evaluated numerically. However, in contrast to the finite-dimensional approximation $p(\mathbf{x}_1, \dots, \mathbf{x}_{N_T})$ of the path-probability density $P[\mathbf{x}]$, the discretisation of Eq. 3.19 has a well-defined limit at $N_T \rightarrow \infty$. As before, both the Freidlin-Wentzell and Onsager-Machlup forms of Φ are statistically equivalent. Furthermore, as showed in [83], an infinite family of expressions of equivalent Φ , which include the OM and FW forms, can be derived from Eq. 3.19 depending on the discretisation scheme.

We can now rewrite Eq. 3.5 in terms of well-defined quantities. Since

$$\mathbb{P}_{\mathbf{X}}(U) = \int_A P_{\mathbf{X}}[\mathbf{x}] \mathcal{D}\mathbf{x} = \int_U \frac{d\mathbb{P}_{\mathbf{X}}}{d\mathbb{P}_{\mathbf{W}}}[\mathbf{x}] P_{\mathbf{W}}[\mathbf{x}] \mathcal{D}\mathbf{x}\tag{3.20}$$

we get

$$\mathbb{P}_{\mathbf{X}}(U) = \int_U \frac{d\mathbb{P}_{\mathbf{X}}}{d\mathbb{P}_{\mathbf{W}}}[\mathbf{x}] d\mathbb{P}_{\mathbf{W}}[\mathbf{x}]\tag{3.21}$$

where we have identified $P_{\mathbf{W}}[\mathbf{x}] \mathcal{D}\mathbf{x} = d\mathbb{P}_{\mathbf{W}}[\mathbf{x}]$. Although Eq. 3.21 was derived via our ill-defined symbolic path-integral expressions, the resulting expression we have arrived at is nevertheless correct [13, 98, 99].

Just as $\mathbb{P}_{\mathbf{W}}$ serves as a measure over the space $C_{\mathbf{x}_0}([0, T])$ of stochastic paths, we can similarly find a well-defined measure over the transition path ensemble $E_{\mathbf{x}_0}^{\mathbf{x}_T}([0, T])$. Let \mathbf{B} be the *Brownian bridge process*, which can be defined as a Wiener process conditioned as $\mathbf{B}(0) = \mathbf{x}_0$ and $\mathbf{B}(T) = \mathbf{x}_T$. In other words, we can write it as

$$\mathbf{B} = \left(1 - \frac{t}{T}\right) \mathbf{W} + \frac{t}{T} (\mathbf{x}_T - \mathbf{x}_0)\tag{3.22}$$

if we let $\mathbf{W}(0) = \mathbf{x}_0$. Then the law $\mathbb{P}_{\mathbf{B}}$ is defined over $E_{\mathbf{x}_0}^{\mathbf{x}_T}([0, T])$, and we have that [13]

$$\mathbb{P}_{\mathbf{X}}(U) = \int_U \frac{d\mathbb{P}_{\mathbf{X}}}{d\mathbb{P}_{\mathbf{B}}}[\mathbf{x}] d\mathbb{P}_{\mathbf{B}}[\mathbf{x}] \quad (3.23)$$

where $\mathbb{P}_{\mathbf{X}}$ is here to be understood as the law of the pinned Itô diffusion, where realisations \mathbf{X} are conditioned as $\mathbf{X}(0) = \mathbf{x}_0$ and $\mathbf{X}(T) = \mathbf{x}_T$. Note that we have used the same symbol $\mathbb{P}_{\mathbf{X}}$ for the law of both the unpinned and pinned processes. Henceforth, $\mathbb{P}_{\mathbf{X}}$ will denote to law of latter, unless explicitly stated otherwise.

Despite the fact that densities over path-spaces are ill-defined, we will continue making use of the path-integrals with respect to the fictitious infinite-dimensional Lebesgue measure. This is primarily due to the ubiquity of the path-integral in the physics, and because it is often intuitively easier to understand densities with respect to a uniform volume density. Mathematically, this will not cause any issues as long as we understand that ill-defined path-integrals correspond to well-defined integrals with respect to the Wiener measure, as in Eq. 3.21 and Eq. 3.23.

3.2 Path-space MCMC methods

In this section we will discuss and apply the *preconditioned Nicolson-Crank* (pCN) algorithm to sample the transition path ensemble of Itô diffusions with additive noise. In Sec. 3.2.1 we begin with an overview of Markov chain Monte Carlo methods, and proceed to reproduce the derivation of the general pCN algorithm in [39, 13, 98, 99, 100]. We will frequently express probabilities in terms of fictitious path-space probability densities with respect to Lebesgue measures, as this is the predominant mathematical language used in the physics literature. The reader may refer to the references for a more rigorous approach. In Sec. 3.2.2 we expand stochastic paths in the Kosambi-Karhunen-Loève (KKL) basis of the Brownian bridge process, and develop a sampling algorithm using Fast-Fourier Transforms. In Sec. 3.2.4 we analyse the band structure of Itô diffusions through the lens of the KKL basis. The treatment here will be further developed in Sec. 3.3, where we extend the pCN algorithm to simultaneously sample multiple transition channels.

3.2.1 The preconditioned Crank-Nicolson algorithm

Markov chain Monte Carlo (MCMC) methods refers to a general class of methods of sampling a target probability measure \mathbb{P} , wherein one constructs a Markov chain that has \mathbb{P} as its steady-state measure. \mathbb{P} is both called the *target measure* of the MCMC protocol, and the *invariant measure* of the Markov chain. The key idea is that as the Markov chain is simulated, each state in the chain will asymptotically sample \mathbb{P} as we simulate for sufficiently many steps.

Here we will consider MCMC methods to sample a general target measure \mathbb{P} with sample space C . We will begin by first discussing general MCMC procedures, and then proceed to define the precondition Crank-Nicolson algorithm. Let P be the probability density of \mathbb{P} with respect to the Lebesgue measure, and we write this relation as $P \sim \mathbb{P}$. We will in general consider C to be an infinite-dimensional functional space, in which case P is a fictitious density in the sense discussed in the introduction of this chapter. We also assume that \mathbb{P} is absolutely continuous with respect to a measure \mathbb{P}_0 , such that we can write

$$\mathbb{P}(U) = \int_U \frac{d\mathbb{P}}{d\mathbb{P}_0}[\mathbf{x}] d\mathbb{P}_0[\mathbf{x}] \quad (3.24)$$

for any measurable subset $A \subset C$. We furthermore assume that \mathbb{P}_0 is a Gaussian measure, and we refer to it as the Gaussian *reference measure* of \mathbb{P} . We express the densities $P_0 \sim \mathbb{P}_0$ and $P \sim \mathbb{P}$ as

$$P_0[\mathbf{x}] \propto \exp(-S_0[\mathbf{x}]) \quad (3.25a)$$

$$P[\mathbf{x}] \propto \exp(-S_0[\mathbf{x}] - \Phi[\mathbf{x}]) = P_0[\mathbf{x}] \exp(-\Phi[\mathbf{x}]) \quad (3.25b)$$

where $S_0[\mathbf{x}]$ is the Gaussian action of $P_0[\mathbf{x}]$ and $\Phi[\mathbf{x}]$ is the relative action, which satisfies $\frac{d\mathbb{P}}{d\mathbb{P}_0} \propto \exp(-\Phi[\mathbf{x}])$. In subsequent subsections we will apply the MCMC method to sample the probability measure $\mathbb{P}_{\mathbf{x}}$ over the sample space $E_{\mathbf{x}_0}^{\mathbf{x}_T}([0, T])$, which has a density with respect to the Gaussian measure $\mathbb{P}_{\mathbf{B}}$.

The aim of the MCMC is to generate samples from the target measure \mathbb{P} . In applications, this is often for the purpose of estimating expectations like Eq. 3.7. Let $\mathbf{x}^{(n)}$, $n = 1, \dots, M$ be M samples from the target measure \mathbb{P} . Then expectations can be approximated as

$$\langle \mathcal{O}[\mathbf{x}] \rangle = \int_C \mathcal{O}[\mathbf{x}] \frac{d\mathbb{P}}{d\mathbb{P}_0}[\mathbf{x}] d\mathbb{P}_0[\mathbf{x}^{(n)}] \approx \frac{1}{M} \sum_{n=1}^M \mathcal{O}[\mathbf{x}^{(n)}]. \quad (3.26)$$

for any observable $\mathcal{O}[\mathbf{x}]$. In the limit $M \rightarrow \infty$, the right-hand side will converge to the true expectation.

Consider a Markov chain with states $\mathbf{x}^{(n)} \in C$, where C is the sample space of a target measure \mathbb{P} . If $\mathbf{x}^{(n)} \in E$ is the current state of the Markov chain, its next step $\mathbf{x}^{(n+1)}$ is drawn from the *transition kernel* $T[\mathbf{x}^{(n)} \rightarrow \mathbf{x}_{i+1}]$, which is a probability distribution in $\mathbf{x}^{(n+1)} \in C$. If $\mathbb{P}_{\mathbf{x}}$ is the invariant measure of the Markov chain then the transition kernel satisfies

$$\int_C P[\mathbf{x}] T[\mathbf{x} \rightarrow \mathbf{y}] \mathcal{D}\mathbf{x} = P[\mathbf{y}]. \quad (3.27)$$

For any given target measure \mathbb{P} there is an infinite family of possible Markov chains, defined by a transition kernel $T[\mathbf{x} \rightarrow \mathbf{y}]$ that has \mathbb{P} as its invariant measure. The particular prescription by which $T[\mathbf{x} \rightarrow \mathbf{y}]$ is constructed given \mathbb{P} is what defines the MCMC.

A popular MCMC variant is the *Metropolis-Hastings scheme*[150, 103], which defines the Markov chain in terms of a *proposal kernel* $Q[\mathbf{x} \rightarrow \mathbf{y}]$ and an *acceptance kernel* $A[\mathbf{x}, \mathbf{y}]$. These are constructed in such a way that the transition kernel satisfies

$$P[\mathbf{x}]T[\mathbf{x} \rightarrow \mathbf{y}] = P[\mathbf{y}]T[\mathbf{y} \rightarrow \mathbf{x}]. \quad (3.28)$$

which in physics is known as a *detailed balance* condition on the Markov chain with respect to \mathbb{P} . The transition kernel is written in terms of the proposal and acceptance kernels as

$$T[\mathbf{x} \rightarrow \mathbf{y}] = Q[\mathbf{x} \rightarrow \mathbf{y}]A[\mathbf{x}, \mathbf{y}] + \delta_x[y] \int_C (1 - A[\mathbf{x}, \mathbf{z}])Q[\mathbf{x} \rightarrow \mathbf{z}]D\mathbf{z}. \quad (3.29)$$

By substituting Eq. 3.29 into Eq. 3.28 we find the following expression for the acceptance probability

$$A[\mathbf{x}, \mathbf{y}] = \min \left\{ 1, \frac{V^T[\mathbf{x}, \mathbf{y}]}{V[\mathbf{x}, \mathbf{y}]} \right\} \quad (3.30)$$

where

$$V[\mathbf{x}, \mathbf{y}] = P[\mathbf{x}]Q[\mathbf{x} \rightarrow \mathbf{y}]. \quad (3.31a)$$

$$V^T[\mathbf{x}, \mathbf{y}] = P[\mathbf{y}]Q[\mathbf{y} \rightarrow \mathbf{x}] \quad (3.31b)$$

are probability densities over $(\mathbf{x}, \mathbf{y}) \in C \times C$ with respect to the measures $\mathbb{V} \sim V$ and $\mathbb{V}^T \sim V^T$, and we will refer to them as the forward and backwards kernels respectively. In general Eq. 3.30 is only well-defined if V^T vanishes whenever V vanishes. In other words, we must have that $\mathbb{V}^T \ll \mathbb{V}$, in which case we can rewrite Eq. 3.30 as

$$A[\mathbf{x}, \mathbf{y}] = \min \left\{ 1, \frac{d\mathbb{V}^T}{d\mathbb{V}}[\mathbf{x}, \mathbf{y}] \right\}. \quad (3.32)$$

We see that the MCMC protocol is only well-defined if the proposal kernel $Q[\mathbf{x} \rightarrow \mathbf{y}]$ is such that the forward and backward kernels satisfy the absolute continuity condition $\mathbb{V}^T \ll \mathbb{V}$.

Rather than by trying to parse Eq. 3.29, the Metropolis-Hastings algorithm can be more easily understood by summarising it algorithmically as follows:

1. Choose an initial state $\mathbf{x}^{(0)} \in E$.
2. Draw a proposal state \mathbf{y} from the distribution $Q[\mathbf{x}^{(n)} \rightarrow \mathbf{y}]$.
3. Compute the *acceptance probability* $A[\mathbf{x}^{(n)}, \mathbf{y}]$.
4. Draw a random number V from $\text{Unif}([0, 1])$.
 - (a) If $V < A[\mathbf{x}^{(n)}, \mathbf{y}]$ then set $\mathbf{x}^{(n+1)} = \mathbf{y}$.

(b) Otherwise set $\mathbf{x}^{(n+1)} = \mathbf{x}^{(n)}$.

5. Repeat step 2.

where $\text{Unif}([0, 1])$ is the uniform distribution over the unit interval. After M steps, we have a chain of states $L_M = \{\mathbf{x}^{(0)}, \mathbf{x}^{(1)}, \dots, \mathbf{x}^{(M)}\}$. Asymptotically, as $M \rightarrow \infty$, the set L_M will converge towards a sample of the target distribution \mathbb{P} . The rate of convergence will in general depend on the implementation of the Metropolis-Hastings rule.

The remaining degree of freedom in the Metropolis-Hastings algorithm, which is to choose the proposal kernel $Q[\mathbf{x} \rightarrow \mathbf{y}]$. A common choice is the update rule

$$\mathbf{y} = \mathbf{x} + \kappa \mathbf{w} \quad (3.33)$$

where κ is a step-size parameter, \mathbf{x} is the current state of the Markov chain, \mathbf{y} is the proposal state, and \mathbf{w} is a sample drawn from the Gaussian distribution \mathbb{P}_0 . The corresponding kernel density can be written in terms of the density $P_0 \sim \mathbb{P}_0$ of the reference measure as

$$Q_{\text{RMW}}[\mathbf{x} \rightarrow \mathbf{y}] \propto \exp(-S_0[\mathbf{x} - \mathbf{y}]/\kappa^2) \quad (3.34)$$

Eq. 3.33 defines the *Gaussian random-walk Metropolis-Hastings scheme* (RMW) [150, 103].

In practice to use the RMW in numerics, or any MCMC, we must prescribe some discretisation procedure on the functional space C . In general this will mean parameterising sample space elements as $\mathbf{x} = \mathbf{x}(\mathbf{a}) \in C$, where $\mathbf{a} \in \mathbb{R}^N$ and N is the discretisation order. Effectively, this induces a target measure \mathbb{P}^N on the sample space

$$C^N = \{\mathbf{x}(\mathbf{a}) : \mathbf{a} \in \mathbb{R}^N\} \subset C \quad (3.35)$$

which is a finite-dimensional subset. Accordingly, the proposal and acceptance kernels now become densities over finite-dimensional distributions $Q(\mathbf{a} \rightarrow \mathbf{b})$ and $A(\mathbf{a}, \mathbf{b})$ respectively. For any finite N , the resulting MCMC algorithm is well-defined and will asymptotically sample \mathbb{P}^N when running the Markov chain for sufficiently many steps. Furthermore, the larger the N , the better will the discretised target measure \mathbb{P}^N approximate the true target measure \mathbb{P} . However, it is well-documented that standard MCMC schemes like the RMW suffer the curse of dimensionality for infinite-dimensional systems [39, 100]. That is, as N is increased the algorithm suffers a curse of dimensionality, so that the number of steps required for the Markov chain to converge onto the target \mathbb{P}^N diverges with N .

The root cause of the divergence of the convergence-times of the RMW under mesh refinement is that the protocol is not well-defined in the $N \rightarrow \infty$ limit. In other words, the RMW is not a well-defined Markov chain on infinite-dimensional spaces. This can be seen by noting that the backwards kernel measure \mathbb{V}^T is not absolutely continuous with respect

to the forward kernel measure \mathbb{V} . If $\mathbb{V}^T \ll \mathbb{V}$, then from Eq. 3.17 we would have that

$$\int_{U \times U'} V[\mathbf{x}, \mathbf{y}] \mathcal{D}\mathbf{x} \mathcal{D}\mathbf{y} = 0 \Rightarrow \int_{A \times A'} V^T[\mathbf{x}, \mathbf{y}] \mathcal{D}\mathbf{x} \mathcal{D}\mathbf{y} = 0 \quad (3.36)$$

where $U \times U' \subset C \times C$. However, if we substitute Eq. ?? into Eq. 3.36, using Eq. 3.31, we find that absolute continuity fails. Due to the symmetry of the RMW proposal kernel it is clear that Eq. 3.36 does hold for arbitrary $U \times U'$.

Recent work by [13, 39, 98, 99] have developed and formalised the theory of MCMC methods so that protocols can remain well-defined on infinite-dimensional functional sample spaces. One of the main results of this work was the *preconditioned Crank-Nicolson* (pCN) algorithm. In contrast to the RMW, and most other common MCMC protocols, the pCN is defined directly on the space of functions. This guarantees that, upon discretisation, the algorithm remains well-defined under mesh refinement $N \rightarrow \infty$.

The pCN algorithm overcomes the degeneracy suffered by the RMW by imposing that its proposal kernel $Q_{\text{pCN}}[\mathbf{x} \rightarrow \mathbf{y}]$ is in detailed balance with a Gaussian reference measure that the target measure is absolutely continuous with respect to. For example, as $\mathbb{P} \ll \mathbb{P}_0$ we may impose

$$P_0[\mathbf{x}] Q_{\text{pCN}}[\mathbf{x} \rightarrow \mathbf{y}] = P_0[\mathbf{y}] Q_{\text{pCN}}[\mathbf{y} \rightarrow \mathbf{x}] \quad (3.37)$$

which ensures that $\mathbb{V}^T \ll \mathbb{V}$. To see this, define the measures $\mathbb{V}_0 \sim P_0[\mathbf{x}] Q_{\text{pCN}}[\mathbf{x} \rightarrow \mathbf{y}]$ and $\mathbb{V}_0^T \sim P_0[\mathbf{y}] Q_{\text{pCN}}[\mathbf{y} \rightarrow \mathbf{x}]$, which from Eq. 3.37 clearly satisfy mutual absolute continuity. $\mathbb{V}^T \ll \mathbb{V}$ then follows from $\mathbb{P} \ll \mathbb{P}_0$, and using the transitivity of absolute continuity. The pCN proposal kernel is defined by

$$\mathbf{y} = \sqrt{1 - \kappa^2} \mathbf{x} + \kappa \mathbf{w} \quad (3.38)$$

where \mathbf{w} is drawn from \mathbb{P}_0 as before. In terms a density, the proposal kernel is

$$Q_{\text{pCN}}[\mathbf{x} \rightarrow \mathbf{y}] \propto \exp(-S_0[\sqrt{1 - \kappa^2} \mathbf{x} - \mathbf{y}] / \kappa^2) \quad (3.39)$$

which satisfies Eq. 3.37. From Eq. 3.30 and Eq. 3.31 we find that the resulting acceptance probability has the elegant expression

$$A_{\text{pCN}}[\mathbf{x}, \mathbf{y}] = \min \{1, \exp(\Phi[\mathbf{x}] - \Phi[\mathbf{y}])\}. \quad (3.40)$$

Now as opposed to $P[\mathbf{x}]$ and $P_0[\mathbf{x}]$, since $\Phi[\mathbf{x}]$ is the exponential factor of the well-defined density $\frac{d\mathbb{P}}{d\mathbb{P}_0}$ it must in-turn also be well-defined for all $\mathbf{x} \in C$. Therefore Eq. 3.40 is also well-defined.

We can now state the pCN algorithm in its entirety:

1. Choose an initial state $\mathbf{x}^{(0)}$.

2. Generate a proposal state

$$\mathbf{y} = \sqrt{1 - \kappa^2} \mathbf{x}^{(n)} + \kappa \mathbf{w} \quad (3.41)$$

where \mathbf{w} is drawn from the reference measure \mathbb{P}_0 .

3. Compute the acceptance probability $A_{\text{pCN}}[\mathbf{x}^{(n)}, \mathbf{y}]$.

4. Draw a random number V from $\text{Unif}([0, 1])$.

- If $V < A_{\text{pCN}}[\mathbf{x}^{(n)}, \mathbf{y}]$ then set $\mathbf{x}^{(n+1)} = \mathbf{y}$.
- Otherwise set $\mathbf{x}^{(n+1)} = \mathbf{x}^{(n)}$.

3.2.2 Kosambi-Karhunen-Loève expansions of stochastic trajectories

In the previous subsection we outlined the pCN algorithm, which was defined directly on general infinite-dimensional functional sample spaces. Here we specialise to transition paths of pinned Itô diffusions. The sample space is now $E_{\mathbf{x}_0}^{\mathbf{x}_T}([0, T])$, the transition path ensemble, and the target measure is the law $\mathbb{P}_{\mathbf{X}}$. Henceforth we will abbreviate the transition path ensemble as $E \equiv E_{\mathbf{x}_0}^{\mathbf{x}_T}([0, T])$. As shown in Eq. 3.23, $\mathbb{P}_{\mathbf{X}}$ has a density with respect to the Brownian bridge law $\mathbb{P}_{\mathbf{B}}$, and we will consider the latter the reference Gaussian measure.

In the second step of the pCN algorithm, we must sample the reference Gaussian measure to generate the proposal state. One method by which to sample $\mathbb{P}_{\mathbf{B}}$ is using the *Kosambi-Karhunen-Loève* (KKL) theorem [? ? 137], which is a representation of a stochastic process as an infinite linear combination of orthogonal basis functions $\phi_k(t)$. The KKL representation is found by solving a homogeneous Fredholm integral equation of the second kind

$$\int K_Y(s, t) \phi_i(s) ds = \lambda_i \phi_i(t) \quad (3.42)$$

where $K_Y(s, t)$ is the covariance function of a given, in this case one-dimensional, stochastic process Y . If Y is *centered* (in other words, if $\langle Y(t) \rangle = 0$ for all $t \in [0, T]$), then the KKL expansion of Y is

$$Y(t) = \sum_{k=1}^{\infty} \sqrt{\lambda_k} Z_k \phi_k(t) \quad (3.43)$$

where $\phi_i(t)$ are pairwise orthonormal functions on $[0, T]$ and Z_i are pairwise uncorrelated random variables with zero mean and unit variance. If Y is a Gaussian process, then the random coefficients Z_k are independent normal random variables distributed as $Z_k \sim \mathcal{N}(0, 1)$, in which case Eq. 3.43 can be used to sample the process. ϕ_k and λ_k are respectively

the eigenfunctions and eigenvalues of the operator T_Y , defined as $T_Y f = \int K_Y(s, t) f(s) ds$. Therefore, as centered Gaussian processes are specified entirely given their covariance functions K_Y , we can see the KKL expansion as a *diagonalisation* of Y .

The solution to Eq. 3.42 for the one-dimensional Brownian bridge process is known. The result, trivially extended to a d -dimensional Brownian bridge process with diffusion constant D , can be written as

$$\mathbf{B}(t) = \mathbf{x}_0 + (\mathbf{x}_T - \mathbf{x}_0) \frac{t}{T} + \sqrt{2D} \sum_{i=1}^{\infty} \mathbf{Z}_k \sqrt{\lambda_k} \phi_k(t) \quad (3.44)$$

where $\mathbf{Z}_k \in \mathbb{R}^d$, $k = 1, \dots, \infty$ are independent d -dimensional normal random variables distributed as $\mathbf{Z}_k \sim \mathcal{N}(0, \mathbb{I}_d)$, and where

$$\phi_k(t) = \sqrt{\frac{2}{T}} \sin(t/\sqrt{\lambda_k}) \quad (3.45a)$$

$$\lambda_k = \frac{T^2}{\pi^2 k^2}, \quad (3.45b)$$

and where $\phi_k(t)$ satisfy

$$\int_0^T \phi_k(t) \phi_l(t) dt = \delta_{kl} \quad (3.46)$$

for all $k, l = 1, \dots, \infty$. We will write the components of the random coefficients as $Z_{ik} \equiv (\mathbf{Z}_k)_i$, $i = 1, \dots, d$, and each component is then distributed as $Z_{ik} \sim \mathcal{N}(0, 1)$. The first two terms in Eq. 3.44 are a result of the fact that Brownian bridge, as we have defined it, is not centred and has mean $\langle \mathbf{B}(t) \rangle = \mathbf{x}_0 + (\mathbf{x}_T - \mathbf{x}_0) \frac{t}{T}$.

In the numerical algorithm, we will make use of Eq. 3.44 to generate samples of the Brownian bridge process using, by truncating the sum to N terms and sampling the dN independent random variables $Z_{ik} \sim \mathcal{N}(0, 1)$. The law $\mathbb{P}_{\mathbf{B}}$ therefore becomes a dN -dimensional probability measure $\mathbb{P}_{\mathbf{B}}^N$. Furthermore, we note that ϕ_k also forms an orthonormal basis for the TPE. Therefore we will also expand transition paths $\mathbf{X}^N \in E$ in the same truncated KKL basis of the Brownian bridge process as

$$\mathbf{X}^N(t; A) = \mathbf{x}_0 + (\mathbf{x}_T - \mathbf{x}_0) \frac{t}{T} + \sqrt{2D} \sum_{k=1}^N \mathbf{A}_k \sqrt{\lambda_k} \phi_k(t) \quad (3.47)$$

where $A = (\mathbf{A}_1 \ \mathbf{A}_2 \ \dots \ \mathbf{A}_N) \in \mathbb{R}^{d \times N}$ is a matrix where the columns $\mathbf{A}_k \in \mathbb{R}^d$, $k = 1, \dots, N$ are the coefficients of the expansion. We will refer to \mathbf{A}_k as the modes of $\mathbf{X}^N(t)$, A as the mode matrix and N the *mode truncation*. We have thus introduced a parameterisation $\mathbf{X}(t; A)$ of transition paths, which in turn defines the subspace

$$E^N = \{\mathbf{X}(t; A) : A \in \mathbb{R}^{d \times N}\} \subset E \quad (3.48)$$

of the transition path ensemble. The dN -dimensional probability measure $\mathbb{P}_{\mathbf{X}}^N$ over E^N is found by projecting Eq. 3.23 onto E^N , and we have

$$\frac{d\mathbb{P}_{\mathbf{X}}^N}{d\mathbb{P}_{\mathbf{B}}^N}(A) \propto \exp(-\Phi[\mathbf{X}(t; A)]). \quad (3.49)$$

Accordingly, the pCN acceptance probability would then be

$$A_{\text{pCN}}[A, A'] = \min \{1, \exp(\Phi[\mathbf{X}(t; A)] - \Phi[\mathbf{X}'(t; A')])\}. \quad (3.50)$$

for a given $A, A' \in R^{d \times N}$. We note that the integral in Eq. 3.18 of the relative action Φ must be computed using a quadrature scheme in numerical applications.

Finally, the pCN rule defined on the KKL mode-representation of transition paths can now be stated as

$$A'_{ik} = \sqrt{1 - \kappa_{ik}^2} A_{ik}^{(n)} + \kappa_{ik} Z_{ik} \quad (3.51)$$

for each $i = 1, \dots, d$ and $k = 1, \dots, N$, where Z_{ik} is sampled from $\mathcal{N}(0, 1)$. In contrast to Eq. 3.41, the pCN update rule on functional space, here we have introduced a tuneable step-size matrix κ_{ik} for each individual mode coefficient. In Sec. 3.2.5 we will discuss how to use the band-structure of the KKL expansion to find a step-size matrices that improve the MCMC correlation time.

There is an analogous expansion to Eq. 3.47, if we were to instead sample $C_{\mathbf{x}_0}^0([0, T])$, the set of stochastic paths starting at \mathbf{x}_0 with open end-point conditions. In that case, the appropriate expansion of stochastic paths would be the KKL basis of the Wiener process. This would in turn induce an N -dimensional subspace of paths, analogous to Eq. 3.48.

3.2.3 Numerical algorithm

We can summarise the pCN sampling algorithm projected onto the truncated Brownian bridge KKL expansion as follows:

1. Choose the mode truncation parameter N .
2. Choose an initial state $A^{(0)} \in \mathbb{R}^{d \times N}$.
3. Generate a proposal state

$$A'_{ik} = \sqrt{1 - \kappa^2} A_{ik}^{(n)} + \kappa_{ik} Z_{ik} \quad (3.52)$$

for each $i = 1, \dots, d$ and $k = 1, \dots, N$, where Z_{ik} is sampled from $\mathcal{N}(0, 1)$ and κ_{ik} is the step-size matrix.

4. Draw a random number U from $\text{Unif}([0, 1])$.

- If $U < A_{\text{pCN}}[A^{(n)}, A']$, then set $A^{(n+1)} = A'$.
- Otherwise set $A^{(n+1)} = A^{(n)}$.

In practice, if the algorithm was run for M iterations, it is often prudent to discard some portion of the first $M_B < M$ of the samples $\{A^{(n)}\}_{n=1}^M$. This is due to the fact that $A^{(0)}$ is in general not a representative sample from the target distribution \mathbb{P}_X . We thus let the MCMC ‘burn in’ for M_B iterations, and discard $\{A^{(n)}\}_{n=1}^{M_B}$. In all numerical experiments in this text, we use a burn-in of $M_B/M = 0.3$.

Recall that in the definition of the acceptance probability Eq. 3.50 we must either use the Onsager-Machlup or the Freidlin-Wentzell form of the relative action Φ . As discussed in the introduction, for the purposes of sampling \mathbb{P}_X there is no difference between the two actions. In all numerical results that follows we have used the Onsager-Machlup action, where we have also verified that the Freidlin-Wentzell action lead to the same result.

Fig. 3.1 shows the result of $M = 10^8$ iterations of the pCN algorithm to a benchmark problem, with burn-in $M_B/M = 0.3$. We sample the TPE of a 1-dimensional overdamped Langevin dynamics of a particle moving between the minima of an asymmetric double-well potential. See Fig. 3.1c for the potential energy profile of the system, and App. B.1 for a detailed specification of the model. Fig. 3.1a shows a sample of 50 trajectories from the TPE, simulated at temperature $\theta/\theta_0 = 2$, where θ_0 is a reference temperature. The reference temperature θ_0 is defined such that at $\theta = \theta_0$ the thermal fluctuations equal the characteristic energy scale of the confining potential energy (See App. B for details on the non-dimensionalisation of the model system). In Fig. 3.1 Fig. 3.1b we show the maximiser of the path-probability density functional Eq. 3.5 (which we call the *instanton*), as well as a sample of 10 trajectories from the TPE simulated at a temperature $\theta/\theta_0 = 0.01$. The

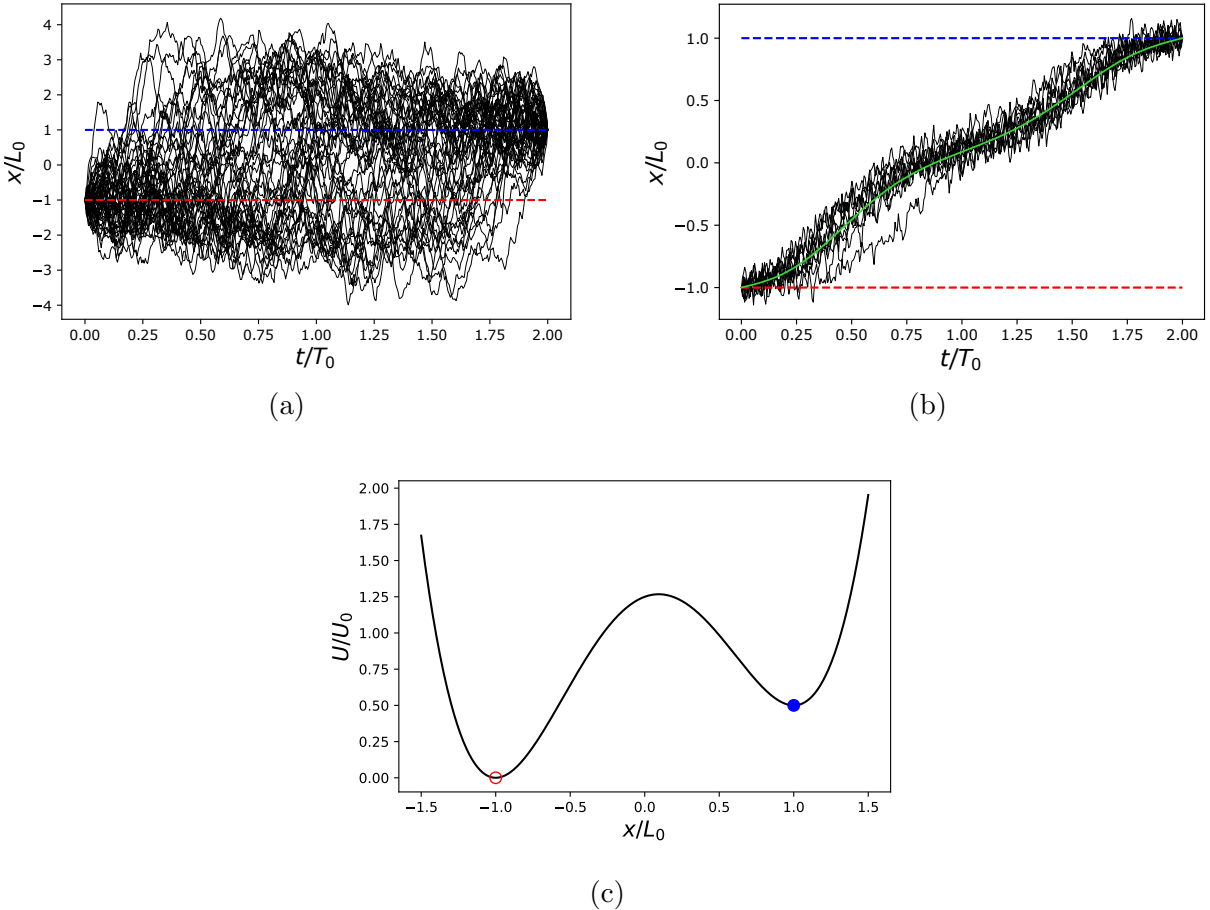


Figure 3.1: Simulation of the 1-dimensional antisymmetric double-well system (defined in App. B.1) using $M = 10^8$ iterations of the pCN algorithm with burn-in $M_B/M = 0.3$. We sampled transition paths of duration $T/T_0 = 2$ between the minima at $x_0/L_0 = -1$ (red dashed lines) to the minima at $x_0/L_0 = 1$ (blue dashed lines), and with mode truncation $N = 200(T/T_0)$. (a) Shows 50 transition paths at temperature $\theta/\theta_0 = 2$. (b) Shows 10 transition paths at temperature θ/θ_0 , and the instanton (green line). (c) The antisymmetric double-well potential, with minima at $x/L_0 = -1$ (hollow red circle) and $x/L_0 = 1$ (filled blue circle). See App. B.1 for its definition.

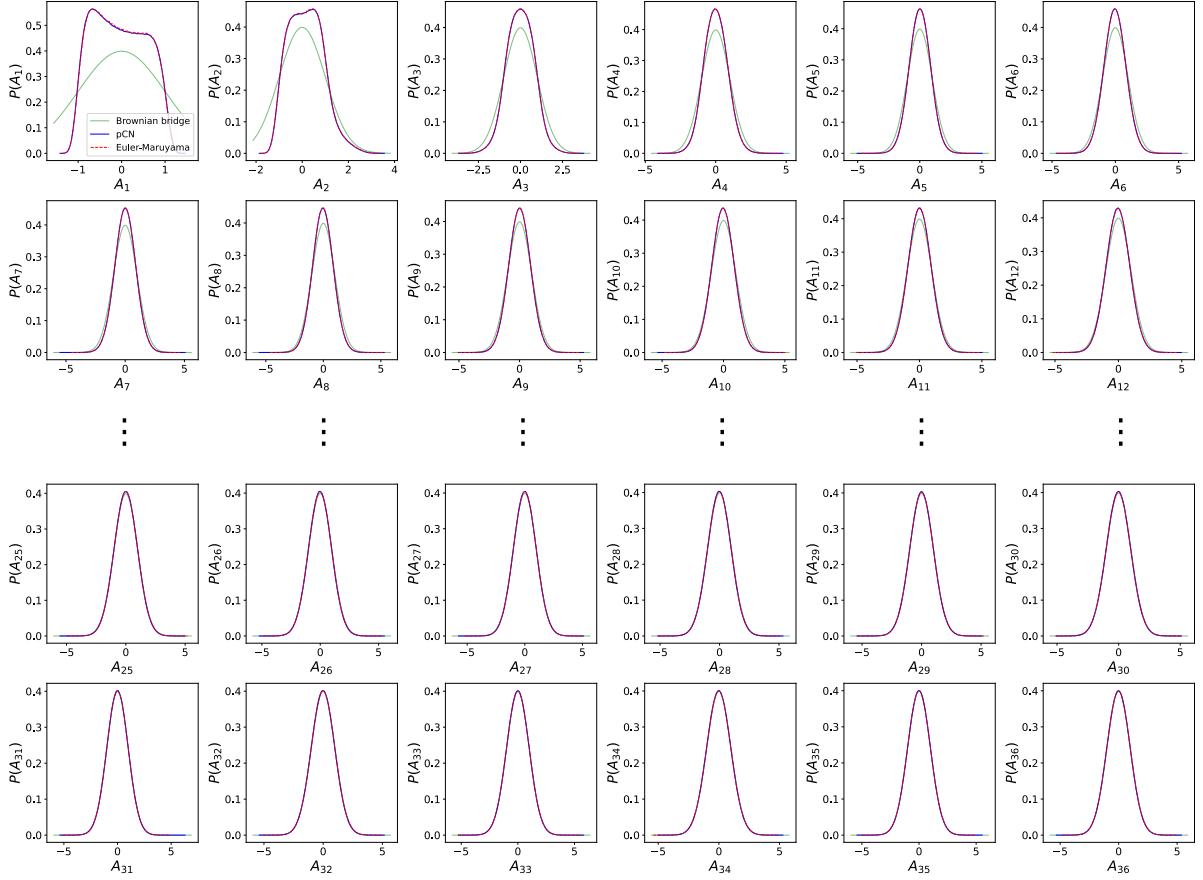


Figure 3.2: Simulation of the 1-dimensional antisymmetric double-well system using both the pCN and the Euler-Maruyama methods. The resulting samples were projected onto the KKL basis of the Brownian bridge process, and the figure shows the marginalised distribution over the coefficients A_k of the sampled TPE. In each sub-plot, the green line are the distributions of a centred normal with unit-variance $Z_k \sim \mathcal{N}(0, 1)$, which corresponds to the modes of the Brownian bridge process. The parameters of the simulation are the same as those of Fig. 3.1 (a).

duration of the transition paths were $T/T_0 = 2$, where T_0 is a reference time-scale. We computed the instanton by minimising the Onsager-Machlup action of the model system, using a Ritz method as described in Ch. 2. Note that, as mentioned in the introduction, at finite temperatures the instanton must be computed using Onsager-Machlup action, as opposed to the Freidlin-Wentzell action [83, 3]. At temperatures $\theta > \theta_0$, where thermal fluctuations (represented by the noise term in the Langevin equation) dominate over the potential, and we see in Fig. 3.1 (a) that the sample paths transition between the two minima several times. On the other hand, at temperatures $\theta \ll \theta_0$, where we would expect that transition events are rare, the TPE is concentrated around the instanton.

To verify that our implementation of the algorithm correctly sampled the TPE, we verified our results using a standard Euler-Maruyama integrator [?]. Using the latter, we generated samples 10^6 of the TPE by collecting trajectories with end-points within a small interval $\tilde{x}(T) \in [1 - \epsilon, 1 + \epsilon]$ around the right minima, where $\epsilon = 10^{-2}$. We

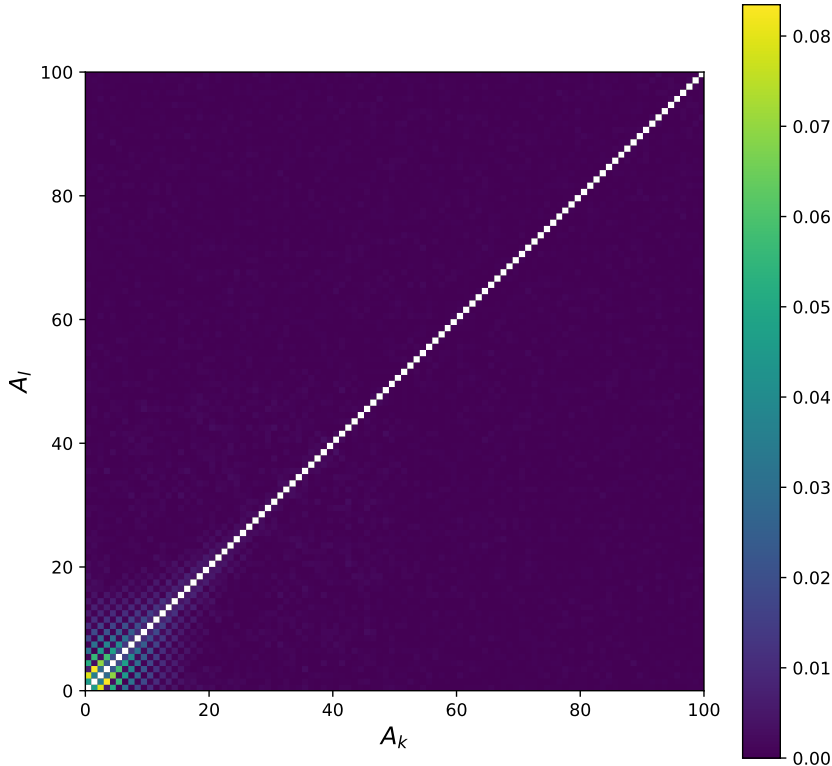


Figure 3.3: The absolute normalised covariances $\rho_{kl} = \langle A_k A_l \rangle / \sqrt{\langle A_k^2 \rangle \langle A_l^2 \rangle}$ of the first 100 modes of the transition paths of the 1-dimensional antisymmetric double-well system. As $\rho_{kk} = 1$, $k = 1, \dots, N$ by definition, we have excluded the diagonal from the plot. We sampled the TPE using the pCN algorithm, with parameters $T/T_0 = 2$, $\theta/\theta_0 = 2$ and $N = 200(T/T_0)$. We see that there is a band-separation between the low and high mode-numbers, where modes beyond the the $k \in [0, 30]$ quadrant are largely uncorrelated.

used a temperature θ/θ_0 as in Fig. 3.1a, as it is unfeasible to use the Euler-Maruyama algorithm to sample the TPE for temperature regimes where transition events are rare. We projected the resulting sample paths onto the KKL basis of the Brownian bridge process, and compared the sample with the result of the pCN method. The results are showed in Fig. 3.2, where we plot the marginalised histograms of the mode distributions against each other.

3.2.4 Mode-space band structure

In Fig. 3.2 we see that the marginalised distributions of the modes of stochastic trajectories in the TPE (blue lines) increasingly coincide with normal distributions of unit variance (green lines) at higher mode orders. The latter corresponds to the modes of the Brownian bridge process, as was established in Sec. 3.2.2. Fig. 3.3 shows the absolute normalised covariances $\rho_{kl} = \langle A_k A_l \rangle / \sqrt{\langle A_k^2 \rangle \langle A_l^2 \rangle}$ of the modes. Here we see the modes also rapidly decorrelate, and are numerically negligible beyond the first 30 modes. Fig. 3.2 and Fig. 3.3 are a first indication that modes of transition paths are approximately distributed like

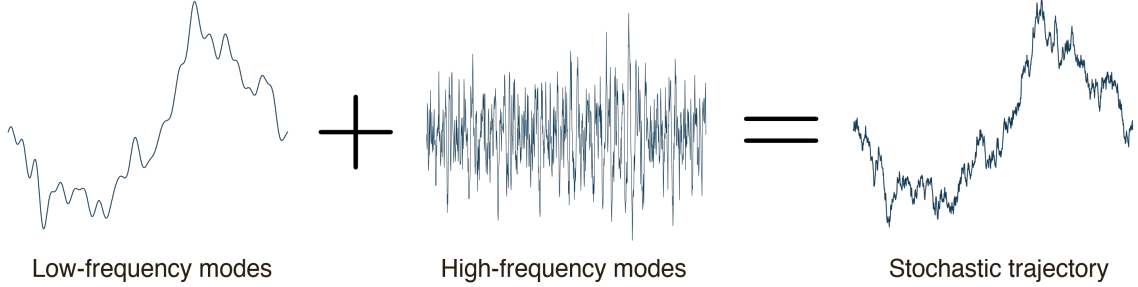


Figure 3.4

a Brownian bridge process for large mode orders k . As we discuss and show below, this holds for *any* Itô diffusion with additive noise, regardless of the drift-field \mathbf{b} .

The law \mathbb{P}_X over the TPE of an Itô diffusion can be seen as a non-linear transformation of \mathbb{P}_B , the law of the Brownian bridge process. They are related via Eq. 3.23 in terms of the density Eq. 3.16, where the latter is an expression entirely in terms of the drift-field. Therefore, the difference in statistical ‘information’ contained in \mathbb{P}_X relative to \mathbb{P}_B is exactly the drift-field \mathbf{b} .

Furthermore, the difference in distribution between \mathbb{P}_X and \mathbb{P}_B is located in the lower-end of the mode-spectrum. For the 1-dimensional benchmark problem, in Fig. 3.3 we can see a division in mode space between a low-frequency and high-frequency band, where the division between the two bands can be conservatively assigned at around $k_l = 40$. The low-frequency band thus correspond to the first k_l modes in the expansion Eq. 3.47, and the high-frequency band correspond to all modes $k > k_l$. We can consider the low-frequency modes the ‘smooth’ and the high-frequency modes the ‘rough’ parts of a stochastic trajectory, as visualised in Fig. 3.4. In the dynamics of an Itô diffusion Eq. 3.3, the stochastic term $\sigma d\mathbf{W}$ dominates over deterministic drift-field \mathbf{b} at short-time scales. In other words, \mathbf{b} only affects the system on long time-scales. Therefore we would intuit that stochastic realisations \mathbf{X} , of the Itô diffusion equation, look like they are undergoing drift-less free diffusion as we ‘zoom in’ on the trajectory. Therefore, if \mathbf{b} is smooth, we would expect that \mathbb{P}_X and \mathbb{P}_B only behave differently in the ‘smooth’ low-frequency band, and behave identically in ‘rough’ high-frequency band. Further numerical evidence of the band-separation is further provided in Sec. 3.2.5 and in later sections in Fig. 3.6 and Fig. 3.7, in addition to the results already discussed for the 1-dimensional antisymmetric double-well system.

Statements analogous to the above would apply if we instead considered the spectrum of the law of an unpinned Itô diffusion, with sample space $C_{x_0}^0([0, T])$, the set of stochastic paths starting at x_0 with open end-point conditions at $t = T$. In that case, using identical arguments, we would find that the spectrum of the \mathbb{P}_X would resemble \mathbb{P}_W in the high-frequency band, where the latter is the law of the Wiener process. Furthermore, below we

will provide an analytical argument.

In the following we expand a unpinned Langevin processes of the form Eq. 3.3 in the KKL basis of the Wiener process \mathbf{W} . For simplicity we only consider the 1-dimensional case, but the results below readily generalises to higher dimensional processes. The KKL expansion of the 1-dimensional Wiener process is

$$W(t) = \mathbf{x}_0 + \sqrt{2D} \sum_{k=1}^{\infty} Z_k \sqrt{\nu_k} \chi_k(t) \quad (3.53)$$

where Z_k , $k = 1, \dots, \infty$ are independent d -dimensional normal random variables distributed as $\mathbf{Z}_k \sim \mathcal{N}(0, \mathbb{1}_d)$, and where

$$\chi_k(t) = \sqrt{\frac{2}{T}} \sin(t/\sqrt{\nu_k}) \quad (3.54a)$$

$$\nu_k = \frac{T^2}{\pi^2 \left(k - \frac{1}{2}\right)^2}, \quad (3.54b)$$

and where $\chi_k(t)$ satisfy $\langle \chi_k, \chi_l \rangle = \delta_{kl}$, where we have defined

$$\langle f, g \rangle = \int_0^T f(t)g(t)dt. \quad (3.55)$$

for any two functions $f, g : [0, T] \rightarrow \mathbb{R}$. We begin with the integral form of the Itô diffusion equation Eq. 3.4

$$X(t) = \int_0^t b(X(t'))dt' + \sqrt{2D} \int_0^t dW(t') \quad (3.56)$$

where $b : \mathbb{R} \rightarrow \mathbb{R}$ is the drift-field, $t \in [0, T]$ and the second term of Eq. 3.56 is an Itô integral. We assume, without loss of generality, that $X(0) = 0$. We now expand the Wiener process in its KKL expansion, and truncate the sum up to order N to approximate Eq. 3.56 as

$$X^N(t) = \int_0^t b(X^N(t'))dt' + \int_0^t dW^N(t') \quad (3.57)$$

where W^N is the truncation of Eq. 3.53, X^N is the truncated stochastic process, and where the second term in Eq. 3.57 is now a Riemann-Stieltjes integral. It is a theorem (known as the *Wong-Zakai theorem*) [219, 206, 65] that as $N \rightarrow \infty$ the sequence of solutions to Eq. 3.57 converges uniformly in probability to the solution of Eq. 3.56¹.

We we will expand X^N as

$$X^N(t) = \sqrt{2D} \sum_{k=1}^N A_k \sqrt{\nu_k} \chi_k(t). \quad (3.58)$$

¹Note that the Wong-Zakai theorem holds for the Stratonovich formulation of Eq. 3.56. However, for additive noise the Itô and Stratonovich formulations are equivalent.

As $X^N(t)$ and $W^N(t)$ are smooth for finite N , we can take the derivative of Eq. 3.57 to find

$$\dot{X}^N(t) = b(X^N(t)) + \dot{W}^N(t). \quad (3.59)$$

We can expand the $\dot{X}^N(t)$ and $\dot{W}^N(t)$ as

$$\dot{X}^N(t) = \sqrt{2D} \sum_{k=1}^N A_k \psi_k(t) \quad (3.60a)$$

$$\dot{W}^N(t) = \sqrt{2D} \sum_{k=1}^N Z_k \psi_k(t) \quad (3.60b)$$

where

$$\psi_k(t) = \sqrt{\nu_k} \dot{\chi}_k(t) = \sqrt{\frac{2}{T}} \cos(t/\sqrt{\lambda_k}). \quad (3.61)$$

As $\langle \psi_k, \psi_l \rangle = \delta_{kl}$, we have that ψ_k forms an orthonormal basis over the space of paths. We can therefore expand the drift-field as

$$b(X^N(t)) = \sqrt{2D} \sum_{k=1}^N b_k \psi_k(t) \quad (3.62)$$

where $b_k = \langle \psi_k, b(X^N) \rangle / \sqrt{2D}$. From Eq. 3.59, and the orthonormality of ψ_k , we get

$$A_k = b_k + Z_k, \quad (3.63)$$

where $k = 1, \dots, N$. This is a spectral version of the Itô diffusion equation, where we have projected Eq. 3.56 onto the truncated KKL spectrum of the Wiener process. Here the mode coefficients A_k are random variables expressed in terms of the drift modes b_k and the modes of the Wiener process Z_k . As $b_k = \langle \psi_k, b(X^N) \rangle / \sqrt{2D}$, we have that $b_k = b_k(A)$ is in general a non-linear equation in terms of the mode coefficients $A = (A_1, \dots, A_N)$. We note that Eq. 3.63 can in principle be used to sample the Itô diffusion equation, by drawing N random numbers $Z_k \sim \mathcal{N}(0, 1)$ and then solving Eq. 3.63 for A .

Any finite choice of the number of modes N will lead to truncation errors, but for increasing N Eq. 3.63 will probabilistically converge to the true infinite-dimensional distribution. For a given X^N , b_k can be seen as the Fourier coefficients of b . Now, using the known convergence-properties of Fourier expansions, we have that

$$|b_k| \leq \frac{C(D, T)}{k} \quad (3.64)$$

where $C(D, T)$ is some function of the system parameters. As Z_k is always of order 1,

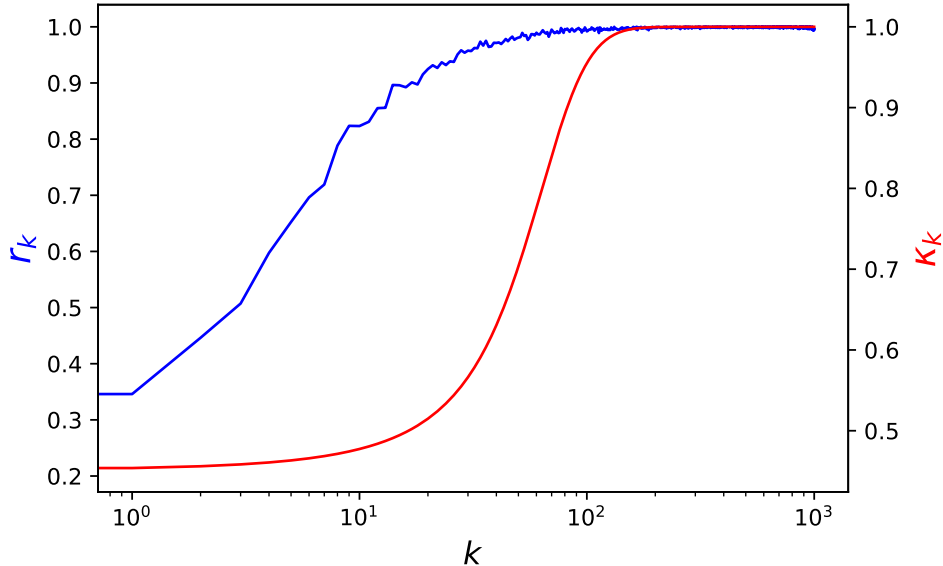


Figure 3.5: The modal acceptance rates r_k^{acc} (red line) for the 1-dimensional asymmetric double-well system, with system parameters identical to those in Fig. 3.1a

Eq. 3.63 tells us that

$$A_k \approx Z_k \quad (3.65)$$

for $k > k_{|}$ for some value of $k_{|}$, and sufficiently large $N > k_{|}$. We thus see that for a given system, there are always only a finite number of physically relevant modes distinct from free diffusion dynamics. In general $k_{|}$ be dependent on the drift-field b , and will be an increasing function of the diffusivity D and duration T .

3.2.5 Mode-dependent step-sizes

The band-structure of the mode-spectrum of Itô processes can potentially be exploited to improve the sampling algorithm. Here, as a simple first attempt, we will use the band-structure to adapt the step-sizes in the pCN algorithm for each individual mode. To construct an adapted step-size matrix κ_{ik} , we need to first have a method by which to estimate the extent to which each mode is distributed like a Gaussian. Note that if $\kappa_{ik} = 1$ for a given i, k , then the proposal Eq. 3.52 at each iteration is an independent random sample from $\mathcal{N}(0, 1)$.

Consider a modified pCN algorithm that, at each iteration step n , only updates a single mode A_{ik} at a time. The algorithm updates the mode in sequence, such that after dN iterations all of the modes A_{ik} , $i = 1, \dots, d$, $k = 1, \dots, N$ will have been updated once. Let r_{ik} be the *modal acceptance rate* of the iterations of the mode A_{ik} , which is the ratio of accepted proposals to the number of iterations $M/(dN)$, where M is the number

of iterations of the whole algorithm. Similarly, let r be the acceptance rate of all modes in the regular pCN algorithm. Figure 3.5 plots the modal acceptance rates (blue line) for the 1-dimensional asymmetric double-well system, with system parameters identical to those in Fig. 3.1a, mode truncation $N = 1000$ and iterations $M = 1000N$. We see that $r_k \approx 1$ for modes $k \geq 50$. Therefore we may consider a sigmoidal step-size profile

$$\kappa_k = \kappa_{\min} + (\kappa_{\max} - \kappa_{\min}) (1 + \exp(-\sigma_\kappa(k - \mu_\kappa))) \quad (3.66)$$

with $\kappa_{\min} = 0.4$, $\kappa_{\max} = 1$, $\mu_k = 50$ and $\sigma_\kappa = 0.05$, which is plotted in Fig. 3.5 (blue line). The base-line step-size κ_{\min} was computed by finding an approximate constant $\kappa_{ik} = \bar{\kappa}$ that yielded an acceptance rate $r \approx 0.3$ in the regular pCN algorithm.

[?]

3.2.6 Generalised end-point conditions

So far we have considered transition path ensembles with fixed end-point conditions. We may consider a TPE of a more general form

$$E_{R_0}^{R_T}([0, T]) = \{\mathbf{X} : \mathbf{X} \in C_{\mathbf{x}_0}([0, T]) \text{ and } \mathbf{X}(T) = \mathbf{x}_T \text{ where } \mathbf{x}_0 \in R_0, \mathbf{x}_T \in R_T\}. \quad (3.67)$$

In other words, $E_{R_0}^{R_T}([0, T])$ is the set of stochastic paths that start in $R_0 \subset \mathbb{R}^d$ and end in $R_T \subset \mathbb{R}^d$. In applications, R_0 and R_T may, for example, be chosen to lie within the basins of attraction of fixed points of the drift-field \mathbf{b} .

A probability measure over $E_{R_0}^{R_T}([0, T])$ can be constructed by simply grafting a probability distribution over the initial condition onto the path-probability measure $\mathbb{P}_{\mathbf{X}}$. Let π_0 be a probability measure over R_0 , with density $p_0 \sim \pi_0$. Let $\tilde{P}_{\mathbf{X}}$ be a probability measure over $E_{R_0}^{R_T}([0, T])$, defined in terms of the density $\tilde{P}_{\mathbf{X}} \sim \tilde{\mathbb{P}}$

$$\tilde{P}_{\mathbf{X}}[\mathbf{x}] \propto p_0(\mathbf{x}(0)) P_{\mathbf{X}}[\mathbf{x}] \quad (3.68)$$

where we have restricted the domain of $\tilde{P}_{\mathbf{X}}[\mathbf{x}]$ to paths that satisfy $\mathbf{x}(0) \in R_0$ and $\mathbf{x}(T) \in R_T$.

We can modify the pCN algorithm to sample $\tilde{P}_{\mathbf{X}}$. In addition to the coefficient matrix $A = (\mathbf{a}_1 \ \mathbf{a}_2 \dots \mathbf{a}_N)$, the MCMC state will now also be specified by the starting- and end-points of the transition path \mathbf{x}_0 and \mathbf{x}_T respectively. We define the new update rule

$$\mathbf{a}'_i = \sqrt{1 - \kappa^2} \mathbf{a}^{(n)} + \kappa \mathbf{Z}_i \quad (3.69a)$$

$$\text{Draw } \mathbf{x}'_0 \text{ from } \pi_0 \quad (3.69b)$$

$$\text{Draw } \mathbf{x}'_T \text{ from } \pi_T \quad (3.69c)$$

where π_T is a distribution over R_T that must be specified. Let $p_T \sim \pi_T$, then the transition kernel density is

$$\tilde{Q}[\mathbf{X} \rightarrow \mathbf{Y}] = p_0(\mathbf{Y}(0))p_T(\mathbf{Y}(T))Q_{\text{pCN}}[\mathbf{X} \rightarrow \mathbf{Y}]. \quad (3.70)$$

From Eq. 3.30 we find the acceptance probability

$$\tilde{A}[\mathbf{X}, \mathbf{Y}] = \min \left\{ 1, e^{\Phi[\mathbf{X}] - \Phi[\mathbf{Y}]} \frac{p_T(\mathbf{X}(T))}{p_T(\mathbf{Y}(T))} \right\}, \quad (3.71)$$

where transition paths are expanded as

$$\mathbf{X}^N(t; A, \mathbf{x}_0, \mathbf{x}_T) = \mathbf{x}_0 + (\mathbf{x}_T - \mathbf{x}_0) \frac{t}{T} + \sqrt{2D} \sum_{i=1}^N \mathbf{a}_i \sqrt{\lambda_i} \phi_i(t). \quad (3.72)$$

The update rule Eq. 3.69 has not been numerically tested, but is rather offered here as a proof-of-concept to show that it is possible to implement generalised initial- and final end-point configurations using the pCN method. Equation 3.69b and Eq. 3.69c are here independent samplers, and in practice implementing random-walk procedures in R_0 and R_T might lead to better convergence.

Finally, some applications may require that we let r of the d degrees of freedom have open end-point conditions (In other words, $R_T = \mathbb{R}^d$). Let X_i be the components of the stochastic process \mathbf{X} , and we consider transition paths where we let X_i , $i = 1, \dots, r$ have open end-point configurations. We may then adapt the pCN algorithm of Sec. 3.2.3 by expanding X_j , $j = r+1, \dots, d$ in the KKL basis of the Brownian bridge process as before, and expanding X_i , $i = 1, \dots, r$ in the KKL basis of the *Wiener process*.

3.3 Sampling multi-modal transition path ensembles

Motivate the algorithm by defining the switch system here (full definition in appendix).

Define transition channel

3.3.1 Quadratic expansions of the Onsager-Machlup action

3.3.2 Calculation of the Gaussian normalisation constants

3.3.3 The Teleporter MCMC method

Perhaps you should first just present a vanilla TMC for finite dimensional distributions.

Here we describe in further detail the *Teleporter MCMC* (TMC) algorithm used in

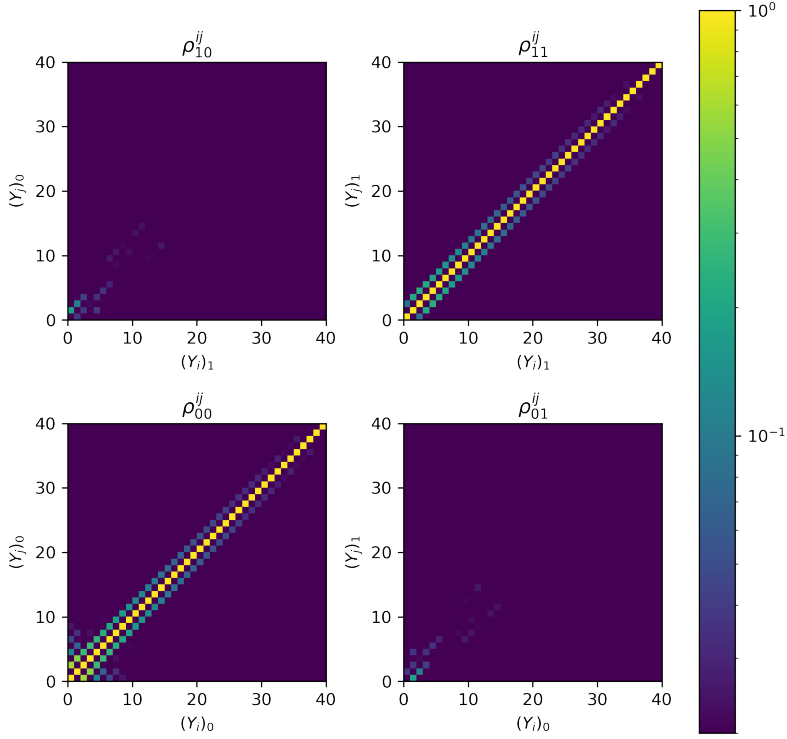


Figure 3.6: The absolute normalised covariance $\rho_{kl}^{ij} = E^{\mathbb{P}} \{(Y_i)_k (Y_j)_l\} / \sqrt{E^{\mathbb{P}} \{(Y_i)_k^2\} E^{\mathbb{P}} \{(Y_j)_l^2\}}$ of the modes of the sample paths in the KKL basis, found by sampling the system with gradient dynamics using the TMC, at $\theta/\theta_0 = 3.36$, $T/T_0 = 3$ and $N = 200(T/T_0)$.

the main text. We start with a discussion of the algorithm in its infinite dimensional form, defined directly on the space of continuous paths, and then proceed to describe a modification of the algorithm adapted to the KKL discretisation.

At each step of the MCMC, with a probability p_{teleport} , we draw an independent proposal step \mathbf{X}' from the mixed Gaussian distribution

$$\bar{\mathbb{P}} = \sum_{\alpha=1}^K w_\alpha \mathbb{P}^{[\alpha]} \quad (3.73)$$

where the weights w_α are parameters that must satisfy $\sum_{\alpha=1}^K w_\alpha = 1$, and where $\mathbb{P}^{[\alpha]}$ are Gaussian distributions with precision operators $\mathcal{H}^{[\alpha]}$ and mean $\bar{\mathbf{x}}$ as defined in previous sections. Using the Metropolis-Hastings condition to ensure that the MCMC samples the target measure \mathbb{P} of the Itô process we find that \mathbf{X}' should be accepted with probability

$$a_{\text{TMC}} [\mathbf{X}', \mathbf{X}^{(n)}] = \min \left\{ 1, \exp (\Phi[\mathbf{X}^{(n)}] - \Phi[\mathbf{X}']) \frac{\sum_\alpha w_\alpha \exp (-\Psi^{[\alpha]}[\mathbf{X}^{(n)}])}{\sum_\alpha w_\alpha \exp (-\Psi^{[\alpha]}[\mathbf{X}'])} \right\} \quad (3.74)$$

where $\mathbf{X}^{(n)}$ is current state of the MCMC, and $\Psi^{[\alpha]}$ is the logarithmic density of $\mathbb{P}^{[\alpha]}$ with respect to the Wiener measure $\frac{d\mathbb{P}^{[\alpha]}}{d\mathbb{P}_W} = \exp(-\Psi^{[\alpha]})$ and

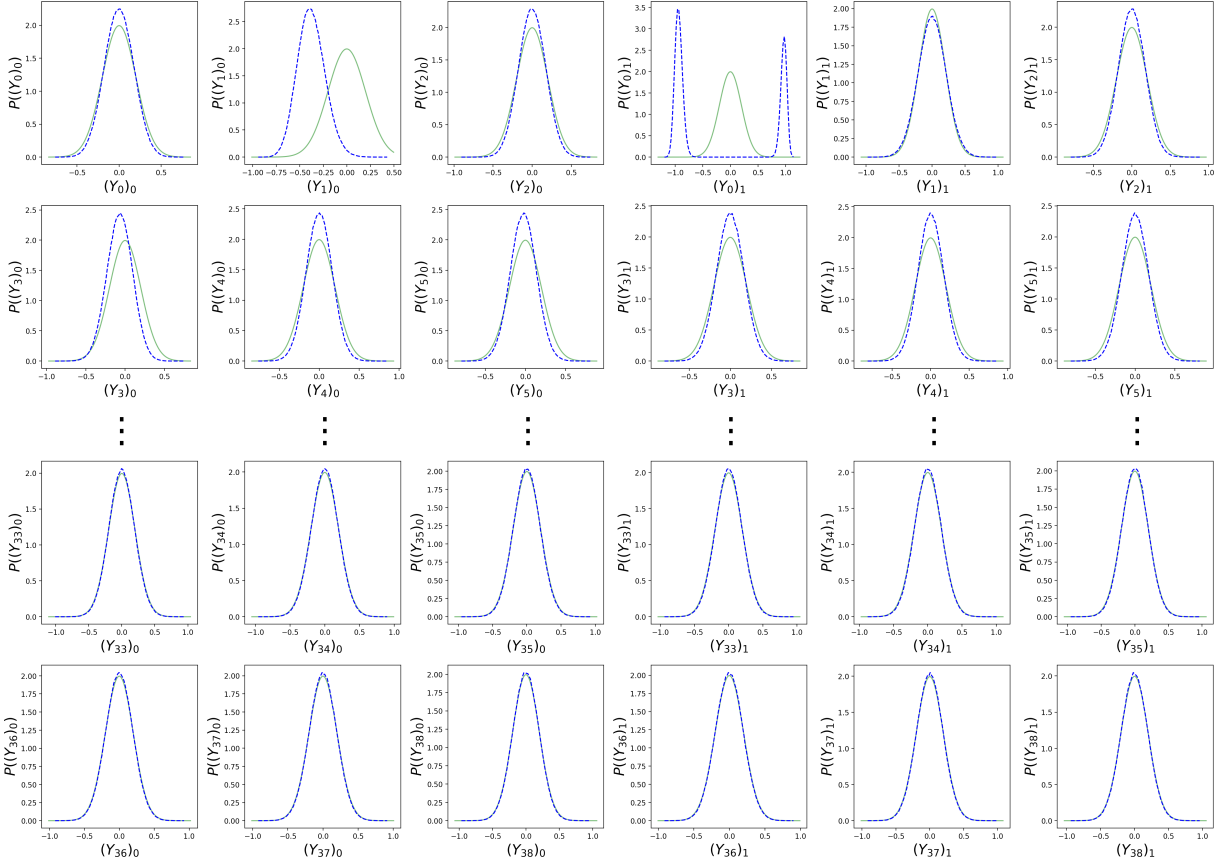


Figure 3.7: The marginalised distributions of the modes of the sample paths (blue) and the Wiener process (green) in the KKL basis, found by sampling the system with gradient dynamics using the TMC, at $\theta/\theta_0 = 3.36$, $T/T_0 = 3$ and $N = 200(T/T_0)$.

$$\Psi^{[\alpha]}[\mathbf{X}] = \Psi_1^{[\alpha]}[\mathbf{X} - \mathbf{x}^{[\alpha]}] + \Psi_2^{[\alpha]}[\mathbf{X}] \quad (3.75)$$

$$\Psi_1^{[\alpha]}[\mathbf{X}] = \int_0^T (2\mathbf{X}^T A(t)d\mathbf{X} + \mathbf{X}^T B(t)\mathbf{X}dt) \quad (3.76)$$

$$\Psi_2^{[\alpha]}[\mathbf{X}] = \frac{\beta}{2\mu} \int_0^T (2\dot{\mathbf{x}}^{[\alpha]T}d\mathbf{X} - |\dot{\mathbf{x}}^{[\alpha]}|^2 dt) \quad (3.77)$$

Thus far, the algorithm has been defined directly on the space of continuous paths, but in numerical applications it is necessary to apply a discretisation procedure. We can approximate $\mathbb{P}^{[\alpha]}$ as a multivariate Gaussian by expanding its precision operator $\mathcal{H}^{[\alpha]}$ in the KKL basis [126, 121, 137] of the Wiener process as $(H_{ij}^{[\alpha]})_{kl} = \langle \mathbf{e}_k \phi_i, \mathcal{H}^{[\alpha]} \mathbf{e}_l \phi_j \rangle$, $i, j = 1, \dots, N$, $k, l = 1, \dots, d$, where, \mathbf{e}_k is a constant vector with one non-zero component $(\mathbf{e}_k)_l = \delta_{kl}$. Due to our discretisation procedure M can be kept small as the noise dominates over the drift for high-frequency modes, which manifests itself as $H_{ij}^{[\alpha]}$ rapidly converging onto the precision matrix of the Wiener measure, $(H_{ij}^W)_{kl} = \frac{\beta}{4\mu} \delta_{ij} \delta_{kl}$, for high mode numbers i, j . This is demonstrated in Fig. 3.6 and Fig. 3.7.

Using the multivariate Gaussian with precision matrix $\tilde{H}^{[\alpha]}$, we construct a grafted Gaussian process $\mathbf{W}^{[\alpha]}(t) = \mathbf{x}^{[\alpha]}(t) + \sqrt{\frac{2\mu}{\beta}} \sum_{i=1}^{\infty} \mathbf{Z}_i^{[\alpha]} \sqrt{\lambda_i} \phi_i(t)$ where $(\mathbf{Z}_1^{[\alpha]}, \dots, \mathbf{Z}_M^{[\alpha]}) \sim \mathcal{N}(0, \tilde{H}^{[\alpha]})$ and $\mathbf{Z}_i^{[\alpha]} \sim \mathcal{N}(0, I_d)$, $i > M$, where I_d is the d -dimensional identity matrix. This defines a Gaussian measure $\tilde{\mathbb{P}}^{[\alpha]}$ on the space of stochastic paths from which we can sample efficiently. Finally, we construct a Gaussian mixture measure as the linear combination

$$\tilde{\mathbb{P}} = \sum_{\alpha=1}^K \tilde{w}_{\alpha} \tilde{\mathbb{P}}^{[\alpha]} \quad (3.78)$$

from which we draw independent samples in the same manner as before. The logarithmic densities of $\tilde{\mathbb{P}}^{[\alpha]}$ with respect to the Wiener measure \mathbb{P}_W are now

$$\tilde{\Psi}^{[\alpha]}[\mathbf{X}] = \sum_{i,j=1}^M \sum_{k,l=1}^d \frac{1}{2} (Y_{ik} - Y_{ik}^{[\alpha]}) \tilde{K}_{ijl}^{[\alpha]} (Y_{jl} - Y_{jl}^{[\alpha]}) + 2 \sum_{i=1}^M \mathbf{Y}_i^{[\alpha]T} \mathbf{Y}_i + \sum_{i=1}^M \mathbf{Y}_i^{[\alpha]T} \mathbf{Y}_i^{[\alpha]}. \quad (3.79)$$

where $\mathbf{X}(t) = \mathbf{x}_0 + \bar{\mathbf{v}}t + \sqrt{\frac{2\mu}{\beta}} \sum_{i=1}^{\infty} \mathbf{Y}_i \sqrt{\lambda_i} \phi_i(t)$, Y_{ik} denotes the k th component of \mathbf{Y}_i , $Y_{ik}^{[\alpha]} = \langle \mathbf{x}^{[\alpha]}, \mathbf{e}_k \phi_i \rangle$, $\left(\tilde{K}_{ij}^{[\alpha]}\right)_{kl} = \langle \mathbf{e}_k \phi_i, (\mathcal{H}^{[\alpha]} - \mathcal{H}^W) \mathbf{e}_l \phi_j \rangle$, $\tilde{L}_{ik}^{[\alpha]} = \frac{\beta}{2\mu}$ using which the acceptance probabilities are computed as in Eq. (3.74).

We now summarise the full algorithm, expressed in the KKL basis:

1. Choose an initial state $\mathbf{Y}^{(0)} \in \mathbb{R}^{N \times d}$.

2. Draw a random number $U^{(n+1)} \sim \text{Unif}([0, 1])$.

- If $U^{(i+1)} > p_{\text{teleport}}$.

(a) Given state $\mathbf{Y}^{(n)}$, the $(n+1)$ -th proposal is

$$\mathbf{Y}'_i = \sqrt{1 - \kappa^2} \mathbf{Y}_i^{(n)} + \kappa \mathbf{Z}_i^{(n)} \quad (3.80)$$

where $\mathbf{Z}_i^{(n)} \sim \mathcal{N}(0, I_d)$ and $i = 1, \dots, N$.

(b) Draw a random number $V^{(n+1)} \sim \text{Unif}([0, 1])$.

- If $V^{(i+1)} < a[\mathbf{x}(t; \mathbf{Y}'), \mathbf{x}(t; \mathbf{Y}^{(n)})]$ then set $\mathbf{Y}^{(n+1)} = \mathbf{Y}'$.
- Otherwise set $\mathbf{Y}^{(n+1)} = \mathbf{Y}^{(n)}$.

- If $U^{(i+1)} \leq p_{\text{teleport}}$:

(a) Given state $\mathbf{Y}^{(n)}$, the $(n+1)$ -th proposal is

$$\mathbf{Y}'_i = \tilde{\mathbf{Z}}_i^{(n)} \quad (3.81)$$

where $\tilde{\mathbf{Z}}^{(n)}$ is drawn from $\tilde{\mathbb{P}}_N$, and $i = 1, \dots, N$.

- (b) Draw a random number $W^{(n+1)} \sim \text{Unif}([0, 1])$.
 - If $W^{(i+1)} < a_{\text{TMC}}[\mathbf{x}(t; \mathbf{Y}'), \mathbf{x}(t; \mathbf{Y}^{(n)})]$ then set $\mathbf{Y}^{(n+1)} = \mathbf{Y}'$.
 - Otherwise set $\mathbf{Y}^{(n+1)} = \mathbf{Y}^{(n)}$.

3. Repeat step 2.

where $\text{Unif}([0, 1])$ is the uniform distribution over the unit interval, $\mathbf{x}(t; \mathbf{Y}) = \mathbf{x}_0 + \bar{\mathbf{v}}t + \sqrt{\frac{2\mu}{\beta}} \sum_{i=1}^N \mathbf{Y}_i \sqrt{\lambda_i} \phi_i(t)$, and $\tilde{\mathbb{P}}_N$ is the truncation of Eq. (3.78) to N modes. In the numerical experiments discussed in the main text, we used $\tilde{w}_1 = \tilde{w}_2 = 1/2$ and $M = 10(T/T_0)$.

As mentioned in the main text, an alternate method to the above would be a synthesis of the two sampling approaches in the above algorithm. We could replace the reference Wiener measure \mathbb{P}_W with the mixed Gaussian $\tilde{\mathbb{P}}$, and thus perform the pCN-MCMC with $\tilde{\mathbb{P}}$ as the invariant measure.

3.3.4 Model system

3.3.5 Gaussian mixture approximation of the transition path ensemble

Here we derive an approximation of the transition path ensemble, using a Gaussian mixture approximation of the path-space probability measure. The subsequent sections give detailed descriptions of the mathematical techniques necessary for the approximation, but we will first give some intuition by drawing an analogy to a one-dimensional probability density.

For a one-dimensional probability density $\rho(x) = \mathcal{N}^{-1} \exp(-V(x))$, where \mathcal{N} is a normalization constant and where the potential $V(x)$ has well-separated relative minima x_α , $\alpha = 1, \dots, K$, we can approximate $\rho(x)$ around x_α using a Gaussian approximation

$$\rho(x) \approx \frac{1}{\mathcal{N}} e^{-V(x_\alpha) - V''(x_\alpha)(x-x_\alpha)^2/2} =: \frac{\mathcal{N}_\alpha}{\mathcal{N}} e^{-V(x_\alpha)} \rho^{[\alpha]}(x) \quad (3.82)$$

with a normalised Gaussian distribution $\rho^{[\alpha]}(x) := \mathcal{N}_\alpha^{-1} e^{-V''(x_\alpha)(x-x_\alpha)^2/2}$ and where $\mathcal{N}_\alpha = \sqrt{2\pi/V''(x_\alpha)}$. Equation 3.82 is a local approximation of $\rho(x)$ around x_α . If $\rho(x)$ is highly peaked around its maxima (for example if $V(x)$ describes a Boltzmann distribution $V(x) = U(x)/(k_B\theta)$ at a low temperature θ), a global approximation of $\rho(x)$ is the Gaussian mixture

$$\rho(x) \approx \sum_{\alpha=1}^K \frac{\mathcal{N}_\alpha}{\mathcal{N}} e^{-V(x_\alpha)} \rho^{[\alpha]}(x) =: \sum_{\alpha=1}^K w_\alpha \rho^{[\alpha]}(x) \quad (3.83)$$

where $w_\alpha = e^{-V(x_\alpha)} \mathcal{N}_\alpha / \mathcal{N}$ are constants that weight the local Gaussian distributions, and where $\mathcal{N} \approx \sum_{\gamma=1}^K e^{-V(x_\gamma)} \mathcal{N}_\gamma$.

Equation (3.83) can be used to approximately evaluate any expectation value. In particular, the probability of being in well α (i.e. around x_α) is given by

$$P(x \in \text{well } \alpha) = \mathbb{E}[\chi_\alpha] = \int_{-\infty}^{\infty} dx \chi_\alpha(x) \rho(x) \approx \sum_{\beta=1}^K w_\beta \int_{-\infty}^{\infty} dx \chi_\alpha(x) \rho^{[\beta]}(x) \quad (3.84)$$

$$\approx w_\alpha \int_{-\infty}^{\infty} dx \rho^{[\alpha]}(x) = w_\alpha = \frac{e^{-V(x_\alpha)} \mathcal{N}_\alpha}{\sum_{\gamma=1}^L e^{-V(x_\gamma)} \mathcal{N}_\gamma}, \quad (3.85)$$

where the indicator function $\chi_\alpha(x)$ is 1 if x is in well α and zero otherwise, and where we assume that the potential wells of $V(x)$ are well-separated so that $\chi_\alpha(x) \rho^{[\beta]}(x)$ is negligibly small whenever $\alpha \neq \beta$.

In the following we apply the same steps as above to the case of the transition path ensemble (TPE). As we are considering Gaussian approximations of probability distributions over infinite-dimensional functional spaces, the mathematical sophistication required is higher, but the intuition remains identical to the above one-dimensional example. In Sec. II.A we derive the local Gaussian approximation for path-probability measures around an instanton (which is based on a second-order functional Taylor approximation), which we in Sec. II.B combine to a Gaussian mixture approximation of the TPE. In Sec. II.D we derive the method we use to calculate the normalisation constants for functional Gaussians (i.e. the infinite-dimensional equivalent of the \mathcal{N}_α from the one-dimensional example above). We put Sec. II.D last as it is a technical result, and is not required to understand the rest of the subsections. In Sec. II.C we use the Gaussian mixture to derive an approximate expression for transition pathway probabilities, which proceeds analogous to the calculation Eq. (3.85).

3.3.6 The quadratic expansion of the Onsager-Machlup action

Here we describe how to formally construct the Gaussian expansion around a given reference path. The variational expansion of the Onsager-Machlup action

$$S_{\text{OM}}[\mathbf{x}(t)] = \int_0^T L(\mathbf{x}(t), \dot{\mathbf{x}}(t)) dt \quad (3.86)$$

$$L(\mathbf{x}, \dot{\mathbf{x}}) = \frac{\beta}{4\mu} |\dot{\mathbf{x}} - \mathbf{F}|^2 + \frac{\mu}{2} \nabla \cdot \mathbf{F}$$

where $\beta = 1/k_B\theta$ is the inverse temperature, is given by

$$S_{\text{OM}}[\bar{\mathbf{x}} + \delta\mathbf{x}] = S_{\text{OM}}[\bar{\mathbf{x}}] + J[\delta\mathbf{x}] + \frac{1}{2} H[\delta\mathbf{x}] + O(\delta\mathbf{x}^3) \quad (3.87)$$

to second order around a reference path $\bar{\mathbf{x}}(t)$, where

$$J[\delta\mathbf{x}] = \int_0^T \left\{ \frac{\partial L}{\partial \mathbf{x}}(\bar{\mathbf{x}}, \dot{\bar{\mathbf{x}}}) \cdot \delta\mathbf{x} + \frac{\partial L}{\partial \dot{\mathbf{x}}}(\bar{\mathbf{x}}, \dot{\bar{\mathbf{x}}}) \cdot \delta\dot{\mathbf{x}} \right\} dt \quad (3.88)$$

$$H[\delta\mathbf{x}] = \int_0^T \left\{ \delta\mathbf{x} \cdot \frac{\partial^2 L}{\partial \mathbf{x} \partial \mathbf{x}}(\bar{\mathbf{x}}, \dot{\bar{\mathbf{x}}}) \cdot \delta\mathbf{x} + 2 \delta\mathbf{x} \cdot \frac{\partial^2 L}{\partial \mathbf{x} \partial \dot{\mathbf{x}}}(\bar{\mathbf{x}}, \dot{\bar{\mathbf{x}}}) \cdot \delta\dot{\mathbf{x}} + \delta\dot{\mathbf{x}} \cdot \frac{\partial^2 L}{\partial \dot{\mathbf{x}} \partial \dot{\mathbf{x}}}(\bar{\mathbf{x}}, \dot{\bar{\mathbf{x}}}) \cdot \delta\dot{\mathbf{x}} \right\} dt. \quad (3.89)$$

In the following we will suppress the arguments of the derivatives of the Lagrangian. We will now recast Eq. (3.87) in terms of self-adjoint operators using integration-by-parts and $\delta\mathbf{x}(0) = \delta\mathbf{x}(T) = 0$. We also note that $\langle \mathbf{f}, P \frac{d}{dt} \mathbf{g} \rangle = -\langle \frac{d}{dt} (P^T \mathbf{f}), \mathbf{g} \rangle$, for any matrix function $P(t) \in \mathbb{R}^{d \times d}$, and where $\langle \mathbf{f}, \mathbf{g} \rangle = \sum_i \int_0^T f_i(t) g_i(t) dt$, which we use to symmetrise the second term in Eq. (3.89). We get

$$S_{OM}[\bar{\mathbf{x}} + \delta\mathbf{x}] = S_{OM}[\bar{\mathbf{x}}(t)] + \langle \mathbf{j}, \delta\mathbf{x} \rangle + \frac{1}{2} \langle \delta\mathbf{x}, \mathcal{H}\delta\mathbf{x} \rangle + O(\delta\mathbf{x}^3) \quad (3.90)$$

where

$$\mathbf{j}(t) = \frac{\partial L}{\partial \mathbf{x}} - \frac{d}{dt} \frac{\partial L}{\partial \dot{\mathbf{x}}} \quad (3.91)$$

$$\mathcal{H} = -\frac{\beta}{2\mu} \frac{d^2}{dt^2} + 2A(t) \frac{d}{dt} + B(t) \quad (3.92)$$

and $A_{ij}(t) = \frac{\partial^2 L}{\partial x_{[i} \partial \dot{x}_{j]}}$, $B_{ij}(t) = \frac{\partial^2 L}{\partial x_i \partial x_j} - \frac{d}{dt} \frac{\partial^2 L}{\partial x_j \partial \dot{x}_i}$, where closed brackets indicate an anti-symmetrisation over indices. By completing the square, we find that Eq. (3.90) defines a Gaussian process $\delta\mathbf{x} \sim \mathcal{N}(-\mathcal{H}^{-1}\mathbf{j}, \mathcal{H}^{-1})$, which describes the quadratic fluctuations around $\bar{\mathbf{x}}$. In the sense of [96], the path-space density of the Gaussian process is $\rho[\delta\mathbf{x}] \propto \exp(-\frac{1}{2} \langle \delta\mathbf{x} + \mathcal{H}^{-1}\mathbf{j}, \mathcal{H}(\delta\mathbf{x} + \mathcal{H}^{-1}\mathbf{j}) \rangle)$. If the reference path solves the Euler-Lagrange equation Eq. (3.109), then $\mathbf{j} = 0$ and the Gaussian process simplifies to $\rho[\delta\mathbf{x}] \propto \exp(-\frac{1}{2} \langle \delta\mathbf{x}, \mathcal{H}\delta\mathbf{x} \rangle)$.

For systems with gradient dynamics $\mathbf{F} = -\nabla U$, the asymmetric term in Eq. (3.92) vanishes, and the form of the operator simplifies to

$$\mathcal{H} = -\frac{\beta}{2\mu} \frac{d^2}{dt^2} + B(t) \quad (3.93)$$

3.3.7 The Gaussian mixture approximation

We now use the quadratic expansion of the Onsager-Machlup action to construct an approximate probability measure over the TPE. Let $\mathbf{x}^{[\alpha]}, \alpha = 1, \dots, K$ be the local instantons of a given Langevin system. For each local instanton we can define a Gaussian measure $\mathbb{P}^{[\alpha]}$ with mean $\mathbf{x}^{[\alpha]}$ and precision $H^{[\alpha]}$. Although the measure $\mathbb{P}^{[\alpha]}$ is defined over the space of C^0 continuous paths, the distribution can be characterised via a density on the Hilbert space of C^2 paths as $\rho^{[\alpha]}[\mathbf{x}] \propto \exp(-\langle \mathbf{x} - \mathbf{x}^{[\alpha]}, \mathcal{H}^{[\alpha]}(\mathbf{x} - \mathbf{x}^{[\alpha]}) \rangle)$ [96, 47].

To approximate the TPE distribution, we construct the mixed Gaussian density $\bar{\rho}[\mathbf{x}] \propto \sum_{\alpha=1}^K e^{-S_{\text{OM}}[\mathbf{x}^{[\alpha]}]} \rho^{[\alpha]}[\mathbf{x}]$. The normalisation constant $\mathcal{N}^{[\alpha]}$ of the densities $\rho^{[\alpha]}[\mathbf{x}]$ are not finite, but can be expressed as ratios with respect to the normalisation of the reference Wiener measure \mathcal{N}^W . This ratio can be shown to be equal to [135, 48]

$$\mathcal{Z}^{[\alpha]} := \frac{\mathcal{N}^{[\alpha]}}{\mathcal{N}^W} = \left(\frac{\det[\mathcal{H}^{[\alpha]}]}{\det[-\frac{\beta}{2\mu} \frac{d^2}{dt^2}]} \right)^{-1/2} \quad (3.94)$$

where the RHS can be computed using the results in the Sec. II-C. Using Eq. (3.94) we can write down the approximation of the TPE as the Gaussian mixture [81]

$$\bar{\mathbb{P}} = \sum_{\alpha=1}^K w_{\alpha} \mathbb{P}^{[\alpha]} \quad (3.95)$$

where $w_{\alpha} = e^{-S_{\text{OM}}[\mathbf{x}^{[\alpha]}]} \mathcal{Z}^{[\alpha]} / \sum_{\gamma=1}^K e^{-S_{\text{OM}}[\mathbf{x}^{[\gamma]}]} \mathcal{Z}^{[\gamma]}$.

3.3.8 Approximations of transition channel probabilities

We now derive an approximation to the probabilities of reactive pathways using the Gaussian mixture approximation of the TPE. Let $E_{\alpha} \subset C^0, \alpha = 1, \dots, K$, which are disjoint open sets in the TPE, be the K reactive pathways under consideration. We define the observable

$$P^{[\alpha]}(\theta, T) = \mathbb{P}[E_{\alpha}] \quad (3.96)$$

which is the probability of observing a path in E_{α} . In low temperatures we can assume that $\mathbb{P}(\cup_{\alpha} E_{\alpha}) \approx 1$, i.e. approximately all stochastic paths transition via one of the reactive pathways. Furthermore, we assume that $\mathbf{x}^{[\alpha]} \in E_{\alpha}$ and that $\mathbb{P}^{[\alpha]}(\cup_{\gamma \neq \alpha} E_{\gamma}) \approx 0$. The latter assumption means that each measure $\mathbb{P}^{[\alpha]}$ is concentrated on E_{α} and lacks support on the other reactive pathways. Under these assumptions we can approximate $P^{[\alpha]}(\theta, T)$ as

$$P^{[\alpha]}(\theta, T) \approx P_G^{[\alpha]}(\theta, T) \equiv w_{\alpha}. \quad (3.97)$$

3.3.9 Calculation of the Gaussian normalisation constants

The regularised normalisation constants of Gaussians defined on functional spaces can be found by computing the determinants of their covariance operators. Equivalently, the normalisation can be found by computing the determinant of their precision operator, which is the inverse of the covariance operator. As for finite-dimensional linear operators, determinants of differential operators can be found by computing their eigenvalues, but this is in general a prohibitively expensive computational procedure. In the following we show that functional determinants, acting on d -dimensional vectors, can be found by

solving d initial value ODEs.

Let the linear operators

$$\mathcal{L} = \frac{d}{dt} \left(P \frac{d}{dt} \right) - R \quad (3.98)$$

and

$$\mathcal{L}_0 = \frac{d}{dt} \left(P \frac{d}{dt} \right) \quad (3.99)$$

be defined for $0 \leq t \leq T$, and where $P(t) \in \mathbb{R}^{d \times d}$ is a positive-definite matrix function and $R(t) \in \mathbb{R}^{d \times d}$ is a matrix function. Let $\gamma^{(k)}$ and $\mathbf{u}^{(k)}(t; \alpha)$ be the eigenvalues and eigenfunctions of \mathcal{L} , which are solutions to the boundary value problem

$$\mathcal{L}\mathbf{u}^{(k)}(t) = \gamma^{(k)}\mathbf{u}^{(k)}(t) \quad (3.100)$$

where $\mathbf{u}^{(k)}(0) = \mathbf{u}^{(k)}(T) = 0$. Similarly, let $\mathbf{u}_0^{(k)}(t)$ and $\gamma_0^{(k)}$ be the eigenfunctions and eigenvalues of \mathcal{L}_0 . Then the *functional determinant* of \mathcal{L} is defined in regularised form as

$$\frac{\det \mathcal{L}}{\det \mathcal{L}_0} = \prod_{k=1}^{\infty} \frac{\gamma^{(k)}}{\gamma_0^{(k)}}. \quad (3.101)$$

As the spectrum of Eq. (3.98) is unknown, and numerically expensive to compute, a much more efficient way of computing Eq. (3.101) is via the Gelfand-Yaglom theorem (GYT) [79, 135, 48]. The GYT states that the functional determinant can be expressed as

$$\left| \frac{\det \mathcal{L}}{\det \mathcal{L}_0} \right| = \left| \frac{\det [Y(T)]}{\det [Y_0(T)]} \right| \quad (3.102)$$

where $Y(t) \in \mathbb{R}^{d \times x}$ with components $Y_{ij}(t) = y_i^{(j)}(t)$, where the $\mathbf{y}^{(j)}(t)$ are solutions to the d second-order ODEs with initial conditions

$$\mathcal{L}\mathbf{y}^{(j)}(t) = 0 \quad (3.103)$$

$$\mathbf{y}^{(j)}(0) = 0 \quad (3.104)$$

$$\frac{d}{dt} y_i^{(j)}(0) = \delta_{ij}. \quad (3.105)$$

and where the matrix $Y_0(t) \in \mathbb{R}^{d \times d}$ is defined similarly, but with \mathcal{L} in Eq. (3.103) replaced with \mathcal{L}_0 .

In the case of gradient dynamics, where \mathcal{H} takes the form in Eq. (3.93), the GYT can be readily applied by setting $P(t) = -\frac{\beta}{2\mu} I_d$ and $R(t) = -B(t)$, where I_d is the identity matrix. We now present a generalisation of the GYT that allows for linear operators of the form

$$\mathcal{L} = \frac{d^2}{dt^2} + U \frac{d}{dt} + R \quad (3.106)$$

where $0 \leq t \leq T$, and where $U(t), R(t) \in \mathbb{R}^{d \times d}$ are matrix functions, which then makes the GYT applicable for systems non-gradient dynamics, with precision operators of the form Eq. (3.92).

We define the linear operator \mathcal{G} which acts on vector functions as

$$\mathcal{G}\mathbf{y} = G\mathbf{y}$$

where $G(t)$ is a matrix function that solves the equation

$$\dot{G} = -\frac{1}{2}UG, \quad (3.107)$$

then the linear operator

$$\tilde{\mathcal{L}} = \mathcal{G}^{-1}\mathcal{L}\mathcal{G} = \frac{d}{dt^2} + G^{-1} \left(R - \frac{1}{2}\dot{U} - \frac{1}{4}U^2 \right) G \quad (3.108)$$

is of the form Eq. (3.98) and $\det \tilde{\mathcal{L}}$ can then be computed using the GYT. As for any two operators \mathcal{A} and \mathcal{B} , we have that $\det \mathcal{A}\mathcal{B} = \det \mathcal{A} \det \mathcal{B}$, and $\det \mathcal{A}^{-1} = 1/\det \mathcal{A}$, and we therefore have that $\det \mathcal{L} = \det \tilde{\mathcal{L}}$. The functional determinant $\det \mathcal{L}$ can thus be computed by first solving Eq. (3.107), constructing $\tilde{\mathcal{L}}$ using Eq. (3.108), and finally using the GYT to compute $\det \tilde{\mathcal{L}}$.

The above theorem can be applied to Eq. (3.92) by setting $P(t) = -\frac{\beta}{2\mu}I_d$, $U = -\frac{4\mu}{\beta}A$ and $R = B$. Using the GYT, and its generalisation presented here, the problem of computing the normalisation constants of Gaussian distributions in functional spaces is reduced to solving d initial value problems.

The TPE is characterized by its corresponding probability measure \mathbb{P} on the space of all continuous transition paths. In the path-integral formalism, this measure is represented by a formal density $\rho[\mathbf{x}(t)] = \exp(-S_{\text{OM}}[\mathbf{x}(t)])$ with respect to a fictitious infinite-dimensional Lebesgue measure [200], with the Onsager-Machlup action [163, 10, 114]

$$S_{\text{OM}}[\mathbf{x}(t)] = \int_0^T \left(\frac{\beta}{4\mu} |\dot{\mathbf{x}} - \mathbf{F}|^2 + \frac{\mu}{2} \nabla \cdot \mathbf{F} \right) dt. \quad (3.109)$$

The variational minima of the action Eq. (3.109) have physical relevance. Namely, because the first term in Eq. (3.109) is inversely proportional to the temperature, at sufficiently low temperature the formal probability density ρ is dominated by paths that aggregate around the variational minima [209, 199, 94]. These variational minima are called the local instantons of the Onsager-Machlup action, and we denote them by $\mathbf{x}^{[\alpha]}(t; \theta, T)$, with

$\alpha = 1, \dots, K$, $\mathbf{x}^{[\alpha]}(0; \theta, T) = \mathbf{x}_0$ and $\mathbf{x}^{[\alpha]}(T; \theta, T) = \mathbf{x}_T$. The arguments of the local instantons indicate that they depend on the temperature and the duration of the path (we suppress these arguments below). For the potential U from Fig. 4.1 (a) we find $K = 2$ local instantons $\mathbf{x}^{[1]} \equiv \mathbf{x}^+$, $\mathbf{x}^{[2]} \equiv \mathbf{x}^-$, going along the upper and lower semi-circles, respectively.

By performing a quadratic functional Taylor expansion of Eq. (3.109) around the α -th local instanton [56, 78, 35],

$$S_{\text{OM}}[\mathbf{x}(t)] \approx S_{\text{OM}}[\mathbf{x}^{[\alpha]}(t)] + \frac{1}{2} \langle \delta \mathbf{x}, \mathcal{H}^{[\alpha]} \delta \mathbf{x} \rangle, \quad (3.110)$$

where $\mathcal{H}^{[\alpha]}$ is a self-adjoint linear differential operator, $\delta \mathbf{x} = \mathbf{x} - \mathbf{x}^{[\alpha]}$ and $\langle \mathbf{f}, \mathbf{g} \rangle = \sum_i \int_0^T f_i(t) g_i(t) dt$, we can formally define a Gaussian measure $\mathbb{P}^{[\alpha]}$ with mean $\mathbf{x}^{[\alpha]}$, precision $\mathcal{H}^{[\alpha]}$, and regularised normalisation constant $\mathcal{Z}^{[\alpha]}$, in the space of paths. The resulting K local approximators of the measure can be combined into a Gaussian mixture approximation [81] of the whole TPE

$$\mathbb{P} \approx \bar{\mathbb{P}} \equiv \sum_{\alpha=1}^K w_{\alpha} \mathbb{P}^{[\alpha]}, \quad (3.111)$$

where the weights $w_{\alpha} = e^{-S_{\text{OM}}[\mathbf{x}^{[\alpha]}]} \mathcal{Z}^{[\alpha]} / \sum_{\gamma=1}^K e^{-S_{\text{OM}}[\mathbf{x}^{[\gamma]}]} \mathcal{Z}^{[\gamma]}$ satisfy $\sum_{\alpha=1}^K w_{\alpha} = 1$, see the SI [1] for more details. Equation (3.111) is the infinite-dimensional analogue to approximating a finite-dimensional multimodal probability density by a sum of Gaussians, with one term for each local maximum of the probability density.

In the numerical verificaiton, show comparison of teleporter with switch and also with biased teleporters.

3.4 Conclusion

Restate main differences between TPS

Field stuff here

Mention multi-level stuff and include Paul

Chapter 4

Diffusivity dependence of transition paths

4.1 Introduction

The fluctuating dynamics of many physical, chemical and biological systems are commonly modelled by stochastic differential equations expressed in Langevin or Itô forms [119, 71, 183, 14]. In such systems it is often of great interest to identify the typical pathways that stochastic paths take to transition from an initial to a final state, as for example in the nucleation of solids, the conformational changes in biomolecules, or shifts in ecological balance [59, 45, 74, 142, 217, 111, 166, 157, 134]. Typically, such transition paths cluster around multiple pathways in the space of configurations and the relative probability of one or the other of these pathways depends on the drift, the diffusivity, and the duration allowed for the transition to take place [163, 10, 114, 113]. As transitions are often rare events, direct simulations are not always practical and other means, analytical or numerical, are required to study them. Methods that allow for a full exploration of the space of transition pathways in stochastic dynamical systems, then, are of substantial theoretical and practical importance.

The theory of large deviations [209, 199, 94, 8] provides an analytical method for obtaining transition pathways - instantons - in regimes dominated by the drift and for very long durations of path. Experimental systems, however, are typically not in a regime where the diffusivity is asymptotically low and durations are asymptotically long [83]. While the relevance of including finite-temperature fluctuations around the instanton [79] is increasingly recognized [155, 36, 138], the physical implications of these fluctuations are far from being understood.

In this chapter, we show that the competition between drift and diffusion in transition pathways can be studied using semi-classical expansions of the path measure of the stochastic dynamics. We use a mixture of Gaussian measures to approximate the path

measure around its local instantons. This allows us to demarcate and transcend the boundaries of the low diffusivity regime. We demonstrate this explicitly for a two-dimensional overdamped mechanical system, with both conservative and non-conservative forces. For this system we uncover a counterintuitive phenomenon where typical transition paths do not concentrate around the most probable path, even at low-to-intermediate diffusivities where the Gaussian approximation is still valid. To validate our results numerically, we construct a Markov Chain Monte Carlo (MCMC) method that allows for simultaneous exploration of multiple transition pathways. We find excellent agreement between the semi-classical expansion and numerical results for a large range of diffusivities and path durations. We now detail our results.

4.2 The transition path ensemble

We consider the stochastic process generated by the d -dimensional overdamped Langevin equation, expressed in Itô form as

$$d\mathbf{X} = \mu\mathbf{F}dt + \sqrt{2D}d\mathbf{W}. \quad (4.1)$$

This represents the stochastic displacement $d\mathbf{X}$ in a time interval dt of a particle with coordinate \mathbf{X} subject to a force field \mathbf{F} and Brownian displacements $\sigma d\mathbf{W}$, where \mathbf{W} is the Wiener process. The particle mobility is μ , the diffusion constant is $D = \mu/\beta$, and the temperature is θ with $\beta^{-1} = k_B\theta$, and k_B the Boltzmann constant. We are interested in realisations $\mathbf{X}(t)$ of Eq. (4.1) that are of duration T and have fixed terminii $\mathbf{X}(0) = \mathbf{x}_0$ and $\mathbf{X}(T) = \mathbf{x}_T$. These trajectories form a set of continuous paths that we call the transition path ensemble (TPE). While in the following we investigate the temperature-dependence of the TPE for specific model systems, the methods we develop are general.

4.3 Model system

We consider the motion of a particle in $d = 2$ dimensions in a potential force field $\mathbf{F} = -\nabla U(\mathbf{x})$; below we will also add a non-conservative force \mathbf{F}^a . The potential $U(\mathbf{x})$ is a deformed Mexican hat, with a maximum at the origin and a manifold of minima on the circle of radius L around the origin, see Fig. 4.1 (a) for a plot of U and the SI for the explicit parametrisation [1]. We consider the TPE for paths of duration T which start at $\mathbf{x}_0 = (-L, 0)$ and end at $\mathbf{x}_T = (L, 0)$. This ensemble features two competing transition channels, namely along the upper and lower semi-circle, which we denote by Γ^+ and Γ^- ; by design the potential along Γ^+ is narrower as compared to along Γ^- .

4.4 Transition channel probabilities

For temperature θ and path duration T we define $P^{[\alpha]}(\theta, T)$ as the probability of observing a transition path travelling via the α -th channel, i.e. close to the α -th instanton. Using Eq. (3.111) we approximate $P^{[\alpha]}(\theta, T)$ as

$$P^{[\alpha]}(\theta, T) \approx P_G^{[\alpha]}(\theta, T) \equiv \frac{e^{-S_{\text{OM}}[\mathbf{x}^{[\alpha]}]} \mathcal{Z}^{[\alpha]}}{\sum_{\gamma=1}^K e^{-S_{\text{OM}}[\mathbf{x}^{[\gamma]}]} \mathcal{Z}^{[\gamma]}}. \quad (4.2)$$

According to Eq. (4.2) the relative channel probabilities are determined by an interplay between the instanton probabilities, as quantified by $e^{-S_{\text{OM}}[\mathbf{x}^{[\alpha]}]}$, and the sizes of the Gaussian fluctuations around the local instantons, $\mathcal{Z}^{[\alpha]}$. It is instructive to compare this ratio with another estimator $P_I^{[\alpha]}(\theta, T) = e^{-S_{\text{OM}}[\mathbf{x}^{[\alpha]}]} / \sum_{\gamma} e^{-S_{\text{OM}}[\mathbf{x}^{[\gamma]}]}$, in which only the instanton probabilities are retained.

To use Eq. (4.2) in practice, we retrieve the instantons $\mathbf{x}^{[\alpha]}$ using a Ritz variational method presented in [123, 83]. We subsequently evaluate the regularised normalisation constants $\mathcal{Z}^{[\alpha]}$ using the Gelfand-Yaglom theorem [48, 79, 135, 35], as well as a generalisation thereof to non-gradient dynamics which we provide in the SI [1].

4.5 Numerical experiments

To infer the range of validity of our semi-analytical approximation it is necessary to compare Eq. (4.2) with numerical simulations. In parameter regimes where transitions are very rare, it is not feasible to sample the TPE using direct simulations. We therefore numerically probe the TPE using a MCMC algorithm built on the *preconditioned Crank-Nicholson algorithm* (pCN) [39, 13, 100], as detailed in the SI [1]. In essence, we approximate the function space of all transition paths by a finite sum of basis functions [125, 121, 137], and perform a random walk on the resulting finite-dimensional space of basis coefficients; the random walk is designed such that the resulting transition path samples are distributed according to the TPE we seek to probe.

A general shortcoming of MCMC methods and also other transition path sampling techniques [18, 16, 42, 41, 66] is that when the distribution to be sampled is multimodal with regions of low probability in between the modes, it may take prohibitively long to obtain converged results. For overdamped Langevin dynamics Eq. (4.1), this corresponds to medium-to-low temperature regimes in systems with competing transition pathways, where the TPE concentrates around the local instantons. One way to overcome this issue is to use replica exchange [66], which requires running several instances of the MCMC algorithm at varying temperatures. Here we introduce a modification of the pCN-MCMC that operates only at one temperature, which we call the *Teleporter MCMC* (TMC), which

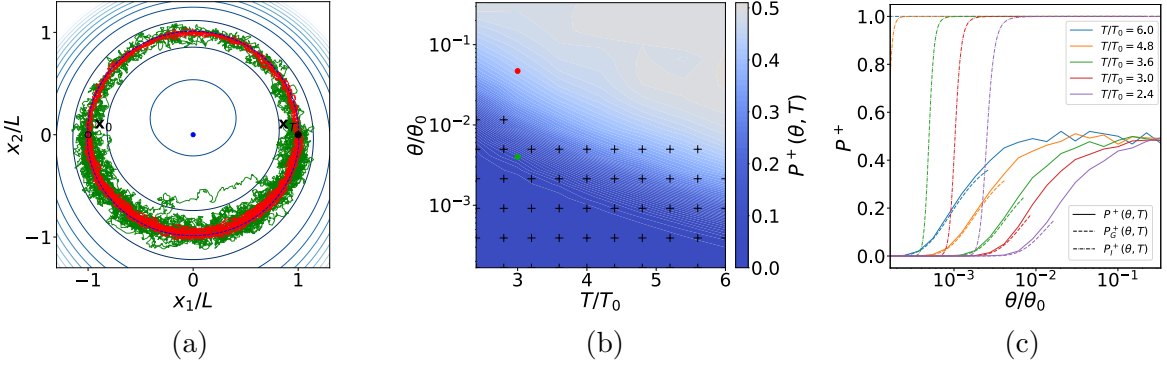


Figure 4.1: Diffusivity-dependence of the transition path ensemble for the conservative model system. Panel (a) shows 50 stochastic trajectories sampled using the TMC method (see text) for overdamped dynamics in the potential $U(x)$ [1]. The dashed blue (green) lines are upper (lower) instantons between initial (circle, \mathbf{x}_0) and final (filled circle, \mathbf{x}_T) points. Upper and lower channels are equally populated at temperature $\theta = 0.047\theta_0$ (green) but the lower channel is preferred at the lower temperature $\theta = 0.004\theta_0$ (red). Trajectories of duration $T = 3T_0$ are sampled with $N = 200(T/T_0)$ modes. Panel (b) is a pseudocolor plot quantifying the variation of the upper and lower channel probabilities with temperature and duration, as obtained from TMC. The plus signs show regions where the Gaussian mixture approximation P_G^+ , defined in Eq. (5), is within a 5% margin of error of the simulated value. The red and green dots correspond to the same color-coded simulations in panel (a). Panel (c) shows a comparison between the TMC, Gaussian mixture and instanton approximations to the upper channel probability as function of temperature for fixed durations of path.

utilises the Gaussian mixture approximation of the TPE. At each step of the TMC there is a small probability to jump between the transition channels, which accelerates mixing between them. We provide a detailed description of the algorithm in the SI [1].

4.6 Results

We now consider the transition behavior of the 2D system depicted in Fig. 4.1 (a). For a range of temperatures θ and total transition times T we first generate ensembles of 10^8 sample transition paths per tuple (θ, T) using the TMC. Let $\tau_D(\theta) = L^2/(\mu k_B \theta)$, which is the diffusive time-scale at temperature θ . We also introduce fixed reference temperature and time-scales $\theta_0 = U_0/k_B$ and $T_0 = \tau_D(\theta_0)$, where U_0 is the energetic well-depth of the potential. Our parameter range is such that $T \ll \tau_D$, for each temperature θ in the range considered. Each sampled ensemble thus describes a rare transition event. For a total transition time $T/T_0 = 3$, and for each of the two temperatures $\theta/\theta_0 = 0.047$ and $\theta/\theta_0 = 0.004$, we show 50 randomly chosen TMC sample paths in Fig. 4.1 (a). We observe that while for the higher temperature the paths are evenly distributed between the two channels, for the lower temperature the lower channel is preferred. In Fig. 4.1 (b) we show TMC results for $P^+(\theta, T) \equiv P^{[1]}(\theta, T)$, the probability of the upper channel, as a function of both θ and T . Consistent with the $\theta/\theta_0 = 0.047$ data from Fig. 4.1 (a), we

observe that for large enough temperature $P^+(\theta, T) \approx 1/2$ (white region), so that upper and lower channel are equally probable. That at large temperature the asymmetry in U becomes irrelevant for the TPE is expected, as in this limit the random force in Eq. (4.1) dominates over the deterministic force. As θ is decreased, the channel around Γ^- becomes dominant, so that $P^+(\theta, T) \rightarrow 0$ (blue region in Fig. 4.1 (b), c.f. $\theta/\theta_0 = 0.004$ data in subplot (a)). The exact temperature at which the crossover from the diffusivity-dominated regime to the drift-dominated regime occurs decreases with increasing T ; this is clearly seen in Fig. 4.1 (c) where vertical sections of subplot (b) are shown for several values of T .

We now compare our numerical TMC results for $P^+(\theta, T)$ with the Gaussian mixture approximation $P_G^+(\theta, T) \equiv P_G^{[1]}(\theta, T)$, defined in Eq. (4.2). Figure 4.1 (b) shows that this approximation is valid in the low-temperature regime (plus signs). This is consistent with the assumptions underlying the Gaussian approximation, as we expect the probability distribution in path space to be dominated by the neighborhoods of the local instantons only for sufficiently low temperature. As Fig. 4.1 (c) shows, $P_G^+(\theta, T)$ quantitatively captures the beginning of the crossover from drift-dominated to diffusivity-dominated transition behaviour for all values of T considered.

For capturing this θ -dependent crossover, the prefactors $\mathcal{Z}^+ = \mathcal{Z}^{[1]}$, $\mathcal{Z}^- = \mathcal{Z}^{[2]}$ in Eq. (4.2) are essential. This becomes apparent by considering $P_I^+(\theta, T)$, which only depends on the relative probabilities of the two local instantons. In Fig. 4.1 (c) we see that for high enough temperatures $P_I^+(\theta, T) \approx 1$, meaning $S_{\text{OM}}[\mathbf{x}^+(t)] < S_{\text{OM}}[\mathbf{x}^-(t)]$ [3]. This limit is understood by comparing the two terms in the action Eq. (3.109). While the first term scales as $1/\theta$, the second term is independent of θ ; for fixed T and large enough θ the second term thus dominates the action. This second term is smaller for the channel around Γ^+ than for the channel around Γ^- , because the former channel is narrower leading to a smaller value of $\nabla \cdot \mathbf{F}$. As θ is decreased for fixed T the first term in Eq. (3.109) becomes dominant. Figure 4.1 (c) shows that this leads to a crossover to $P_I^+(\theta, T) \approx 0$, meaning \mathbf{x}^- becomes more probable than \mathbf{x}^+ . While this low-temperature limit is consistent with the numerical results, the temperature at which we observe the crossover in $P_I^+(\theta, T)$ is smaller as compared to $P^+(\theta, T)$. For example, we see in Fig. 4.1 (c) that for $T/T_0 = 2.4$ the crossover of $P_I^+(\theta, T)$ is at $\theta/\theta_0 < 10^{-2}$, whereas the crossover for $P^+(\theta, T)$ occurs at $\theta/\theta_0 > 10^{-2}$. In particular this implies that for $\theta/\theta_0 = 10^{-2}$ the most probable path goes along Γ^+ , while most transition paths go along Γ^- . This highlights that even at intermediate-to-low temperatures, where the Gaussian mixture approximation Eq. (4.2) is already valid, the probabilities of the local instantons alone are insufficient to obtain the actual transition behaviour. Instead it is the prefactors \mathcal{Z}^\pm in Eq. (4.2) that dominate the crossover behaviour in Fig. 4.1 (b); these Gaussian normalisation constants are, in a sense, an entropic contribution, as they measure the effective volume in path space of the support around the respective local instanton. Even though for $T/T_0 = 2.4$, $\theta/\theta_0 = 10^{-2}$

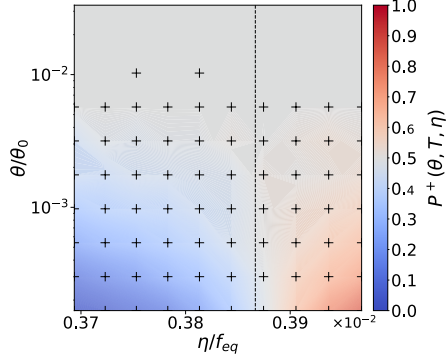


Figure 4.2: Diffusivity-dependence of the transition path ensemble for the non-conservative model system. Pseudocolour plot of the probability of the upper channel, $P^+(\theta, T, \eta)$, for the non-gradient system with $T/T_0 = 3$, as a function of the temperature θ and the circular force-strength η . The black plus signs show regions where the variational approximation $P_G^+(\theta, T, \eta)$, defined in Eq. (4.2), is within a 5% margin of error of the simulated value. The dashed line shows the crossover force strength $\eta_c/f_{\text{eq}} \approx 0.00387$, where f_{eq} is the characteristic strength of the gradient force [1].

the instanton \mathbf{x}^+ is more probable than \mathbf{x}^- , this is more than offset by the larger number of paths that behave similar to \mathbf{x}^- . As we discuss in the SI [1], the prefactors \mathcal{Z}^\pm remain relevant even in the Freidlin-Wentzell-Graham limit [209, 94] of vanishing temperature and infinite path duration.

For non-gradient forms of the drift, the prefactors \mathcal{Z}^\pm can also drive the crossover behaviour of the system, as we show now by adding a force of strength η that acts perpendicular to the radius vector in the clockwise direction. For positive force strength η , this non-conservative force biases towards the upper channel Γ^+ . In Fig. 4.2 we show numerical results for $P^+(\theta, T, \eta)$ as a function of η and θ for $T/T_0 = 3$. For small $\eta/f_{\text{eq}} \rightarrow 0$, with f_{eq} the characteristic strength of the gradient force [1], we recover the results from Fig. 4.1 (b), (c). Thus at small but finite temperature the dominant transition channel is the one where particles travel against the weak non-conservative force. As η is increased to $\eta_c/f_{\text{eq}} \approx 0.00387$, we observe a crossover from Γ^- -channel dominated transitions to Γ^+ -channel dominated transitions in the low-temperature regime. This switch is also captured by the Gaussian approximation (plus signs in Fig. 4.2). On the other hand, throughout the parameter regime considered in Fig. 4.2, we find that $P_I^+(\theta, T, \eta) \approx 1$, meaning that the local instanton \mathbf{x}^+ is always more probable than \mathbf{x}^- for finite η . This again highlights the relevance of considering Gaussian fluctuations around the instantons for determining the dominant transition pathway.

4.7 Conclusion

For a system with two competing transition pathways, we have studied how the dominant transition pathway depends on both the temperature and the total duration. To quantify the relative importance of the competing pathways, we have constructed semi-analytical approximators which are valid in the low-to-intermediate temperature regime. We have validated our approximators via comparison with a continuous-time MCMC method that is dimensionally robust and efficiently samples systems with multiple reactive pathways.

Our results show that even in the low-to-intermediate temperature regime the global instanton, or most probable path, itself is not sufficient to determine the dominant transition pathway. Rather, it is vital that fluctuations around this path be incorporated. This has a simple one-dimensional equivalent: For a probability density $\rho(x) \sim \exp(-V(x))$ for some potential $V(x)$ with relative minima x_α , the probabilistically most relevant minimum is not the global one, but that with the largest well probability, i.e. the x_α that maximizes $P(\text{well around } x_\alpha) \sim e^{-V(x_\alpha)} \sqrt{2\pi/V''(x_\alpha)}$, where we use a quadratic Taylor approximation of V around x_α . The most probable well is thus determined by an interplay of $e^{-V(x_\alpha)}$ (which corresponds to the instanton probability $e^{-S_{\text{OM}}[x^{[\alpha]}]}$) and $\sqrt{2\pi/V''(x_\alpha)}$ (which corresponds to the regularised normalisation constant $\mathcal{Z}^{[\alpha]}$).

In the present paper we consider a paradigmatic example system with two competing transition pathways. The method of instantons is an established technique in theoretical chemistry and statistical physics [50, 49, 89, 88, 189, 46, 62, 123, 105], and the method of Gaussian mixtures presented here scales as $O(d^2)$ with the number of degrees of freedom d [1]. It is therefore feasible to apply the methods we developed here to more realistic many-particle systems to study e.g. nucleation pathways [49, 140, 177] or conformational rearrangements in macromolecules [178, 66, 67?].

Our quantification here of the finite-temperature breakdown of instanton theories is important for relating such theories to experiments, which are always at finite temperatures. Our insights into path-space probability distributions for diffusive stochastic dynamics, together with our MCMC method, will therefore be valuable for going beyond the regime of asymptotically low diffusivity in both large deviations theory [209, 207, 50, 76] and the study of rare events [91].

Part II

Geometric mechanics of soft, slender matter

Chapter 5

Introduction

Something more should be said here, prefacing the geometricisation programme. Below are some notes and random scribbles.

We provide a general framework with which to derive the kinematic and dynamical equations of motion of continuum system with both internal and external degrees of freedom. For instance, the purview of continuum mechanics is the dynamics of sub-manifolds of \mathbb{E}^3 . Continuum mechanics thus considers systems where the external configuration space is \mathbb{E}^3 , but there are no internal degrees of freedom. Our framework can generalise these dynamics to settings where the point-continua have internal degrees of freedom, such as orientation or spin.

Extending the continuum mechanics analogy, we can consider a system that is a sub-manifold $M_{\text{ext}} \subset \mathbb{X}$ of some homogeneous space \mathbb{X} , corresponding to the external degrees of freedom of the system. Each point-continua M_{ext} can also have an internal configuration, which can take values in some Lie group H . When we can write $\mathbb{X} = G/H$, then the configuration of the whole system described as $M \subset G$, which includes both external and internal degrees of freedom. We call this class of system *generalised Cosserat media*. An example is that of a Cosserat rod, which is a 1-dimensional rod embedded in 3-dimensional Euclidean space, where at each material point along the rod there is attached an orthonormal frame $(\mathbf{e}_1, \mathbf{e}_2, \mathbf{e}_3)$. We thus have $\mathbb{X} = \mathbb{E}^3 = SE(3)/SO(3)$, and $H = SO(3)$, and $G = SE(3)$. We also consider the case when the total kinematic configuration space is not a Lie group.

We consider the dynamics of systems that can be described as sub-manifolds of a Lie group G . In the case where there is a natural division G/H and H , corresponding to external and internal degrees of freedom respectively, we call this class of systems *generalised Cosserat media*.

By kinematics we mean that equations of motion that upon integration ensures that the system remains within its own configuration space. By dynamics we mean that the dynamical equations of motion are, in the conservative case, Lagrangian equations of

motion for a given Lagrangian. We also generalise the dynamics to the non-conservative case.

References:

soft robotics [181, 95, 180, 24, 22, 23, 179, 210, 153]

cell membranes [129, 176]

biological tissue [187, 221]

soft matter:

active filaments [132, 133, 118?]

filaments [77, 85, 86, 84]

Many applicaitons in engineering and continuum mechanics: soils [197], polycrystalline [63] and composite materials [6], granular and powder-like materials [52, 151, 127], masonries [196], cellular [162] or porous media and foams [112], bones [168], liquid crystals [57, 87], as well as electromagnetic and ferromagnetic media [116, 167, 115]

Notation App. A

5.1 Classical Cosserat theory

Classical continuum mechanics study elastic materials as manifolds $M \subset \mathbb{E}$ of point-continua $\mathbf{x} \in M$, where $\mathbb{E} \cong \mathbb{R}^3$ is 3-dimensional Euclidean space. Points in the material have three translational degrees of freedom, and the elastic response to displacements away from the rest configuration is determined by the symmetric Cauchy stress 2-tensor $\boldsymbol{\sigma}$. The momentum transport within the continuum is given by the *Cauchy momentum equation*

$$\rho \frac{D\mathbf{v}}{Dt} = \nabla \cdot \boldsymbol{\sigma} + \mathbf{f} \quad (5.1)$$

where ρ is the mass density, \mathbf{v} is the flow velocity field, \mathbf{f} are body forces per unit volume (e.g. gravity $\mathbf{f} = \rho\mathbf{g}$), and D/Dt the material derivative. Eq. (5.1) is a non-linear PDE in three spatial dimensions and time. In the treatment of a given system, these equations of motion must thus be satisfied at each material point $\mathbf{x} \in M$ as well as obey necessary conditions at the boundaries ∂M of the body.

However, many systems have geometric properties that make them amenable to simplified treatments. Slender systems, for instance, are ‘thin’ in one or more spatial dimensions. This often makes it feasible to model slender shells in two spatial dimensions and time, and slender rods in one spatial dimension and time. In such cases the continuum configuration of the bulk can then be suitably substituted with other, model-specific, internal degrees of freedom.

The suite of models proposed by the Cosserat brothers [38] in 1909 are one of the more prominent approaches by which one can study slender materials. Their approach is

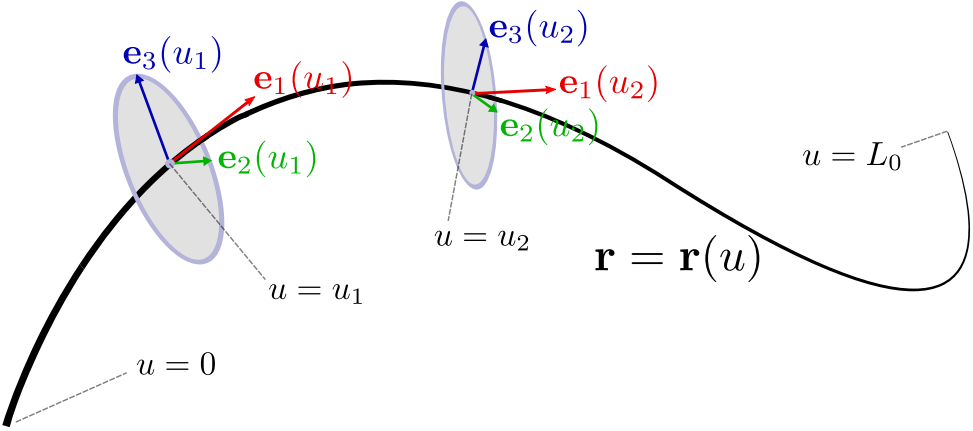
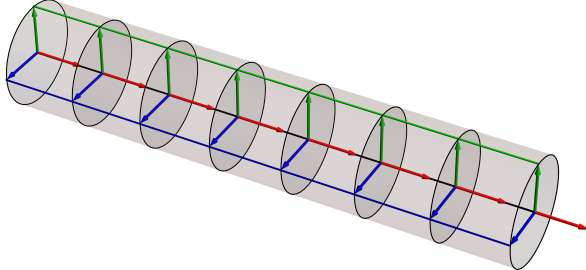


Figure 5.1: Illustration of the kinematics degrees of freedom of the Cosserat rod. The black line is the *center-line* $\mathbf{r} = \mathbf{r}(u)$ where $u \in [0, L_0]$ is the *material coordinate* along the length of the rod, where L_0 is a positive real number. When specifying constitutive dynamics, L_0 often becomes the *rest-length* of the rod. Two cross-sections at $u = u_1$ and $u = u_2$ are shown with the material frame attached $E = (\mathbf{e}_1 \ \mathbf{e}_2 \ \mathbf{e}_3)$, which are the red, green and blue arrows respectively, of which the latter two are the *directors* of the rod. Note that having two directors, as opposed to a single director normal to the cross-section, allows for a twisting degree of freedom as can be seen in Fig. 5.2d.

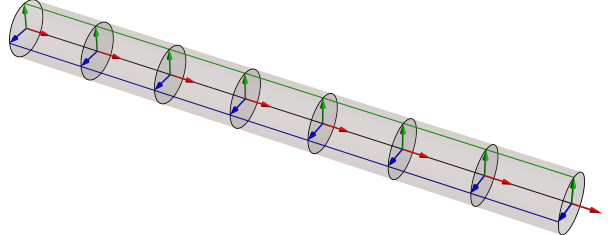
that of an extended continuum theory that, in addition to the manifold of point-continua M , included a set of *directors* (three-dimensional vectors) at each point $\mathbf{x} \in M$. We thus refer to these systems as *directed media*, as opposed to the undirected media of classical continuum mechanics. The physical interpretation of the directors are a matter of constitutive modelling. For three-dimensional continuum bodies, the directors could represent polar continua which has been used to study the properties of asymmetric Cauchy stress tensors, as in the case of liquid crystals [58].

When M is a lower-dimensional sub-manifold of \mathbb{R}^3 , the polar continua would then often represent the substitutive internal degrees of freedom of the neglected bulk continuum. In the elastic theory of shells, a single director can model the material fibre running across its thickness, and for rods two directors are used to model the material fibres through the cross-section. We now continue to define the latter in detail.

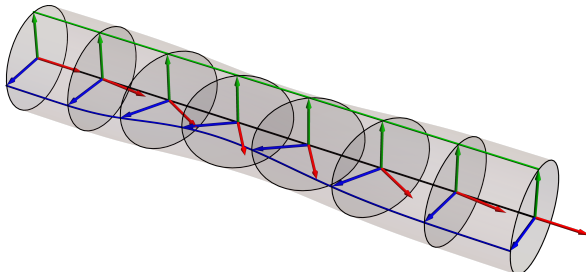
A Cosserat rod can be defined as a curve in Euclidean space $\mathbf{r}(u) \in \mathbb{R}^3$, $u \in [0, L_0]$, known as the *center-line* and where L_0 is (in a dynamical setting) the *rest-length* of the rod, and an orthogonal triad $E(u) = (\mathbf{e}_1(u) \ \mathbf{e}_2(u) \ \mathbf{e}_3(u)) \in \mathbb{R}^3$. The *material frame* $E(u)$ represents the, in general ellipsoidal, cross-section of the rod at each *material point* u along the center-line. The vectors $\mathbf{e}_2(u)$ and $\mathbf{e}_3(u)$ are the aforementioned directors of the Cosserat rod, which can vary in length and represent the semi-minor and semi-major axes of the cross-section at u . The vector $\mathbf{e}_1(u)$ is normal to the cross-section at u and is defined as $\mathbf{e}_1(u) = (\mathbf{e}_2(u) \times \mathbf{e}_3(u)) / |\mathbf{e}_2(u) \times \mathbf{e}_3(u)|$, where \times is the 3-dimensional cross-product and $|\cdot|$ is the standard norm in Euclidean space.



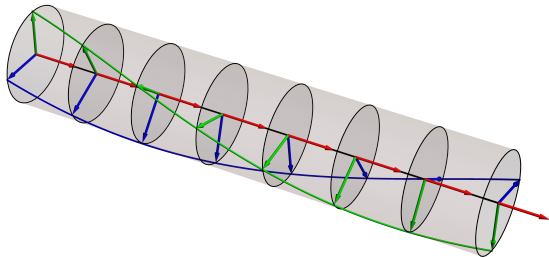
(a) Straight Cosserat rod



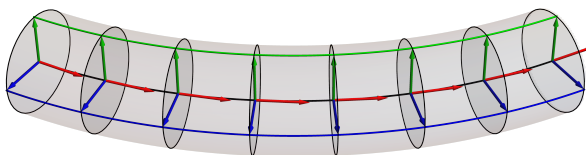
(b) Extending Cosserat rod



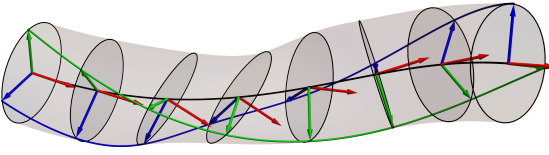
(c) Shearing Cosserat rod



(d) Twisting Cosserat rod



(e) Bending Cosserat rod



(f) Bending, shearing and twisting Cosserat rod

Figure 5.2: Examples of deformations of the Cosserat rod. The transparent gray tubes is the bulk of the Cosserat rod, with the center-line (black line) running through its radial center. The material frame and cross-section are shown at intermittent points along the center-line, along with the surface fibres traced out by the directors \mathbf{e}_2 and \mathbf{e}_3 , green and blue respectively. The tubular radii of the rods depicted were exaggerated in size for illustrative purposes. (a) A straight Cosserat rod suffering no deformation. (b-f) Examples of extension, shearing, twisting and bending deformations.

The deformations and rotations of the center-line and material frame comprise the full kinematic degrees of freedom of the Cosserat rod. Often in applications the cross-section is approximated to be of constant shape along the rod, in which case we restrict the directors to be inextensible and orthogonal, and thus $E(u)$ is then an orthonormal triad. See Fig. 5.1 for an illustration of a Cosserat rod with circular cross-section. In the literature this class of Cosserat rod is known as a *special Cosserat rod* [7, 186, 6]. Henceforth, unless stated otherwise, by Cosserat rod we mean a special Cosserat rod.

The kinematic degrees of freedom of the rod are thus: smooth translations of the curve \mathbf{r} and smooth rotations the material frame-field E . In other words, the center-line can bend, and the cross-section can shear and twist around the center-line and extend tangentially across its length, as is illustrated in Fig. 5.1. The extension of the rod can be captured by the scalar $h(u) = |\frac{\partial \mathbf{r}}{\partial u}|$, which can be seen as the square root of the metric on the center-line induced by the Euclidean metric on \mathbb{R}^3 . h relates the material coordinate u to the arc-length coordinate s as

$$ds = h(u)du \quad (5.2)$$

such that $|\frac{\partial \mathbf{r}}{\partial s}| = 1$ for all $s \in [0, L]$ where

$$L[h(u)] = \int_0^{L_0} h(u)du \quad (5.3)$$

is the total arc-length of the center-line. Thus any point u for which $h(u) = 1$ is not suffering an extension. Shear and twist deformations can be distinguished by noting that the former denotes the orientation \mathbf{e}_1 of the cross-section deviating from being parallel to the center-line, whilst the latter denotes rotations of the material frame around $\mathbf{e}_1(u)$. Henceforth we will also distinguish the length elements ds and du as the *length element* and *material length element* respectively.

We now add time to the picture, and consider the motion of the Cosserat rod as the result of arbitrary translational and angular velocity fields. Let the center-line $\mathbf{r}(t, u)$ and the material frame $\mathbf{e}_i(t, u)$ be functions of time, then the temporal evolution of the rod is

$$\dot{\mathbf{r}} = \mathbf{V} \quad (5.4a)$$

$$\dot{\mathbf{e}}_i = \boldsymbol{\Omega} \times \mathbf{e}_i \quad (5.4b)$$

from initial boundary conditions at $t = 0$, and where $\mathbf{V} = \mathbf{V}(t, u)$ and $\boldsymbol{\Omega} = \boldsymbol{\Omega}(t, u)$ are arbitrary translation and angular velocities.

Dynamical equations of motion for the Cosserat rod are found by imposing balance laws on the momentum and moments of the polar continua. For undirected media, the conservation of mass and linear momentum balance are used to determine the dynamics, given constitutive and body forces. For directed media, in addition to the above, further

conservation laws must be imposed to establish the director dynamics.

For a Cosserat rod with mass density ρ_0^V and cross-sectional area A in its reference configuration, the linear momentum of the rod is $\mathbf{P} = \rho_0^V A \dot{\mathbf{V}}$, as is the case in classical continuum mechanics. We also introduce the director angular momentum $\mathbf{L} = I\Omega$, where $I \in \mathbb{R}^{3 \times 3}$ is a moment of inertia matrix for the cross-section. As will be shown in Sec. 6, imposing the conservation of the linear momentum of the rod and the director angular momentum leads, as was first derived in [38], to

$$\dot{\mathbf{P}} = \mathbf{F}' + \mathbf{f} \quad (5.5a)$$

$$\dot{\mathbf{L}} = \mathbf{M}' + \mathbf{r}' \times \mathbf{F} + \mathbf{m}, \quad (5.5b)$$

$$\mathbf{F} = 0, \text{ at } u = 0 \text{ and } u = L_0 \quad (5.5c)$$

$$\mathbf{M} = 0, \text{ at } u = 0 \text{ and } u = L_0 \quad (5.5d)$$

where \mathbf{F} are the constitutive forces acting on the rod, \mathbf{f} the body forces per unit material length, \mathbf{M} the constitutive director moments and \mathbf{m} the body moment per unit material length. Eq. 5.5a is in a form familiar to classical continuum mechanics, which can be seen by comparing it to Eq. 5.1, whilst Eq. 5.5b is particular to the setting of directed media. Equation 5.5 and Eq. 5.4 together form a closed set of first-order equations in time and space for the kinematics and dynamics of a Cosserat rod.

We note here that up until this point we have considered an open Cosserat rod where $\mathbf{r}(0, t) \neq \mathbf{r}(L_0, t)$. The dynamics of a closed Cosserat rod, for which the center-line and frame are periodic functions of u , are identical with the exception of the omission of the boundary conditions Eq. 5.5c and Eq. 5.5d.

Equation 5.5 can be derived directly from the balance laws of classical continuum mechanics, as shown in [169, 186], under the kinematic assumption that the cross-sections traced out by the directors correspond to the bulk of a three-dimensional tube of undirected point-continua. For illustrative purposes this kinematic assumption deserves further elaboration. In precise mathematical language, let $M \subset \mathbb{E}$ and let $\mathbf{x} : D \rightarrow M$ be the *material coordinate* function from the domain

$$D = \{(X_1, X_2, X_3) : X_1^2 + X_2^2 = R^2 \text{ and } X_3 \in [0, L_0]\} \quad (5.6)$$

where R is a given fixed tubular radius of the Cosserat rod. Given a Cosserat rod configuration (\mathbf{r}, E) , we define M via the material coordinate function as

$$\mathbf{x}(\mathbf{X}) = \mathbf{r}(X_3) + X_j \mathbf{e}_j, \quad j = 2, 3 \quad (5.7)$$

such that M is the image of \mathbf{x} . Here the material coordinate X_3 corresponds to the coordinate u . We see how the Cosserat rod can be viewed as the result of a coarse-graining

procedure from the full three-dimensional continuum setting, replacing the cross section at each u with two directors, thus reducing the spatial coordinates of the system from three to one.

We now conclude this section by making some remarks, prefacing the discussions in subsequent chapters, on the geometric properties of the Cosserat rod. The kinematic equations of motion Eq. 5.4a and Eq. 5.4b shows explicitly that the rod moves according to infinitesimal translations $\mathbf{V}dt$ and rotations $\boldsymbol{\Omega} \times \mathbf{e}_i$ respectively. This entails that we can identify the kinematic structure of the Cosserat rod with the *Lie group* of Euclidean transformations of translations and rotations $SE(3)$ [194, 193]. In particular the rod itself can be parametrised in terms of sub-manifolds of $SE(3)$ and, as will be the main subject of Sec. 6, from which geometricised kinematic and dynamical equations of motion can be derived programmatically. In the following section some mathematical foundations will be introduced, necessary for the subsequent chapters of this part of the thesis.

I think this should reference some more beneficial properties of using Lie group, like the lack of coordinateitisation and some rereferec to parameterising using the Lie algebra / differential invariants. But I can add that later when I've written the subsequent mathematical subsections.

Should also introduce Cosserat sheet, althouhg can do that later after you've derived the equations of motion etc.

5.2 Mathematical preliminaries

As will be further discussed in Ch. 6, directed media can be seen as either sub-manifolds of *homogeneous spaces* or sub-manifolds of *Lie groups*. Through this lens, a fully geometricised and non-coordinate form of the equations of motion of such systems can be derived. This section serves primarily to establish establish the mathematical foundation and rigour of the programme, and therefore has a level of mathematical abstraction higher than that of the subsequent chapters. The reader not interested in these details may proceed to Ch. 6, and return to this section intermittently to fill gaps in notation and conceptual knowledge.

For a fuller treatment of the concepts introduced in this section the reader can consult the following references for further exposition [34, 124, 149, 147].

5.2.1 Differential geometry

Pullbacks and pushforwards

Define the Lie bracket in component form

$$[X, Y] = (X^j \partial_j Y^i - Y^j \partial_j X^i) \partial_i \quad (5.8)$$

5.2.2 Exterior calculus

In calculus, the differential of a scalar function $f : \mathbb{R}^3 \rightarrow \mathbb{R}$ is often written as

$$df = \frac{\partial f}{\partial x} dx + \frac{\partial f}{\partial y} dy + \frac{\partial f}{\partial z} dz. \quad (5.9)$$

This can be generalised for differentiable manifolds. Let M be a smooth d -dimensional manifold, $p \in M$ a point on the manifold, $X \in \Gamma(TM)$ a vector field on M and $f \in C^\infty(M)$ be a smooth function on M . We define the map $df : TM \rightarrow \mathbb{R}$ as

$$(df(X))(p) = X_p(f). \quad (5.10)$$

Here df is an example of a *scalar-valued 1-form*. Analogously, scalar functions $f \in C^\infty(M)$ are known as *scalar-valued 0-forms*. Scalar-valued p -form are linear maps $\prod_{i=1}^p TM \rightarrow \mathbb{R}$, where \prod signifies the repeated Cartesian product. The operator d is the *exterior derivative*, which in general maps p -forms to $(p+1)$ -forms. Any $(p+1)$ -form that can be written as the exterior derivative of a p -form is referred to as *exact*. Conversely, any p -form ϕ that satisfies $d\phi = 0$ is *closed*. Locally, closed p -forms are always exact, which is known as the *Poincaré lemma*.

Let $x^i : U \rightarrow \mathbb{R}$, $i = 1, \dots, d$ be coordinate functions for some neighbourhood $U \subset M$. Then df can then be locally expressed in U as

$$df = \frac{\partial f}{\partial x_i} dx^i \quad (5.11)$$

such that $df(X) = \frac{\partial f}{\partial x^i} dx^i(X) = \frac{\partial f}{\partial x^i} X^i$, where $X \in \Gamma(TM)$. Not all 1-forms are closed, and can thus not be written in the form of Eq. 5.11, but they can always be expanded in a coordinate basis as $\phi = a_i dx^i$, where $a_i \in C^\infty(M)$, $i = 1, \dots, d$ are the coefficients of ϕ in this basis.

The *symmetric product* of a p -form x and q -form y is written as $x \otimes y$. For $p = q = 1$, we have

$$(x \otimes y)(X, Y) = \phi(X)\psi(Y) \quad (5.12)$$

where $X, Y \in \Gamma(TM)$ are two vector fields. For a general 1-form, its exterior derivative can be expressed locally as

$$d\phi = da_i \wedge dx^i. \quad (5.13)$$

where \wedge is the *wedge product*. Let x and y be a p -form and a q -form respectively, then $x \wedge y$ is a $(p+q)$ -form defined as

$$x \wedge y = x \otimes y - y \otimes x \quad (5.14)$$

and satisfies

$$y \wedge x = (-1)^{pq} x \wedge y. \quad (5.15)$$

and

$$d(x \wedge y) = dx \wedge y + (-1)^p x \wedge dy. \quad (5.16)$$

The wedge product of a sequence of forms can be written as

$$\bigwedge_{i=1}^n z^i = dz^1 \wedge dz^2 \wedge \cdots \wedge dz^n \quad (5.17)$$

where each z^i is a p^i -form. Due to the anti-symmetry of the wedge products of 1-forms, we have that $df \wedge df = 0$ for any $f \in C^\infty(M)$. If x and y are two 1-forms, then the product $x \wedge y$ is a mapping $TM \times TM \rightarrow \mathbb{R}$, and can be evaluated on two vector fields $X, Y \in \Gamma(M)$ as

$$(x \wedge y)(X, Y) = x(X)y(Y) - x(Y)y(X). \quad (5.18)$$

We will now derive a coordinate-free expression for the exterior derivative of a 1-form. Let $\phi = a_i dx^i$, then

$$\begin{aligned} d\phi(X, Y) &= da_i(X)Y^i - da_i(Y)X^i \\ &= \frac{\partial a_i}{\partial x^k} X^k Y^i - \frac{\partial a_i}{\partial x^k} Y^k X^i \\ &= \left(X^k \frac{\partial}{\partial x^k}(a_i Y^i) - a_i X^k \frac{\partial Y^i}{\partial x_k} \right) - \left(Y^k \frac{\partial}{\partial x^k}(a_i X^i) - a_i Y^k \frac{\partial X^i}{\partial x_k} \right) \\ &= X^k \frac{\partial}{\partial x^k}(a_i Y^i) - Y^k \frac{\partial}{\partial x^k}(a_i X^i) - a_i \left(X^k \frac{\partial Y^i}{\partial x_k} - Y^k \frac{\partial X^i}{\partial x_k} \right) \\ &= X(\phi(Y)) - Y(\phi(X)) - \phi([X, Y]) \end{aligned} \quad (5.19)$$

where we used Eq. 5.8.

Intuitively, a 1-form can be seen as measuring an infinitesimal oriented length. A 2-form can be seen as measuring an infinitesimal oriented area. A p -form measures an infinitesimal oriented p -dimensional volume. There is therefore a natural notion of integrals of p -forms. In general, a p -form ϕ defined on a manifold M can be integrated on a p -dimensional sub-manifold of M .

If M is d -dimensional, then the integration of d -forms and 1-forms coincides with the usual notion of integration in multi-variate calculus. Let $U \subset M$ with coordinates $x^i : U \rightarrow \mathbb{R}^d$, and let $\gamma \subset U$ be a 1-dimensional sub-manifold of U , and let $\phi = h_i dx^i$ be a

general 1-form and $\psi = g \bigwedge_{i=1}^d dx^i$ a general d -form then

$$\int_{\gamma} \phi = \int_{\gamma} h_i dx^i \quad (5.20a)$$

$$\int_U \psi = \int_U g \bigwedge_{i=1}^d dx^i = \int_U g dx^1 dx^2 \dots dx^d \quad (5.20b)$$

where the right-most term in the equalities are the standard multi-variate integrals. For a d -dimensional manifold, a d -form like ψ is called a *volume form*. If $V \subset M$ is a $(p - 1)$ -dimensional sub-manifold and ϕ is a p -form, then it can be shown that

$$\int_V d\phi = \int_{\partial V} \phi \quad (5.21)$$

where ∂V signifies the boundary of V . Eq. 5.21 is called *Stokes' theorem*.

Consider a 1-form expressed locally as $\phi = a_i dx^i$. Under change of coordinates, it transforms as

$$a_i dx^i = a_i \frac{\partial x^i}{\partial \tilde{x}^i} d\tilde{x}^i. \quad (5.22)$$

From Eq. 5.22, it can be shown that d -forms transform as

$$f \bigwedge_{i=1}^d dx^i = \left(\det \left[\frac{\partial \mathbf{x}}{\partial \tilde{\mathbf{x}}} \right] f \right) \bigwedge_{i=1}^d d\tilde{x}^i \quad (5.23)$$

where $\frac{\partial \mathbf{x}}{\partial \tilde{\mathbf{x}}}$ is the Jacobian matrix of the coordinate transformation.

5.2.3 Lie groups

Definition 5.2.1. A d -dimensional Lie group is a set G that is both a group and a differentiable manifold of dimensions d , where the multiplication map $G \times G \rightarrow G$

$$(g, h) \mapsto gh \in G \quad (5.24)$$

and inverse $G \rightarrow G$

$$g \mapsto g^{-1} \quad (5.25)$$

are smooth maps.

For all Lie groups under our consideration, G can be represented as sub-manifold of $GL(n)$ under a map, the group of $n \times n$ invertible matrices for some $n \geq d$, under the map $g : G \rightarrow \subset GL(n)$. We call the image of this map \tilde{G} , which is the set of invertible matrices in $GL(n)$ that forms a representation of G . Henceforth, unless stated to be otherwise explicitly, we will use the short-hand $g \in G$ instead of $g \in \tilde{G}$, thus essentially identifying

the matrix Lie group representation with the Lie group itself.

For each element $g \in G$, the *left multiplication* map $L_g : G \rightarrow G$ is defined as $L_g h = gh$ where $h \in G$. Similarly, the *right multiplication* map $R_g : G \rightarrow G$ is defined as $R_g h = hg$. For maps between smooth manifolds $\Psi : M \rightarrow N$, we define its *derivative* at $p \in M$ as the mapping $D\Psi_p : T_p M \rightarrow T_{\Psi(p)} N$ given by the formula

$$D\Psi_p(v)(f) = v(f \circ \Psi) \quad (5.26)$$

for $v \in T_p M$ and $f \in C^\infty(N)$. In particular, the derivative of the left multiplication at $h \in G$ is a mapping $(DL_g)_h : T_h G \rightarrow T_{gh} G$, which can be shown to be equal to

$$(DL_g)_h(X) = gX \quad (5.27)$$

where $X \in T_h G$. For any Lie group G there is an associated *Lie algebra* \mathfrak{g} , which is the tangent space $T_e G$ at the identity, where $e \in G$ is the identity element. \mathfrak{g} is thus a vector space of the same dimension d as G . For any vector $V \in \mathfrak{g}$, we can define a *left-invariant vector field* \tilde{V} defined on each $g \in G$ as

$$\tilde{V}_g = (DL_g)_e(V). \quad (5.28)$$

Now let E_i , $i = 1, \dots, d$ be a basis for \mathfrak{g} , then it can be shown that the corresponding left-invariant vector-fields \tilde{E}_i form a global basis for the tangent bundle TG . This implies that the tangent bundle of Lie groups G are isomorphic to the Cartesian product $TG \cong G \times \mathfrak{g}$. Furthermore, it is notable that the global basis is constructed without specifying coordinate functions on the manifold.

The *exponential map* $\exp : \mathfrak{g} \rightarrow G$ relates Lie algebra elements to corresponding Lie group elements, and for matrix Lie groups this is explicitly given by the matrix exponential. Intuitively this mapping can be understood by considering the curve $\gamma(t) = \exp(tV) \in G$, where $V \in \mathfrak{g}$. Differentiating the curve gives us

$$\begin{aligned} \frac{d}{dt}\gamma(t) &= \exp(tV)V \\ &= (DL_{\exp(tV)})_e(V) = \tilde{V}_g \end{aligned} \quad (5.29)$$

The curve γ is thus a flow-line of the left-invariant vector field \tilde{V} .

The Lie algebra \mathfrak{g} also has a product structure known as the *Lie bracket* $[\cdot, \cdot] : \mathfrak{g} \times \mathfrak{g} \rightarrow \mathfrak{g}$ given by

$$[X, Y] = XY - YX \quad (5.30)$$

for $X, Y \in \mathfrak{g}$. To see its relation to the Lie group, we introduce the *adjoint action* of a Lie

group on its Lie algebra $\text{Ad} : G \times \mathfrak{g} \rightarrow \mathfrak{g}$ given by

$$\text{Ad}_g Y = gYg^{-1} \quad (5.31)$$

for each $g \in G$, Ad_g is thus an automorphism of the Lie algebra. Let $g(t) = \exp(tX)$, with Taylor expansion $g(t) = I + tX + O(t^2)$. The infinitesimal action of the automorphism Ad_g can then be found by expanding it as

$$\text{Ad}_g Y = Y + t[X, Y] + O(t^2). \quad (5.32)$$

This motivates the definition of the adjoint action of the Lie algebra *on itself* $\text{ad} : \mathfrak{g} \times \mathfrak{g} \rightarrow \mathfrak{g}$ given by

$$\text{ad}_X Y = [X, Y]. \quad (5.33)$$

Let E_a , $a = 1, \dots, d$ be a basis for Lie algebra \mathfrak{g} , then the Lie bracket can also be written in terms of its *structure constants* $f_{bc}^a \in \mathbb{R}$

$$[E_a, E_b] = f_{ab}^c E_c, \quad a, b, c = 1, \dots, d. \quad (5.34)$$

The Lie algebra can be *defined* as a vector space \mathfrak{g} equipped with Lie bracket, where the latter is fully specified by the structure constants. If G is connected, then G is exactly equal to the image of \mathfrak{g} under the exponential map ¹. This is known as the *Lie algebra-Lie group correspondence*. We thus see that the structure constants encapsulates the full geometry of the Lie group.

For a d -dimensional Lie group G , with Lie algebra \mathfrak{g} , a linear map $\prod_{i=1}^p TG \rightarrow \mathfrak{g}$ is a *Lie algebra-valued p-form*. A general Lie algebra-valued 1-form $X : TG \rightarrow \mathfrak{g}$ can be written as

$$X = a_i^a E_a dx^i \quad (5.35)$$

where E_a , $a = 1, \dots, d$ is a basis for \mathfrak{g} , $x^i \in C^\infty(G)$, $i = 1, \dots, d$ are global coordinate functions on G , and $a_i^a \in C^\infty(G)$, $i, a = 1, \dots, d$ are the coefficients of X in this basis. The exterior derivative of a Lie-algebra valued form can be computed by simply applying it directly on the scalars in the expression. For example, the exterior derivative of a Lie algebra-valued 1-form is

$$dX = E_a d(a_i^a dx^i). \quad (5.36)$$

Similarly, let $Y = b_i^a E_a dx^i$, then the wedge product of two 1-forms can be computed as

$$X \wedge Y = E_a E_b a_i^a b_j^b dx^i \wedge dx^j \quad (5.37)$$

¹If G is not connected, $\exp(\mathfrak{g})$ is equal to the sub-group of G that is connected to the identity element $e \in G$.

where $E_a E_b$ denotes ordinary matrix multiplication. Note that the wedge product of two Lie algebra-valued forms is not necessarily Lie algebra-valued.

The following are some examples of Lie groups:

- The positive real numbers \mathbb{R}^+ equipped with multiplication forms an *abelian* Lie group, where all elements commute with each other.
- The orthogonal group $O(n)$ which is the space of orthogonal $n \times n$ matrices. Its Lie algebra $\mathfrak{o}(n)$ comprises the space of anti-symmetric $n \times n$ matrices.
- The special orthogonal group $SO(n)$ is the set of matrices $R \in SO(n)$ for which $\det R = 1$. Its Lie algebra $\mathfrak{so}(n)$ is equal to $\mathfrak{o}(n)$.
- The translation group $T(n)$ is the group of translations in n -dimensional Euclidean space.
- The special Euclidean group $SE(n)$ is the group of translations and rotations in n -dimensional space, and can be written as the semi-direct product $SE(n) = T(n) \rtimes SO(n)$.

5.2.4 Homogeneous spaces

List all the main homogeneous spaces found in

Introduce principal bundles.

Define transitive action. Define homogeneous space both as a quotient G/H but also as a topological space where a group G acts transitively.

Introduce Euclidean space \mathbb{E}^d , as the vector space \mathbb{R}^d equipped with an inner product.

5.2.5 The Maurer-Cartan form

We have seen that the Lie group G can be fully reconstructed using the structure constants f_{ab}^c of its Lie algebra \mathfrak{g} . The same geometric information is also contained in its left-invariant vector fields Eq. 5.28², which can be encapsulated using a Lie algebra-valued 1-form called the *Maurer-Cartan form* $\omega : TG \rightarrow \mathfrak{g}$, which is defined as

$$\omega(v) = (DL_{g^{-1}})_g(v) \quad (5.38)$$

for any $v \in T_g G$. The Maurer-Cartan form thus maps the tangent spaces at any point g to the tangent space at the identity \mathfrak{g} .

²Equivalently, the right-invariant vector fields contains the same information.

Let $X, Y \in \mathfrak{g}$ and let $v_X = (DL_g)_e(X)$ and $v_Y = (DL_g)_e(Y)$ be their corresponding left-invariant vector fields. Then the Maurer-Cartan form satisfies

$$\omega([v_X, v_Y]) = [X, Y] \quad (5.39)$$

where the argument of ω on the left-hand side is the Lie bracket of vector fields. Eq. 5.39 can be derived by noting that for any diffeomorphism $\Psi : M \rightarrow N$, we have that $D\Psi([v, w]) = [D\Psi(v), D\Psi(w)]$ where $v, w \in \Gamma(TM)$. By recovering the Lie bracket of the Lie algebra from the Maurer-Cartan form, we thus see that it encapsulates all geometric information about the Lie group.

From Eq. 5.19 we have that

$$d\omega(v, w) = v(\omega(w)) - w(\omega(v)) - \omega([v, w]). \quad (5.40)$$

If v and w are left-invariant, then $v(\omega(w)) = w(\omega(v)) = 0$, and we get

$$d\omega(v, w) + \omega([v, w]) = 0 \quad (5.41)$$

but as left-invariant vectors span the whole tangent bundle, this equation must also hold for arbitrary for all vector fields. Eq. 5.41 is known as the *Maurer-Cartan equation*, and can be seen as the defining equation for ω , and will be instrumental in future chapters.

For the applications in the coming chapters, it is more convenient to work in a matrix representation of the Maurer-Cartan form, given by

$$\omega = g^{-1}dg. \quad (5.42)$$

To explain the above expression, we temporarily reintroduce the distinction between abstract Lie group elements $x \in G$, and their matrix representations $g(x) \in \tilde{G}$. Eq. 5.42 is more accurately written as $\omega_x = g(x)^{-1}Dg_x$ where $x \in G$ is here an abstract (non-matrix) Lie group element. To see the correspondence between Eq. 5.38 and Eq. 5.42, we first note that the derivatives of linear maps $\Psi : M \rightarrow N$, defined in Eq. 5.26, is equivalent to the exterior derivative of a 0-form. Thus $dg = Dg$, and $dg_x : T_x G \rightarrow T_{g(x)} \tilde{G}$, which is computed as a matrix of 1-forms. Finally we then left-translate dg to get $g^{-1}dg : TG \rightarrow \mathfrak{g}$.

Finally, we derive Eq. 5.41 in matrix form. We take the exterior derivative of Eq. 5.42

$$\begin{aligned} d\omega &= d(g^{-1}dg) \\ &= -(g^{-1}dgg^{-1}) \wedge dg + g^{-1}d^2g \\ &= -\omega g^{-1} \wedge dg, \end{aligned} \quad (5.43)$$

to get

$$d\omega + \omega \wedge \omega = 0 \quad (5.44)$$

where we have used the fact that dg is a matrix of closed 1-forms, so that $d^2g = 0$, that the wedge product commutes with matrix multiplication, and $d(g^{-1}g) = 0$ to find an expression for dg^{-1} .

5.2.6 Sub-manifolds of homogeneous spaces

The exposition in this section follows closely that of [34]. The Maurer-Cartan form and the Maurer-Cartan equation are particularly useful when studying sub-manifolds of homogeneous spaces. If $M \subset G/H$, let $\Phi : W \rightarrow M$ be a differentiable map, where W is some n -dimensional manifold, where \mathbb{T}^n is the n -dimensional torus, for some n . The *pullback bundle* Φ^*G of the principal bundle $\pi : G \rightarrow G/H$ is defined as

$$\Phi^*G = \{(u, g) \in W \times G : \Phi(u) = \pi(g)\}, \quad (5.45)$$

i.e. Φ^*G is a principal bundle over W , such that its fibre over $u \in W$ is equal to the fibre of G over $\Phi(u) \in G/H$. Φ^*G has the map $\hat{\Phi} : \Phi^*G \rightarrow G$

$$\hat{\Phi}(u, g) = g \quad (5.46)$$

A *lifting* $\tilde{\Phi} : W \rightarrow G$ is a map that satisfies

$$(\pi \circ \tilde{\Phi})(u) = \Phi(u), \quad \forall u \in W. \quad (5.47)$$

In subsequent chapters, Φ will be identified with the space-time kinematic configuration of a system, and the lifting $\tilde{\Phi}$ a G -valued field on W that reconstructs Φ . The homogeneous space G/H is then the kinematic configuration space of the system, and $W = (\text{time domain}) \times (\text{material domain})$ will be referred to as the *kinematic base space*. To make this analogy explicit, consider a Cosserat rod with material coordinate $u \in [0, L_0]$ and temporal coordinate $t \in [0, T]$, then $W = [0, T] \times [0, L_0]$ and $\Phi(t, u)$ is the (G/H -valued) configuration of the material point u at time t . The manifolds $[0, L_0]$ and $[0, T]$ will be called the *material base space* and the *time domain* respectively.

Similarly to how the Maurer-Cartan form can be shown to contain the geometrical information of a Lie group G , we will now also show that it can play a similar role for Φ . Let $\tilde{\Phi} : W \rightarrow G$ be a differentiable map and let $\xi := \tilde{\Phi}^*\omega$ be the pull-back of the Maurer-Cartan form onto W . As $\omega : TG \rightarrow \mathfrak{g}$, we have that $\xi : TW \rightarrow \mathfrak{g}$. To derive the

matrix expression for ξ we note that for any $v \in T_u W$ and $u \in W$ we have

$$\begin{aligned}\xi(v) &= \tilde{\Phi}^* \omega(v) = \omega(D\tilde{\Phi}(v)) = (DL_{\tilde{\Phi}(u)^{-1}})_{\tilde{\Phi}(u)}(D\tilde{\Phi}(v)) \\ &= \tilde{\Phi}(u)^{-1}(D\tilde{\Phi})_u(v)\end{aligned}\tag{5.48}$$

where the definition of the Maurer-Cartan form Eq. 5.38. We can thus write

$$\begin{aligned}\xi &= \tilde{\Phi}^{-1} d\tilde{\Phi} \\ &= g^{-1} dg, \quad g \in \tilde{\Phi}(W)\end{aligned}\tag{5.49}$$

where used $D\tilde{\Phi} = d\tilde{\Phi}$. The following lemma will show that all information in Φ is encapsulated by ξ , up to global transformations $g \in G$.

Lemma 5.2.1. *Let W be an n -dimensional differentiable manifold, and let $\tilde{\Phi}_1, \tilde{\Phi}_2 : W \rightarrow G$ be two differentiable maps, and $\xi_i = \tilde{\Phi}_i^* \omega$, $i = 1, 2$. Then there exists a $g \in G$ such that*

$$\tilde{\Phi}_1(u) = g\tilde{\Phi}_2(u), \quad \forall u \in U\tag{5.50}$$

if and only if $\xi_1 = \xi_2$ where ω is the Maurer-Cartan form of G .

Proof. The following is a reproduction of results in [34], but where we have relaxed the condition that $\dim(W) = n \leq \dim(G/H)$, to allow for arbitrary n . There exists a function $f : W \rightarrow G$ such that

$$\tilde{\Phi}_1(u) = f(u)\tilde{\Phi}_2(u), \quad \forall u \in W.\tag{5.51}$$

Differentiating the above, we get

$$d\tilde{\Phi}_1 = df\tilde{\Phi}_2 + f d\tilde{\Phi}_2\tag{5.52}$$

Thus we have

$$\begin{aligned}\xi_1 &= \tilde{\Phi}_1^* \omega = \tilde{\Phi}_1^{-1} d\tilde{\Phi}_1 \\ &= \tilde{\Phi}_1^{-1} (df\tilde{\Phi}_2 + f d\tilde{\Phi}_2) \\ &= \tilde{\Phi}_1^{-1} df\tilde{\Phi}_2 + \tilde{\Phi}_1^{-1} f \tilde{\Phi}_2 \tilde{\Phi}_2^{-1} d\tilde{\Phi}_2 \\ &= \tilde{\Phi}_1^{-1} df\tilde{\Phi}_2 + \xi_2,\end{aligned}\tag{5.53}$$

from which it follows that $\xi_1 = \xi_2$ if and only if $df = 0$. \square

The same steps taken to derive Eq. 5.43 can be repeated to find that ξ satisfies

$$d\xi + \xi \wedge \xi = 0.\tag{5.54}$$

which are in this context also sometime referred to as the Maurer-Cartan equations. More precisely, they can be seen as the pull-back of the Maurer-Cartan equations on to W . The

above lemma, along with Eq. 5.54, are the corner-stones of the general kinematic theory of directed continuum materials, whose kinematic configuration space is a Lie group or homogeneous space, which we will develop in the subsequent chapters. It tells us that *all geometric information in Φ is encoded in ξ* , subject to global transformations Eq. 5.50, and furthermore that ξ is invariant under said transformations.

In Cartan's *theory of moving frames*, the Maurer-Cartan form is utilised to establish the equivalence of sub-manifolds of homogeneous spaces [136, 34, 161, 72]. For a given homogeneous space G/H , d -dimensional sub-manifolds can be characterised by a set of *differential invariants*, which are scalar functions defined on the sub-manifold. These differential invariants capture the intrinsic geometry of the sub-manifold, and are invariant under transformations in H . For example, space-curves $\gamma : [0, 1] \rightarrow \mathbb{R}^3$ can be seen as sub-manifolds the homogeneous space $SE(3)/SO(3) \cong \mathbb{R}^3$. Any such curve is uniquely determined, up to global rigid-body rotations in $SO(3)$, by its *torsion* $\tau(u)$ and *curvature* $\kappa(u)$, where $u \in [0, 1]$. The equations that recover γ from the two scalar differential invariants are the celebrated *Frenet-Serret* equations. In the language of physics, such a space curve is called a *filament*, and will be treated in Ch. 6.

However, the relevance of the above results go beyond being a mathematical nicety. In simulations, working directly with Lie group-valued objects like Φ can be impractical. As all Lie groups G will in practice be represented as a sub-Lie group of $GL(n)$, numerical errors will in general take values in the space of n -by- n matrices. Let $h \in \mathbb{R}^{n \times n}$ represent the error accrued in a single time-step, and let $g \in G$ represent the current state of a simulation. Then it is clear that $g + h \notin G$. This is inherently due to the non-linearity of the space G . In the later chapters, we will instead use the Maurer-Cartan form to formulate the kinematics and dynamics of sub-manifolds of G in terms of its Lie algebra \mathfrak{g} . The state of the system thus take values in a linear space, as do the errors, which ensures that in simulations the system never falls out of the correct space.

We have considered a map Φ and showed its relation to the pullback of the Maurer-Cartan form ξ . In applications we will most often have some $\xi : TW \rightarrow \mathfrak{g}$ and then reconstruct its corresponding Φ . From Eq. 5.49, we have

$$d\tilde{\Phi} = \tilde{\Phi}\xi. \quad (5.55)$$

This is a matrix ODE that can be solved numerically.

Note that for many systems the kinematic configuration space will be an entire Lie group G (e.g. a Cosserat rod), rather than a homogeneous space G/H (e.g. a filament, without a material frame). In this case we can use that $G \cong G/e$ and all of the above will still apply. Consequently, we must have $\tilde{\Phi} = \Phi$ as $G = G/H$. Conversely if H is not trivial there is an infinite dimensional space of admissible $\tilde{\Phi}$ for a given Φ . This latter fact will later be described as a *gauge freedom* in the kinematic description of the system.

Chapter 6

Cosserat rod models and geometric mechanics

Add some remarks that what you will do here builds up to a generalised version in the subsequent chapter.

6.1 Geometric mechanics of a rigid body

Before we study the kinematics and dynamics of Cosserat rods, we first consider the case of a free rigid body which undergo translations and rotations (equivalent to a ‘Cosserat point particle’). We will first formulate the Lagrangian mechanics of the rigid body, expressing it in terms of its kinematic configuration space $SE(3)$, the group of special Euclidean transformations. We then construct a reduced Lagrangian density that take values in the corresponding Lie algebra $se(3)$. The canonical example of this procedure is the rotating free rigid body and was introduced in [149, 108, 31], which we here generalise to include translation.

We consider mechanics in \mathbb{R}^3 , starting from the point-of-view of some observer with a *fixed* or *spatial* frame $B = (\mathbf{b}_1 \ \mathbf{b}_2 \ \mathbf{b}_3) \in \mathbb{R}^{3 \times 3}$. As we are working in Euclidean space, we will make use of the isomorphism $\mathbb{R}^3 \cong T\mathbb{R}^3$. Vectors $\mathbf{v} \in \mathbb{R}^3$ will be expressed in terms of their components in the fixed frame as $\mathbf{v} = \tilde{v}_i \mathbf{b}_i$, where the tilde denotes the fixed frame.

Let $\mathcal{M} \subset \mathbb{R}^3$ be the *reference configuration* of a rigid body, let $\mathbf{X} \in M$ denote the *material coordinates* of \mathcal{M} , and let $\rho_0^V(\mathbf{X})$ be the mass density per unit material volume of the rigid body at \mathbf{X} . We define the material coordinates to be in the centre-of-mass frame, such that $\int_{\mathcal{M}} \rho_0^V(\mathbf{X}) X_i d^3 X = 0$, $i = 1, 2, 3$.

At time t the location of the material point at \mathbf{X} is given by $\mathbf{x}(\mathbf{X}, t)$. The latter can be related to the former as

$$\mathbf{x}(\mathbf{X}, t) = \mathbf{r}(t) + R(t)\mathbf{X}, \quad \mathbf{X} \in \mathcal{M} \tag{6.1}$$

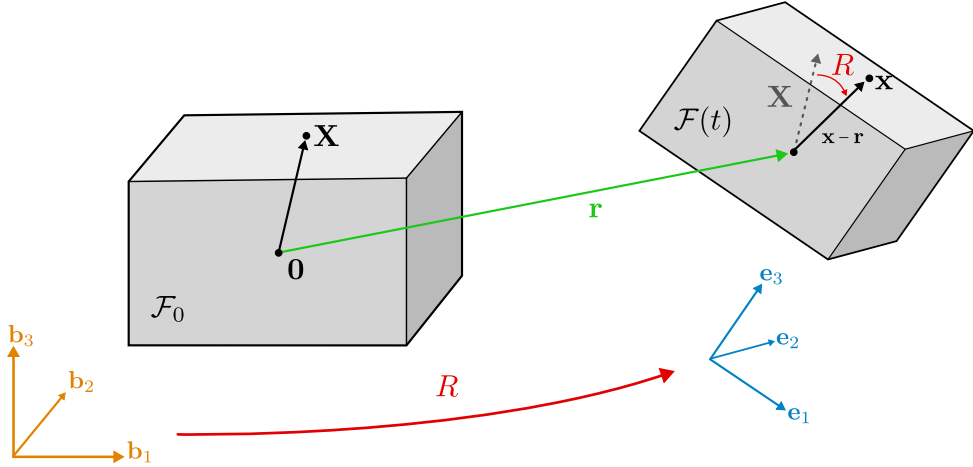


Figure 6.1: Illustration of the mapping from the reference configuration \mathcal{F}_0 to the current configuration $\mathcal{F}(t)$ of a rigid body. The configuration of the rigid body is specified via a translation of the center-of-mass \mathbf{r} (green), and rotation R (red), relative to a reference configuration with a center-of-mass located at $\mathbf{0}$. Material points \mathbf{X} in the reference configuration are thus mapped to $\mathbf{x}(\mathbf{X}) = \mathbf{r} + R\mathbf{X}$. An observer that sits on the rigid body and moves with it will have a frame $E = (\mathbf{e}_1 \mathbf{e}_2 \mathbf{e}_3)$ (blue), which rotates relative to the fixed frame of a still observer $B = (\mathbf{b}_1 \mathbf{b}_2 \mathbf{b}_3)$ (orange) as $E = RB$.

where $\mathbf{r}(t)$ is the location of the centre-of-mass and $R(t)$ is the rotation of the rigid body relative to its reference configuration. Now consider the second term in Eq. 6.1,

$$R\mathbf{X} = \tilde{X}_i \mathbf{e}_i \quad (6.2)$$

where $\mathbf{e}_i = R\mathbf{b}_i$ is the *moving* or *body* frame, which we write as $E = (\mathbf{e}_1 \mathbf{e}_2 \mathbf{e}_3) \in \mathbb{R}^{3 \times 3}$ and satisfies $E = RB$, and is illustrated in Fig. 6.1. The configuration of the rigid body can thus be written as a matrix

$$\mathcal{F}(t) = \begin{pmatrix} 1 & \mathbf{0}^T \\ \mathbf{r}(t) & E(t) \end{pmatrix} \quad (6.3)$$

and we can relate it to the reference configuration as

$$\mathcal{F}(t) = \mathcal{F}_0 \Phi(t) \quad (6.4)$$

where

$$\mathcal{F}_0 = \begin{pmatrix} 1 & \mathbf{0}^T \\ \mathbf{0} & B \end{pmatrix} \quad (6.5)$$

is the reference configuration and

$$\Phi(t) = \begin{pmatrix} 1 & \mathbf{0}^T \\ B^T \mathbf{r} & B^T R(t) B \end{pmatrix} \quad (6.6)$$

is for each $t \in [0, T]$ an element of the special Euclidean group $SE(3)$ of translations and rotations. We will thus henceforth identify the configuration of the rigid body with Φ , up to a global rotation of \mathcal{F}_0 .

The form of Eq. 6.6 merits some explanation. $B^T \mathbf{r}$ can be seen as the component of coefficients of \mathbf{r} expressed in the fixed frame B , and $B^T R B$ is then the rotation R in that same basis. We therefore introduce the notation $\tilde{\mathbf{v}} = B^T \mathbf{v}$ for vectors $\mathbf{v} \in \mathbb{R}^3$. Similarly we write

$$\vec{v} = E^T \mathbf{v} \quad (6.7)$$

where \vec{v} is a vector $\mathbf{v} \in \mathbb{R}^3$ expressed in the moving frame E , with components $v_i = \mathbf{e}_i \cdot \mathbf{v}$. We thus have that $\mathbf{v} = v_i \mathbf{e}_i = \tilde{v}_i \mathbf{d}_i$.

We now derive the kinematic equations of motion of the rigid body, parametrised as a point $\Phi(t)$ in the Lie group $SE(3)$. The ‘velocity’ of the rigid body is $\dot{\Phi}(t) \in T_{\Phi(t)}SE(3)$, a vector in the tangent space at $\Phi(t)$, which incorporates both the translation of the centre-of-mass and the rotation of the frame. As $SE(3)$ is a Lie group, there is a natural map from $T_{\Phi(t)}SE(3)$ to its Lie algebra $\mathfrak{se}(3) \cong T_e SE(3)$ by left (or right)-translation

$$\Phi^{-1} \dot{\Phi} = N \in \mathfrak{se}(3) \quad (6.8)$$

which allows us to express the kinematics of the rigid body in terms of generalised velocities all taking values in the same Lie algebra. Equation 6.8 is an ordinary matrix differential equation and can be solved to find $\Phi(t)$ given a velocity $Y(t)$.

We now derive the kinematic equations of motion of the rigid body in terms of more familiar quantities. Let \vec{V} be the translational velocity of the center-of-mass, and $\hat{\Omega}$ the angular velocity of the rigid body, expressed in the moving frame basis. We write N as

$$N = \begin{pmatrix} 0 & \vec{0}^T \\ \vec{V} & \hat{\Omega} \end{pmatrix} \quad (6.9)$$

where $\hat{\Omega} \in \mathbb{R}^{3 \times 3}$ is the angular velocity under the hat-map. We can see N as a generalised velocity, defined on the Lie algebra. The inverse of Eq. 6.6 is given by

$$\Phi^{-1} = \begin{pmatrix} 1 & \mathbf{0}^T \\ -B^T R^T \mathbf{r} & B^T R^T B \end{pmatrix}. \quad (6.10)$$

We now evaluate the left-hand side of Eq. 6.8 to get

$$\begin{aligned}\Phi^{-1}\dot{\Phi} &= \mathcal{F}^{-1}\dot{\mathcal{F}} = \begin{pmatrix} 0 & \vec{0}^T \\ B^T R^T \dot{\mathbf{r}} & B^T R^T \dot{R}B \end{pmatrix} \\ &= \begin{pmatrix} 0 & \vec{0}^T \\ E^T \dot{\mathbf{r}} & E^T \dot{E} \end{pmatrix}\end{aligned}\tag{6.11}$$

Equating Eq. 6.9 and Eq. 6.11, we get the kinematic equations of motion

$$\dot{\mathbf{r}} = \mathbf{V} \tag{6.12a}$$

$$\dot{E} = E\hat{\Omega}. \tag{6.12b}$$

which describes the translational motion of the centre-of-mass and the rotation of the frame E , respectively. Equation 6.12b can also be written as

$$\begin{aligned}\dot{\mathbf{e}}_j &= \mathbf{e}_i \hat{\Omega}_{ij} \\ &= \boldsymbol{\Omega} \times \mathbf{e}_i.\end{aligned}\tag{6.13}$$

where $\boldsymbol{\Omega} = \Omega_i \mathbf{e}_i$. Eq. 6.13 provides a clear interpretation of the angular velocity. At time t the i th component of the angular velocity in the moving frame $\Omega_i(t)$ gives the rate at which the rigid body rotates around the axis \mathbf{e}_i .

We note that the derivations above would simplify to some extent if we let the fixed frame equal the identity matrix $B = \mathbb{1}$, in which case $E = R$. In this section we will keep the distinction so as to make the distinction clear between the moving frame E and the fixed frame B . It is clear that \mathcal{F} (and \mathcal{F}_0) could also be considered Lie group-valued, and indeed $\Phi^{-1}\dot{\Phi} = \mathcal{F}^{-1}\dot{\mathcal{F}}$. In the subsequent section we will make this identification.

Now we will consider the dynamics of the rigid body. We will start with the Euler-Lagrange equations defined on the Lie group, and then show the corresponding action principle defined on the Lie algebra. The kinetic energy of the rigid body is given by

$$\mathcal{K}(\dot{\Phi}) = \frac{1}{2} \int_{\mathcal{M}} \rho_0^V(\mathbf{X}) |\dot{\mathbf{x}}(\mathbf{X})|^2 d^3 X \tag{6.14}$$

which is here written explicitly as a function of $\dot{\Phi}$. To see this note that

$$\begin{pmatrix} 1 \\ \mathbf{x} \end{pmatrix} = \mathcal{F}_0 \Phi \mathcal{F}_0^{-1} \begin{pmatrix} 1 \\ \mathbf{X} \end{pmatrix} \tag{6.15}$$

and so \mathbf{x} can be seen as a function of Φ . The dynamical equations of motions of a free

rigid body with Lagrangian density $L : SE(3) \times TSE(3) \rightarrow \mathbb{R}$

$$\mathcal{L}(\Phi, \dot{\Phi}) = \mathcal{K}(\dot{\Phi}) \quad (6.16)$$

are found by invoking *Hamilton's principle*

$$\delta \int_0^T \mathcal{L}(\Phi(t), \dot{\Phi}(t)) dt = 0 \quad (6.17)$$

under variations $\Phi(t) \rightarrow \Phi(t) + \delta\Phi(t)$, where $\delta\Phi(t)$ is a variational test function which must vanish at the temporal boundaries, and where T is the upper-bound of the time-domain considered. The resulting equations of motion will be second-order equations for Φ in time. This formulation is often undesirable, as in numerical simulations errors accrue such as to push Φ out of the sub-manifold $SE(3) \subset \mathbb{R}^{4 \times 4}$. We will next formulate the corresponding equations of motion on the Lie algebra instead.

We have that

$$\mathcal{K}(\dot{\Phi}) = \frac{1}{2}m|\dot{\mathbf{r}}|^2 + \frac{1}{2} \int_{\mathcal{M}} \rho_0^V(\mathbf{X}) |\dot{R}\mathbf{X}|^2 d^3X \quad (6.18)$$

where we have used that $\int_M \rho_0^V(\mathbf{X}) \mathbf{X} d^3X = 0$. Now, since

$$|\dot{R}\mathbf{X}| = |\dot{E}B^T X| = |\dot{E}\tilde{X}| = |E^T \dot{E}\tilde{X}| = |\hat{\Omega}\tilde{X}| = |\vec{\Omega} \times \tilde{X}| \quad (6.19)$$

we see that the rotational kinetic energy is a quadratic form in terms of the angular velocity $\vec{\Omega}$. Furthermore, as $|\dot{\mathbf{r}}| = |\vec{V}|$ we can write

$$\mathcal{K}(N) = \frac{1}{2}m|\vec{V}|^2 + \frac{1}{2}\vec{\Omega}^T \mathbb{I}\vec{\Omega} \quad (6.20)$$

where $\mathbb{I} \in \mathbb{R}^{3 \times 3}$ is the *moment of inertia* tensor, which is, unless the body is incidental to a line, positive-definite. Eq. 6.20 is now a function of the Lie algebra-valued $N \in \mathfrak{se}(3)$. We define the *reduced Lagrangian density* $\ell : \mathfrak{se}(3) \rightarrow \mathbb{R}$

$$\ell(N) = \mathcal{K}(N) \quad (6.21)$$

which coincides with the regular Lagrangian density $\mathcal{L}(\Phi, \dot{\Phi}) = \ell(N)$ when $\Phi^{-1}\dot{\Phi} = N$. To find the corresponding Hamilton's principle

$$\delta \int_0^T \ell(N) dt = 0 \quad (6.22)$$

defined on the Lie algebra, we identify the space of admissible variations δN in terms of

the variations on the Lie group-level $\delta\Phi$. We vary Eq. 6.8 to find

$$\delta N = -\Phi^{-1}\delta\Phi\Phi^{-1}\dot{\Phi} + \Phi^{-1}\delta\dot{\Phi}. \quad (6.23)$$

where we used $\delta(\Phi\Phi^{-1}) = 0$ to find $\delta\Phi^{-1}$. We define the variational test function $\eta = \Phi^{-1}\delta\Phi$, which satisfies $\dot{\eta} = -N\eta + \Phi^{-1}\delta\dot{\Phi}$. We get

$$\begin{aligned} \delta N &= \dot{\eta} + [N, \eta] \\ &= \dot{\eta} + \text{ad}_N\eta. \end{aligned} \quad (6.24)$$

As we will compute the corresponding variational principle for the Cosserat rod in the subsequent section, we will not go through the detailed derivation here. If the variation Eq. 6.22 is computed using Eq. 6.24, the resulting equations of motion are

$$\frac{d}{dt}\frac{\partial\ell}{\partial N} = \text{ad}_N^*\frac{\partial\ell}{\partial N} \quad (6.25)$$

where $\text{ad}_N^* : \mathfrak{se}(3)^* \rightarrow \mathfrak{se}(3)^*$ is the dual of the adjoint action, defined on the dual $\mathfrak{se}(3)^*$ to the Lie algebra, and $\frac{\partial\ell}{\partial N}$ is the matrix partial derivative. Equation 6.25 is the result of the *Euler-Poincaré theorem* [147, 149, 147, 172], and is also thus referred to as the *Euler-Poincaré equation*. Further details, and its derivation in the continuum case, will follow in the subsequent sections. Evaluating Eq. 6.25 leads to

$$\dot{\vec{V}} = \vec{V} \times \vec{\Omega} \quad (6.26a)$$

$$\dot{\vec{\Omega}} = \mathbb{I}\vec{\Omega} \times \vec{\Omega}. \quad (6.26b)$$

Eq. 6.8 and Eq. 6.26 together fully specify the kinematics and dynamics of the free rigid body respectively. Note that Eq. 6.26 is expressed in the moving frame, and reduces to $\dot{\vec{V}} = 0$ and $\dot{\vec{\Omega}} = 0$ in a non-moving frame.

We will now briefly consider the case of a rigid body under the influence of an external force. As the more general case of a continuum of rigid bodies will be treated in the following section, we will leave out many mathematical details, and only state some results here to preface the results that will follow.

External forcing of the rigid body can be included by considering the more general *Lagrange-D'Alembert principle* [149], which is, in integral form

$$\delta \int_0^T \mathcal{L}(\Phi, \dot{\Phi}) dt + \int_0^T (\mathbf{T}(\Phi, \dot{\Phi}))(\delta\Phi) dt = 0 \quad (6.27)$$

where $\mathcal{L}(\Phi, \dot{\Phi})$ is the Lagrangian density of the free rigid body, and $\mathbf{T} \in T^*SE(3)$ is a covector, where its argument is the variational test function $\delta\Phi$. \mathbf{T} is here a generalised

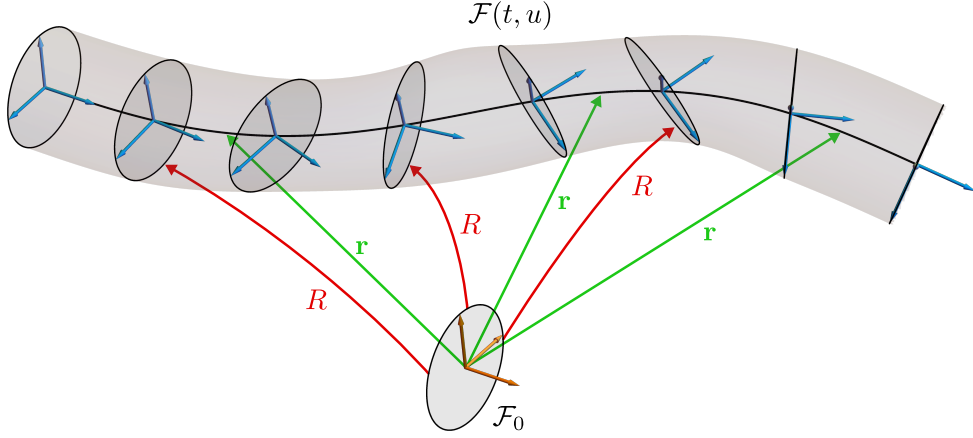


Figure 6.2: Illustration of the mapping from the reference configuration \mathcal{F}_0 to the current configuration $\mathcal{F}(t, u)$ of a Cosserat rod. The configuration of a Cosserat rod is specified by the center-line $\mathbf{r}(u)$, $u \in [0, L_0]$ and a rigid body cross section attached at each u , related to a reference configuration \mathcal{F}_0 , via translation (red) and rotation (red) respectively.

external force on the rigid body, containing both the force and the moment applied on the rigid body. As shown in [216], Eq. 6.27 in reduced form leads to

$$\delta \int_0^T \ell(N) dt + \int_0^T \langle T, \eta \rangle dt = 0 \quad (6.28)$$

where T is the generalised external force pulled-back onto the dual Lie algebra $\mathfrak{se}(3)^*$, η the variational test function defined on the Lie algebra, and $\langle \cdot, \cdot \rangle : \mathfrak{se}(3)^* \times \mathfrak{se}(3) \rightarrow \mathbb{R}$ is an inner product. If we let the \vec{f} and \vec{m} be the external force and moment respectively, the resulting equations of motion are

$$\dot{\vec{V}} = \vec{V} \times \vec{\Omega} + \vec{f} \quad (6.29a)$$

$$\dot{\vec{\Omega}} = \mathbb{I}\vec{\Omega} \times \vec{\Omega} + \vec{m}. \quad (6.29b)$$

In the following section we will generalise these equations of motion for the Cosserat rod.

6.2 Geometric Cosserat rod mechanics

6.2.1 Cosserat rod kinematics

General Cosserat media can be described as a microstructured sub-manifold of Euclidean space. At each point-continua on the sub-manifold n directors are attached, where each director can in general vary in both magnitude and direction independently. The *special Cosserat rod* is an example of a Cosserat system where the one-dimensional continuum body is called the *center-line* $\mathbf{r}(u)$, with two orthogonal directors at each material point

$u \in [0, L_0]$, where L_0 is the rest length of the rod, that are constrained to be *inextensible* (constant magnitude) and orthogonal. Equivalently, we can thus see the special Cosserat rod as a connected string of rigid body cross-sections. These cross-sections are represented as orthonormal frames we call the *material frames* $E(u) = (\mathbf{e}_1(u) \ \mathbf{e}_2(u) \ \mathbf{e}_3(u))$, which rotate relative to each other along the material coordinate u . A pair $\mathbf{r}(u), E(u)$) is known as a *trihedron*. See Fig. 5.1 for an illustration.

We will show that the kinematic configuration space of the Cosserat rod is the Lie group of special Euclidean transformations $SE(3)$, and then proceed to formulate its kinematic equations of motion on the corresponding Lie algebra $\mathfrak{se}(3)$.

Lie group–Lie algebra correspondence

The center-of-mass of the cross-section at u is given by $\mathbf{r}(u)$, and its orientation is specified by the material frame $E(u) = (\mathbf{e}_1(u) \ \mathbf{e}_2(u) \ \mathbf{e}_3(u))$, which is an orthonormal triad. As E is a basis for \mathbb{E}^3 , the vector of components in the material frame basis $\vec{v} = E^T \mathbf{v}$ will be said to be expressed in the *moving frame*. The configuration of the Cosserat rod is thus specified by the center-line and material frame, which we write as

$$\mathcal{F}(t, u) = \begin{pmatrix} 1 & \mathbf{0}^T \\ \mathbf{r}(t, u) & E(t, u) \end{pmatrix} \quad (6.30)$$

We can relate rod configurations to a reference coordinate system as

$$\mathcal{F}(t, u) = \mathcal{F}_0 \Phi(t, u) \quad (6.31)$$

where

$$\mathcal{F}_0 = \begin{pmatrix} 1 & \mathbf{0}^T \\ \mathbf{0} & B \end{pmatrix} \quad (6.32)$$

is the reference coordinate system, and $\Phi(t, u) \in SE(3)$ is the transformation between the two. See Fig. 6.2 for an illustration. In contrast the previous section, here we set the fixed frame to $B = \mathbb{1}_{3 \times 3}$, to simplify the notation. Such that $\mathcal{F}_0 = \mathbb{1}_{4 \times 4}$ and

$$\Phi(t, u) = (\mathbf{r}; E) = \begin{pmatrix} 1 & \mathbf{0}^T \\ \mathbf{r}(t, u) & E(t, u) \end{pmatrix} \in SE(3). \quad (6.33)$$

where we have introduced the short-hand notation for $\Phi = (\mathbf{r}; E)$ for $SE(3)$ elements. We thus have that $\mathcal{F}(t, u) = \Phi(t, u)$, and we will henceforth identify the Cosserat rod configuration with the group element $\Phi(t, u)$. The kinematic motion of the Cosserat rod can thus be fully specified by a space-time sheet $\Phi(t, u) \in SE(3)$ in the Lie group of special Euclidean transformations. In other words, the spatio-temporal configuration of

the Cosserat rod can be described as a 2-dimensional immersion $N \subset SE(3)$, defined by the map $\Phi : W \rightarrow SE(3)$, where we call $W = [0, T] \times [0, L_0]$ the *kinematic base space*, and $N = \Phi(W)$. Therefore we call $SE(3)$ the *kinematic configuration space* of the Cosserat rod, and Φ the *spatio-temporal configuration* of the system. In other words, N can be seen as a ‘sheet’ in $SE(3)$, and is parametrised by the function Φ . The manifolds $[0, L_0]$ and $[0, T]$ will be called the *material base space* and the *time domain* respectively. Furthermore, we may draw a distinction between the *internal configuration space* $SO(3)$, corresponding to the material frame, and the *external configuration space* $\mathbb{E}^3 \cong SE(3)/SO(3)$, corresponding to the center-line.

At a point $\Phi(t, u) \in N$, we can consider velocities in the temporal and spatial directions $\dot{\Phi}(t, u)$ and $\Phi'(t, u)$ respectively. Thus by differentiating the map Φ we get a vector field

$$d\Phi = \dot{\Phi}dt + \Phi'du \quad (6.34)$$

as discussed in Sec. 5.2.5, where $d\Phi(t, u) \in T_{\Phi(t, u)}N$ for all $(t, u) \in W$. Here it is worth clarifying a technical point to avoid confusion. Although we say $d\Phi$ is a vector field on N , we have written it as a 1-form on the kinematic base space W . These two notions are not contradictory. Precisely, $d\Phi$ is a *TN -valued 1-form on W* .

Via left-translation, we can relate $d\Phi$ to a $\mathfrak{se}(3)$ -valued 1-form on W

$$\xi = \Phi^{-1}d\Phi \quad (6.35)$$

where $\xi = \Phi^*\omega$, the pull-back $\Phi^*\omega$ of the Maurer-Cartan ω form, as discussed in Sec. 5.2.6. ξ contains all geometric information contained in Φ , up to rigid body transformations, and as a Lie algebra-valued object ξ will turn out to be easier to work with than Φ or $d\Phi$. In what follows, we will formulate the kinematics of the Cosserat rod entirely within the Lie algebra using ξ .

Kinematic equations of motion

Equation 6.35 shows how to construct ξ from the Lie group function Φ . For our purposes it will be more relevant to go the other direction: Given a ξ , is there a corresponding Φ ? The answer can be formulated in terms of integrability. As a motivating and intuitive example from multi-variate calculus, consider a vector-valued function $\mathbf{F} : \mathbb{R}^3 \rightarrow \mathbb{R}^3$. There exists a potential $U : \mathbb{R}^3 \rightarrow \mathbb{R}$ such that $\mathbf{F} = -\nabla \cdot U$ if and only if the differential $\phi = \frac{\partial F_i}{\partial x^i} dx^i$ is *exact*. In \mathbb{R}^3 , and for Lie groups, this is equivalent to $d\phi = 0$ ¹. In Sec. 5.2.6, we showed that there is a Φ for which the right-hand side of Eq. 6.35 holds true if and only if

$$d\xi + \xi \wedge \xi = 0. \quad (6.36)$$

¹This is known as the *Poincaré lemma* and holds true locally for arbitrary manifolds.

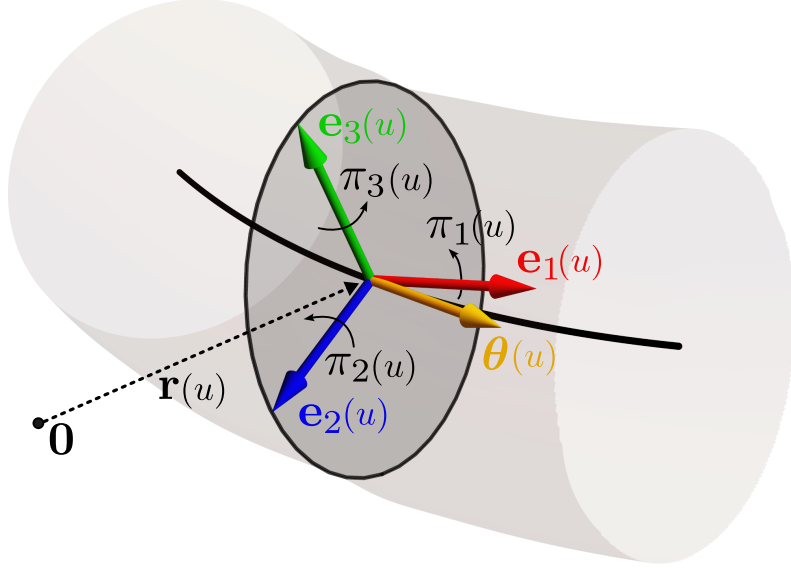


Figure 6.3: Depicts the rate-of-change along u of the material frame located at $\mathbf{r}(u)$ (dashed line). The spatial derivative of the center-line (solid black line) at u is $\boldsymbol{\theta}(u) = \mathbf{r}'(u)$ (yellow arrow), and π_1 , π_2 and π_3 is the angular rate-of-change of the material frame around \mathbf{e}_1 (red), \mathbf{e}_2 (blue) and \mathbf{e}_3 (green) respectively. The analogous description holds true for \vec{V} and $\vec{\Omega}$, but in time t rather than material coordinate u .

This is an integrability condition on ξ , and is a Maurer-Cartan equation on the sub-manifold N . As we will show, Eq. 6.36 is in fact a concise expression of the kinematics of a Cosserat rod. We expand ξ in terms of its temporal and spatial components

$$\xi = Ndt + Xdu \quad (6.37)$$

where $X(t, u), N(t, u) \in \mathfrak{se}(3)$, which we write as

$$X = \{\vec{\theta}; \vec{\pi}\} = \begin{pmatrix} 0 & \vec{0}^T \\ \vec{\theta} & \hat{\pi} \end{pmatrix} \quad (6.38a)$$

$$N = \{\vec{V}; \vec{\Omega}\} = \begin{pmatrix} 0 & \vec{0}^T \\ \vec{V} & \hat{\Omega} \end{pmatrix} \quad (6.38b)$$

where $\vec{\theta}(t, u), \vec{\pi}(t, u), \vec{V}(t, u), \vec{\Omega}(t, u) \in \mathbb{R}^3$ are vectors expressed in the material frame basis, and where we have introduced the notation $X = \{\vec{\theta}; \vec{\pi}\}$ as a shorthand for matrices like Eq. 6.38a. We will call X the *spatial reconstruction field* and N the *generalised velocity field*. Following a similar derivation as in Eq. 6.11, we find

$$\Phi^{-1}d\Phi = \begin{pmatrix} 0 & \vec{0}^T \\ E^T d\mathbf{r} & E^T dE \end{pmatrix}. \quad (6.39)$$

From Eq. 6.38 we then find that

$$d\mathbf{r} = \mathbf{e}_i V_i dt + \mathbf{e}_i \theta_i du \quad (6.40a)$$

$$d\mathbf{e}_j = \mathbf{e}_i \hat{\Omega}_{ij} dt + \mathbf{e}_i \hat{\pi}_{ij} du \quad (6.40b)$$

which we can also write as

$$d\mathbf{r} = \mathbf{V} dt + \boldsymbol{\theta} du \quad (6.41a)$$

$$dE = E \hat{\Omega} dt + E \hat{\pi} du. \quad (6.41b)$$

We can thus identify $\mathbf{V} = E\vec{V} = \partial_t \mathbf{r}$ as the translational velocity of the center-line, $\boldsymbol{\theta} = E\vec{\theta} = \partial_u \mathbf{r}$ as rate-of-change of the center-line along the material coordinate, and from Eq. 6.40b it follows that

$$\dot{\mathbf{e}}_i = \boldsymbol{\Omega} \times \mathbf{e}_i \quad (6.42a)$$

$$\mathbf{e}'_i = \boldsymbol{\pi} \times \mathbf{e}_i \quad (6.42b)$$

which show that $\boldsymbol{\Omega} = E\vec{\Omega}$ and $\boldsymbol{\pi} = E\vec{\pi}$ are the temporal and ‘spatial’ angular velocities of the material frame respectively. The spatial part of Eq. 6.40 is illustrated in Fig. 6.3. We can thus see N as a generalised velocity in the Lie algebra. Equation 6.40b also shows how derivatives of vector functions $\mathbf{v}(t, u)$ can be expressed in terms of $\vec{v}(t, u)$ in the moving frame basis. We have

$$\begin{aligned} d\mathbf{v} &= d(\mathbf{e}_i v_i) \\ &= \mathbf{e}_i (dv_i) + (d\mathbf{e}_i)v_i \\ &= E(d\vec{v}) + (E\hat{\pi} + E\hat{\Omega})v_i \\ &= E(D_t \vec{v} dt + D_u \vec{v} du) \end{aligned} \quad (6.43)$$

such that $E^T d\mathbf{v} = D_u \vec{v} du + D_t \vec{v} dt$, where

$$D_t = \partial_t + \hat{\Omega} \quad (6.44a)$$

$$D_u = \partial_u + \hat{\pi} \quad (6.44b)$$

are the spatial and temporal *material derivatives* respectively. We thus have that $E^T \mathbf{v}' = D_u \vec{v}'$ and $E^T \dot{\mathbf{v}} = D_t \vec{v}'$.

For a given spatio-temporal velocity field $N(t, u)$, Eq. 6.36 imposes a condition on the spatial reconstruction field $X(t, u)$. The resulting equations are the kinematic equations of motion. Substituting Eq. 6.37 into the left-hand side of Eq. 6.36

$$\begin{aligned} d\xi + \xi \wedge \xi &= N' dt \wedge du + \dot{X} dt \wedge du + X N dt \wedge du + N X dt \wedge du \\ &= (\dot{X} - N' + [N, X]) dt \wedge du, \end{aligned} \quad (6.45)$$

we get

$$\dot{X} = \mathcal{D}_u N. \quad (6.46)$$

where we have defined

$$\mathcal{D}_u = \partial_u + \text{ad}_X. \quad (6.47)$$

Equation 6.46 is the kinematic equation of motion for the Cosserat rod, which expresses the evolution of the spatial configuration X , in terms of the generalised velocity N . To express the kinematics in terms of the non-generalised velocities, we substitute Eq. 6.38 into Eq. 6.46 to find

$$D_t \vec{\theta} = D_u \vec{V} \quad (6.48a)$$

$$\partial_t \vec{\pi} = D_u \vec{\Omega}, \quad (6.48b)$$

which are equivalent to Eq. 6.46 and are the kinematic equations of motion expressed in the moving frame. At the Lie group-level the corresponding equations are

$$\dot{\mathbf{r}} = \mathbf{V} \quad (6.49a)$$

$$\dot{\mathbf{e}}_i = \boldsymbol{\Omega} \times \mathbf{e}_i \quad (6.49b)$$

From the numerical standpoint, the benefit of Eq. 6.48b over Eq. 6.49b is clear. Errors in integrating the latter can in general lead to $|\mathbf{e}_i| \neq 1$ and $\mathbf{e}_i \cdot \mathbf{e}_j \neq 0$, whilst by errors in Eq. 6.48b are by construction Lie algebra-valued. In other words, errors in Eq. 6.49b accrue in $\mathbb{R}^{3 \times 3}$, whilst errors in Eq. 6.48b accrue within the Lie group itself. Mathematically, this is due to the fact that Eq. 6.46 is defined on the linear space $W \times \mathfrak{se}(3)$, as opposed to Eq. 6.49 which is defined on the non-linear space $G \times TG$.

Types of deformations

Fig. 5.2 shows the various types of deformations that are kinematically possible for the Cosserat rod. Here we will describe how these deformations are encoded in $\vec{\theta}$ and $\vec{\pi}$. Since $\boldsymbol{\theta} = \mathbf{r}'$ we have that if $\vec{\theta}(u) \propto (1 \ 0 \ 0)$ then the material frame at u , pointing in the direction $\mathbf{e}_1(u)$ is aligned with the center-line. We thus see that $\vec{\theta}$ measures the *shear* of the rod. Note that this is because $\vec{\theta}$ is expressed in the moving frame; $\boldsymbol{\theta}$ does not contain any information about the shear.

Twist is the rotation of the material frame around \mathbf{e}_1 , and the rate of twist along the material coordinate is given by π_1 . Similarly, the rotation of the material frame around \mathbf{e}_2 and \mathbf{e}_3 are given by π_2 and π_3 respectively, as depicted in Fig. 6.3.

In a non-moving frame the *bending* of the center-line is encoded in \mathbf{r} , likewise $\boldsymbol{\theta}$. In the moving frame it is encoded in both $\vec{\theta}$ and $\vec{\pi}$ simultaneously. For instance, if $\vec{\theta}$ is constant

along u and π_2 or π_3 are non-zero along u , then the rod is bending.

In general velocities \vec{V} will cause the Cosserat to *extend*. Locally, the extension is described by the scalar $h(u) = |\mathbf{r}'| = |\vec{\theta}|$, which can be seen as the square root of the metric on the center-line induced by the Euclidean metric on \mathbb{R}^3 . Using h we can define an arc-length coordinate as

$$ds = h(u)du \quad (6.50)$$

which relates the arc-length increment ds to the material length increment du . In the arc-length parametrisation we thus have $|\frac{\partial \mathbf{r}}{\partial s}| = 1$ for all $s \in [0, L]$ where

$$L[h(u)] = \int_0^{L_0} h(u)du \quad (6.51)$$

is the total arc-length of the center-line. $h(u)$ thus measures the local extension of the rod, where $h(u) = |\vec{\theta}| = 1$ indicates that the rod is not suffering an extension at u .

We define a unit-vector tangent to the center-line $\mathbf{t} = \boldsymbol{\theta}/|\boldsymbol{\theta}|$. The *curvature* of the center-line is then a scalar defined as

$$\kappa = |\mathbf{t}'|. \quad (6.52)$$

In the literature it is more common to define the curvature in terms of the arc-length parametrisation, which we write as $\tilde{\kappa} = |\partial_s \mathbf{t}| = |\partial_s^2 \mathbf{r}|$.

Reconstructing the Cosserat rod from ξ

Solving Eq. 6.46, for a given velocity N , yields the Lie algebra-valued 1-form ξ which contains, in infinitesimal form, information from which the Cosserat rod \mathcal{F} can be reconstructed. Firstly, recall that we can reconstruct Φ , the representation of the Cosserat rod as a space-time sheet in the Lie group, from ξ using Eq. 6.35. Secondly, from Eq. 6.31 we note that $\Phi^{-1}d\Phi = \mathcal{F}^{-1}d\mathcal{F}$. Therefore we can reconstruct the Cosserat rod from ξ by solving the equation

$$d\mathcal{F} = \mathcal{F}\xi. \quad (6.53)$$

We will now put the above into a form solvable as a matrix ordinary differential equation. By expanding $\mathcal{F}^{-1}d\mathcal{F}$ into its components, and from Eq. 6.37 we find that

$$\mathcal{F}^{-1}\mathcal{F}' = X \quad (6.54a)$$

$$\mathcal{F}^{-1}\dot{\mathcal{F}} = Y. \quad (6.54b)$$

For fixed $t = \bar{t}$ and given initial conditions Eq. 6.54a can be used to find $\mathcal{F}(u, \bar{t})$ for $u \in [0, L_0]$, and for fixed $u = \bar{u}$ and given initial conditions Eq. 6.54b can be used to find

$\mathcal{F}(\bar{u}, t)$ for $t \in [0, T]$. We can therefore trace out and reconstruct $\mathcal{F}(t, u)$ by repeatedly solving Eqs. 6.54a and 6.54b. Due to Eq. 6.36, which ensures that $d\mathcal{F}$ is an ‘exact’ differential, the resulting $\mathcal{F}(t, u)$ is invariant with respect to the particular path in (t, u) -space taken to reconstruct it. Therefore, a suitable scheme to reconstruct \mathcal{F} is to first reconstruct the Cosserat rod in time along $u = 0$ by solving

$$\bar{\mathcal{F}}(t) = \bar{\mathcal{F}}(t)\dot{\bar{\mathcal{F}}}(t), \quad (6.55)$$

with initial condition $\bar{\mathcal{F}}(0) = \mathcal{F}^{0,0}$, where the latter corresponds to choosing values for $\mathbf{r}(0, 0)$ and $E(0, 0)$. Secondly, for any given time $t = \bar{t}$ we can reconstruct the Cosserat rod in space by solving

$$\mathcal{F}(u, \bar{t}) = \mathcal{F}(u, \bar{t})\mathcal{F}(u, \bar{t})', \quad (6.56)$$

with initial condition $\mathcal{F}(0, \bar{t}) = \bar{\mathcal{F}}(\bar{t})$. See App. D.1 for a detailed description of the numerical algorithm.

Closed Cosserat rods

Thus far we have considered *open* Cosserat rods, for which $\mathbf{r}(0) \neq \mathbf{r}(L_0)$ and $E(0) \neq E(L_0)$. For *closed* Cosserat rods the material coordinate $u \in [0, L_0]$ is periodic in its domain, and the center-line and material frame must also be periodic and continuous in u . Although seemingly complicated, the following derivations will result in showing that the case of a closed Cosserat can be in practice treated equivalently to an open Cosserat rod.

A closed rod implies that

$$X(0) = X(L_0). \quad (6.57)$$

However, Eq. 6.57 is only a necessary, but not sufficient, condition for the rod to close. The sufficient condition is for the constraint

$$\mathcal{F}(0, t) = \mathcal{F}(L_0, t) \quad (6.58)$$

to hold for all t . This is an integral constraint on X , as formally we can write

$$\mathcal{F}(L_0, t) = \mathcal{F}(0, t)\mathcal{U} \exp \left\{ \int_0^{L_0} X du \right\} \quad (6.59)$$

where \mathcal{U} denotes a u -ordered integral. The integral constraint on X is therefore

$$\mathcal{U} \exp \left\{ \int_0^{L_0} X du \right\} = 1. \quad (6.60)$$

However, if N is a smooth function of u , the kinematic equations of motion will preserve Eq. 6.60. This means that if the rod is initialised to obey Eq. 6.60 at $t = 0$, it will continue

to do so for all t .

In practice, in order to simulate a closed filament we must thus first construct on the Lie group-level a periodic $\mathcal{F}(u, 0)$, and then use Eq. 6.54a to find $X(u, 0)$ that obeys Eq. 6.60.

6.2.2 Cosserat rod dynamics

Constitutive dynamics

Thus far we have considered the Cosserat rod abstractly as a sub-manifold of $SE(3)$. Physically, the Cosserat rod is a kinematic approximation of a deformable and slender tube. Let $\mathcal{M} = D \times [0, L_0] \subset \mathbb{R}^3$ be the reference configuration of such a tube, where $D \subset \mathbb{R}^2$ is the cross-section of the tube and is of arbitrary shape. Let $\mathbf{X} \in \mathcal{M}$ denote the material coordinates of \mathcal{M} , such that $X_1 \in [0, L_0]$ and $(X_2, X_3) \in \mathcal{D}$ and for simplicity let ρ_0^V be a constant mass density per unit material volume at each \mathbf{X} . At time t the location of the material point at \mathbf{X} is given by $\mathbf{x}(\mathbf{X}, t)$, which are the deformed coordinates. We define (X_2, X_3) to be in the centre-of-mass of the cross-section, such that $\int_{\mathcal{D}} X_\gamma dX_2 dX_3 = 0$, $\gamma = 2, 3$.

The Cosserat rod models the slender deformable tube under the kinematic assumption that the material fibres that run radially from the center of \mathcal{D} to its edge are fixed. In other words we impose that

$$\mathbf{x}(\mathbf{X}, t) = \mathbf{r}(t, u) + X_\gamma \mathbf{e}_\gamma(t, u), \quad \gamma = 2, 3 \quad (6.61)$$

where $\mathbf{r}(t, u)$ is the center-line of the rod and where $u = X_1$ is the material coordinate along the center-line. The three-dimensional tube has thus been replaced with the Cosserat rod, which only has one spatial dimension. In this coarse-graining, the two missing spatial dimensions have been replaced by rigid body cross-sections attached at each $u \in [0, L_0]$, with orientation specified by the two directors \mathbf{e}_2 and \mathbf{e}_3 .

As in Sec. 6.1 we formulate the dynamics of the Cosserat rod via a Lagrangian formulation. We will again be using a reduction of the Lagrangian to construct dynamics defined on the Lie algebra. We derive the constitutive dynamics by first computing the kinetic energy of the rod in terms of its generalised velocity $N = \{\vec{V}; \vec{\Omega}\}$.

We assume that the dynamics is defined by a Lagrangian density of the form $\mathcal{L}(\Phi, d\Phi)$, and that its kinetic energy term is given by

$$\int_0^{L_0} \mathcal{K}(\dot{\Phi}) du = \frac{1}{2} \int_{\mathcal{M}} \rho_0^V |\dot{\mathbf{x}}|^2 d^3X \quad (6.62)$$

where \mathcal{K} is the kinetic energy density along the material coordinate u . Substituting in

Eq. 6.61 we get

$$\int_0^{L_0} \mathcal{K}(\dot{\Phi}) du = \frac{1}{2} \int_0^{L_0} \rho_0 |\mathbf{V}|^2 du + \frac{1}{2} \rho_0^V \int_{\mathcal{M}} \mathbf{V} \cdot \dot{\mathbf{e}}_\gamma X_\gamma d^3X + \frac{1}{2} \rho_0^V \int_{\mathcal{M}} |X_\gamma \dot{\mathbf{e}}_\gamma|^2 d^3X \quad (6.63)$$

where $\rho_0 = A\rho_0^V$ is the mass density per unit material length, and $A = \int_D dX_2 dX_3$ is the area of the cross-section, and we have used $\dot{\mathbf{r}} = \mathbf{V}$. The second term in Eq. 6.63 vanishes when the integral over D is evaluated. To evaluate the third term, let $\bar{\mathbf{X}} = X_\gamma \mathbf{e}_\gamma$, and note that $\mathbf{e}_i = \boldsymbol{\Omega} \times \mathbf{e}_i$, and so

$$|X_\gamma \dot{\mathbf{e}}_\gamma|^2 = |X_\gamma \boldsymbol{\Omega} \times \mathbf{e}_\gamma|^2 = |\boldsymbol{\Omega} \times \bar{\mathbf{X}}|^2 = |E(\vec{\Omega} \times \vec{X})|^2 = |\vec{\Omega} \times \vec{X}|^2 \quad (6.64)$$

where we used $(E\vec{\Omega}) \times (E\vec{X}) = E(\vec{\Omega} \times \vec{X})$. As $|(\vec{\Omega} \times \vec{X})|^2$ is a quadratic form in $\vec{\Omega}$, we can write

$$\frac{1}{2} \rho_0^V \int_{\mathcal{M}} |X_\gamma \dot{\mathbf{e}}_\gamma|^2 d^3X = \frac{1}{2} \int_0^{L_0} \vec{\Omega}^T \mathbb{I} \vec{\Omega} du \quad (6.65)$$

where \mathbb{I} is the cross-sectional moment-of-inertia per unit material length. We can thus write the kinetic energy of the Cosserat rod as $K(N) = \int_0^{L_0} \mathcal{K}(N) du$ where

$$\mathcal{K}(N) = \frac{1}{2} \rho_0 |\vec{V}|^2 + \frac{1}{2} \vec{\Omega}^T \mathbb{I} \vec{\Omega} \quad (6.66)$$

is the kinetic energy per material unit length, which is now explicitly a function of the generalised velocity N .

Having established that the kinetic energy of the Cosserat rod has a reduced form, we now assume that we have a reduced Lagrangian density of the form

$$\ell(\xi) = \mathcal{K}(N) - \mathcal{U}(X) \quad (6.67)$$

where $\mathcal{U}(X)$ is the potential energy per material unit length of a given spatial configuration $X = \{\vec{\theta}; \vec{\pi}\}$, and $\ell(\xi)$ is here a Lagrangian density defined on the Lie algebra. The reduced Lagrangian density satisfies $\ell(\xi) = \mathcal{L}(\Phi, d\Phi)$ when $\xi = \Phi^{-1}d\Phi$.

The reduced Lagrangian density Eq. 6.67 is explicitly invariant under Galilean transformations, as it is written in terms of the invariant quantities X and N . Physically, the fact that a Lagrangian $\mathcal{L}(\Phi, d\Phi)$ admits a reduction $\ell(\xi)$ entails that only differential deformations couple to the dynamics. In other words the Lagrangian is really only a function of the tangent space $\mathcal{L}(d\Phi)$. We will henceforth omit the argument in Φ when the Lagrangian density admits a reduced form.

The *generalised conjugate momentum* of the Cosserat rod is

$$S := \frac{\partial \ell}{\partial N} = \frac{\partial \mathcal{K}}{\partial N} = \begin{pmatrix} 0 & \vec{P}^T \\ \vec{0} & \vec{L}^T \end{pmatrix} \in \mathfrak{se}(3)^* \quad (6.68)$$

where $\vec{P} = \rho_0 \vec{V}$ and $\vec{L} = \mathbb{I}\vec{\Omega}$. It will become clear that \vec{P} is the linear momentum of the center-line per unit material length, and \vec{L} is the angular momentum per unit material length of the material frame. We use the short-hand $S = \{\vec{P}; \vec{L}\}$ as for Lie algebra elements. The matrix derivative $\frac{\partial \ell}{\partial N}$ is evaluated only with respect to the non-zero components of N , for which we have $S_{ji} = \frac{\partial \ell}{\partial N_{ij}}$, and $S_{ji} = 0$ otherwise. S can be seen to take values in the dual Lie algebra $\mathfrak{se}(3)^*$, which is the space of linear operators $\mathfrak{se}(3) \rightarrow \mathbb{R}$ on the Lie algebra. To see this, note that $\mathcal{K}(N)$ can be written as

$$\mathcal{K}(N) = \frac{1}{2} \langle N, P \rangle \quad (6.69)$$

where $\langle \cdot, \cdot \rangle : \mathfrak{se}(3) \times \mathfrak{se}(3)^* \rightarrow \mathbb{R}$ is an inner product defined as

$$\langle A, B \rangle = \vec{a} \cdot \vec{b} + \vec{m} \cdot \vec{n} \quad (6.70)$$

where $A = \{\vec{a}; \vec{m}\} \in \mathfrak{se}(3)$ and $B = \{\vec{b}; \vec{n}\} \in \mathfrak{se}(3)^*$. Similarly, we can define a *generalised stress*, conjugate to the spatial configuration X , as

$$Q := \frac{\partial \mathcal{U}}{\partial X}. \quad (6.71)$$

We write its components as $Q = \{\vec{F}; \vec{M}\}$ where

$$F_i = \frac{\partial \mathcal{U}}{\partial \theta_i} \quad (6.72a)$$

$$M_i = \frac{\partial \mathcal{U}}{\partial \pi_i} \quad (6.72b)$$

are, as will be shown, the force on the center-line and the moment on the material frame respectively.

To find dynamic equations of motion for P and Q , we invoke Hamilton's principle that variations

$$\delta \int_W \ell(\xi) dt \wedge du \quad (6.73)$$

must vanish, where $\ell(\xi)$ is again the reduced Lagrangian density for the system. As for the rigid body in Sec. 6.1, we must first derive the permissible form of the variations. We first consider the Lagrangian density $\mathcal{L} : SE(3) \times TSE(3) \rightarrow \mathbb{R}$ defined on the Lie group, which satisfies $\mathcal{L}(\Phi, d\Phi) = \ell(\xi)$ when $\Phi^{-1}d\Phi = \xi$. The Euler-Lagrange equations are found by imposing

$$\delta \int_W \mathcal{L}(\Phi, d\Phi) dt \wedge du = 0 \quad (6.74)$$

under variations $\Phi \rightarrow \Phi + \delta\Phi$, where $\delta\Phi(t, u) \in TSE(3)$ is a variational test function which must vanish at the temporal boundaries. We will now assume that the Lagrangian

density can be written as a function $\mathcal{L} = \mathcal{L}(d\Phi)$, purely in terms of the tangent vectors $d\Phi$. Repeating similar steps as in Sec. 6.1, we vary $\xi = \Phi^{-1}d\Phi$ to get

$$\delta\xi = -\Phi^{-1}\delta\Phi\Phi^{-1}d\Phi + \Phi^{-1}\delta(d\Phi). \quad (6.75)$$

We define the variational test function $\eta = \Phi^{-1}\delta\Phi$, which satisfies $d\eta = -N\eta + \Phi^{-1}\delta(d\Phi)$, to get

$$\begin{aligned} \delta\xi &= d\eta + \text{ad}_\xi\eta \\ &= (\dot{\eta} + \text{ad}_N)dt + (\eta' + \text{ad}_X\eta)du \\ &= \delta X du + \delta N dt \end{aligned} \quad (6.76)$$

We now proceed to evaluate Eq. 6.73. We first note that since

$$\begin{aligned} \delta\ell &= \frac{\partial\ell}{\partial X_{ij}}\delta X_{ij} + \frac{\partial\ell}{\partial N_{ij}}\delta N_{ij} \\ &= \langle S, \delta N \rangle - \langle Q, \delta X \rangle, \end{aligned} \quad (6.77)$$

we have

$$\begin{aligned} \delta \int_W \ell(\xi) dt \wedge du &= \int_W \{ \langle \delta N, S \rangle - \langle \delta X, Q \rangle \} dt \wedge du \\ &= \int_W \{ \langle \dot{\eta} + \text{ad}_N\eta, S \rangle - \langle \eta' + \text{ad}_X\eta, Q \rangle \} dt \wedge du \\ &= \int_W \left\{ \left\langle \eta, \left(-\frac{\partial}{\partial t} - \text{ad}_N^* \right) S \right\rangle - \left\langle \eta, \left(-\frac{\partial}{\partial u} - \text{ad}_X^* \right) Q \right\rangle \right\} dt \wedge du \\ &\quad + \int_0^{L_0} [\langle \eta, S \rangle]_0^T du - \int_0^T [\langle \eta, Q \rangle]_0^{L_0} dt \\ &= 0 \end{aligned} \quad (6.78)$$

where we used integration-by-parts and where $\text{ad}_A^* : \mathfrak{se}(3)^* \rightarrow \mathfrak{se}(3)^*$ is the dual of the adjoint action, defined as $\langle \text{ad}_A^* B, C \rangle = -\langle B, \text{ad}_A C \rangle$. We impose that the variation vanishes at the temporal boundaries, to get

$$\mathcal{D}_t^* S = \mathcal{D}_u^* Q \quad (6.79a)$$

$$Q = 0, \quad u = 0, L_0 \quad (6.79b)$$

where

$$\mathcal{D}_t^* = \partial_t + \text{ad}_N^* \quad (6.80a)$$

$$\mathcal{D}_u^* = \partial_u + \text{ad}_X^* \quad (6.80b)$$

which was first derived in [107, 82], where Eq. 6.79b arises from imposing that $\int_0^T [\langle Q, \eta \rangle]_0^{L_0} dt =$

0 for arbitrary variations η . As $Q = Q(X)$, Eq. 6.79b is a boundary condition on X . Equation 6.79 is the local balance law of linear and angular momentum in the absence of external forces, and together with Eq. 6.46 completely determines the constitutive kinematics and dynamics of a Cosserat rod. These equations are first-order partial differential equations in both time t and space u . The corresponding equations of motion for a closed rod are identical, with the exception that Eq. 6.79b no longer applies.

We now evaluate Eq. 6.79 in terms of the components of S , Q , X and Y . To do this we must first compute action of the dual adjoint ad_B^* . As ad_B is a linear operator, it can be represented in matrix form as

$$[\text{ad}_A] = \begin{pmatrix} \hat{n} & \hat{a} \\ 0_{3 \times 3} & \hat{n} \end{pmatrix} \in \mathbb{R}^{6 \times 6} \quad (6.81)$$

where $A = \{\vec{a}; \hat{n}\}$ and acts as $[\text{ad}_A]\vec{B}$, where we have represented $B = \{\vec{b}; \vec{m}\}$ as vectors $\vec{B} = (\vec{b}^T \vec{m}^T)^T \in \mathbb{R}^6$. Now we have

$$\begin{aligned} \langle B, \text{ad}_A C \rangle &= \vec{B}^T [\text{ad}_A] \vec{C} \\ &= -([\text{ad}_A^*] \vec{B})^T \vec{C} \\ &= -\vec{B}^T [\text{ad}_A^*]^T \vec{C}. \end{aligned} \quad (6.82)$$

We thus have that

$$[\text{ad}_A^*] = -[\text{ad}_A]^T = \begin{pmatrix} \hat{n} & 0_{3 \times 3} \\ \hat{a} & \hat{n} \end{pmatrix} \in \mathbb{R}^{6 \times 6} \quad (6.83)$$

where we used $\hat{a}^T = -\hat{a}$ for anti-symmetric matrices. Using Eq. 6.83 we get

$$D_t \vec{P} = D_u \vec{F} \quad (6.84a)$$

$$D_t \vec{L} = D_u \vec{M} + \vec{\theta} \times \vec{F} \quad (6.84b)$$

$$\vec{M} = 0, \quad u = 0, L_0 \quad (6.84c)$$

$$\vec{F} = 0, \quad u = 0, L_0 \quad (6.84d)$$

where we used the definitions of S , Q , X and Y and the covariant derivative. In the non-moving frame the equations of motion are

$$\dot{\vec{P}} = \vec{F}' \quad (6.85a)$$

$$\dot{\vec{L}} = \vec{M}' + \vec{r}' \times \vec{F} \quad (6.85b)$$

where $\vec{F} = \vec{M} = 0$ at $u = 0, L_0$, which are the classical force and moment balance equations for a Cosserat rod [38, 194]. Here we see explicitly that \vec{F} and \vec{M} is a constitutive force on the center-line and a constitutive moment on the material frame respectively,

with dimensions of force and moment respectively. We can also identify \mathbf{P} as the linear momentum per unit material length of the center-line, and \mathbf{L} as the angular momentum per unit material length of the material frame. The second term in Eq. 6.85b is the moment exerted on the material frame by the force. Note that linear force balance Eq. 6.85a is the 1-dimensional analogue of the Cauchy momentum equation Eq. 5.1, where the force that arise from constitutive stresses is here \mathbf{F} . We thus see that the physical description of the Cosserat rod is consistent with classical continuum mechanics. For a discussion on how the dimensions of the kinematic and dynamic quantities are arrived at, as well as how to nondimensionalise the dynamics, see App. C.

The generalised momentum can be written in a compact form as

$$\vec{S} = \mathbf{M}\vec{N} \quad (6.86)$$

where

$$\mathbf{M} = \begin{pmatrix} \rho_0 \mathbb{I}_{3 \times 3} & 0_{3 \times 3} \\ 0_{3 \times 3} & \mathbb{I} \end{pmatrix} \quad (6.87)$$

is a generalised mass matrix. Similarly, in many applications the constitutive potential energy density can be written as a quadratic form

$$\mathcal{U} = \frac{1}{2}(\vec{X} - \vec{X}_0)^T \mathbf{K}(\vec{X} - \vec{X}_0) \quad (6.88)$$

where \mathbf{K} is a symmetric and positive-definite matrix, representing the elastic stiffness of the rod, and \vec{X}_0 is a given rest state. In which case the generalised stress can be written as

$$\vec{Q} = \mathbf{K}\vec{X}. \quad (6.89)$$

Henceforth we will write $S = \mathbf{M}\vec{N}$ and $Q = \mathbf{K}\vec{X}$, where the action of matrices like \mathbf{M} are to be understood in the sense of Eq. 6.86.

Body forces and non-conservative dynamics

In the preceding sections we considered a stress $Q = \frac{\partial \mathcal{U}}{\partial X}$, leading to conservative dynamics. In general, the dynamics does not have to be variational (i.e. derived from a potential \mathcal{U}). When this is not the case, we say that the dynamics is *non-conservative*. Furthermore external or internal *body* forces and moments, like gravity and friction, are absent in Eq. 6.79.

The following is a generalisation of the derivations in [216, 172, 148] for continuum systems. We write the continuum analogue of the *integral Lagrange-d'Alembert* principle

as [149, 108]

$$\delta \int_W \mathcal{L}(d\Phi) dt \wedge du + \int_W (\mathbf{T}(\Phi, d\Phi, \dots))(\delta\Phi) dt \wedge du = 0 \quad (6.90)$$

where $\mathbf{T}(\Phi, d\Phi, \dots) \in T^*SE(3)$ is a covector field we call the *generalised body force* and can be an arbitrary function of Φ and its derivatives, and where it is acting on the variational test function $\delta\Phi$. Henceforth we will suppress its arguments and write $(\mathbf{T}(\Phi, d\Phi, \dots))(\delta\Phi) = \mathbf{T}(\delta\Phi)$. Analogous to previous section, we presume that the Lagrangian density can be reformulated to a reduced form $\ell(\xi)$. Compare with Eq. 6.27. Note that the way \mathbf{T} appears in the integral, as a density over the kinematic base space W , shows that it is indeed a generalised *body* force. Eq. 6.90 is a generalisation of Hamilton's principle Eq. 6.74 that also incorporates body forces.

By the Euler–Poincaré theorem [216], the first term in Eq. 6.90 evaluates as previously to Eq. 6.78. The second term can be written as

$$\begin{aligned} \int_W \mathbf{T}(\delta\Phi) dt \wedge du &= \int_W \mathbf{T}(\Phi\eta) dt \wedge du \\ &= \int_W \mathbf{T}(L_\Phi\eta) dt \wedge du \\ &= \int_W \langle \eta, T \rangle dt \wedge du \end{aligned} \quad (6.91)$$

where we used $\eta = \Phi^{-1}\delta\Phi$, and where $T = L_\Phi^*\mathbf{T}$ is the generalised body force mapped to the dual Lie algebra and is thus a map $T : W \rightarrow \mathfrak{se}(3)^*$, and $L_\Phi^* : T_\Phi^*SE(3) \rightarrow \mathfrak{se}(3)^*$ is a mapping from the cotangent bundle to the dual Lie algebra defined as $\mathbf{T}(L_\Phi\eta) = \langle L_\Phi^*\mathbf{T}, \eta \rangle$. The resulting dynamical equations of motion, which now include arbitrary body forces and moments, are

$$\mathcal{D}_t^*S = \mathcal{D}_u^*Q + T \quad (6.92a)$$

$$Q = 0, \quad u = 0, L_0. \quad (6.92b)$$

The analogous equation for non-continuum systems can be found Eq. 4 in [147] and Eq. 6 in [216]. Expressed in non-Lie algebraic terms, by setting $\vec{T} = \{\vec{f}; \vec{m}\}$, the equations of motion in the moving frame are

$$D_t \vec{P} = D_u \vec{F} + \vec{f} \quad (6.93a)$$

$$D_t \vec{L} = D_u \vec{M} + \vec{\theta} \times \vec{F} + \vec{m} \quad (6.93b)$$

where \vec{f} and \vec{m} are the body force and moment respectively, with units of force and moment per unit material length respectively, and $\vec{F} = \vec{M} = 0$ at $u \in 0, L_0$ as before.

Finally, in the non-moving frame, we have

$$\dot{\mathbf{P}} = \mathbf{F}' + \mathbf{f} \quad (6.94a)$$

$$\dot{\mathbf{L}} = \mathbf{M}' + \mathbf{r}' \times \mathbf{F} + \mathbf{m} \quad (6.94b)$$

where $\mathbf{F} = \mathbf{M} = 0$ at $u = 0, L_0$. Note that \mathbf{f} and \mathbf{m} (and \vec{f} and \vec{m}) have dimension force per unit material length and moment per unit material length respectively.

Although technical, the derivation in Eq. 6.91 shows in what form the generalised body force appears in the equations of motion. In practice however, we do not need to evaluate $L_\Phi^* \mathbf{T} \in \mathfrak{se}(3)^*$, but can instead find the expression for the body forces and moments by first defining them in the non-moving frame. For example, to incorporate gravity we would have a body force $\mathbf{f} = -\rho_0 g \mathbf{d}_3$, where g is here the gravitational constant. In the moving frame, the force is then $\vec{f} = E^T \mathbf{f}$. We see that the static force \mathbf{f} becomes state-dependent in the moving frame. In this context \vec{f} is referred to as an *advection force*, and is treated in detail in [108, 32, 106].

As the example of gravity highlights, in general body forces and moments can be functions of the Lie group-level configuration Φ , or indeed functions of space-time (t, u) or the Lie algebra-valued X and N , and any of their derivatives. In this general case the dynamics are thus no longer defined purely on the Lie algebra. For simulations, this mean that Φ needs to be reconstructed from ξ for every time t , in order to evaluate the dynamics. In Sec. 6.2.1 we showed how to reconstruct Φ from ξ .

Finally, we now consider non-variational constitutive forces. For a point particle, the Euler-Lagrange equations can be shown to be a special case of D'Alembert's principle where the applied force is derives from a potential energy function. Consider point particle with configuration space Q , and a Lagrangian density $\mathcal{L} : Q \times TQ \rightarrow \mathbb{R}$ given by $\mathcal{L}(\mathbf{q}, \dot{\mathbf{q}}) = \mathcal{K}(\dot{\mathbf{q}}) - \mathcal{U}(\mathbf{q})$, where \mathbf{q} are coordinates on Q . Then from Hamilton's principle $\delta \int_0^T \mathcal{L} = 0$ we find

$$\int_0^T \left(\frac{\partial \mathcal{K}}{\partial \dot{\mathbf{q}}} \cdot \delta \dot{\mathbf{q}} - \frac{\partial \mathcal{U}}{\partial \mathbf{q}} \cdot \delta \mathbf{q} \right) dt = 0. \quad (6.95)$$

We can identify $\mathbf{P} = \frac{\partial \mathcal{K}}{\partial \dot{\mathbf{q}}}$ and $\mathbf{F} = \frac{\partial \mathcal{U}}{\partial \mathbf{q}}$ as the inertial and external forces respectively, which we also identify as covectors $\mathbf{P}, \mathbf{F} \in T^*Q$ as they contract with tangent vectors. Now if we promote F_i to be an arbitrary non-variational force, then we have

$$\int_0^T (\mathbf{P} \cdot \delta \dot{\mathbf{q}} - \mathbf{F} \cdot \delta \mathbf{q}) dt = 0. \quad (6.96)$$

which is D'Alembert's principle in integral form for a point particle.

By analogy to the previous example, we construct D'Alembert's principle for the constitutive dynamics of a Cosserat rod, which reduce to the Euler-Poincaré equations

when the forces and moments are conservative. As shown in Eq. 6.78, the variation of $\int_W \ell \, dt \wedge du$ leads to

$$\int_W \{ \langle \delta N, S \rangle - \langle \delta X, Q \rangle \} \, dt \wedge du = 0, \quad (6.97)$$

where previously $Q = \frac{\partial U}{\partial X}$ was variational. However if we let Q to be non-variational in general, we can take Eq. 6.97 to be a D'Alembert's principle for constitutive mechanics in the absence of body forces. Thus we present a final generalisation of the integral Lagrange-d'Alembert principle

$$\int_W \{ \langle \delta N, S \rangle - \langle \delta X, Q \rangle \} \, dt \wedge du + \int_W \langle \eta, T \rangle \, dt \wedge du = 0 \quad (6.98)$$

which incorporates both body and non-conservative forces and moments. The resulting equations of motion are identical to Eq. 6.92, but where Q is now an arbitrary function of X .

Equation 6.98 should be compared with Eq. 6.28, which is the corresponding principle for rigid bodies. As rigid bodies are in-effect modelled as oriented point particles, they suffer no internal stresses. There is therefore no notion of a constitutive dynamics for a rigid body, as there are for a continuum bodies. For the latter, the first term in Eq. 6.28 is now instead the first term in Eq. 6.98, which accommodates for general non-conservative internal stresses.

6.2.3 Summary and discussion

Here we give a brief overview and summary of the steps taken to derive the kinematic and dynamic equations of motion of the Cosserat rod.

In Eq. 6.31 we showed that the configuration space of the Cosserat rod can be seen as the Lie group of special Euclidean transformations $SE(3)$, and its spatio-temporal configuration can thus be seen as a group-valued function $\Phi(t, u) \in SE(3)$, where $t \in [0, T]$ and $u \in [0, L_0]$. We referred to $M = [0, L_0]$ as the material base space, and $W = [0, T] \times M$ the kinematic base space. Through the Lie group-Lie algebra correspondence, Eq. 6.35, the configuration of the rod can additionally be described as a Lie algebra-valued function $\xi(t, u) \in \mathfrak{se}(3)$. The kinematic equations of motion Eq. 6.46, formulated in the Lie algebra, can then be derived by imposing the integrability condition Eq. 6.36.

Dynamically, we modelled the Cosserat rod as a kinematic approximation of a thin three-dimensional tube. We wrote down the general Lagrangian density for the constitutive mechanics of the latter in Eq. 6.62, and then proceeded to derive the corresponding reduced Lagrangian density defined on the Lie algebra Eq. 6.67. By performing Lie algebraic variations of the reduced Lagrangian density, we arrived at the Euler-Poincaré for the constitutive dynamics of the Cosserat rod Eq. 6.79.

Finally, we derived a generalised integral Lagrange-d'Alembert principle Eq. 6.98, that allows for both non-variational (non-conservative) constitutive forces and moments, as well as body forces and moments.

The full set of kinematic and dynamical equations of motion for the Cosserat rod can thus be written as

$$\dot{X} = (\partial_u + \text{ad}_X)N \quad (6.99a)$$

$$(\partial_t - \text{ad}_N^*) S = (\partial_u - \text{ad}_X^*) Q + T \quad (6.99b)$$

$$Q = 0, \quad u = 0, L_0, \quad (6.99c)$$

and the equations close using $P = MN$, where ad_X^* is defined in Eq. 6.83. Using $X = \{\vec{\theta}; \vec{\pi}\}$, $N = \{\vec{V}; \vec{\Omega}\}$ and $P = \{\rho_0 \vec{V}; \vec{L}\}$ the equations of motion in the moving frame become

$$D_t \vec{\theta} = D_u \vec{V} \quad (6.100a)$$

$$\partial_t \vec{\pi} = D_u \vec{\Omega} \quad (6.100b)$$

$$D_t \vec{P} = D_u \vec{F} + \vec{f} \quad (6.100c)$$

$$D_t \vec{L} = D_u \vec{M} + \vec{\theta} \times \vec{F} + \vec{m} \quad (6.100d)$$

with $\vec{F} = \vec{M} = 0$ at $u = 0, L_0$, and the equations close using $\vec{P} = \rho_0 \vec{V}$ and $\vec{L} = \mathbb{I} \vec{\Omega}$, and D_u and D_t are defined in Eq. 6.44.

The equations of motion that would have resulted from varying the Lagrangian density $\mathcal{L}(\Phi, d\Phi)$ in Eq. 6.74, defined on the Lie group, would have resulted in equations of motion defined on the *non-linear* space $SE(3) \times TSE(3)$ and $SE(3) \times T^*SE(3)$. In contrast, varying the reduced Lagrangian density Eq. 6.73 results in equations of motion Eq. 6.99 defined on $W \times \mathfrak{se}(3)$ and $W \times \mathfrak{se}(3)^*$, which are linear spaces². This drastic simplification of the dynamics is inherently made possible due to the properties of a Lie group G , allowing for the trivialisation $G \times TG \cong G \times \mathfrak{g}$.

When the dynamics is constitutive then it is notable that the above equations of motion are entirely formulated within the Lie algebra. That is, the dynamical variables are the Lie algebra-valued X and N , and all forces and moments are expressed as functions of them. The invariance of the constitutive dynamics under rigid body rotations and translations is inherent in Eq. 6.99, as all quantities in the equations are in themselves invariant.

In the next section we will consider kinematically constrained Cosserat rods, and in particular the *filament*, which has as kinematic configuration space the homogeneous space $SE(3)/SO(3)$. The results of this and the next section will be generalised in Ch. 7 to systems where the kinematic configuration space is a general Lie group or homogeneous space, and the material base space is a general manifold.

²Note that this is not strictly-speaking true in general, if T is a function of Φ

$$\mathcal{F}(u, t) \in SE(3)$$

$$\mathcal{F}(u, t) \in SE(3)/SO(3) \cong \mathbb{E}^3$$

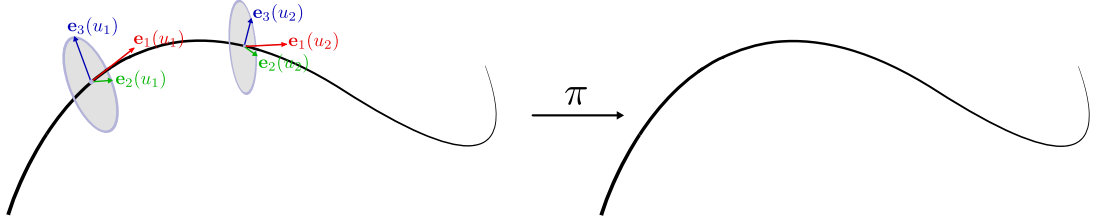


Figure 6.4: (Left) A Cosserat rod, with configuration space $SE(3)$. (Right) A filament, with configuration space in $SE(3)/SO(3) \cong \mathbb{E}^3$.

We conclude this section with the remark that it is possible to view the mathematical formalism that we have developed from a field-theoretic lens. The spatio-temporal configuration Φ can be seen as a $SE(3)$ -valued field defined over the base space $M = [0, L_0]$. The kinematic and dynamic equations of motion are then the field equations, defined in terms of the Lie algebra.

6.3 Mechanics of kinematically constrained Cosserat rods

Thus far we have considered the material frame E and the center-line \mathbf{r} as independent degrees of freedom, modelling a rod that can shear and twist in addition to bending and extending. In many applications it suffices to consider pure center-line dynamics where the cross-section does not shear [54, 202, 84, 195, 158, 102]. We shall refer to these systems as *filaments*, and can be seen as a Cosserat rod model with a kinematically constrained material frame. As we will show, kinematic constraints can often be implemented by first identifying an appropriate Lie subgroup $H \subset SE(3)$ such that the homogeneous space $SE(3)/H$ is the kinematically constrained configuration space, and then by making a ‘gauge choice’ $h(u) \in H$ which fixes a parametrisation of $SE(3)/H$. In addition to the filament, we will also consider the case of a *twisting filament*, where the cross-section is allowed to twist around the center-line [174, 170, 86].

6.3.1 Kinematic constraints and gauge freedoms

The configuration space of a filament can be found by ‘rotating away’ the material frame $E(u)$ at each u . Therefore the appropriate Lie subgroup is $H = SO(3)$, and the configuration space is $SE(3)/SO(3) \cong \mathbb{E}^3$, where \mathbb{E}^3 is the three-dimensional Euclidean space. Conceptually, that $SE(3)/SO(3)$ represents the configuration space of the filament can be understood by recalling the definition of a homogeneous space. For any Lie group

G and Lie subgroup $H \subset G$ then G/H is the set

$$G/H = \{gH \mid g \in G\} \quad (6.101)$$

where $gH = \{gh \mid h \in H\}$ is the left coset. Now consider the case when $G = SE(3)$ and $H = SO(3)$. Let $g_1 = (\mathbf{r}, E_1)$ and $g_2 = (\mathbf{r}, E_2)$ denote two cross-sections that are located at the same point \mathbf{r} , but have two different material frames E_1 and E_2 , and furthermore we can trivially identify these as elements $g_1, g_2 \in SE(3)$. As E_1 is related to E_2 by a rotation in $SO(3)$, we have that $g_1H = g_2H$. In other words, in the homogeneous space $SE(3)/SO(3)$, g_1 and g_2 belong to the same element $g_1H = g_2H \in SE(3)/SO(3)$. Therefore, a filament can mathematically be described as a Cosserat rod where we have, for each u , identified all material frames $E(u)$ at $\mathbf{r}(u)$ as belonging to the same equivalence class. See Fig. 6.4 for an illustration.

Now let $\Phi : W \rightarrow SE(3)/SO(3)$ be the spatio-temporal configuration of the filament. As discussed in Sec. 5.2.6, we can write Φ as

$$\Phi = \pi \circ \tilde{\Phi} \quad (6.102)$$

where \circ denotes compositions of maps and $\pi : SE(3) \rightarrow SE(3)/SO(3)$ relates elements in $SE(3)$ to elements in the homogeneous space and can be defined as

$$\pi((\mathbf{r}; E)) = \mathbf{r}, \quad (6.103)$$

and $\tilde{\Phi} : W \rightarrow SE(3)$ is a *framing*, or an *adapted frame field*, of Φ [34], and is a Lie group-valued function on W that satisfies Eq. 6.102.

We can map any framing $\tilde{\Phi}$ to a spatio-temporal filament configuration Φ using Eq. 6.102. Note however that this map is not injective. Let $h : W \rightarrow SO(3)$ be an arbitrary $SO(3)$ -valued smooth function and let $\tilde{\Phi}_1 : W \rightarrow SE(3)$ and $\tilde{\Phi}_2 : W \rightarrow SE(3)$, then if $\tilde{\Phi}_1(t, u) = h(t, u)\tilde{\Phi}_2(t, u)$ maps to the same Φ . Any given choice of $\tilde{\Phi}$ is called a *framing* of Φ [34]. There is thus a *gauge freedom* in the choice of $\tilde{\Phi}$.

In principle, the kinematic and dynamical equations for a Cosserat rod Eq. 6.99 apply to the filament as well. We could initialise Eq. 6.99 with some $\tilde{\Phi}(u, 0)$ that maps to the true initial condition $\Phi(u, 0)$, then simulate the equations of motion to find $\tilde{\Phi}(t, u)$, and then finally use Eq. 6.102 to find $\Phi(t, u)$. In this case, it is important that all constitutive and body forces and moments only couple to the center-line \mathbf{r} , and not the material frame E . For example, for conservative constitutive dynamics we could have a potential energy density $\mathcal{U} \propto \kappa^2$, where κ is the scalar curvature of the center-line defined in Eq. 6.52.

However, the above would mean simulating equations of motion of higher-dimensionality than the system in question, where the extra degrees of freedom (the material frame)

are non-physical. In the following we will instead choose a particular *gauge* and form an injective map between $\tilde{\Phi}$ and Φ . In other words, by choosing a gauge we choose a particular prescription for how to frame a given space-curve. Beyond the fact that the resulting dynamics will be defined directly on the lower dimensional $SE(3)/SO(3)$ rather than $SE(3)$, it is also often easier to formulate constitutive dynamics given a particular framing, rather than formulating it in terms of the degrees of freedom of a general Cosserat rod. The programmatic construction of such gauges is better known as the *theory of moving frames* [28, 136]. We note that the terminological use of ‘gauge’, although well-motivated in this context, is not standard in the theory of moving frames.

All gauge choices are ultimately mathematically equivalent, however some choices are more practically useful than others. Our procedure to construct a gauge will be to write the material frame $E = (\mathbf{e}_1 \mathbf{e}_2 \mathbf{e}_3)$ as a function of the center-line \mathbf{r} . Thus one-to-one map between Φ and $\tilde{\Phi}$ is formed. As a first step towards finding an appropriate gauge, we set

$$\mathbf{e}_1 = \frac{\mathbf{r}'}{h} \quad (6.104)$$

where $h = |\mathbf{r}'|$, such that \mathbf{e}_1 is a unit-vector tangent to \mathbf{r} at u . This means that given \mathbf{e}_1 we can write the center-line as

$$\mathbf{r}(t, u) = \mathbf{r}(0, t) + \int_0^u h\mathbf{e}_1 du. \quad (6.105)$$

There is now a remaining $SO(2)$ gauge freedom in specifying the material frame vectors \mathbf{e}_2 and \mathbf{e}_3 . In the gauges found in the literature [15, 145, 34, 27, 190], most abide Eq. 6.104, and are thus all related by an $SO(2)$ gauge transformation of \mathbf{e}_2 and \mathbf{e}_3 .

The Frenet-Serret gauge

In the *Frenet-Serret* gauge [64, 191], we set

$$\mathbf{e}_2 = \frac{\mathbf{e}'_1}{\kappa} \quad (6.106)$$

where $\kappa = |\mathbf{e}'_1|$ is the scalar curvature, such that $\mathbf{e}_2(u)$ is a unit-vector pointing in the direction of the center-line $\mathbf{r}(t, u)$ curves towards at time t . Eq. 6.106 fully specifies the frame, as $\mathbf{e}_3 = \mathbf{e}_1 \times \mathbf{e}_2$. In this context \mathbf{e}_1 , \mathbf{e}_2 and \mathbf{e}_3 are called the tangent, normal and binormal vectors respectively. co

Now recall the equations of motion of \mathbf{r} and \mathbf{e}_i along u , given by Eq. 6.40, which we

write as

$$\mathbf{r}' = \mathbf{e}_i \theta_i \quad (6.107a)$$

$$\mathbf{e}'_j = \mathbf{e}_i \hat{\pi}_{ij}. \quad (6.107b)$$

Since $\mathbf{r}' = h\mathbf{e}_1$ we have that

$$\vec{\theta} = (h \ 0 \ 0)^T, \quad (6.108)$$

and as $\mathbf{e}'_1 = \kappa \mathbf{e}_2$ we have that $\hat{\pi}_{21} = -\hat{\pi}_{12} = \kappa$ and $\hat{\pi}_{31} = -\hat{\pi}_{13} = 0$. This leaves only one more possible parameter $\hat{\pi}_{23} = -\hat{\pi}_{32}$, to which we assign the scalar parameter τ , known as the *torsion*. We thus have

$$\hat{\pi} = \begin{pmatrix} 0 & -\kappa & 0 \\ \kappa & 0 & -\tau \\ 0 & \tau & 0. \end{pmatrix} \quad (6.109)$$

or, in vector form, $\vec{\pi} = (\tau \ 0 \ \kappa)^T$. Finally, we get the *Frenet-Serret equations*

$$\begin{aligned} \mathbf{e}'_1 &= \kappa \mathbf{e}_2 \\ \mathbf{e}'_2 &= -\kappa \mathbf{e}_1 + \tau \mathbf{e}_3 \\ \mathbf{e}'_3 &= \tau \mathbf{e}_2 \end{aligned} \quad (6.110)$$

which together with Eq. 6.105 reconstructs the framing $\tilde{\Phi} \cong (\mathbf{r}, E)$, from which get the filament configuration $\Phi \cong \mathbf{r}$.

We see that by choosing a gauge, we have effectively constrained the spatial configuration X to only take values in a subset $V \subset \mathfrak{se}(3)$, where $X = X(h, \kappa, \tau)$ is now parametrised by the three scalars (h, κ, τ) that are functions of space and time. Note that V is not a Lie subalgebra. This constraint establishes an injective mapping between V -valued fields $X : W \rightarrow V$ and \mathbb{E}^3 -valued fields $\Phi : W \rightarrow \mathbb{E}^3$. In this context (h, κ, τ) are known as the *differential invariants* of the filament, as they uniquely define the filament up to rigid body transformations.

We should stress that in the mathematical literature, the purview of the theory of moving frames are in general space curves (rather than space-time curves). Furthermore, in that context the metric h along the center-line is of little importance (and is usually not referred to as a differential invariant), and thus the arc-length parameterisation is preferred. Eq. 6.110 is therefore more commonly written in terms of arc-length derivatives

$$\begin{aligned} \partial_s \mathbf{e}_1 &= \tilde{\kappa} \mathbf{e}_2 \\ \partial_s \mathbf{e}_2 &= -\tilde{\kappa} \mathbf{e}_1 + \tilde{\tau} \mathbf{e}_3 \\ \partial_s \mathbf{e}_3 &= \tilde{\tau} \mathbf{e}_2 \end{aligned} \quad (6.111)$$

where $\tilde{\kappa} = h\kappa$ and $\tilde{\tau} = h\tau$ are the scalar curvature and torsion in the arc-length parame-

terisation.

Intuitively, we can visualise the motion of (\mathbf{r}, E) as a function of u , for fixed t , in the Frenet-Serret gauge as follows. We can imagine an airplane which is travelling in the direction of \mathbf{e}_1 and with the floor of the plane aligned with \mathbf{e}_3 . Its trajectory traces out a center-line $\mathbf{r}(u)$, at ‘speed’ h . The Frenet-Serret frame corresponds to a plane that navigates *pitching* (at a rate κ) and *rolling* (at a rate τ), but never *yaws*.

We now consider the kinematics along time t . The same kinematic equations of motion Eq. 6.48 for the Cosserat rod still apply. However, substituting $\vec{\theta} = (h \ 0 \ 0)^T$ and $\vec{\pi} = (\tau \ 0 \ \kappa)^T$ into Eq. 6.48 we find the following constraints

$$\Omega_1 = (\Omega_3\tau - \Omega'_2)/\kappa \quad (6.112a)$$

$$\Omega_2 = -h^{-1}(D_u \vec{V})_3 \quad (6.112b)$$

$$\Omega_3 = h^{-1}(D_u \vec{V})_2. \quad (6.112c)$$

It is intuitive that the angular velocity of the filament, with a cross-section constrained to be aligned with the center-line, is completely determined as a function of the differential invariants and the translational velocity \vec{V} . Eq. 6.112, together with Eq. 6.48, completely specify the kinematics of the filament. Just as we have three scalar parameters (h, κ, τ) that determine the spatial configuration of the filament, the temporal evolution is determined by the three scalars in $\vec{V} = (V_1 \ V_2 \ V_3)$. Using Eq. 6.48 and Eq. 6.112, we can write the kinematic equations of motion for the filament compactly as

$$\dot{h} = V'_1 - \kappa V_2 \quad (6.113a)$$

$$\dot{\kappa} = \Omega'_3 + \tau \Omega_2 \quad (6.113b)$$

$$\dot{\tau} = \Omega'_1 - \kappa \Omega_2 \quad (6.113c)$$

$$(6.113d)$$

where $\vec{\Omega}$ is given by Eq. 6.112. The temporal evolution of the filament is thus specified by the velocity field \vec{V} alone.

The twisting filament

We can model a filament that can twist around its center-line by keeping the $SO(2)$ gauge freedom of $(\mathbf{e}_2, \mathbf{e}_3)$ and promoting it to a kinematic degree of freedom. The resulting degrees of freedom are then $\vec{\theta} = (h \ 0 \ 0)^T$ as before and $\vec{\pi}$ has all three of its components. The resulting constraints on $\vec{\Omega}$ are then

$$\Omega_2 = -h^{-1}(D_u \vec{V})_3 \quad (6.114a)$$

$$\Omega_3 = h^{-1}(D_u \vec{V})_2. \quad (6.114b)$$

instead of Eq. 6.112. The resulting kinematic equations of motion are thus

$$\dot{h} = V'_1 - \kappa V_2 \quad (6.115a)$$

$$\dot{\vec{\pi}} = D_u \vec{\Omega} \quad (6.115b)$$

The temporal evolution of the twisting filament is thus specified by the rate of twist Ω_1 and the velocity field \vec{V} .

In our airplane analogy, the twisting filament travels (again, as a function of u for fixed t) by rolling (at a rate π_1), yawing (at a rate π_2) and pitches (at a rate π_3).

6.3.2 Kinematically constrained dynamics

The formulation of the dynamics for kinematically constrained rods carries through less programmatically than in the case of the Cosserat rod. In general, extra care must be taken formulating the dynamics when the configuration space is a homogeneous space G/H . Issues of under- or over-determination in the equations of motion may arise due to the fact that $\dim(G/H) < \dim(G)$ if $\dim(H) \neq 0$.

Filament dynamics

For a filament, though its configuration space is $SE(3)/SO(3) \cong \mathbb{E}^3$ rather than $SE(3)$ as for the Cosserat rod, $SE(3)$ acts *transitively* on \mathbb{E}^3 . By which we mean that for any two elements $\mathbf{x}, \mathbf{y} \in \mathbb{E}^3$, there exists an element $g \in SE(3)$ such that $\mathbf{y} = g\mathbf{x}$. As before, we can define a Lagrangian density $\mathcal{L} : SE(3) \times TSE(3) \rightarrow \mathbb{R}$, with reduction $\ell : \mathfrak{se}(3) \rightarrow \mathbb{R}$, or use the Lagrange-D'Alembert principle as the starting point. The derivation of the dynamics then proceed as before in Sec. 6.2.2, and we find the same general equations of motion Eq. 6.99.

However, issues arise as the dimension of the Lie algebra $\dim(\mathfrak{se}(3)) = 6$ is larger than the configuration space $\dim(\mathbb{E}^3) = 3$. This is in principle partially ameliorated by choosing a gauge, such as the Frenet-Serret gauge, but if this is done naively then the resulting equations of motion are untenable. Consider the dynamical equations of motion that would result if we consider a filament with the Frenet-Serret frame, starting from the Lagrange-D'Alembert principle Eq. 6.98. As before, we let $S = \frac{\partial \mathcal{K}}{\partial N}$, where the reduced kinetic energy \mathcal{K} of the Cosserat rod was derived in Eq. 6.66 and we repeat it here

$$\mathcal{K}(N) = \frac{1}{2} \rho_0 |\vec{V}|^2 + \frac{1}{2} \vec{\Omega}^T \mathbb{I} \vec{\Omega}. \quad (6.116)$$

Consider now, in particular, the moment balance equation for the filament

$$D_t \vec{L} = D_u \vec{M} + \vec{\theta} \times \vec{F} + \vec{m}, \quad (6.117)$$

where $\vec{L} = \mathbb{I}\vec{\Omega}$. Due to Eq. 6.112, $\vec{\Omega}$ is not an independent degree of freedom, but a function of \vec{V} and the differential invariants. Therefore Eq. 6.117 over-determines the system, and is in general an intractable constraint.

To address this issue, we first note that it stems from the particular method by which we have parametrised the filament. In the fixed frame, the dynamics of the filament can be unambiguously written as

$$\rho_0\ddot{\mathbf{r}} = \mathbf{F}' + \mathbf{f} \quad (6.118)$$

where we used $\mathbf{P} = \rho_0\dot{\mathbf{r}}$, which can be seen as the 1-dimensional analogue of the Cauchy momentum equation in the Lagrangian point-of-view, where \mathbf{F} would correspond to the *first Piola-Kirchhoff stress tensor* in continuum dynamics.

In the geometric formulation presented here, we parametrise the filament in terms of its intrinsic geometry κ and τ , which corresponds to a given framing, rather than its center-line $\mathbf{r}(t, u)$ as in Eq. 6.118. This means that we must consider how the forces on the filament corresponds to moments on the moving frame $(\mathbf{e}_1, \mathbf{e}_2, \mathbf{e}_3)$. However, as the filament is ultimately described as a center-line, the model does not accommodate the angular momentum of its frame as an independent degree of freedom. In the literature the issue of Eq. 6.117 is avoided by taking the overdamped limit modelling a filament immersed in a highly viscous fluid [54, 202, 84, 195, 158, 102, 174, 86], or by considering filament statics [170]. Here, we avoid this limit and present a derivation of inertial filament dynamics.

Let $\mathcal{K}(N) = \frac{1}{2}\rho_0|\vec{V}|^2$, so that we get $S = \{\vec{P}; \vec{0}\}$ where $\vec{P} = \rho_0\vec{V}$, therefore implicitly assuming the angular momentum of the filament to be negligible. The moment balance equation then becomes

$$0 = D_u\vec{M} + \vec{\theta} \times \vec{F} + \vec{m}. \quad (6.119)$$

To find self-consistent constitutive dynamics, we consider moment balance in the absence of external moments $\vec{m} = 0$, to find

$$0 = (D_u\vec{M})_1 \quad (6.120a)$$

$$F_2 = h^{-1}(D_u\vec{M})_3 \quad (6.120b)$$

$$F_3 = -h^{-1}(D_u\vec{M})_2. \quad (6.120c)$$

Thus we see that combined we can only independently specify three of the six force and moment components in total. The kinematic and dynamical equations of motion for the

filament are thus

$$\dot{h} = V'_1 - \kappa V_2 \quad (6.121a)$$

$$\dot{\kappa} = \Omega'_3 + \tau \Omega_2 \quad (6.121b)$$

$$\dot{\tau} = \Omega'_1 - \kappa \Omega_2 \quad (6.121c)$$

$$D_t \vec{P} = D_u \vec{F} + \vec{f}, \quad (6.121d)$$

where the material derivatives are computed as before, using $\vec{\pi} = (\tau \ 0 \ \kappa)$ and $\vec{\Omega}$ given by Eq. 6.112, and where the force must obey the conditions Eq. 6.120. We note that \vec{M} does not appear explicitly in the dynamics, and we can indeed in theory write down the three arbitrary constitutive force components \vec{F} , which would induce a moment via Eq. 6.120 that has no impact on the dynamics. This is however not how the constitutive forces and moments are defined in practice, as we will now show.

We now move on to treat conservative constitutive dynamics. As discussed in [136], when the Lie algebra, that acts transitively on the configuration space, is of a higher dimension than the configuration space the resulting Lagrangian dynamics (i.e. conservative dynamics) is under-determined. For a Cosserat rod we have $Q = \frac{\partial \mathcal{U}}{\partial X} = \{\vec{F}; \vec{M}\}$ which results in Eq. 6.72. In contrast, as $\vec{\theta} = (h \ 0 \ 0)^T$ and $\vec{\pi} = (\tau \ 0 \ \kappa)^T$ for a filament, the only components that are determined for a general constitutive \mathcal{U} are

$$F_1 = \frac{\partial \mathcal{U}}{\partial h} \quad (6.122a)$$

$$M_1 = \frac{\partial \mathcal{U}}{\partial \tau} \quad (6.122b)$$

$$M_3 = \frac{\partial \mathcal{U}}{\partial \kappa} \quad (6.122c)$$

leaving M_2 , F_2 and F_3 undetermined by \mathcal{U} . However we see that by having chosen a gauge, these force and moment components are given by moment balance Eq. 6.120. The conservative constitutive forces and moments on a filament are thus determined by Eq. 6.122 and Eq. 6.120 together. Note that it was necessary to let M_1 , F_2 and F_3 be undetermined by \mathcal{U} , rather than setting $M_1 = F_2 = F_3 = 0$, which would conflict with moment balance. The above is consistent with the force and moment balance equations found for the filament in the overdamped setting [174] and in statics [170].

It is standard for filament dynamics to associate an energetic cost to the square of the curvature and extension $\mathcal{U} = \frac{1}{2} \epsilon \kappa^2$. From Eq. 6.122 and Eq. 6.120 we then find, expressed in a non-moving frame

$$\mathbf{M} = \epsilon \kappa \mathbf{e}_3 \quad (6.123)$$

where ϵ is the bending stiffness. Eq. 6.123 agree with classical Bernoulli-Euler beam theory [174, 195, 158]. Note that as the notion of torsion τ appears from the gauge choice, rather

than representing a physical property of the filament, a τ^2 term is usually not included in \mathcal{U} . Therefore $M_1 = M_2 = 0$ for a filament in the Frenet-Serret frame in practice.

In the overdamped limit, the results of Sec. 6.5 and Eq. 6.149 applies as before, under the constraints Eq. 6.108 and Eq. 6.109, Eq. 6.112 and Eq. 6.120. Setting $\vec{f} = -\gamma_T \vec{V}$ we get

$$\dot{h} = V'_1 - \kappa V_2 \quad (6.124a)$$

$$\dot{\kappa} = \Omega'_3 + \tau \Omega_2 \quad (6.124b)$$

$$\dot{\tau} = \Omega'_1 - \kappa \Omega_2 \quad (6.124c)$$

$$\vec{V} = \mu_T D_u \vec{F}, \quad (6.124d)$$

where $\mu_T = \gamma_T^{-1}$.

Twisting filament dynamics

For a twisting filament, the angular velocity component Ω_1 is now a dynamic degree of freedom, and we therefore permit angular momentum along the tangential direction. We assume the principal axes of the moment of inertia \mathbb{I} coincide with the moving frame \mathbf{e}_i , $i = 1, 2, 3$, and that the angular momentum is negligible along the normal and binormal directions, setting $\vec{L} = (\mathbb{I}^{(1)} \Omega_1 \ 0 \ 0)^T$, where $\mathbb{I}^{(1)}$ is the eigenvalue of \mathbb{I} along \mathbf{e}_1 . The resulting kinematic and dynamical equations of motion are

$$\dot{h} = V'_1 - \kappa V_2 \quad (6.125a)$$

$$\dot{\pi} = D_u \vec{\Omega} \quad (6.125b)$$

$$D_t \vec{P} = D_u \vec{F} + \vec{f} \quad (6.125c)$$

$$\mathbb{I}^{(1)} \dot{\Omega}_1 = (D_u \vec{M})_1 + m_1 \quad (6.125d)$$

where the constraints on the force are

$$F_2 = h^{-1} (D_u \vec{M})_3 \quad (6.126a)$$

$$F_3 = -h^{-1} (D_u \vec{M})_2, \quad (6.126b)$$

which should be compared with Eq. 6.121 and Eq. 6.120. For conservative constitutive we now have the relations

$$F_1 = \frac{\partial \mathcal{U}}{\partial h} \quad (6.127a)$$

$$M_i = \frac{\partial \mathcal{U}}{\partial \pi_i}. \quad (6.127b)$$

6.4 The hyperelastic Cosserat rod model

In many applications the conservative part of the constitutive dynamics arise from a potential of the form Eq. 6.88 [2, 211, 75, 201], where the potential \mathcal{U} is a quadratic form in X , with coefficients given by the symmetric and positive-definite stiffness matrix $K \in \mathbb{R}^{6 \times 6}$. Here we derive the form of K from first principles, given constitutive assumptions on the material that the rod is composed of. Specifically, we model the Cosserat rod as a slender tube of hyper-elastic *Saint Venant-Kirchoff* material [11], but the derivation carries through regardless of what constitutive assumption.

We consider a straight rod $\mathcal{M} = \mathcal{D} \times [0, L_0]$ at rest, where \mathcal{D} is a disc of arbitrary shape, and L_0 is the length of the rod. As before, \mathbf{X} is the material coordinate on \mathcal{M} , and we align $X_1 \in [0, L_0]$ along the length of the rod, and $(X_2, X_3) \in \mathcal{D}$. We will use $u = X_1$ and X_1 interchangeably. Deformations of \mathcal{M} are given by $\mathbf{x}(\mathbf{X})$, which we will refer to as the *deformed coordinate*. The material and deformed coordinates can be related as

$$d\mathbf{x} = \mathcal{P}d\mathbf{X} \quad (6.128)$$

where $\mathcal{P} = \frac{\partial \mathbf{x}}{\partial \mathbf{X}}$ is here the *deformation gradient tensor*, and we write its components in the moving frame $\mathcal{P}_{ij} = \mathbf{e}_i \cdot (\frac{\partial \mathbf{x}}{\partial \mathbf{X}} \mathbf{e}_j)$. Following [131], we consider the change in infinitesimal distances between two material points \mathbf{X}_1 and \mathbf{X}_2 in the rod after a deformation. In the undeformed state, the distance between \mathbf{X}_1 and \mathbf{X}_2 is $d\ell^2 = |d\mathbf{X}|^2$. After deformation we have

$$\begin{aligned} d\ell'^2 &= |d\mathbf{x}|^2 = (Pd\mathbf{X})^T (\mathcal{P}d\mathbf{X}) \\ &= d\mathbf{X}^T \mathcal{P}^T \mathcal{P} d\mathbf{X} \\ &= d\ell^2 + 2d\mathbf{X}^T E d\mathbf{X} \\ &= d\mathbf{X}^T (I + 2E) d\mathbf{X} \end{aligned} \quad (6.129)$$

where

$$E = \frac{1}{2} \left(\frac{\partial \mathbf{u}}{\partial \mathbf{X}} + \left(\frac{\partial \mathbf{u}}{\partial \mathbf{X}} \right)^T + \left(\frac{\partial \mathbf{u}}{\partial \mathbf{X}} \right)^T \frac{\partial \mathbf{u}}{\partial \mathbf{X}} \right) \quad (6.130)$$

is the *Lagrangian strain tensor* and $\mathbf{u}(\mathbf{X}) = \mathbf{x} - \mathbf{X}$ is the *deformation vector*. For small deformations, we can approximate Eq. 6.135 as $E \approx \frac{1}{2} \left(\frac{\partial \mathbf{u}}{\partial \mathbf{X}} + \left(\frac{\partial \mathbf{u}}{\partial \mathbf{X}} \right)^T \right)$, in which case we can express it as

$$E = \frac{1}{2} (\mathcal{P} + \mathcal{P}^T - 2\mathbb{1}). \quad (6.131)$$

The Lagrangian strain tensor can be seen as giving the relative deformations along the principle axes of a material, where the latter are defined as the eigenvectors E . The elastic energy density of the material in a deformed state is a function of E , and we assume it to be a quadratic form

$$W(E) = \frac{1}{2} C_{ijkl} E_{ij} E_{kl} \quad (6.132)$$

where C_{ijkl} is a fourth-order tensor of elastic constants, which is known as the Saint Venant-Kirchoff constitutive assumption [11], and materials that are well-approximated under this assumption are known as *Saint Venant-Kirchoff materials*. If we assume that C is isotropic, in which case it has the form

$$C_{ijkl} = \lambda\delta_{ij}\delta_{kl} + \mu_1\delta_{ik}\delta_{jl} + \mu_2\delta_{il}\delta_{jk} \quad (6.133)$$

then Eq. 6.132 can be shown to reduce to

$$W(E) = \mu\text{Tr}(E^2) + \frac{\lambda}{2}\text{Tr}(E)^2 \quad (6.134)$$

where λ and $\mu = \mu_1 + \mu_2$ are known as the *Lamé constants*.

We will now proceed to derive the potential energy per unit material length of a Cosserat rod under the constitutive assumption of Eq. 6.134. We impose the kinematic assumption Eq. 6.61, which we write again here as

$$\mathbf{x}(\mathbf{X}) = \mathbf{r}(X_1) + \mathbf{e}_\xi X_\xi, \quad \xi = 2, 3 \quad (6.135)$$

which constrains deformations to preserve the area and shape of the cross-section at each X_1 . Since

$$\frac{\partial \mathbf{x}}{\partial X_1} = \theta_i \mathbf{e}_i + \mathbf{e}_i \hat{\pi}_{i\gamma} X_\gamma, \quad \gamma = 2, 3 \quad (6.136)$$

where we used Eq. 6.40, we have

$$\begin{aligned} \mathcal{P}_{i1} &= \theta_i + \pi_{i\gamma} X_\gamma \\ \mathcal{P}_{i\gamma} &= \delta_{i\gamma}. \end{aligned} \quad (6.137)$$

The Lagrangian strain tensor E can then be computed using Eq. 6.131, and since Eq. 6.137 is expressed entirely in terms of $X = \{\vec{\theta}; \vec{\pi}\}$, we can express the energy volume density W as a function of X as well. To find the energy density per unit-length $\mathcal{U}(\vec{\theta}, \vec{\pi})$ of the rod, we must integrate out the cross-section

$$\mathcal{U}(\vec{\theta}, \vec{\pi}) = \int_{\mathcal{D}} W(E) dX_2 dX_3. \quad (6.138)$$

For simplicity, we assume a circular cross-section, for which we have that

$$\begin{aligned}
\int_{\mathcal{D}} dA &= \pi R^2 \\
\int_{\mathcal{D}} X_\alpha dA &= 0 \\
\int_{\mathcal{D}} X_\alpha X_\beta dA &= \frac{\pi R^4}{4} \delta_{\alpha\beta} \\
\int_{\mathcal{D}} X_\alpha X_\beta X_\gamma dA &= 0 \\
\int_{\mathcal{D}} X_\alpha X_\beta X_\gamma X_\delta dA &= \begin{cases} \frac{\pi R^6}{8}, & \alpha = \beta = \gamma = \delta \\ \frac{\pi R^6}{24}, & \alpha = \beta \text{ and } \gamma = \delta \\ \frac{\pi R^6}{24}, & \alpha = \gamma \text{ and } \gamma = \beta \end{cases}
\end{aligned} \tag{6.139}$$

where $\alpha, \beta, \gamma, \delta = 2, 3$ and R is the radius of the rod. From Eq. 6.139, Eq. 6.139, Eq. 6.131 and Eq. 6.134, the potential energy per unit material length evaluates to

$$\mathcal{U}(\vec{\theta}, \vec{\pi}) = \frac{k_1}{2}(\theta_1 - 1)^2 + \frac{k_2}{2}(\theta_2^2 + \theta_3^2) + \frac{\epsilon_1}{2}\hat{\pi}_1^2 + \frac{\epsilon_2}{2}(\hat{\pi}_2^2 + \hat{\pi}_3^2) \tag{6.140}$$

where $k_1 = \pi R^2(\lambda + 2\mu)$, $k_2 = \frac{\pi R^2}{2}\lambda$, $\epsilon_1 = \frac{\pi R^4}{4}\lambda$ and $\epsilon_2 = \frac{\pi R^4}{4}(\lambda + 2\mu)$. Equation 6.140 is consistent with the is consistent with the quadratic Cosserat free energies found in the literature [82, 26, 186]. For a non-circular cross-section we will in general have a potential energy of the form

$$\mathcal{U}(\vec{\theta}, \vec{\pi}) = \frac{k_1}{2}(\theta_1 - 1)^2 + \frac{k_2}{2}\theta_2^2 + \frac{k_3}{2}\theta_3^2 + \frac{\epsilon_1}{2}\hat{\pi}_1^2 + \frac{\epsilon_2}{2}\hat{\pi}_2^2 + \frac{\epsilon_3}{2}\hat{\pi}_3^2. \tag{6.141}$$

We can interpret the form of the potential energy by recalling how $\vec{\theta}$ and $\vec{\pi}$ encodes the various kinematic deformations of the Cosserat rod, described in Sec. 6.2.1. The first three terms in Eq. 6.141 penalises both shearing of the material frame, as well as extension of the center-line. The π_1 term penalises twisting of the material frame along \mathbf{e}_1 , and π_2 and π_3 penalises the rotation of the material frame along \mathbf{e}_2 and \mathbf{e}_3 respectively.

The stiffness matrix of a hyper-elastic Cosserat rod can thus be written as

$$\mathbf{K} = \begin{pmatrix} K^{(1)} & 0_{3 \times 3} \\ 0_{3 \times 3} & K^{(2)} \end{pmatrix} \tag{6.142}$$

where $K^{(1)} = \text{diag}\{k_1, k_2, k_3\}$ and $K^{(2)} = \text{diag}\{\epsilon_1, \epsilon_2, \epsilon_3\}$, with rest state

$$\vec{\theta}_0 = (1 \ 0 \ 0)^T \tag{6.143a}$$

$$\vec{\pi}_0 = (0 \ 0 \ 0)^T. \tag{6.143b}$$

The resulting constitutive force and moments are

$$\vec{F} = \frac{\partial \mathcal{U}}{\partial \vec{\theta}} = K^{(1)}(\vec{\theta} - \vec{\theta}_0) \quad (6.144a)$$

$$\vec{M} = \frac{\partial \mathcal{U}}{\partial \vec{\pi}} = K^{(2)}\vec{\pi}. \quad (6.144b)$$

We see that in this constitutive model, the force \vec{F} acts on the center-line such as to align with its material frame. In other words, if the material frame is shearing, then the center-line will bend such as to be tangent to \mathbf{e}_1 . If the material frame is rotating along u , which corresponds to a non-zero $\vec{\pi}$, then the moment \vec{M} acts so as to render it non-rotating. We thus see that a shearing material frame *induces* bend. This effect happens despite the fact that $\vec{\theta}$ and $\vec{\pi}$ do not couple in \mathcal{U} , which inherently due to the geometric non-linearities in the kinematics of the Cosserat rod. Conversely, a bending center-line which is aligned with the material frame will induce shear. Note that there is no direct energetic cost for the bending of the center-line itself (as \mathcal{U} is not a function of the scalar curvature κ), however the energetic cost of shearing, combined with the energetic cost of a rotating material frame, conspire together so as to straighten segments of the rod that bend.

6.5 Dissipative and overdamped dynamics

Equation 6.93 allows us to model general dissipative dynamics. We consider the case of a Cosserat rod that suffers both internal and external friction

$$\dot{X} = (\partial_u + \text{ad}_N)X \quad (6.145a)$$

$$(\partial_t - \text{ad}_N^*)S = (\partial_u - \text{ad}_X^*)Q - \mathbf{H}\dot{X} - \mathbf{G}N \quad (6.145b)$$

$$Q = 0, \quad u = 0, L_0, \quad (6.145c)$$

where we have set $T = -\mathbf{H}\dot{X} - \mathbf{G}N$, and where \mathbf{H} and \mathbf{G} are positive-definite matrices of damping coefficients of the internal and external friction respectively. Note that $\mathbf{H}\dot{X}$ in Eq. 6.145b is evaluated by substituting in Eq. 6.145a. If let the frictional matrices be block-diagonal in the translational and angular components as

$$\mathbf{H} = \begin{pmatrix} \gamma_T^{\text{in}} & 0_{3 \times 3} \\ 0_{3 \times 3} & \gamma_R^{\text{in}} \end{pmatrix} \quad (6.146a)$$

$$\mathbf{G} = \begin{pmatrix} \gamma_T & 0_{3 \times 3} \\ 0_{3 \times 3} & \gamma_R \end{pmatrix} \quad (6.146b)$$

where γ_T^{in} , γ_R^{in} , γ_T and γ_R are positive-definite 3×3 -matrices, we can write the equations of motion as

$$D_t \vec{\theta} = D_u \vec{V} \quad (6.147\text{a})$$

$$\partial_t \vec{\pi} = D_u \vec{\Omega} \quad (6.147\text{b})$$

$$D_t \vec{P} = D_u \vec{F} - \gamma_T^{\text{in}} \dot{\vec{\theta}} - \gamma_T \vec{V} \quad (6.147\text{c})$$

$$D_t \vec{L} = D_u \vec{M} + \vec{\theta} \times \vec{F} - \gamma_R^{\text{in}} \dot{\vec{\pi}} - \gamma_R \vec{\Omega} \quad (6.147\text{d})$$

where again $\gamma_T^{\text{in}} \dot{\vec{\theta}}$ and $\gamma_R^{\text{in}} \dot{\vec{\pi}}$ can be evaluated using the kinematic equations of motion, and $\vec{F} = \vec{M} = 0$, $u = 0, L_0$.

We can consider a limit where the dissipative forces dominate over the inertial forces (which correspond to the left-hand side of Eq. 6.145b). In this limit, we set $S \approx 0$, or equivalently $\vec{P} \approx 0$ and $\vec{L} = \mathbb{I} \vec{\Omega} \approx 0$. The resulting equations are *overdamped* equations of motion

$$\dot{\vec{X}} = (\partial_u + \text{ad}_X) N \quad (6.148\text{a})$$

$$\mathbf{G}N = (\partial_u - \text{ad}_X^*) Q + \mathbf{H}\dot{\vec{X}} \quad (6.148\text{b})$$

$$Q = 0, \quad u = 0, L_0. \quad (6.148\text{c})$$

where we must solve for N in Eq. 6.148b to compute Eq. 6.148a. In terms of the translational and angular velocities, the equations of motion are

$$D_t \vec{\theta} = D_u \vec{V} \quad (6.149\text{a})$$

$$\partial_t \vec{\pi} = D_u \vec{\Omega} \quad (6.149\text{b})$$

$$\gamma_T \vec{V} = D_u \vec{F} - \gamma_T^{\text{in}} \dot{\vec{\theta}} \quad (6.149\text{c})$$

$$\gamma_R \vec{\Omega} = D_u \vec{M} + \vec{\theta} \times \vec{F} - \gamma_R^{\text{in}} \dot{\vec{\pi}} \quad (6.149\text{d})$$

where again we must solve for \vec{V} and $\vec{\Omega}$ in the latter two equations and substitute them into the kinematic equations of motion. We note that the overdamped equations of motion are first-order in time t and second-order in space u (as opposed to first-order in the underdamped case). Furthermore, the only degree of freedom is here $X = \{\vec{\theta}; \vec{\Omega}\}$, and so the dynamics are 6-dimensional as opposed to 12-dimensional in the underdamped case.

The presence of the internal friction $\mathbf{H}\dot{\vec{X}}$ significantly complicates the evaluation of the overdamped dynamics. Substituting Eq. 6.148a into Eq. 6.148b we get a self-consistency relation for N

$$\mathbf{G}N = (\partial_u - \text{ad}_X^*) Q + \mathbf{H}(\partial_u + \text{ad}_X) N \quad (6.150)$$

and formally we can write N as

$$N = \mathcal{A}^{-1} (\partial_u - \text{ad}_X^*) Q \quad (6.151)$$

where $\mathcal{A} = \mathsf{G} - \mathsf{H}(\partial_u + \text{ad}_X)$. In simulations, which invariably employ some discretisation scheme, \mathcal{A} becomes a matrix that can be inverted numerically. If, however, we neglect internal dissipation we have $N = \mathsf{G}^{-1} (\partial_u - \text{ad}_X^*) Q$, and we can write the equations of motion in a compact form as

$$\dot{\vec{X}} = (\partial_u + \text{ad}_X) [\mathsf{G}^{-1} (\partial_u - \text{ad}_X^*) Q] \quad (6.152)$$

or

$$D_t \vec{\theta} = D_u [\mu_T D_u \vec{F}] \quad (6.153a)$$

$$\partial_t \vec{\pi} = D_u [\mu_R D_u \vec{M}] \quad (6.153b)$$

where $\mu_{T,R} = \gamma_{T,R}^{-1}$, which would be the overdamped equations of motion of a Cosserat rod immersed in a viscous medium.

Chapter 7

Geometric continuum mechanics on Lie group- and homogeneous configuration spaces

In Ch. 6, we derived the kinematic and dynamical equations of motion of the Cosserat rod and filament, systems in one material dimension with configuration space $SE(3)$ and $SE(3)/SO(3)$ respectively. In the subsequent section we provide a generalisation of Ch. 6 to systems with general material bases spaces and homogeneous configuration spaces. We call this the *geometrisation programme*. Mathematically, the geometrisation programme can be seen as a general field theory of Lie group- or homogeneous space-valued fields defined over topological manifolds. The derivations of the results are provided in Sec. 7.2.1 and Sec. 7.2.2.

We have separated the exposition of the results and their derivation, as the latter require a level of mathematical abstraction not necessary in the presentation of the geometrisation programme itself. The primary mathematical challenge stems from allowing arbitrary topologies in the material base space, which entails that it longer admits a global set of coordinates. An example of such a system would be a closed surface, like the membrane of a cell. This necessitated further geometrical abstraction that was not required in the case of the Cosserat rod.

In Sec. 7.3 we use the geometrisation programme to derive the equations of motion for a set of example systems. This section is called ‘Applications’, meant to be understood in the sense that our general geometric framework is *applied* to derive the kinematic and dynamic theories of the given example systems. When these systems are well-established in the literature, we show that our framework recovers the correct equations of motion. Finally, in Sec. 7.1.4 we conclude with a summary and discussion on the geometrisation programme.

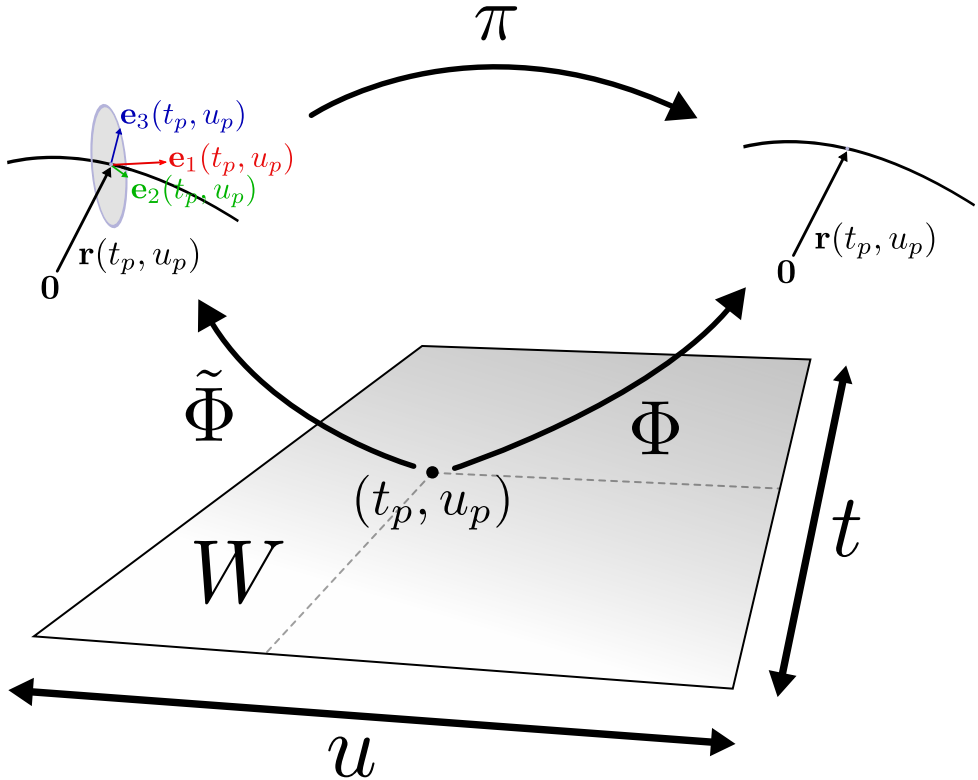


Figure 7.1: The relation between the spatio-temporal configuration Φ and the adapted frame field $\tilde{\Phi}$ of a filament. In the top-left and top-right we show the mapping of (t_p, u_p) , a point in the kinematic base space W , to $\tilde{\Phi}(t_p, u_p)$ and $\Phi(t_p, u_p)$, which are related by the projection map π .

7.1 The geometrisation programme

Here we generalise the results of Sec. 6.2 to systems with an arbitrary material base space and homogeneous configuration space. To aid understanding it will be helpful to reintroduce some nomenclature, and to relate and contextualise the mathematical formulation of the Cosserat rod and the filament to the general systems that we describe in what follows. This preamble will thus serve as a brief overview of the results given in the subsequent subsections.

The *material base space* of an open Cosserat rod is the manifold $M = [0, L_0]$, and its *kinematic configuration space* is the Lie group $SE(3)$. The *spatio-temporal configuration* of the Cosserat rod is a map $\Phi : W \rightarrow SE(3)$, where $W = [0, T] \times M$ is the *kinematic base space* and $[0, T]$ the time domain. In Sec. 6.3 we showed that a filament can be considered a kinematically constrained Cosserat rod, and its configuration space is the homogeneous space $SE(3)/SO(3)$. The spatio-temporal configuration of the filament is thus $\Phi : W \rightarrow SE(3)/SO(3)$. However, the kinematics on the homogeneous space $SE(3)/SO(3)$ can be related to kinematics on the Lie group $SE(3)$ using an *adapted frame field* (or *framing*) $\tilde{\Phi} : W \rightarrow SE(3)$ via the composition $\Phi = \pi \circ \tilde{\Phi}$, where $\pi : SE(3) \rightarrow SO(3)$ is the projection map and is defined as $\pi((\mathbf{r}; E)) = \mathbf{r}$. A given Cosserat rod configuration

was thus seen as an adapted frame of the filament. This relationship is illustrated in Fig. 7.1.

The mathematical formulation of the $SE(3)$ -configured Cosserat rod, and its relation to the $SE(3)/SO(3)$ -configured filament, is analogous to the more general setting we will develop here. We first consider kinematic configuration spaces that is a general Lie group G , and we will denote \mathfrak{g} as its Lie algebra. Secondly, we let the material base space M be a general manifold. Thirdly, given a Lie subgroup $H \subset G$ known as the *stabiliser*, we can relate the kinematics and dynamics of the G -configured system to a corresponding G/H -configured system by choosing a *gauge* in H . Therefore, as in Ch. 6, it suffices to at first consider the kinematics and dynamics of the G -configured system with material base space M . The corresponding G/H -configured system can then be modelled by applying kinematic constraints on the G -configured system.

The spatio-temporal configurations of the general systems in consideration are therefore $\Phi : M \rightarrow G$, or $\Phi : M \rightarrow G/H$. We can thus see the geometrisation programme as a general theory of G - or G/H -valued fields on topological manifolds M . The majority of the mathematical technology we introduce is then for the purpose of formulating the field equations of motion on the Lie algebra \mathfrak{g} , which locally acts transitively on G/H (and on G , trivially).

In Sec. 7.1.1 and Sec. 7.1.2 we present the kinematic and dynamic equations of motion of a general G -configured system with material base space M , formulated in terms of Lie algebraic quantities. In Sec. 7.1.3 we describe the procedure by which G/H -configured systems can be modelled via kinematically constraining the G -configured system. We conclude with a discussion of the geometrisation programme in Sec. 7.1.4.

7.1.1 Kinematics

A physical system can be kinematically described using the geometrisation programme if it is possible to identify its kinematic configuration with an element of a Lie group G . Alternatively, the programme is also applicable if the kinematic configuration space is a homogeneous space, upon which G acts transitively. Respectively, the Cosserat rod (Sec. 6.2) and the filament (Sec. 6.3) are examples of this respectively, and further examples can be found in Sec. 7.3. We will first treat the case where the kinematic configuration space is a Lie group, and then return to homogeneous configuration spaces in Sec. 7.1.3.

We consider a system with a d -dimensional material base space M and kinematic configuration space G , where M is a general manifold and G is an n -dimensional Lie group with Lie algebra \mathfrak{g} . Let the kinematic base space W be a $(d+1)$ -dimensional manifold of the form $W = [0, T] \times M$, where $[0, T]$ is the time domain. The spatio-temporal configuration of the system is $\Phi : W \rightarrow G$.

As the material base space M is a general manifold, it does not admit global coordinates

in general. Instead, we must have an atlas \mathcal{A} that covers M . We denote its elements as $\mathcal{A} = \{(U_a, \mathbf{u}_a) \mid a \in I\}$, where $U_a \subset M$ and $\mathbf{u}_a : M \rightarrow \mathbb{R}^d$ and I is an index set. Due to the product structure of the kinematic base space W , \mathcal{A} extends trivially to an atlas $\mathcal{A}_W = \{(U_a \times [0, T], \mathbf{x}_a) \mid a \in I\}$ over W , where $\mathbf{x}_a = (u_a^1, \dots, u_a^d, t)$. We stress that the only kinematically relevant property of M is its topological character, as the kinematics do not depend on any metric structure on M . Therefore, in practice, suitable choices for M are often d -dimensional cuboids, spheres or toruses. Conceptually, we can see M as a continuous multi-dimensional ‘index’ over the system.

The G -valued spatio-temporal configuration can be related to a \mathfrak{g} -valued 1-form as

$$\xi = \Phi^{-1} d\Phi \quad (7.1)$$

where $\xi = \tilde{\Phi}^* \omega : W \rightarrow \mathfrak{g}$ is the pull-back of the Maurer-Cartan ω form onto W , and will henceforth for the sake of brevity be referred to as the Maurer-Cartan form. In a local chart $(U, \mathbf{u}) \in \mathcal{A}$ we can write

$$\xi = N dt + X_\alpha du^\alpha \quad (7.2)$$

where $X_\alpha : [0, T] \times U \rightarrow \mathfrak{g}$, $\alpha = 1, \dots, d$ are the *spatial reconstruction fields* and $N : [0, T] \times U \rightarrow \mathfrak{g}$ is a *generalised velocity field*. Locally, we will write functions on W in terms of their coordinates, i.e. $X_\alpha(t, \mathbf{u})$.

The Maurer-Cartan form obeys the integrability condition

$$d\xi + \xi \wedge \xi = 0 \quad (7.3)$$

from which we can find the kinematic equations of motion expressed in a local chart

$$\partial_t X_\alpha = \mathcal{D}_\alpha N \quad (7.4)$$

where $\alpha = 1, \dots, d$, and the spatial integrability conditions

$$\partial_\beta X_\alpha = \mathcal{D}_\alpha X_\beta \quad (7.5)$$

where $\alpha = 1, \dots, d-1$ and $\beta = \alpha+1, \dots, d$, and where we have defined

$$\mathcal{D}_\alpha = \partial_\alpha + \text{ad}_{X_\alpha}. \quad (7.6)$$

and where $\partial_\alpha = \frac{\partial}{\partial u^\alpha}$. The d spatial reconstruction fields X_α are not independent, as the spatial integrability condition Eq. 7.5 must be obeyed at all times t . However, as spatial integrability is preserved by the equations of motions Eq. 7.4, it suffices that the initial conditions satisfy Eq. 7.5 at $t=0$. Spatial integrability also implies that the total number of degrees of freedom is $\dim(G) = d$.

It is important to note that the local expression of all 1-forms must transform correctly under change of charts. If ξ is written in a chart $(U', \mathbf{u}') \in \mathcal{A}$ as $\xi = Ndt + X'_\alpha du'^\alpha$, then we must have

$$X'_\beta = X_\alpha \frac{\partial u^\alpha}{\partial u'^\beta} \quad (7.7)$$

on $[0, T] \times (U \cap U')$. The \mathfrak{g} -valued X_α thus transform as scalar 1-forms. If M does not admit global coordinates Eq. 7.4 must be integrated consistently over a set of charts that cover M .

To reconstruct the spatio-temporal configuration Φ from the Maurer-Cartan form ξ , we simply integrate Eq. 7.1. For see a detailed numerical algorithm, see App. D.2.

7.1.2 Dynamics

The starting point for modelling the dynamics of a system using the geometrisation programme is to identify its kinetic energy density $\mathcal{K}(\Phi)$ in terms of the spatio-temporal configuration Φ , and a reduction $\mathcal{K}(N)$ in terms of the Lie algebra-valued generalise velocity. The kinetic energy is then used to define the generalised conjugate momentum. This was done systematically for the Cosserat rod in Sec. 6.2.2. Secondly, the generalised stresses and body forces on the system must be defined. As with Cosserat rod dynamics, we can consider both constitutive and non-constitutive dynamics, as well as non-conservative dynamics. As before, the conservative case can be derived as a special case of the non-conservative case. We will be working in local material coordinates, in a chart $(U, \mathbf{u}) \in \mathcal{A}$.

The dynamic quantities correspond analogously to those in Sec. 6.2.2. Let Q^α , $\alpha = 1, \dots, d$ be the generalised constitutive stress fields, and T the generalised body force on the system, which both take values in \mathfrak{g}^* and are defined over M and can be time-dependent in general. The generalised conjugate momentum field is given by

$$S = \frac{\partial \mathcal{K}}{\partial N} \quad (7.8)$$

where $\mathcal{K} = \mathcal{K}(N)$ is a kinetic energy density defined on the system, and S takes values in the dual Lie algebra \mathfrak{g}^* . The general dynamic equations of motion of the system are then

$$\mathcal{D}_t^* S = \mathcal{D}_\alpha^* Q^\alpha + T \quad (7.9a)$$

$$n_\alpha Q^\alpha = 0, \quad \text{on } \partial M. \quad (7.9b)$$

where

$$\mathcal{D}_t^* = \partial_t + \text{ad}_N^* \quad (7.10a)$$

$$\mathcal{D}_\alpha^* = \partial_\alpha + \text{ad}_{X^\alpha}^*. \quad (7.10b)$$

and $n \in T^*M$ is a normal covector field that is tangent to the material boundary ∂M . To give an intuitive example that illustrates the implementation of Eq. 7.9b, we can consider the case where $M = [0, L_0^1] \times [0, L_0^2] \times \cdots \times [0, L_0^d]$ and $L_0^\alpha \in \mathbb{R}^+$. Then from Eq. 7.9b we would have that $Q^\alpha = 0$ on $u^\alpha = 0, L_0^\alpha$. In physical applications S is always related linearly to N , and the kinematic and dynamic equations of motion thus close by solving for $N = N(S)$. The total number of degrees of freedom of the system is thus $2d$, which are encoded in the spatial reconstruction fields X_α and N .

Note that in general the generalised body force T is a function of the spatio-temporal configuration Φ . In this case we must reconstruct Φ from the spatial reconstruction fields X_α to compute T at any time t . See App. D.2 for a detailed algorithm.

For many physical systems we often care about formulating purely constitutive and conservative dynamics. In this case the stress can be derived from a potential energy. As we did in Sec. 6.4 for the Cosserat rod, the starting point would be to formulate a Lagrangian density $\mathcal{L}(\Phi, d\Phi)$. If the dynamics is purely constitutive, then the Lagrangian can not be a function of the global state Φ . Rather, only deformations $d\Phi$ energetically. Therefore the Lagrangian is only a function of the tangent space of G , and we write it as $\mathcal{L}(d\Phi)$. In such cases, $\mathcal{L}(d\Phi)$ admits a reduced form $\ell(\xi)$, that satisfies $\ell(\xi) = \mathcal{L}(d\Phi)$ when $\xi = \Phi^{-1}d\Phi$. Often, the reduced Lagrangian can be written in the form

$$\ell(\xi) = \mathcal{K}(N) - \mathcal{U}(X_\alpha). \quad (7.11)$$

Applying the Euler-Poincaré theorem, we arrive at the same equations Eq. ?? with the body force absent and where the generalised internal stresses are given by

$$Q^\alpha = -\frac{\partial \ell}{\partial X_\alpha} = \frac{\partial \mathcal{U}}{\partial X_\alpha}. \quad (7.12)$$

which takes values in the dual Lie algebra \mathfrak{g}^* .

An example of how to derive a body force is given in the latter half of Sec. 6.2.2, where we incorporate gravity into the Cosserat rod model. In general, if the body force is a function of the spatio-temporal configuration Φ , then for all times t we must solve the equations $\partial_\alpha \Phi = \Phi X_\alpha$ for Φ to evaluate the body force.

Note that in practice it is often the case that Lagrangians are formulated in coordinate-form as densities, as was the case in Sec. 6.2. However, if M does not admit global coordinates it is important that the densities are defined such that for any pair of charts $(U, \mathbf{u}), (U', \mathbf{u}') \in \mathcal{A}$ where $U \cap U' \neq \emptyset$ we have

$$\mathcal{L}'(\Phi, d\Phi) = |J| \mathcal{L}(\Phi, d\Phi). \quad (7.13)$$

and

$$\ell'(\xi) = |J| \ell(\xi). \quad (7.14)$$

on $[0, T] \times U \cap U'$, where $J = \left| \det \left[\frac{\partial \mathbf{u}}{\partial \mathbf{u}'} \right] \right|$, and $\frac{\partial \mathbf{u}}{\partial \mathbf{u}'}$ is the Jacobian matrix of the coordinate transformation between the two charts.

7.1.3 Kinematic constraints

We will now consider implementing kinematic constraints on a Lie group-configured system to model a system that is homogeneous space-configured. The reader will notice that this procedure is less programmatic than the Lie group-configured case. The process of implementing kinematic constraints requires some care in order to develop consistent and physical equations of motion. We will therefore describe the process of kinematic constraints in as much detail as is possible whilst keeping the same level of abstraction. We will repeatedly refer to the example of the filament, treated in Sec. 6.3.1, to illustrate the discussion.

We consider a system where the kinematic configuration space is a homogeneous space. Let $\Phi : W \rightarrow G/H$ be the spatio-temporal configuration, where $H \subset G$ is an r -dimensional Lie subgroup we call the *stabiliser*. The d -dimensional Lie group G is now called a *symmetry group* over the homogeneous space G/H , over which it acts transitively. There is a natural projection map $\pi : G \rightarrow G/H$ from G to G/H , given by

$$\pi(g) = gH \quad (7.15)$$

which describes G as a principal bundle over G/H . In Sec. 6.3.1, we had $G = SE(3)$, $H = SO(3)$ and the projection $\pi((\mathbf{r}; E)) = \mathbf{r}$.

An *adapted frame field*, or *framing*, of the spatio-temporal configuration is a map $\tilde{\Phi} : G \rightarrow G/H$ which satisfies $\Phi = \pi \circ \tilde{\Phi}$. The relation between Φ , $\tilde{\Phi}$ and π is summarised by the commutative map

$$\begin{array}{ccc} & G & \\ \tilde{\Phi} \nearrow & \searrow \pi & \\ W & \xrightarrow{\Phi} & G/H \end{array}$$

and Fig. 7.1. If the stabiliser is trivial $H = \{e\}$, where $e \in G$ is the identity element, then the kinematic configuration space is $G/H \cong G$ and $\tilde{\Phi} = \Phi$.

The projection map π allows us to describe the kinematics of the system in terms of Lie group motions, using adapted frame fields. All the mathematical technology introduced in Sec. 7.1.1 and Sec. 7.1.2 apply as before, but here in terms of the adapted frame field $\tilde{\Phi}$ and its Maurer-Cartan form $\xi = \tilde{\Phi}^{-1}\tilde{\Phi}$. The kinematic and dynamic equations of motion are thus as before Eq. 7.4 and Eq. 7.9 respectively.

Ostensibly the spatial reconstruction fields X_α , $\alpha = 1, \dots, d$ and the generalised velocity field N (or, alternatively, the generalised conjugate momentum S) together comprise $2d$ independent degrees of freedom, once the spatial integrability conditions are factored in. However, the kinematic configuration space G/H is $(n - r)$ -dimensional, leaving r un-physical and superfluous degrees of freedom under-determined by the equations of motion. In principle there is nothing that prevents us from modelling the G/H -configured system using a G -configured system (analogously, there is nothing that prevents us to model the $SE(3)/SO(3)$ -configured filament using the $SE(3)$ -configured Cosserat rod), although as the kinematics of the latter is not adapted to the intrinsic geometry of the former formulating the dynamics can be difficult. Alternatively, we can eliminate the r -superfluous degrees of freedom.

For a given Φ , the space of admissible frame fields $\tilde{\Phi}$ is equal to the space of smooth functions of the form $h : W \rightarrow H$. Explicitly, if $\tilde{\Phi}_1$ is a framing of Φ then

$$\tilde{\Phi}_2(p) = h(p)\tilde{\Phi}_1(p), \quad \forall p \in W \tag{7.16}$$

is also a frame. We call this a *gauge freedom* in the specification of $\tilde{\Phi}$. Only if H is trivial and $r = 0$ is there a unique choice of $\tilde{\Phi}$ for each Φ .

Choosing a gauge is equivalent to prescribing a one-to-one map between spatio-temporal configurations $\Phi : W \rightarrow G/H$ and adapted frames $\tilde{\Phi} : W \rightarrow G$. In Sec. 6.3 this was done by ‘locking’ \mathbf{e}_1 and \mathbf{e}_2 of the trihedron $(\mathbf{r}, E) : W \rightarrow G = SE(3)$ to its center-line $\mathbf{r} : W \rightarrow G/H$. Thus, we had the one-to-one map $\mathbf{r} \mapsto (\mathbf{r}, E(\mathbf{r}))$. We then saw that the choice of gauge on the Lie group-level induced a d -dimensional sub-vector space $V \subset \mathfrak{se}(3)$ on the Lie algebra, where the spatial reconstruction field X only takes values in V . Note that though, in the filament case, we had ‘locked’ the spatial configuration of the material frame to $\partial_u \mathbf{r}$, in principle it is also possible to lock it to the velocity $\partial_t \mathbf{r} = \mathbf{V}$. See Sec. 7.3.4 for an explicit example of this.

In general, the choice of gauge will result in only $n - r$ components of the Maurer-Cartan form ξ to be independent, which in turn means that the kinematic equations of motion yields r constraints. See Eq. 6.112 for an example. Care must be taken to ensure to eliminate superfluous dynamic degrees of freedom. In Sec. 6.3.2 we did this by setting $S_{ij} = 0$ for every vanishing component $N_{ij} = 0$ of the generalised velocity. In turn, this will lead to r constraints on the generalised stress from the dynamical equations of motion Eq. 7.9. These r constraints are consistent with the fact that we cannot specify n generalised forces independently for a system with only $n - r$ degrees of freedom.

Though all gauge choices are theoretically equivalent, some are more ‘natural’ than others. In the case of the filament, a 1-dimensional sub-manifold of \mathbb{E}^3 , we have the Frenet-Serret, as well as the *Bishop* [15, 27], frames. A generalisation of natural moving frames to arbitrary sub-manifolds of \mathbb{E}^d can be found in [29, 30, 136]. A further generalisation

of the theory of moving frames to arbitrary sub-manifolds of Lie groups can be found in [161, 60, 61, 160].

7.1.4 Summary and discussion

The geometrisation programme can be summarised as follows. We can model a given physical system by taking the following steps.

1. Identify the material base space M of the system. Only the topology of M is of kinematic relevance. For example, if the system is a closed surface (like the membrane of a cellular organism), then an appropriate material base space is $M = S^2$.
2. Identify the kinematic configuration space. In general this will be a homogeneous space G/H . If H is trivial then the kinematic configuration space is the Lie group G . This entails constructing adapted frames $\tilde{\Phi} : W \rightarrow G/H$ such that the spatio-temporal configuration $\Phi = \pi \circ \tilde{\Phi}$ kinematically encodes the state of the system.
3. Relate the Lie group-valued adapted frame to the corresponding Maurer-Cartan form ξ , using $\xi = \tilde{\Phi}^{-1}d\tilde{\Phi}$. As was done for the Cosserat rod, we can expand ξ and $\tilde{\Phi}^{-1}d\tilde{\Phi}$ in terms of their constitutive sub-matrices in order to interpret the kinematic equations of motion.
4. Write down the kinematic equations of motion Eq. 7.4 of the system, formulated on the Lie algebra \mathfrak{g} .
5. Write down a kinetic energy density of the system in terms of $d\Phi$, and its corresponding reduction $\mathcal{K}(N)$. Compute the generalised conjugate momentum $S = \frac{\partial \mathcal{K}}{\partial N}$.
6. Define the generalised stresses Q^α and generalised body force T . The conservative part of the constitutive dynamics can be derived by defining a potential energy density $\mathcal{U}(\partial_\alpha \Phi)$, with reduction $\mathcal{U}(X_\alpha)$. The generalised stresses are then $Q^\alpha = \frac{\partial \mathcal{U}}{\partial X_\alpha}$.
7. Write down the dynamic equations of motion Eq. 7.9 of the system, formulated on the dual Lie algebra \mathfrak{g}^* . Note that if the generalised body force T is Φ -dependent, then Φ must be reconstructed from X_α to compute T (see App. D.2 for a detailed algorithm).
8. If the stabiliser H satisfies $\dim(H) = r > 0$, then kinematic constraints should be applied to eliminate the r superfluous degrees of freedom.

Combined, the kinematic and dynamic equations of the motion can be written as the system of equations

$$\partial_t X_\alpha = \mathcal{D}_\alpha N \quad (7.17a)$$

$$\mathcal{D}_t^* S = \mathcal{D}_\alpha^* Q^\alpha + T \quad (7.17b)$$

$$\partial_\beta X_\alpha = \mathcal{D}_\alpha X_\beta \quad (7.17c)$$

$$n_\alpha Q^\alpha = 0, \quad \text{on } \partial M \quad (7.17d)$$

that close under $S = \frac{\partial \mathcal{K}}{\partial N}$, where $\alpha = 1, \dots, d-1$ and $\beta = \alpha+1, \dots, d$ and where Eq. 7.17c are the spatial integrability conditions and Eq. 7.17d are boundary conditions on the generalised stress on ∂M . In the rest of this subsection we will discuss the geometrisation programme.

Internal and external degrees of freedom. Although not necessary for the application of the geometrisation programme, we can introduce some further conceptual distinctions for systems with Lie group-valued kinematic configurations. For many systems there is a natural distinction to be made between the *external* and *internal* degrees of freedom. For a Cosserat rod the center-line $\mathbf{r}(t, u)$, which take values in $SE(3)/SO(3) = \mathbb{E}^3$, and the material frame E , which take values in $SO(3)$, can be seen as external and internal degrees of freedom respectively. The combination of the two, the trihedron (\mathbf{r}, E) , takes values in the combination of the two spaces $SE(3)$. We can generalise this to arbitrary systems with a configuration space G . If G admits some Lie subgroup $H \subset G$, then we may deem it natural to designate the homogeneous space G/H as the *external configuration space* and H as the *internal configuration space*, or vice versa. We should note that in general G can contain many Lie subgroups, and the distinction between the external and internal configuration spaces for a given system would be a matter of convention.

Both the results of Ch. 6, as well as the various applications in Sec. 7.3 provide examples of the implementations of the above steps, as well as a demarcation of the internal and external configuration spaces. Our aim with the chosen examples was to show that the generality of the programme allows for modelling a very broad class of systems with relative ease. The wide applicability of the programme stems from the fact that the kinematic configurations of most physical systems can be said to take values in either a homogeneous space or a Lie group. In addition, allowing for a general material base space M enables us to model continuum systems of arbitrary topologies.

Dynamics on G/H vs. dynamics on \mathfrak{g} . It should be noted that in principle the kinematics and dynamics of a G/H -configured system could be formulated entirely in terms of the G/H -valued spatio-temporal configuration $\tilde{\Phi}$ and its derivative $d\tilde{\Phi}$, as opposed to on the Lie algebra \mathfrak{g} of its symmetry group G as we have done here. This is perhaps the most common way of modelling many systems in classical continuum and Cosserat

mechanics [153, 174, 196, 26]. When simulating systems in this formulation, it requires the discretisation of the G - or G/H -valued system configuration. As G and G/H are always numerically embedded in \mathbb{R}^m , for some $m > \dim(G)$ or $m > \dim(G/H)$, numerical errors accrue in such a manner so that the configuration leaves the sub-manifold $G \subset \mathbb{R}^m$ or $G/H \subset \mathbb{R}^m$. The benefit of the geometrisation programme stems from the fact that it exploits the trivialisation $TG \rightarrow G \times \mathfrak{g}$, which enables us to formulate the kinematics and dynamics in terms of the linear vector space \mathfrak{g} , as opposed to the non-linear space G .

Furthermore, the geometrisation programme thus naturally leads to a formulation of the dynamics in terms of the intrinsic geometry of the system. For constitutive dynamics, this is reflected in the fact that the Lagrangian admits a reduction. The reduction procedure ‘subtracts’ all global information from the dynamics, such that only differential deformations are energetically relevant. These deformations are precisely encompassed in the Maurer-Cartan form ξ . To illustrate the difference between a G/H -based approach and a \mathfrak{g} -based approach, recall the filament system defined in Sec. 6.3. A typical potential energy for a filament is quadratic in its scalar curvature κ and extension h [195, 84]

$$U = \int_0^{L_0} (k(h - 1)^2 + \epsilon\kappa^2) du, \quad (7.18)$$

where k and ϵ are constants. As we showed in Sec. 6.3 κ is a component of the Maurer-Cartan form ξ once kinematic restrictions have been imposed. Equation 7.18 can be rewritten in terms of the $\mathbb{E}^3 \cong SE(3)/SO(3)$ -valued center-line $\mathbf{r}(u)$. However as intrinsic geometry of a space-curve $\mathbf{r}(u)$ is translation-invariant, the resulting expression is not a function of \mathbf{r} but its derivatives $\partial_u \mathbf{r}$ and $\partial_u^2 \mathbf{r}$. We find

$$U = \int_0^{L_0} \left\{ k(|\partial_u \mathbf{r}| - 1)^2 + \epsilon |\partial_u (\partial_u \mathbf{r} / |\partial_u \mathbf{r}|)|^2 \right\} du. \quad (7.19)$$

Aside from the fact that Eq. 7.18 might be aesthetically preferred over Eq. 7.19, the evaluation of the latter will be highly sensitive to numerical errors due to the derivatives.

Time as a privileged axis. As our formulation of the geometrisation programme is primarily geared towards continuum mechanics, our notation has singled-out time as a privileged axis. To remove this notational quirk, we could simply exclude the temporal part of the kinematic base space $W = [0, T] \times M \rightarrow W = M$, and thus consider configurations $\Phi : M \rightarrow G/H$. The resulting system of equations that determines the system configuration

are then

$$\mathcal{D}_\alpha^* Q^\alpha + T = 0 \quad (7.20a)$$

$$\partial_\beta X_\alpha = \mathcal{D}_\alpha X_\beta \quad (7.20b)$$

$$n_\alpha Q^\alpha = 0, \quad \text{on } \partial M \quad (7.20c)$$

$$(7.20d)$$

where $\alpha = 1, \dots, d-1$ and $\beta = \alpha + 1, \dots, d$. Equation 7.17 and Eq. 7.20 are formally equivalent. The former can be recovered from the latter by setting $M = [0, T] \times \tilde{M}$, where \tilde{M} is then a given material base space. In Eq. 7.20 we do not explicitly privilege a time-direction. However, note that we could in general consider the material base space M to be some $(d+1)$ -dimensional space-time manifold.

Field theories and non-linear σ models. The geometrisation programme can be viewed from a field-theoretic lens, in which case the spatio-temporal configuration Φ can be seen as a G/H -valued *field* over the base space M . The geometrisation programme is thus a formulation of the field dynamics in terms of the locally transitive action of the Lie algebra \mathfrak{g} , resulting in the Lie algebraic field equations Eq. 7.20. Notably though, as opposed to the vector-valued fields we often find in many field theories (e.g. electromagnetic field theory), Φ takes values ‘outside’ of the base space M . This is the reason why M does not necessitate a metric structure in the geometrisation programme. In principle, however, it would be possible to imbue M with a metric, and couple Φ with dynamic vector fields defined on TM in a Lagrangian formulation of the dynamics.

As a concrete example to illustrate the field-theoretic perspective, consider a Lagrangian density of the form

$$\mathcal{L} = \frac{1}{2} \eta^{\mu\nu} g(\partial_\mu \Phi, \partial_\nu \Phi) \quad (7.21)$$

where g is a (in general Φ -dependent) metric on G/H and η is the Minkowski metric (or the Euclidean metric for flat space-times). Equation 7.21 is a *non-linear σ model* [122, 146], and in this context Φ is a field that takes values in *target manifold* G/H . If Eq. 7.21 admits a reduction, then the geometrisation programme can be applied to derive the equations of motion for Φ . This would result in Eq. 7.20, with $Q^\alpha = -\frac{\partial \ell}{\partial X_\alpha}$, where ℓ is the reduction of \mathcal{L} . In Sec. 7.3.5 we use the geometrisation programme to derive the field equations for the $O(3)$ non-linear σ model. Furthermore, we note that Cosserat dynamics with a Lagrangian

$$\mathcal{L} = \frac{1}{2} \vec{N}^T \mathbf{M} \vec{N} + \frac{1}{2} \vec{X}^T \mathbf{K} \vec{X}, \quad (7.22)$$

of which the constitutive dynamics described in Sec. 6.4 is an example, is in the form of Eq. 7.21. Lagrangian Cosserat dynamics with a quadratic potential energy is thus a non-linear σ model.

Soft modes. Consider the case when the dynamics of the system is described by a constitutive Lagrangian \mathcal{L} which admits a reduction $\ell(\xi)$. We can note that the existence of the reduction $\ell(\xi)$ implies that the Lagrangian can only be dependent on the tangent space TG . In other words, \mathcal{L} has only gradient terms, and no ‘mass’ terms. Note that the components of the spatial reconstruction fields $X_\alpha = \Phi^{-1}\partial_\alpha\Phi$ are the ‘gradients’ of Φ , and therefore potential energies $\mathcal{U}(X_\alpha)$ are thus by construction ‘massless’. Consequently, each kinematic degree of freedom in such systems behave like *soft modes* [192, 33]. This can be understood intuitively by considering the Cosserat rod and the elastic energy derived in Sec. 6.4. The elastic energy cost of long wavelength deformations of the rod (whether twist, extension, bend or shear) go continuously to zero, as the wavelength is taken to infinity. This gives rise to sound modes (from extension), shearing waves and curvature waves.

7.2 Derivation of the geometric kinematic and dynamical equations of motion

Here we provide detailed derivations of the results in Sec. 7.1. For the sake of clarity, we had presented the kinematics and dynamics of Lie group-configured and homogeneous space-configured systems separately, and had formulated the latter as a kinematically constrained version of the former. Here, we will treat both cases simultaneously by considering a general system with a homogeneous configuration space. Note that for a Lie group G and $H = \{e\}$, where $e \in G$ is the identity element, then $G/H \cong G$. Therefore G is trivially a homogeneous space.

7.2.1 Kinematics

Let the kinematic base space W be a $(d + 1)$ -dimensional manifold of the form $W = [0, T] \times M$, where M is the d -dimensional material base space and $[0, T]$ is the time domain. The spatio-temporal configuration of the system is the map $\Phi : W \rightarrow G/H$, where G is an n -dimensional the symmetry group on G/H , with Lie algebra \mathfrak{g} , and the stabiliser $H \subset G$ is a r -dimensional Lie subgroup. The kinematic configuration space is the $(n - r)$ -dimensional homogeneous space G/H , upon which G acts transitively.

Let \mathcal{A} be an atlas over the material base space M , with elements $\mathcal{A} = \{(U_a, \mathbf{u}_a) \mid a \in I\}$, where $U_a \subset M$ and $\mathbf{u}_a : M \rightarrow \mathbb{R}^d$ and I is an index set. Due to the product structure of W , \mathcal{A} extends trivially to an atlas $\mathcal{A}_W = \{([0, T] \times U_a, \mathbf{x}_a) \mid a \in I\}$ over the kinematic base space W , where $\mathbf{x}_a = (t, u_a^1, \dots, u_a^d)$.

We define a projection map $\pi : G \rightarrow G/H$ as

$$\pi(g) = gH \quad (7.23)$$

which describes G as a principal bundle over G/H . Given the projection π , we can write the spatio-temporal configuration as $\Phi = \pi \circ \tilde{\Phi}$, where we $\tilde{\Phi} : W \rightarrow G$ is then an adapted frame field of Φ . In general there is no unique choice of $\tilde{\Phi}$ for a given Φ . In the case where the stabiliser is the trivial group $H = \{e\}$, where $e \in G$ is the identity element, then $G/H \cong G$ and we must have $\Phi = \tilde{\Phi}$. This was the case for the Cosserat rod.

The kinematics will be formulated with respect to the frame field $\tilde{\Phi}$, after which the projection π can be used to construct the spatio-temporal configuration Φ . The goal of this subsection is thus to formulate a mathematical programme with which we can kinematically construct $\tilde{\Phi}$. That is, given initial conditions on the time-slice at the initial time boundary, and a velocity field defined over W , we want to compute $\tilde{\Phi}$ at all future times. The vector field $d\tilde{\Phi} : W \rightarrow TG$ contains the infinitesimal information required to reconstruct Φ . As discussed in Sec. 5.2.6, we can left-translate $d\tilde{\Phi}$ to relate it to the Lie algebra-valued vector field

$$\xi = \tilde{\Phi}^{-1} d\tilde{\Phi} \quad (7.24)$$

where $\xi = \tilde{\Phi}^* \omega : W \rightarrow \mathfrak{g}$. Compactly, we write ξ locally as

$$\xi = Z_\gamma dx^\gamma \quad (7.25)$$

where $\gamma = 0, \dots, d$, such that $Z_0 = N$ and $Z_\alpha = X_\alpha$, $\alpha = 1, \dots, d$. As shown in Sec. 5.2.6, the Maurer-Cartan form satisfies the integrability condition

$$d\xi + \xi \wedge \xi = 0. \quad (7.26)$$

Substituting Eq. 7.2 into Eq. 7.26, locally we get the equations

$$\dot{X}_\alpha = (\partial_\alpha + \text{ad}_{X_\alpha})N, \quad \alpha = 1, \dots, d \quad (7.27a)$$

$$\begin{aligned} \partial_\beta X_\alpha &= (\partial_\alpha + \text{ad}_{X_\alpha})X_\beta, & \alpha &= 1, \dots, d-1, \\ && \beta &= \alpha + 1, \dots, d, \end{aligned} \quad (7.27b)$$

where we used the linear independence of the 2-form basis $du^\alpha \wedge du^\beta$ and $du^\alpha \wedge dt$. Eq. 7.27 are a set of $(d+1)d/2$ conditions on ξ , which must be simultaneously satisfied. Eq. 7.27b can be seen as spatial integrability conditions on X_α , which must be satisfied at all times t , and Eq. 7.27a are then the kinematic equations of motion. To see that Eq. 7.27b and

Eq. 7.27a are compatible, we take the time-derivative of the former to get

$$\begin{aligned}
& \partial_t (\partial_\beta X_\alpha - (\partial_\alpha + \text{ad}_{X^\alpha}) X_\beta) \\
&= \partial_\beta \dot{X}_\alpha - \partial_\alpha \dot{X}_\beta - [\dot{X}_\alpha, X_\beta] - [X_\alpha, \dot{X}_\beta] \\
&= (\partial_\beta + \text{ad}_{X_\beta}) \dot{X}_\alpha - (\partial_\alpha + \text{ad}_{X_\alpha}) \dot{X}_\beta \\
&= \partial_\beta ([X_\alpha, N]) + [X_\beta, \partial_\alpha N] + [X_\beta, [X_\alpha, N]] \\
&\quad - \partial_\alpha ([X_\beta, N]) - [X_\alpha, \partial_\beta N] - [X_\alpha, [X_\beta, N]] \\
&= -[\partial_\alpha X_\beta, N] + [X_\beta, [X_\alpha, N]] \\
&\quad + [\partial_\beta X_\alpha, N] - [X_\alpha, [X_\beta, N]] \\
&= [\partial_\beta X_\alpha, N] - [\partial_\alpha X_\beta, N] + [[X_\beta, X_\alpha], N]
\end{aligned} \tag{7.28}$$

where we used the Jacobi identity $[A, [B, C]] = -[C, [A, B]] - [B, [C, A]]$. Finally, we get

$$\partial_t (\partial_\beta X^\alpha - (\partial_\alpha + \text{ad}_{X^\alpha}) X^\beta) = [\partial_\beta X^\alpha - (\partial_\alpha + \text{ad}_{X^\alpha}) X^\beta, N]. \tag{7.29}$$

If X_α satisfies Eq. 7.27b at time $t = 0$, then the right-hand side of Eq. 7.29 vanishes. Therefore we see that the kinematic equations of motion Eq. 7.27a preserves the spatial integrability conditions Eq. 7.27b at all future times. Equation 7.29 shows how the error in spatial integrability grows in time.

The frame field $\tilde{\Phi}$ can thus be kinematically constructed by first integrating Eq. 7.27a to find ξ , and then solving by Eq. 7.24. The spatio-temporal configuration can be found using the projection map π , as $\Phi = \pi \circ \tilde{\Phi}$.

7.2.2 Dynamics

We now consider the dynamics of a general G/H -configured system with material base space M . The derivation requires a higher level of mathematical abstraction than that of Sec. 6.2, as we are considering material bases spaces that do not admit global coordinates in general.

We will begin by first treating the case of purely-constitutive and conservative dynamics, and then proceed to include non-conservative dynamics and body forces. We will make use of the celebrated Euler-Poincaré equation, which was first derived in [148, 172] to consider the dynamics of G/H -configured point particles (that is, M is a zero-dimensional manifold). Here we apply the Euler-Poincaré theorem to general G/H -configured continuum systems. This has previously been done in the specific case of the Cosserat rod in [82].

As was analogously the case in Sec. 6.3.2 for the Cosserat rod and filament, there is no difference in the resulting equations of motion whether kinematic configuration space is G or G/H . The dynamics is formulated with respect to the transitive action of G on G/H ,

and therefore the generalised forces will always ostensibly be \mathfrak{g}^* -valued. Consequently, if kinematic constraints are not explicitly implemented, the resulting dynamical equations of motion will be undetermined (as was also stated in [148, 172]).

Conservative dynamics

The conservative and constitutive dynamics of the system can be described by a volume form $L(d\Phi)$ on W we call the *Lagrangian*. In local coordinates $(U, \mathbf{u}) \in \mathcal{A}$ we write

$$L(d\Phi) = \mathcal{L}(d\Phi) dt \wedge d\mathbf{u} \quad (7.30)$$

on U , where $\mathcal{L}(d\Phi)$ is a Lagrangian density, where $d\mathbf{u} = \bigwedge_{\alpha=1}^d du^\alpha$.

Note that in contrast to Sec. 6.2, where we used Lagrangian densities, here the Lagrangian is a volume form. However, in practice the Lagrangian is often defined locally in terms of densities. These densities must follow the appropriate transformation law under change of charts. Let $(U, \mathbf{u}), (U', \mathbf{u}') \in \mathcal{A}$ where $U \cap U' \neq \emptyset$. Then we must have

$$\mathcal{L}'(d\Phi) = |J| \mathcal{L}(\Phi, d\Phi). \quad (7.31)$$

on $[0, T] \times U \cap U'$, where $J = |\det [\frac{\partial \mathbf{u}}{\partial \mathbf{u}'}]|$, and $\frac{\partial \mathbf{u}}{\partial \mathbf{u}'}$ is the Jacobian matrix of the coordinate transformation between the two charts.

The dynamical equations of motion can be found from Hamilton's principle

$$\delta \int_W L(d\Phi) = 0 \quad (7.32)$$

under variations $\Phi(t) \rightarrow \Phi(t) + \delta\Phi(t)$, where $\delta\Phi(\mathbf{u}, t) \in TG$ must vanish at the temporal boundaries. As before, we define an equivalent Hamilton's principle in terms of the reduced Lagrangian

$$\delta \int_W l(\xi) = 0 \quad (7.33)$$

under permissible variations $\delta\xi = \delta(\Phi^{-1}d\Phi)$, where $l(\xi)$ is the reduced Lagrangian and a volume form on W , and in local coordinates $(U, \mathbf{u}) \in \mathcal{A}$ is expressed as

$$l(\xi) = \ell(\xi) d\mathbf{x} \quad (7.34)$$

on $[0, T] \times U$, where $d\mathbf{x} = dt \wedge d\mathbf{u}$. We have that $\ell(\xi) = \mathcal{L}(d\Phi)$ when $\xi = \Phi^{-1}d\Phi$. Analogously to Sec. 6.2.2, we find

$$\delta\xi = d\eta + \text{ad}_\xi\eta \quad (7.35)$$

where $\eta : W \rightarrow \mathfrak{g}$ is an arbitrary Lie algebra-valued test function. In local coordinates

$(U_a, \mathbf{u}_a) \in \mathcal{A}$ we have

$$\delta\xi = \delta Z_\gamma du^\gamma \quad (7.36a)$$

$$\delta X_\alpha = \partial_\alpha \eta + \text{ad}_{X_\alpha} \eta, \quad \alpha = 1, \dots, d \quad (7.36b)$$

$$\delta N = \partial_t \eta + \text{ad}_N \eta \quad (7.36c)$$

on $[0, T] \times U$.

To express Eq. 7.32 and Eq. 7.33 in terms of local coordinates, we assume there exists a subset $\{(U_a, \mathbf{u}_a) \mid a \in J\} = \mathcal{B} \subset \mathcal{A}$, where $J \subset I$ is an index set, such that

$$\bigcup_{a \in J} \bar{U}_a = M \quad (7.37)$$

and $U_a \cap U_b = \emptyset$, $a, b \in J$ for $a \neq b$, where \bar{U}_k denotes the closure of the open set U_k . In other words, \mathcal{B} is a patchwork of charts over M , known as a *partition of unity*, such that their domains do not intersect but the union of their closures completely covers M . Then Hamilton's principle can be expressed in terms of local coordinates as

$$\delta \sum_{a \in J} \int_{U_a \times [0, T]} \mathcal{L}^{(a)}(d\Phi) \, d\mathbf{x}_a = 0 \quad (7.38)$$

or

$$\delta \sum_{a \in J} \int_{U_a \times [0, T]} \ell^{(a)}(\xi) \, d\mathbf{x}_a = 0. \quad (7.39)$$

From the Euler-Poincaré theorem [148, 172, 149] we have that the two variational principles Eq. 7.32 and Eq. 7.33 are equivalent, and we can thus use the latter to derive dynamical equations of motion expressed in the Lie algebra.

Let us now consider evaluating the variation over a single chart $(U, \mathbf{u}) \in \mathcal{A}$. Let e_i , $i = 1, \dots, n$ and E_i , $i = 1, \dots, n$ be bases for the Lie algebra \mathfrak{g} and its dual space \mathfrak{g}^* respectively, so that we can write $B = B_i e_i \in \mathfrak{g}$ and $C = C_i E_i \in \mathfrak{g}^*$ in terms of their components. We then have

$$\begin{aligned} \delta \int_{[0, T] \times U} \ell(\xi) \, d\mathbf{x} &= \int_{[0, T] \times U} A_i^\gamma \delta(Z_\gamma)_i \, d\mathbf{x} \\ &= \int_{[0, T] \times U} \langle \delta Z_\gamma, A^\gamma \rangle \, d\mathbf{x} \end{aligned} \quad (7.40)$$

where we sum over the index i , and where we have defined

$$A^\gamma = \frac{\partial \ell}{\partial Z_\gamma} \in \mathfrak{g}^* \quad (7.41)$$

and where the inner product $\langle \cdot, \cdot \rangle : \mathfrak{g} \times \mathfrak{g}^* \rightarrow \mathbb{R}$ is given by

$$\langle B, C \rangle = B_i C_i \quad (7.42)$$

for $B \in \mathfrak{g}$ and $C \in \mathfrak{g}^*$. We will now massage Eq. 7.40 into a coordinate-free form, so that the variation can be performed without recourse to charts.

Whilst the topology of the material base space M is of kinematic importance, as it dictates whether multiple charts are needed to parametrise the entire space, its differential geometry is irrelevant to both the kinematics as well as the dynamics. Nevertheless, for the following, we will require a volume form on M . For the derivation to proceed the choice is arbitrary, but one natural choice is the reduced Lagrangian l . However, to emphasise that the choice is arbitrary we will consider a general volume form, which can be written in a local chart $([0, T] \times U, \mathbf{u}) \in \mathcal{A}_W$ as $\omega = w d\mathbf{x}$.

We define the \mathfrak{g}^* -valued vector field

$$\begin{aligned} \Gamma &= w^{-1} A^\gamma \frac{\partial}{\partial x^\gamma} \\ &= w^{-1} (S^{(a)} \partial_t - Q_\alpha^{(a)} \partial_\alpha) \end{aligned} \quad (7.43)$$

such that

$$\begin{aligned} i_\Gamma \omega &= \sum_{\gamma=0}^d (-1)^\gamma A^\gamma \bigwedge_{\kappa \neq \gamma} dx^\kappa \\ &= S^{(a)} d\mathbf{u}_a + \sum_{\alpha=1}^d (-1)^\alpha Q_\alpha^{(a)} dt \wedge \left(\bigwedge_{\alpha \neq \beta} du_a^\beta \right) \end{aligned} \quad (7.44)$$

where $i_\Gamma \omega$ denotes the interior product of Γ and ω , and we have written $S = A^0$ and $Q^\alpha = A^\alpha$, $\alpha = 1, \dots, d$. It can be verified that Eq. 7.40 transforms as a vector under change of charts, using Eq. 7.31 and Eq. 7.7.

We can now rewrite Eq. 7.40 as

$$\int_{[0,T] \times U} \langle \delta\xi \wedge i_\Gamma \omega \rangle = 0 \quad (7.45)$$

where we have defined the inner wedge product

$$\langle B \wedge C \rangle = B_i \wedge C_i. \quad (7.46)$$

for \mathfrak{g} - and \mathfrak{g}^* -valued 1-forms B and C respectively. Now as $\delta\xi$ and $\langle \delta\xi \wedge i_\Gamma \omega \rangle$ are 1- and $(d+1)$ -forms respectively, $i_\Gamma \omega$ must be a \mathfrak{g}^* -valued d -form. Since Eq. 7.45 is chart-

independent we can write Hamilton's principle as

$$\int_W \langle \delta\xi \wedge i_\Gamma\omega \rangle = 0. \quad (7.47)$$

Now using Eq. 5.16 we have

$$d\langle \eta, i_\Gamma\omega \rangle = \langle d\eta \wedge i_\Gamma\omega \rangle + \langle \eta, di_\Gamma\omega \rangle \quad (7.48)$$

with which we can perform integration-by-parts, to get

$$\begin{aligned} \int_W \langle \delta\xi \wedge i_\Gamma\omega \rangle &= \int_W \{ \langle d\eta \wedge i_\Gamma\omega \rangle + \langle \text{ad}_\xi\eta \wedge i_\Gamma\omega \rangle \} \\ &= \int_W \{ d\langle \eta, i_\Gamma\omega \rangle - \langle \eta, di_\Gamma\omega \rangle - \langle \eta, \text{ad}_\xi^*(i_\Gamma\omega) \rangle \} \\ &= \int_{\partial W} \langle \eta, i_\Gamma\omega \rangle - \int_W \{ \langle \eta, (d + \text{ad}_\xi^*)i_\Gamma\omega \rangle \} \\ &= 0 \end{aligned} \quad (7.49)$$

where we used Stokes' theorem Eq. 5.21, and $\text{ad}_B^* : \mathfrak{g}^* \rightarrow \mathfrak{g}^*$ is the dual of the adjoint action defined as $\langle \text{ad}_D B, C \rangle = \langle B, \text{ad}_D^* C \rangle$ for $D, B \in \mathfrak{g}$ and $C \in \mathfrak{g}^*$.

For arbitrary η that vanishes at the temporal boundaries, the integral Eq. 7.49 must vanish. We first consider the boundary term in local coordinates

$$\begin{aligned} &\int_{\partial W} \left\{ \langle \eta, S \rangle d\mathbf{u} + \sum_{\alpha=1}^d (-1)^\alpha \langle \eta, Q^\alpha \rangle dt \wedge \left(\bigwedge_{\alpha \neq \beta} du^\beta \right) \right\} \\ &= \int_{\partial W} \sum_{\alpha=1}^d (-1)^\alpha \langle \eta, Q^\alpha \rangle dt \wedge \left(\bigwedge_{\alpha \neq \beta} du^\beta \right) \\ &= \int_0^T dt \int_{\partial M} \sum_{\alpha=1}^d (-1)^\alpha \langle \eta, Q^\alpha \rangle \bigwedge_{\alpha \neq \beta} du^\beta \end{aligned} \quad (7.50)$$

where we used that η vanishes at the temporal boundaries. The integral over ∂W and ∂M in Eq. 7.50 is an abuse of notation, and meant to be understood as an integral over the boundary covered by the chart. Consider the tangent and cotangent spaces $T_p M$ and $T_p^* M$ at a point $p \in \partial M$, and we trivially consider $T_p \partial M$ as a subset $T_p \partial M \subset T_p M$. Up to scalar multiplication, there is a single covector $n_p \in T_p^* M$ such that $n_p(v) = 0$ for all $v \in T_p \partial M$. We extend this to all $p \in \partial M$, to define the normal covector field n . Now let us assume that the chart $(U, \mathbf{u}) \in \mathcal{A}$ is defined such that the coordinates of the boundary satisfies $u^1 = 0$ and the interior $u^1 > 0$. In other words, we have that $(u^1)^{-1}(0) = \partial W \cap \bar{U}$. In these coordinates we have that $n_1 = -1$ and $n_\alpha = 0$, $\alpha \neq 1$. Eq. 7.50 can then be

rewritten as

$$\begin{aligned}
& \int_0^T dt \int_{\partial M} (-1)^\kappa \langle \eta, Q^1 \rangle \bigwedge_{\alpha \neq \kappa} du^\beta \\
&= \int_0^T dt \int_{\partial M} \langle \eta, Q^1 \rangle du^2 \dots du^d \\
&= \int_0^T dt \int_{\partial M} n_\alpha \langle \eta, Q^\alpha \rangle du^2 \dots du^d
\end{aligned} \tag{7.51}$$

where the integrals in the second and third lines are the standard integral in multi-variate calculus, and we sum over α in the third line. As Eq. 7.51 must vanish for arbitrary η , we find the boundary condition

$$n_\alpha Q^\alpha = 0, \tag{7.52}$$

in the given chart. To see that Eq. 7.52 is chart-independent, note that $n_\alpha = \frac{\partial u'^\beta}{\partial u^\alpha} n'_\beta$ and that Q_α transforms as a vector density

$$Q_\alpha = \frac{\partial \ell}{\partial X_\alpha} = |J| \frac{\partial \ell'}{\partial X'_\beta} \frac{\partial X'_\beta}{\partial X_\alpha} = |J| Q'_\beta \frac{\partial u^\alpha}{\partial u'^\beta} \tag{7.53}$$

where $J = \det \left[\frac{\partial \mathbf{u}'}{\partial \mathbf{u}} \right]$ and we used Eq. 7.7 and Eq. 7.31. We thus have that $n_\alpha Q_\alpha = |J| n'_\alpha Q'_\alpha$, which preserves Eq. 7.52 as $|J| \neq 0$.

From the second term in the Eq. 7.49 we find

$$\mathcal{D}^*(i_\Gamma \omega) = 0 \tag{7.54a}$$

which are the dynamical equations of motion in invariant form, where we have defined

$$\mathcal{D}^* = d + \text{ad}_\xi^*. \tag{7.55}$$

By substituting Eq. 7.44 into Eq. 7.54 we get the equations of motion in a local chart

$$\mathcal{D}_t^* P = \mathcal{D}_\alpha^* Q^\alpha \tag{7.56a}$$

$$n_\alpha Q^\alpha = 0, \quad \text{on } \partial M. \tag{7.56b}$$

where we sum over $\alpha = 1, \dots, d$, and have defined

$$\mathcal{D}_t^* = \partial_t + \text{ad}_N^* \tag{7.57a}$$

$$\mathcal{D}_\alpha^* = \partial_\alpha + \text{ad}_{X_\alpha}^*. \tag{7.57b}$$

Volumetric force forms and non-conservative dynamics

Here we generalise the above to include non-conservative constitutive dynamics and volumetric forces. In Sec. 6.2.2 we called the latter the *body forces* and *body moments* on the Cosserat rod. Here the analogous mathematical object is a *covector*-valued volume form, which we call the generalised body force density on the system.

We start with the *Lagrange-D'Alembert principle*, by adding an additional term to Eq. 7.32

$$\delta \int_W L(d\Phi) + \int_W (\mathbf{T}(\Phi, d\Phi, \dots))(\delta\Phi) = 0 \quad (7.58)$$

where \mathbf{T} is a T^*G -valued volume form we call the *generalised volumetric force*, and is acting on $\delta\Phi \in TG$. Henceforth we will suppress its arguments and write $(\mathbf{T}(\Phi, d\Phi, \dots))(\delta\Phi) = \mathbf{T}(\delta\Phi)$. The second-term in Eq. 7.58 is analogous to external forces in classical Euler-Poincaré theory for point-particles [148, 149]. In particular, compare Eq. 7.58 with the integral Lagrange-D'Alembert principle for point-particles in [149, Eq. 7.8.5].

As before we want to express Eq. 7.58 in reduced form. As in Sec. 6.2.2 we have that $\mathbf{T}(\delta\Phi) = \langle \eta, T \rangle$, where $T = L_\Phi^* \mathbf{T} = (\Phi^T)^{-1} \mathbf{T}$ is the generalised volumetric force and is a \mathfrak{g}^* -valued volume form, and $L_\Phi^* : T_\Phi^* G \rightarrow \mathfrak{g}^*$ is a mapping from the cotangent bundle to the dual Lie algebra defined as $\mathbf{T}(L_\Phi \eta) = \langle L_\Phi^* \mathbf{T}, \eta \rangle$. From the reduced form of Eq. 7.58, and following the same steps in Eq. 7.49, we get

$$\int_{\partial W} \langle \eta, i_\Gamma \omega \rangle - \int_W \{ \langle \eta \wedge \mathcal{D}^* i_\Gamma \omega \rangle \} + \int_W \langle \eta, T \rangle = 0. \quad (7.59)$$

and the equations of motion

$$\mathcal{D}^*(i_\Gamma \omega) = T \quad (7.60a)$$

with the same boundary conditions as before. In local coordinates we have

$$\mathcal{D}_t^* S = \mathcal{D}_\alpha^* Q^\alpha + T \quad (7.61a)$$

$$n_\alpha Q^\alpha = 0, \quad \text{on } \partial M. \quad (7.61b)$$

The argument for how to include non-conservative constitutive dynamics mimics that of Sec. 6.2.2. Here, we need only consider a more general Eq. 7.44, where Q^α is non-variational in general. We can thus write down a *generalised Lagrange-D'Alembert principle* for continuum systems as

$$\int_W \langle \delta\xi \wedge i_\Gamma \omega \rangle + \int_W \langle \eta, T \rangle = 0. \quad (7.62)$$

where the generalised internal stresses Q^α are non-variational in general for each $a \in I$,

and η must vanish at the temporal boundaries. In terms of local charts we have

$$\int_{[0,T] \times U} \{\langle \delta N, S \rangle - \langle \delta X_\alpha, Q^\alpha \rangle\} d\mathbf{x} + \int_{[0,T] \times U} \langle \eta, T \rangle = 0 \quad (7.63)$$

where we sum over $\alpha = 1, \dots, d$, and δN and δX_α are given in Eq. 7.36, from which general non-variational dynamics, including constitutive and body forces, can be derived.

7.3 Applications

Here we will apply the geometric framework derived in the preceding sections to various example systems. In contrast to the treatment of the Cosserat rod in Sec. 6.2, we will not the derivations of the equations of motion in details. Rather, we will take the results of Sec. 7.1 as a given and apply them directly. In doing so we mean to emphasise that our framework is programmatic, flexible and applicable to a wide variety of systems.

Sections 7.3.1 and 7.3.2 derive the classical theories of Cosserat bodies and surfaces, which are analogous to the Cosserat rod in two and three material dimensions respectively. Furthermore, we show that when the internal angular momenta are neglected, these models reduce to the theory of classical continuum mechanics, but expressed in terms of the intrinsic geometry of the bodies. Sections 7.3.3 and 7.3.4 provide examples of generalised Cosserat rods, where the external configuration spaces are not \mathbb{E}^3 , but the 2-sphere and Minkowski space respectively. When appropriate, we will point out if there is a natural division between internal and external degrees of freedom in the kinematic configuration spaces, which was a distinction that was introduced in Sec. 7.1.4.

In Sec. 7.3.5 we present a final example where we apply the geometrisation programme to the $O(N)$ non-linear σ model, as a showcase and illustration for the connection between our formalism and field theory

7.3.1 Three-dimensional Cosserat media

In Sec. 6 we approximated the kinematics and dynamics of a slender tube with the Cosserat rod model, which in that setting was seen as a coarse-graining of the tube into a 1-dimensional deformable rod of rigid body cross-sections. In general however, classical Cosserat media can exist in up to three spatial dimensions, and their point-continua can have an arbitrary number of directors, as discussed in Sec. 5.1. Here we consider a Cosserat *body* in three material dimensions (u, v, w) with two orthonormal directors, where the latter will be represented as material frames attached at each material point (u, v, w) . This is thus analogous to the Cosserat rod in three material dimensions. However, here the the micro-structure of the point-continua are not the result of a coarse-graining procedure,

but rather represent true internal degrees of freedom. Examples of such systems include liquid crystals [57, 87] as well as electromagnetic and ferromagnetic media [116, 167, 115].

Let the material base space be a connected and bounded subset $M \subset \mathbb{R}^3$. For example $M = [0, L_0^u] \times [0, L_0^v] \times [0, L_0^w]$ would be an appropriate material base space for a system with a cuboidal rest configuration. As for the Cosserat rod, the total configuration space is $SE(3)$, and the external and internal configuration spaces are $\mathbb{E}^3 = SE(3)/SO(3)$ and $SO(3)$ respectively. Let $\mathbf{u} = (u, v, w) : M \rightarrow \mathbb{R}^3$ be global material coordinates on the body, and let $\mathbf{r} : [0, T] \times M \rightarrow \mathbb{E}^3$ be the spatial configuration of the continuum body at time t , and let $E(t, \mathbf{u}) = (\mathbf{e}_1, \mathbf{e}_2, \mathbf{e}_3) \in SO(3)$ be the material frame at the material point \mathbf{u} at time t . As before, we have

$$\Phi(t, \mathbf{u}) = (\mathbf{r}(t, \mathbf{u}); E(t, \mathbf{u})) = \begin{pmatrix} 1 & \mathbf{0}^T \\ \mathbf{r}(t, \mathbf{u}) & E(t, \mathbf{u}) \end{pmatrix} \quad (7.64)$$

and we write the Maurer-Cartan form as

$$\xi = N dt + X_u du + X_v dv + X_w dw \quad (7.65)$$

where

$$N = \{\vec{V}; \vec{\Omega}\} \quad (7.66a)$$

$$X_u = \{\vec{\theta}_u; \vec{\pi}_u\} \quad (7.66b)$$

$$X_v = \{\vec{\theta}_v; \vec{\pi}_v\} \quad (7.66c)$$

$$X_w = \{\vec{\theta}_w; \vec{\pi}_w\}. \quad (7.66d)$$

From $\Phi^{-1} d\Phi = \xi$ we find that

$$d\mathbf{r} = \mathbf{V} dt + \boldsymbol{\theta}_u du + \boldsymbol{\theta}_v dv + \boldsymbol{\theta}_w dw \quad (7.67a)$$

$$dE = E \hat{\vec{\Omega}} dt + E \hat{\vec{\pi}}_u du + E \hat{\vec{\pi}}_v dv + E \hat{\vec{\pi}}_w dw. \quad (7.67b)$$

From Eq. 7.4 we have that the kinematic equations of motion are

$$\dot{X}_\alpha = \mathcal{D}_\alpha N \quad (7.68a)$$

where $\alpha = u, v, w$, and where the spatial reconstruction fields X_α must satisfy the $d(d+1)/2 = 6$ spatial integrability conditions Eq. 7.5 at all times. As spatial integrability is preserved by the forward equations Eq. 7.68, it suffices that X_α satisfy Eq. 7.5 at $t = 0$.

Substituting Eq. 7.66 into Eq. 7.68 we get

$$D_t \vec{\theta}_\alpha = D_\alpha \vec{V} \quad (7.69a)$$

$$\dot{\vec{\pi}}_\alpha = D_\alpha \vec{\Omega} \quad (7.69b)$$

where $D_t = \partial_t + \hat{\vec{\Omega}}$ and $D_\alpha = \partial_\alpha + \hat{\vec{\pi}}_\alpha$, $\alpha = u, v, w$.

From Eq. 7.9 we find the dynamical equations of motion

$$\mathcal{D}_t^* S = \mathcal{D}_u^* Q^u + \mathcal{D}_v^* Q^v + \mathcal{D}_w^* Q^w + T \quad (7.70a)$$

$$n_\alpha Q^\alpha = 0, \quad \text{on } \partial M. \quad (7.70b)$$

where ad^* was given in Eq. 6.81, and where

$$S = \frac{\partial \mathcal{K}}{\partial N} = \{\vec{P}; \vec{L}\} \quad (7.71a)$$

$$Q^u = \{\vec{F}^u; \vec{M}^u\} \quad (7.71b)$$

$$Q^v = \{\vec{F}^v; \vec{M}^v\} \quad (7.71c)$$

$$Q^w = \{\vec{F}^w; \vec{M}^w\}. \quad (7.71d)$$

We now define the kinetic energy per unit material volume as

$$\mathcal{K} = \mathcal{K}(N) = \frac{1}{2} \rho_0 |\vec{V}|^2 + \frac{1}{2} \vec{\Omega}^T \mathbb{I} \vec{\Omega} \quad (7.72)$$

where ρ_0 is the mass density per unit material volume and \mathbb{I} is the moment-of-inertia per unit material volume, and we have $\vec{P} = \rho_0 \vec{V}$ and $\vec{L} = \mathbb{I} \vec{\Omega}$. Substituting Eq. 7.66 and Eq. 7.71 into Eq. 7.70 we get

$$D_t \vec{P} = D_\alpha \vec{F}^\alpha + \vec{f} \quad (7.73a)$$

$$D_t \vec{L} = D_\alpha \vec{M}^\alpha + \vec{\theta}_\alpha \times \vec{F}^\alpha + \vec{m} \quad (7.73b)$$

$$n_\alpha \vec{F}^\alpha = n_\alpha \vec{M}^\alpha = 0, \quad \text{on } \partial M \quad (7.73c)$$

where we sum over repeated indices of $\alpha = u, v, w$. Let L, T and M refer to the dimensions of material length, time and mass respectively. The dimensions of all kinematic and dynamic quantities can be found by first noting that from Eq. 7.67 we have that $[\vec{V}] = LT^{-1}$, $[\vec{\theta}_\alpha] = 1$, $[\vec{\Omega}] = T^{-1}$ and $[\vec{\pi}_\alpha] = L^{-1}$. As $\mathcal{K}(N)$ has units of energy per unit material volume, and $\vec{P} = \frac{\partial \mathcal{K}}{\partial \vec{V}}$ and $\vec{L} = \frac{\partial \mathcal{K}}{\partial \vec{\Omega}}$, we have that $[\vec{P}] = ML^{-2}T^{-1}$ and $[\vec{L}] = ML^{-1}T^{-1}$. Similarly, as $\vec{F}^\alpha = \frac{\partial \mathcal{U}}{\partial \vec{\theta}_\alpha}$ and $\vec{M}^\alpha = \frac{\partial \mathcal{U}}{\partial \vec{\pi}_\alpha}$ for conservative dynamics, we have that $[\vec{F}^\alpha] = ML^{-1}T^{-2}$ and $[\vec{M}^\alpha] = MT^{-2}$. We thus conclude that \vec{P} and \vec{L} have units of momentum and angular momentum per unit material volume respectively, and \vec{F}^α and \vec{M}^α force and moment per

unit material area respectively. The body force \vec{f} and \vec{m} have units of force and moment per unit material volume respectively.

Equations 7.69 and 7.73 together completely determine the kinematics and dynamics of the Cosserat body, where the initial conditions must obey the spatial integrability constraints Eq. 7.5, and are consistent with the equations of motion found in the literature [186]. The equations close using $\vec{P} = \rho_0 \vec{V}$ and $\vec{L} = \mathbb{I} \vec{\Omega}$.

We will now show that Eq. 7.73 is consistent with the dynamic laws of classical continuum mechanics. We can recognise Eq. 7.73a as the *Cauchy momentum equation* in Lagrangian coordinates with respect to a reference configuration. This is especially clear in the non-moving frame. We define $\nabla_{\circ} = (\partial_u \ \partial_v \ \partial_w)^T$ and

$$\Sigma = \begin{pmatrix} F^u & F^v & F^w \end{pmatrix} \quad (7.74a)$$

$$\Sigma = E\Sigma = \begin{pmatrix} \mathbf{F}^u & \mathbf{F}^v & \mathbf{F}^w \end{pmatrix} \quad (7.74b)$$

such that $\nabla_{\circ} \cdot \Sigma^T = \partial_{\alpha} \mathbf{F}_{\alpha} = ED_{\alpha} \vec{F}_{\alpha}$. Then Eq. 7.73a in the non-moving frame becomes

$$\rho_0 \ddot{\mathbf{r}} = \nabla_{\circ} \cdot \Sigma^T + \mathbf{f}, \quad (7.75)$$

which is the *Cauchy momentum equation*, written in terms of the *first Piola-Kirchhoff* stress tensor Σ . Equation 7.73a can thus in turn be seen as the Cauchy momentum equation in curvilinear coordinates. The first Piola-Kirchoff stress tensor is related to the Cauchy stress tensor σ as $\mathcal{P}\Sigma^T = \det[\mathcal{P}]\sigma$ where $\mathcal{P} = \frac{\partial \mathbf{r}}{\partial \mathbf{u}}$ is the deformation gradient tensor, using which we can relate Eq. 7.75 to Eq. 5.1 Analogously, Eq. 7.73b can thus also be seen as a conservation equation for the internal angular momentum of the system.

In Eq. 7.74 we see saw that the first Piola-Kirchoff in the moving frame was Σ . Similarly, if we define

$$\Theta = \begin{pmatrix} \vec{\theta}_u & \vec{\theta}_v & \vec{\theta}_w \end{pmatrix} \quad (7.76)$$

we have that $\mathcal{P} = E\Theta$. We thus see that Θ is the deformation gradient tensor in the moving frame. Furthermore we have that if \mathcal{U} is the density of potential energy stored in the system, then since in classical continuum mechanics [19]

$$\Sigma = \frac{\partial \mathcal{U}}{\partial \mathcal{P}} \quad (7.77)$$

we have that

$$\Sigma = E^T \frac{\partial \mathcal{U}}{\partial \mathcal{P}} = \frac{\partial \mathcal{U}}{\partial \Theta} \quad (7.78)$$

which recovers $\vec{F}_{\alpha} = \frac{\partial \mathcal{U}}{\partial \vec{\theta}_{\alpha}}$.

We have thus shown that conservative Cosserat body dynamics is consistent with conservative continuum dynamics, and reduces to it when eliminating the internal degrees

of freedom through kinematic restriction. This elimination is trivial in the case of the Cosserat body. As the material frame lies in the tangent space of the body at all points $\mathbf{e}_i(t, \mathbf{u}) \in T_{\mathbf{r}(t, \mathbf{u})}\mathbb{E}^3$, the frame is always adapted. Therefore one simple gauge choice is to use a non-moving frame by setting $\vec{\pi} = \vec{\Omega} = 0$, thus neglecting Eq.7.73b

Finally, we can also relate $\vec{\theta}_\alpha$ and $\vec{\pi}_\alpha$ to well-known quantities in differential geometry. Let \tilde{d} be a ‘spatial’ exterior derivative, which we define such that $\tilde{d}\mathbf{r} = \boldsymbol{\theta}_\alpha du^\alpha$. At time t , the metric $g_{\alpha\beta}$ of the manifold $\mathbf{r}(M) \subset \mathbb{E}^3$ satisfies

$$\tilde{d}\mathbf{r} \cdot \tilde{d}\mathbf{r} = g_{\alpha\beta} du^\alpha du^\beta \quad (7.79)$$

we can thus identify $g_{\alpha\beta} = \vec{\theta}_\alpha^T \vec{\theta}_\beta$, or $g = \Theta^T \Theta$. Furthermore, in Euclidean space the *Christoffel symbols* are defined as

$$\partial_\alpha \mathbf{e}_j = \Gamma_{j\alpha}^i \mathbf{e}_i \quad (7.80)$$

we can thus identify $(\hat{\pi}_\alpha)_{ij} = \Gamma_{j\alpha}^i$, and D_α as the covariant derivative on $\mathbf{r}(M)$.

7.3.2 Cosserat surfaces

We consider a thin shell with reference configuration $\mathcal{M} = [-L_0^1/2, L_0^1/2] \times [0, L_0^2] \times [0, L_0^3]$, material coordinates $\mathbf{X} \in \mathcal{M}$ and with constant mass density per unit material volume ρ_0^V . We assume that the body is slender along the first spatial dimension, meaning that L_0^1 is small relative to L_0^2 and L_0^3 . At time t the location of the material point at \mathbf{X} is given by $\mathbf{x}(\mathbf{X}, t)$, which are the deformed coordinates. We also define X_1 such that $\int_{\mathcal{M}} X_1 d\mathbf{X} = 0$.

As we did in Sec. 6.2.2 for a slender tube, we will now kinematically approximate the thin shell with a Cosserat system of lower dimensionality. We consider a Cosserat surface, with material base space $M = [0, L_0^2] \times [0, L_0^3]$, and we denote its material coordinates as $(u, v) = (X_2, X_3)$. A single inextensible director \mathbf{e}_1 is attached at each material point (u, v) . Then, the Cosserat surface approximates the slender body under the kinematic assumption that the fibres along \mathbf{e}_1 are rigid bodies. In other words we have

$$\mathbf{x}(\mathbf{X}, t) = \mathbf{r}(t, u, v) + X_1 \mathbf{e}_1. \quad (7.81)$$

where $X_1 \in [-L_0^1/2, L_0^1/2]$ and $\mathbf{r}(t, u, v)$ is the mid-surface. Equation 7.81 is illustrated in Fig. 7.2. Notably the Cosserat surface only has a single director, as opposed to the two directors of the Cosserat rod. This means that the internal configuration space of the Cosserat surface is $S^2 = SO(3)/SO(2)$ rather than $SO(3)$. However, for the sake of convenience we may add an additional orthonormal director \mathbf{e}_2 such that we have a full material frame $E \in SO(3)$. We thus introduce a gauge freedom in the physical description of the system, but due to the abelian nature of $SO(2)$ this will not cause any issues in the physical description of the system.

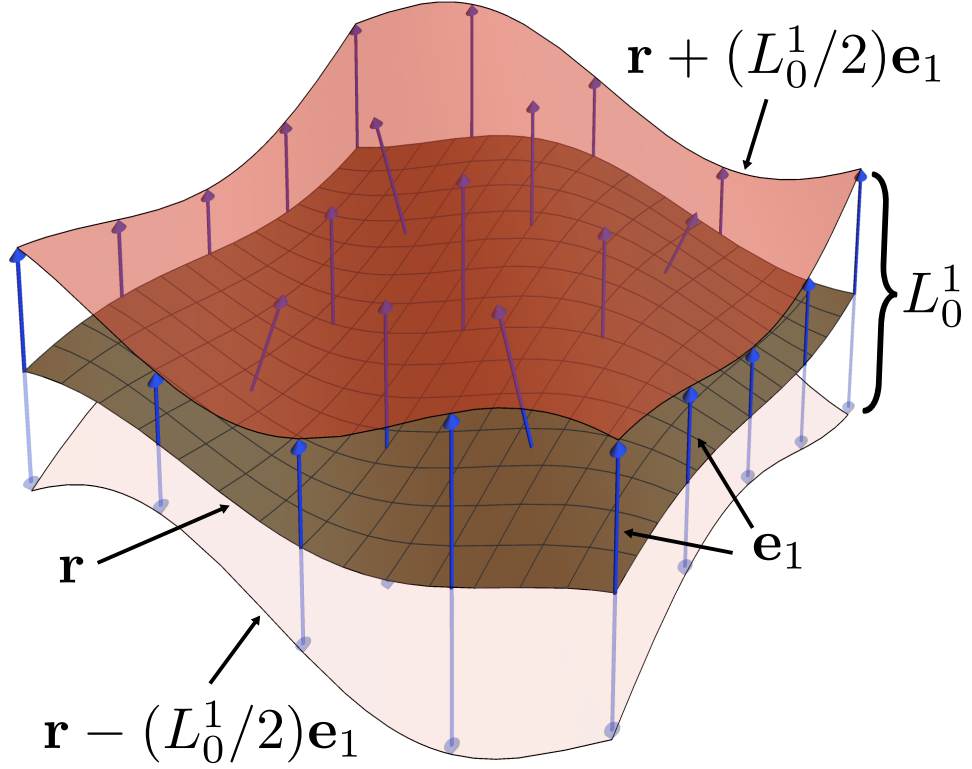


Figure 7.2: The director field $\mathbf{e}_1(u, v)$ (blue arrows) and the midsurface $\mathbf{r}(u, v)$ (brown surface) of the Cosserat surface approximates a thin shell by constraining the material fibres along the director to be fixed. The upper and lower boundaries of the shell (transparent red surfaces) are given by $\mathbf{r}(u, v) \pm (L_0^1/2)\mathbf{e}_1(u, v)$ respectively.

We write $\Phi(t, u, v) = (\mathbf{r}(t, u, v); E(t, u, v))$ as before and

$$\xi = Ndt + X_u du + X_v dv \quad (7.82)$$

where

$$N = \{\vec{V}; \vec{\Omega}\} \quad (7.83a)$$

$$X_u = \{\vec{\theta}_u; \vec{\pi}_u\} \quad (7.83b)$$

$$X_v = \{\vec{\theta}_v; \vec{\pi}_v\}. \quad (7.83c)$$

From $\Phi^{-1}d\Phi = \xi$ we find

$$d\mathbf{r} = \mathbf{V}dt + \boldsymbol{\theta}_u du + \boldsymbol{\theta}_v dv \quad (7.84a)$$

$$dE = E\hat{\Omega}dt + E\hat{\pi}_u du + E\hat{\pi}_v dv. \quad (7.84b)$$

and from Eq. 7.4 we find the kinematic equations of motion

$$\dot{X}_u = \mathcal{D}_u N \quad (7.85a)$$

$$\dot{X}_v = \mathcal{D}_v N \quad (7.85b)$$

where the spatial reconstruction fields X_u and X_v must obey the spatial integrability conditions

$$\partial_v X_u = \mathcal{D}_u X_v. \quad (7.86)$$

We now derive the dynamical equations of motion. Carrying out the analogous derivation as we did in Sec. 6.2.2, we find that the kinetic energy density per unit material area is

$$\mathcal{K} = \frac{1}{2} \rho_0 |\vec{V}|^2 + \frac{1}{2} \vec{\Omega}^T \mathbb{I} \vec{\Omega} \quad (7.87)$$

where $\rho_0 = L_0^1 \rho_0^V$ and \mathbb{I} is the moment-of-inertia of the material frame per unit material area.

From Eq. 7.9 we find the dynamical equations of motion

$$\mathcal{D}_t^* S = \mathcal{D}_u^* Q^u + \mathcal{D}_v^* Q^v + T \quad (7.88a)$$

$$n_\alpha Q^\alpha = 0, \quad \text{on } \partial M. \quad (7.88b)$$

where we sum over $\alpha = u, v$ and ad^* was given in Eq. 6.81, and where

$$S = \frac{\partial \mathcal{K}}{\partial N} = \{\vec{P}; \vec{L}\} \quad (7.89a)$$

$$Q^u = \{\vec{F}^u; \vec{M}^u\} \quad (7.89b)$$

$$Q^v = \{\vec{F}^v; \vec{M}^v\} \quad (7.89c)$$

and $\vec{P} = \rho_0 \vec{V}$ and $\vec{L} = \mathbb{I} \vec{\Omega}$. Substituting Eq. 7.83 and Eq. 7.89 into Eq. 7.88 we get

$$D_t \vec{P} = D_\alpha \vec{F}^\alpha + \vec{f} \quad (7.90a)$$

$$D_t \vec{L} = D_\alpha \vec{M}^\alpha + \vec{\theta}_\alpha \times \vec{F}^\alpha + \vec{m} \quad (7.90b)$$

$$n_\alpha \vec{F}^\alpha = n_\alpha \vec{M}^\alpha = 0, \quad \text{on } \partial M \quad (7.90c)$$

where we sum over repeated indices of $\alpha = u, v$, and is consistent with the dynamical equations of motion found in the literature [6]. Repeating the same dimensional arguments as in Sec. 7.3.1, we can conclude that \vec{P} and \vec{L} have units of momentum and angular momentum per unit material area respectively, and \vec{F}^α and \vec{M}^α force and moment per unit material length respectively. The body force \vec{f} and \vec{m} have units of force and moment per unit material area respectively.

Note that the component L_1 of the angular momentum of the material frame is unphysical if the Cosserat surface is seen as an approximate model for a slender shell. For conservative dynamics, this means that \mathcal{U} should not couple to π_1 , which is the rate-of-twist of the material frame around \mathbf{e}_1 . In general, this entails that $M_1^\alpha = m_1^\alpha = 0$.

In the above we have considered a rectangular material base space M . However, in general for *open* Cosserat surfaces the material base space can be any bounded and compact subset $M \subset \mathbb{R}^2$. Furthermore, *closed* Cosserat surfaces may have $M = S^2$, in which case the material base space no longer admits global coordinates. The kinematic and dynamical equations of motion above still apply in the case of a closed surface, but they must then be simultaneously and consistently simulated over multiple charts that cover M .

7.3.3 Cosserat rods on 2-spheres

We consider the constitutive dynamics of a generalised Cosserat rod, lying on the 2-dimensional surface of a sphere $S^2 = \{\mathbf{x} \in \mathbb{E}^3 \mid |\mathbf{x}| = r\}$ where r is the radius of the sphere. Some recent applications of such systems can be found in [144, 109]. The external configuration space of the rod is thus $S^2 = SO(3)/SO(2)$, and the internal configuration space is $SO(2)$. Let $\mathbf{r}(t, u) = r\mathbf{e}_0(t, u)$ denote the center-line of the rod, where $\mathbf{n}(t, u) \in \mathbb{E}^3$ is a unit-vector, and $u \in [0, L_0]$, $t \in [0, T]$. The material frame $E = (\mathbf{e}_1(t, u), \mathbf{e}_2(t, u))$ of the rod are two orthonormal vectors that are tangent to S^2 at \mathbf{r} , and can be seen as an element of $SO(2)$. We also have that the triad $(\mathbf{n} \ \mathbf{e}_1 \ \mathbf{e}_2)$ are mutually orthogonal, and $\mathbf{n}(t, u)$ is normal to S^1 at $\mathbf{r}(t, u)$ and $(\mathbf{e}_1 \ \mathbf{e}_2)$ forms a basis for $T_{\mathbf{r}(t,u)}S^2$. Furthermore, as the triad forms an orthogonal matrix with unit determinant we can identify it as an element of $SO(3)$, and will thus write $\Phi = (\mathbf{n} \ \mathbf{e}_1 \ \mathbf{e}_2)$. The configuration space of the Cosserat rod on the sphere is thus $G = SO(3)$, with kinematic base space $W = [0, T] \times [0, L_0]$ which admits a global basis. As in Ch. 6 we will distinguish between vectors $\mathbf{v} \in \mathbb{E}^3$ in the fixed frame and vectors $\vec{v} \in \mathbb{R}^3$ in the moving frame, and relate the two as $\vec{v} = \Phi^T \mathbf{v}$. We shall write the components of vectors in the moving frame as $\vec{v} = (v_n, v_1, v_2)$.

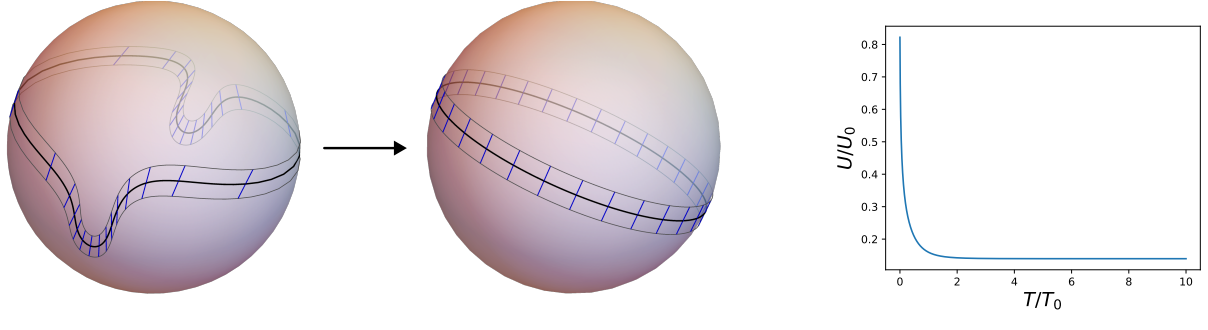
We shall write the Maurer-Cartan form as

$$\xi = \hat{N}dt + \hat{X}du \quad (7.91)$$

where $\hat{N}(t, u), \hat{X}(t, u) \in \mathfrak{so}(3)$, and we write

$$\vec{N} = (\Omega_n, -V_2/r, V_1/r)^T \quad (7.92a)$$

$$\vec{X} = (\pi_n, -\theta_2/r, \theta_1/r)^T \quad (7.92b)$$



(a) Overdamped Cosserat rod relaxing to a ground-state

(b) Potential energy

Figure 7.3: (a) Overdamped Cosserat rod on 2-sphere relaxing from a deformed initial configuration (left) to a ground-state (right). Solid black lines are the rod center-lines, and the blue lines are the directors \mathbf{e}_2 . (b) Potential energy of the Cosserat rod.

and

$$\vec{V} = (0, V_1, V_2)^T \quad (7.93a)$$

$$\vec{\theta} = (0, \theta_1, \theta_2)^T \quad (7.93b)$$

$$\vec{\Omega} = (\Omega_n, 0, 0)^T \quad (7.93c)$$

$$\vec{\pi} = (\pi_n, 0, 0)^T. \quad (7.93d)$$

From $\Phi^{-1}d\Phi = \xi$ we find

$$d\mathbf{r} = r d\mathbf{n} = \mathbf{e}_i V_i dt + \mathbf{e}_i \theta_i du \quad (7.94a)$$

$$= \mathbf{V} dt + \boldsymbol{\theta} du$$

$$d\mathbf{e}_1 = (\Omega_n \mathbf{e}_2 - (V_1/r) \mathbf{n}) dt + (\pi_n \mathbf{e}_2 - (\theta_1/r) \mathbf{n}) du \quad (7.94b)$$

$$d\mathbf{e}_2 = (-\Omega_n \mathbf{e}_1 - (V_2/r) \mathbf{n}) dt + (-\pi_n \mathbf{e}_1 - (\theta_2/r) \mathbf{n}) du. \quad (7.94c)$$

We can identify $\mathbf{V}(t, u) \in T_{\mathbf{r}(t,u)}S^2$ as the velocity of the center-line at $\mathbf{r}(t, u)$ and likewise $\boldsymbol{\theta}(t, u) \in T_{\mathbf{r}(t,u)}S^2$ as the rate-of-change of the center-line along the material coordinate u . We can also identify $\Omega_n(t, u)$ and $\pi_n(t, u)$ as the angular velocity and angular rate-of-rotation of the material frame around \mathbf{n} , and thus $\Omega(t, u), \pi(t, u) \in \mathfrak{so}(2)$.

From Eq. 7.4 we can find the kinematic equations of motion

$$\begin{aligned} \dot{\vec{X}} &= \mathcal{D}_u \vec{N} \\ &= \vec{N}' + \vec{X} \times \vec{N} \end{aligned} \quad (7.95)$$

using $\overrightarrow{[\hat{X}, \hat{N}]} = \vec{X} \times \vec{N}$. We define the Lagrangian

$$\mathcal{L}(d\Phi) = \mathcal{K}(\dot{\Phi}) - \mathcal{U}(\Phi') \quad (7.96a)$$

$$\mathcal{K} = \frac{1}{2}\rho_0|\mathbf{V}|^2 + \frac{1}{2}\mathbb{I}_n\Omega_n^2 \quad (7.96b)$$

where \mathcal{U} is constitutive potential energy, ρ_0 is the mass density per unit material length and $\mathbb{I}_n \in \mathbb{R}$ is the moment-of-inertia per unit material length of the material frame. In its reduced form, the Lagrangian is

$$\ell(\xi) = \mathcal{K}(N) - \mathcal{U}(X) \quad (7.97a)$$

$$\mathcal{K} = \frac{1}{2}\rho_0|\vec{V}|^2 + \frac{1}{2}\mathbb{I}_n\Omega_n^2. \quad (7.97b)$$

The conjugate moment and stress are $\vec{P} = \frac{\partial \ell}{\partial \vec{N}}$ and $\vec{Q} = -\frac{\partial \ell}{\partial \vec{X}}$ respectively, and we get

$$\vec{P} = (L_n, p_2 r, -p_1 r)^T \quad (7.98a)$$

$$\vec{Q} = (M_n, F_2 r, -F_1 r)^T \quad (7.98b)$$

where $\vec{F} = (0, F_1, F_2)^T$ and $\vec{p} = (0, \rho_0 V_1, \rho_0 V_2)^T$ is the force on the center-line and its linear momentum density per unit material length respectively, and where $\vec{M} = (M_n, 0, 0)$ and $\vec{L} = (\mathbb{I}_n\Omega_n, 0, 0)^T$ are the moment on the material frame and its angular momentum per unit material length respectively. From Eq. 7.9 we find the dynamical equations of motion

$$(\partial_t + \hat{N})\vec{S} = (\partial_u + \hat{X})\vec{Q} + \vec{T} \quad (7.99a)$$

$$Q_\alpha = 0, \quad u = 0, L_0. \quad (7.99b)$$

where we used $[\text{ad}_X] = \hat{X}$ and $[\text{ad}_X^*] = -[\text{ad}_X]^T$, and where \vec{T} is a generalised body force. In the absence of body forces, and using the definitions of S, Q, N and X , we get

$$\dot{\vec{L}} = M' + \vec{\theta} \times \vec{F} \quad (7.100a)$$

$$\dot{\vec{P}} = D_u \vec{F} - c\vec{\Omega} \times \vec{V} + \frac{1}{r^2} \vec{M} \times \vec{\theta} \quad (7.100b)$$

where $c = \rho_0 + \mathbb{I}_n/r^2$. $\vec{\theta} \times \vec{F}$ is the moment exerted on the material frame due to the force, $\frac{1}{r^2} \vec{M} \times \vec{\theta}$ is the force exerted on the center-line due to the moment, and $-c\vec{\Omega} \times \vec{V}$ can be seen as a Coriolis force that arises due to the rotating frame. Equations 7.95 and 7.100a together form a set of equations that completely determine the kinematics and dynamics of the system.

We will now consider the example of ‘overdamped’ Cosserat rod dynamics on the 2-sphere. We define the frictional body force $\vec{T} = \gamma \vec{N}$, where $\gamma \in \mathbb{R}^{3 \times 3}$ is a symmetric and

positive-definite matrix, and the constitutive potential

$$\mathcal{U} = \frac{1}{2}\epsilon(\vec{X} - \vec{X}_0)^T \mathsf{K}(\vec{X} - \vec{X}_0) \quad (7.101)$$

where $\vec{X}_0 = (0\ 1\ 0)^T$ and $\mathsf{K} \in \mathbb{R}^{3 \times 3}$ is a positive definite matrix. We take the overdamped limit, eliminating the inertial degrees of freedom $\vec{P} \approx 0$, to get

$$\dot{\vec{X}} = \vec{N}' + \vec{X} \times \vec{N} \quad (7.102a)$$

$$\gamma \vec{N} = (\partial_u + \hat{X}) \vec{Q}. \quad (7.102b)$$

Fig. 7.3 shows the result of a simulation of Eq. 7.102, depicting the relaxation of an initial deformed state to a ground-state that minimises Eq. 7.101.

7.3.4 Relativistic Cosserat rods

Here we derive the kinematic equations of relativistic motion of a Cosserat rod. We work in units where the speed-of-light constant is set to unity $c = 1$. The Minkowski vector space $\mathbb{M}^{1,3}$ is the vector space \mathbb{R}^4 equipped with the *Minkowski inner product* $\langle \cdot, \cdot \rangle_M : \mathbb{M}^{1,3} \times \mathbb{M}^{1,3} \rightarrow \mathbb{R}$ with signature $(1, 3)$. In other words, given some basis $B = (\mathbf{b}_0, \mathbf{b}_1, \mathbf{b}_2, \mathbf{b}_3)$ for \mathbb{R}^4 , the *Minkowski metric*

$$\eta_{ij} = \langle \mathbf{b}_i, \mathbf{b}_j \rangle_M \quad (7.103)$$

has 1 negative eigenvalue and 3 positive eigenvalues. Henceforth we will assume that the basis is defined such that

$$\eta = \text{diag}(-1, 1, 1, 1). \quad (7.104)$$

Any basis that diagonalises η as in Eq. 7.104 will be called an *orthonormal* basis. A $\mathbf{v} \in \mathbb{M}^{1,3}$ is known as *time-like* if $\langle \mathbf{v}, \mathbf{v} \rangle_M < 0$, *space-like* if $\langle \mathbf{v}, \mathbf{v} \rangle_M > 0$ and *light-like* if $\langle \mathbf{v}, \mathbf{v} \rangle_M = 0$. We can thus identify \mathbf{b}_0 as the time-like direction in this basis, and $(\mathbf{b}_1, \mathbf{b}_2, \mathbf{b}_3)$ as the space-like directions.

The *space-time coordinates* $\mathbf{r}(\tau)$ of an observer is a function $\mathbf{r} : \mathbb{R} \rightarrow \mathbb{M}^{1,3}$ where τ is the time measured by clocks co-moving with the observer, known as the *proper time*. The *4-velocity* of the observer is given by the time-like vector $\mathbf{U} = \partial_\tau \mathbf{r}$. The *inertial frame* of the observer at proper time τ is an orthonormal basis $E(\tau) = (\mathbf{e}_0(\tau), \mathbf{e}_1(\tau), \mathbf{e}_2(\tau), \mathbf{e}_3(\tau))$ such that

$$\vec{U} = E^{-1} \mathbf{U} = (1\ 0\ 0\ 0)^T. \quad (7.105)$$

Intuitively, this corresponds to the fact that an observer is always stationary in its own co-moving inertial reference frame. Such a basis can be found by setting $\mathbf{e}_0 = \mathbf{U}$, and the remaining three basis elements $(\mathbf{e}_1, \mathbf{e}_2, \mathbf{e}_3)$ specify the spatial orientation of the observer. Vectors $\vec{v} = E^{-1} \mathbf{v}$ are thus expressed in the inertial frame E . We shall use the notation \tilde{v}

to refer to the spatial components of \vec{v} , such that $\vec{v} = (v_0 \ \tilde{v}^T)^T$.

Any two inertial frames E_1 and E_2 can be related by a *Lorentz transformation*

$$E_2 = \Lambda E_1 \quad (7.106)$$

where $\Lambda \in SO(1, 3)$, and where $SO(1, 3)$ is the *Lorentz group* on $\mathbb{M}^{1,3}$ and is defined as

$$SO(1, 3) = \{\Lambda \in \mathbb{R}^{4 \times 4} \mid \langle \Lambda \mathbf{v}, \Lambda \mathbf{v} \rangle_M = \langle \mathbf{v}, \mathbf{v} \rangle_M \ \forall \mathbf{v} \in \mathbb{M}^{3,1}\}. \quad (7.107)$$

which is the group of rotations in space and *Lorentz boosts*. The Lorentz group is thus the set of linear transformations that preserves the Minkowski inner product. Combined with the group of translations on $\mathbb{M}^{1,3}$, we have the *Poincaré group*

$$M(1, 3) = \left\{ \begin{pmatrix} 1 & \mathbf{0}^T \\ \mathbf{t} & \Lambda \end{pmatrix} \in \mathbb{R}^{5 \times 5} \mid \mathbf{t} \in \mathbb{M}^{1,3}, \Lambda \in SO(3, 1) \right\} \quad (7.108)$$

of space-time translations and rotations.

Now consider a continuous ‘string’ of inertial observers with space-time coordinates $\mathbf{r}(\tau, u)$ and inertial frames $E(\tau, u)$, parametrised by u . If $\mathbf{e}_0(\tau, u) = \partial_\tau \mathbf{U}(\tau, u)$ then this can be considered a *relativistic* Cosserat rod, where $(\mathbf{e}_1, \mathbf{e}_2, \mathbf{e}_3)$ is here the material frame of the rod. In order to avoid confusing using the word ‘frame’ in reference to both material and inertial frames, we will henceforth refer to the former as the Cosserat cross-section. Given a reference frame B and origin $\mathbf{0} \in \mathbb{M}^{1,3}$, we can write the configuration of the Cosserat rod as

$$\mathcal{F} = \mathcal{F}_0 \Phi \quad (7.109)$$

where

$$\mathcal{F} = (\mathbf{r}; E) = \begin{pmatrix} 1 & \mathbf{0}^T \\ \mathbf{r} & E \end{pmatrix} \quad (7.110)$$

and $\mathcal{F}_0 = (\mathbf{0}; B)$ and $\Phi = (B^{-1}\mathbf{r}; B^{-1}\Lambda B)$, and where Λ satisfies $E = \Lambda B$. As in Sec. 6.2.1, we now simplify our notation by letting $B = \mathbb{1}_{4 \times 4}$, such that $\Lambda = E \in SO(1, 3)$ and we can thus write $\Phi = \mathcal{F}$.

We write the Maurer-Cartan form as

$$\xi = N d\tau + X du \quad (7.111)$$

where

$$N = \{\vec{U}; O\} = \begin{pmatrix} 0 & \vec{0}^T \\ \vec{U} & O \end{pmatrix} \quad (7.112a)$$

$$X = \{\vec{\theta}; \Xi\} = \begin{pmatrix} 0 & \vec{0}^T \\ \vec{\theta} & \Xi \end{pmatrix} \quad (7.112b)$$

and $N(\tau, u), X(\tau, u) \in \mathfrak{m}(1, 3)$ and $O, \Xi \in \mathfrak{so}(1, 3)$. From $\Phi^{-1}d\Phi = \xi$ we find

$$d\mathbf{r} = \mathbf{U}d\tau + \boldsymbol{\theta}du \quad (7.113a)$$

$$= \mathbf{e}_0 d\tau + \boldsymbol{\theta}du$$

$$d\mathbf{e}_\beta = \mathbf{e}_\alpha O_{\alpha\beta} d\tau + \mathbf{e}_\alpha \Xi_{\alpha\beta} du, \quad \alpha, \beta = 0, 1, 2, 3 \quad (7.113b)$$

where we used $\mathbf{e}_0 = \mathbf{U}$, which should be seen as a kinematic restriction on the Lie group-valued Φ (although note that it is not a kinematic restriction from the physical perspective, as real inertial observers always are always stationary with respect to themselves). Because we have parametrised the Cosserat rod with respect to the co-moving inertial frames, we have that $\vec{U}(\tau, u) = (1 \ 0 \ 0 \ 0)^T$. Therefore the kinematic movement of the rod is not specified in \vec{U} as in Sec. 6.2, but must instead be encoded in O .

The Lie algebra element $O \in \mathfrak{so}(1, 3)$ can be written as

$$O = \begin{pmatrix} 0 & \tilde{a}^T \\ \tilde{a} & \hat{\tilde{\Omega}} \end{pmatrix} \quad (7.114)$$

where $\tilde{a} = (a_1, a_2, a_3)$ and $\hat{\tilde{\Omega}} \in \mathfrak{so}(3)$. Henceforth the tilde will designate spatial 3-vectors. To interpret these quantities, we first note that

$$\partial_\tau \mathbf{e}_i = \mathbf{e}_i \hat{\tilde{\Omega}}_{ij}, \quad i = 1, 2, 3 \quad (7.115)$$

from which we identify that $\tilde{\Omega}(\tau, u)$ is the angular velocity of the Cosserat cross-section at u in its inertial frame. Secondly, we can compute the 4-acceleration $\mathbf{a} = \partial_\tau^2 \mathbf{r}$ as

$$\mathbf{a} = \partial_\tau \mathbf{e}_i = \mathbf{e}_i a_i, \quad i = 1, 2, 3. \quad (7.116)$$

such that $\vec{a} = E^{-1}\mathbf{a} = (0 \ \tilde{a}^T)^T$, which is the correct expression for the co-moving 4-acceleration in special relativistic kinematics [182, p. 99]. We thus see that $\tilde{a}(\tau, u)$ is the acceleration of the Cosserat cross-section at u in its co-moving inertial frame. Therefore the kinematics of the relativistic Cosserat rod is specified by the spatial acceleration \tilde{a} of the center-line and the angular velocity $\tilde{\Omega}$ of the cross-section. This stands in contrast to the non-relativistic Cosserat rod, where we instead specify the velocity of the center-line.

We can understand this difference by noting that velocity is *itself* a kinematic degree of freedom in special relativity, in addition to position and orientation. Only the latter two are kinematic degrees of freedom in non-relativistic systems. Mathematically, we have that the relative velocity of an inertial observer with frame E_1 with respect to another observer with frame E_2 is encoded in the Lorentz transformation that relates the two, as in Eq. 7.106. This is therefore the reason why we must specify the *acceleration* of the frame, as opposed to its *velocity*, in the kinematics.

The kinematic equations of motion are given by Eq. 7.4, from which we find

$$\partial_\tau \vec{\theta} = -O\vec{\theta} + \Xi \vec{U} \quad (7.117a)$$

$$\partial_\tau \Xi = \partial_u O + [\Xi, O]. \quad (7.117b)$$

If we let

$$O = \begin{pmatrix} 0 & \tilde{t}^T \\ \tilde{t} & \hat{\pi} \end{pmatrix} \quad (7.118)$$

then the kinematic equations of motion can be written as

$$\partial_\tau \theta_i = a_i \theta_i \quad (7.119a)$$

$$\tilde{D}_\tau \tilde{\theta} = -\theta_0 \tilde{a} + \tilde{t} \quad (7.119b)$$

$$\tilde{D}_\tau \tilde{t} = \tilde{D}_u \tilde{a} \quad (7.119c)$$

$$\partial_\tau \tilde{\pi} = \tilde{D}_u \tilde{\Omega} \quad (7.119d)$$

where $i = 1, 2, 3$ and $\tilde{D}_\tau = \partial_\tau + \hat{\tilde{\Omega}}$ and $\tilde{D}_u = \partial_u + \hat{\tilde{\pi}}$.

7.3.5 The $O(N)$ non-linear σ model

Here we give an example of the geometrisation programme applied to a field theory. We consider a field $\vec{n} : W \rightarrow S^N \subset \mathbb{R}^N$, where W is the base space and \vec{n} is a unit-vector in \mathbb{R}^N for all $p \in W$. We call $S^N \subset \mathbb{R}^N$ the *target manifold* of the field theory. We let $W = \mathbb{M}^{1,d}$, which is the $(d+1)$ -dimensional Minkowski space, although what follows is easily generalisable to Euclidean space or any arbitrary base space. We define coordinates $(t, u^1, u^2, \dots, u^d)$ on $\mathbb{M}^{1,d}$, and we will write partial derivatives as ∂_γ , $\gamma = 0, 1, \dots, d$, where $\partial_0 = \frac{\partial}{\partial t}$ and $\partial_\alpha = \frac{\partial}{\partial u^\alpha}$, $\alpha = 1, \dots, d$.

The $O(N)$ *non-linear σ model* [122] is defined by the Lagrangian density

$$\mathcal{L} = \frac{1}{2} \eta^{\gamma\kappa} (\partial_\gamma \vec{n})^T (\partial_\kappa \vec{n}) \quad (7.120)$$

which is expressed in some local coordinate chart of $\mathbb{M}^{1,d}$, where η is the Minkowski metric on $\mathbb{M}^{1,d}$ with signature $(1, d)$.

Let the $SO(N)$ -valued field $\Phi : \mathbb{M}^{1,d} \rightarrow SO(3)$ satisfy $\vec{n} = \Phi \vec{n}_0$ where $\vec{n}_0 \in S^N$ is some constant reference vector. We can then rewrite Eq. 7.120 as

$$\mathcal{L} = \frac{1}{2} \eta^{\gamma\kappa} (\partial_\gamma \Phi \vec{n}_0)^T (\partial_\kappa \Phi \vec{n}_0) \quad (7.121)$$

Now, we have

$$\begin{aligned} (\partial_\gamma \Phi \vec{n}_0)^T (\partial_\kappa \Phi \vec{n}_0) &= (\Phi^{-1} \partial_\gamma \Phi \vec{n}_0)^T (\Phi^{-1} \partial_\kappa \Phi \vec{n}_0) \\ &= (\hat{Z}_\gamma \vec{n}_0)^T (\hat{Z}_\kappa \vec{n}_0) \end{aligned} \quad (7.122)$$

for all $\gamma, \kappa = 1, \dots, d$, where we have defined $\hat{Z}_\gamma = \Phi^{-1} \partial_\gamma \Phi \in \mathfrak{so}(N)$. As before we will be making use of the hat-map to convert anti-symmetric 3×3 -matrices \hat{Z}_γ to 3-vectors \vec{Z}_γ . Let us now assume that the coordinates are defined such that $\eta = \text{diag}(-1, 1, \dots, 1)$. The Lagrangian then has a reduced form

$$\ell(\xi) = -\frac{1}{2} \vec{N}^T \mathbf{N}_0 \vec{N} + \frac{1}{2} \sum_{\alpha=1}^d \vec{X}_\alpha^T \mathbf{N}_0 \vec{X}_\alpha \quad (7.123)$$

where $\vec{N} = \vec{Z}_0$ and $\vec{X}_\alpha = \vec{Z}_\alpha$, $\alpha = 1, \dots, d$ and $\mathbf{N}_0 = \hat{n}_0^T \hat{n}_0$ and we have used $|\hat{Z}_\gamma \vec{n}_0| = |\vec{Z}_\gamma \times \vec{n}_0| = |\hat{n}_0 \vec{Z}_\gamma|$.

We can then readily apply the geometrisation programme to the system, to get the field equations of motion

$$\partial_t \vec{X}_\alpha = (\partial_\alpha + \hat{X}_\alpha) N \quad (7.124a)$$

$$(\partial_t + \hat{N}) \vec{S} = \sum_{\alpha=1}^d (\partial_\alpha + \hat{X}_\alpha) \vec{Q}^\alpha \quad (7.124b)$$

where $\vec{N} = \vec{Z}_0$, $\vec{X}_\alpha = \vec{Z}_\alpha$, $\alpha = 1, \dots, d$, $S = \frac{\partial \ell}{\partial N}$ and $Q^\alpha = \frac{\partial \ell}{\partial X_\alpha}$. The spatial reconstruction fields X_α must satisfy the spatial integrability conditions

$$\partial_\beta X_\alpha = \mathcal{D}_\alpha X_\beta \quad (7.125)$$

at all times t , where $\alpha = 1, \dots, d-1$ and $\beta = \alpha+1, \dots, d$.

Note that only two of the three components of S are independently determined by Eq. 7.124b, as \mathbf{N}_0 is only a rank 2 matrix. To see this let $\vec{n}_0 = (1 \ 0 \ 0)^T$ such that $\mathbf{N}_0 = \text{diag}(0, 1, 1)$. We then have that $\vec{S} = (0, N_2, N_3)$ and $Q^\alpha = (0, X_2, X_3)$. This reflects the fact that rotations of \vec{n} around its own axis is a gauge freedom in our formulation of the $O(N)$ non-linear σ model.

Chapter 8

Geometric numerical integrators

- 8.1 Geometric numerical integrators for sub-manifolds of Lie groups
- 8.2 Geometric numerical integrators for Cosserat rods
- 8.3 Geometric numerical integrators for Cosserat surfaces
- 8.4 Geometric numerical integrators for Cosserat rods on 2-spheres

Chapter 9

Conclusion

References

- [1] See the supplementary information.
- [2] *Nonlinear Problems of Elasticity*, volume 107 of *Applied Mathematical Sciences*. Springer-Verlag, New York, 2005. ISBN 978-0-387-20880-0. doi: 10.1007/0-387-27649-1.
- [3] Artur B. Adib. Stochastic actions for diffusive dynamics: Reweighting, sampling, and minimization. *The Journal of Physical Chemistry B*, 112(19):5910–5916, May 2008. ISSN 1520-6106, 1520-5207. doi: 10.1021/jp0751458.
- [4] Rosalind J Allen, Patrick B Warren, and Pieter Rein Ten Wolde. Sampling rare switching events in biochemical networks. *Physical Review Letters*, 94(1):018104, 2005.
- [5] Rosalind J Allen, Chantal Valeriani, and Pieter Rein ten Wolde. Forward flux sampling for rare event simulations. *Journal of Physics: Condensed Matter*, 21(46):463102, 2009.
- [6] Holm Altenbach and Victor A. Eremeyev. Cosserat Media. In Holm Altenbach and Victor A. Eremeyev, editors, *Generalized Continua from the Theory to Engineering Applications*, CISM International Centre for Mechanical Sciences, pages 65–130. Springer, Vienna, 2013. ISBN 978-3-7091-1371-4. doi: 10.1007/978-3-7091-1371-4_2.
- [7] Stuart S. Antman. The Special Cosserat Theory of Rods. In Stuart S. Antman, editor, *Nonlinear Problems of Elasticity*, Applied Mathematical Sciences, pages 259–324. Springer, New York, NY, 1995. ISBN 978-1-4757-4147-6. doi: 10.1007/978-1-4757-4147-6_8.
- [8] Ludwig Arnold. *Stochastic Differential Equations: Theory and Applications*. Wiley, April 1974. ISBN 978-0-471-03359-2.
- [9] Jared L Aurentz and Lloyd N Trefethen. Chopping a chebyshev series. *ACM Transactions on Mathematical Software (TOMS)*, 43(4):33, 2017.

- [10] A. Bach, D. Dürr, and B. Stawicki. Functionals of paths of a diffusion process and the Onsager-Machlup function. *Zeitschrift für Physik B Condensed Matter and Quanta*, 26(2):191–193, June 1977. ISSN 0340-224X, 1434-6036. doi: 10.1007/BF01325272.
- [11] Yavuz Basar and Dieter Weichert. *Nonlinear Continuum Mechanics of Solids: Fundamental Mathematical and Physical Concepts*. Springer Science & Business Media, November 2013. ISBN 978-3-662-04299-1.
- [12] Jean-Paul Berrut and Lloyd N Trefethen. Barycentric lagrange interpolation. *SIAM review*, 46(3):501–517, 2004.
- [13] Alexandros Beskos, Gareth Roberts, Andrew Stuart, and Jochen Voss. MCMC METHODS FOR DIFFUSION BRIDGES. *Stochastics and Dynamics*, 08(03):319–350, September 2008. ISSN 0219-4937, 1793-6799. doi: 10.1142/S0219493708002378.
- [14] A. T. Bharucha-Reid. *Elements of the Theory of Markov Processes and Their Applications*. Courier Corporation, April 2012. ISBN 978-0-486-15035-2.
- [15] Richard L. Bishop. There is More than One Way to Frame a Curve. *The American Mathematical Monthly*, 82(3):246–251, 1975. ISSN 0002-9890. doi: 10.2307/2319846.
- [16] Peter G. Bolhuis and David W. H. Swenson. Transition Path Sampling as Markov Chain Monte Carlo of Trajectories: Recent Algorithms, Software, Applications, and Future Outlook. *Advanced Theory and Simulations*, 4:2000237. ISSN 2513-0390. doi: 10.1002/adts.202000237.
- [17] Peter G Bolhuis, David Chandler, Christoph Dellago, and Phillip L Geissler. Transition path sampling: Throwing ropes over rough mountain passes, in the dark. *Annual Review of Physical Chemistry*, 53(1):291–318, 2002.
- [18] Peter G. Bolhuis, David Chandler, Christoph Dellago, and Phillip L. Geissler. Transition Path Sampling: Throwing Ropes Over Rough Mountain Passes, in the Dark. *Annual Review of Physical Chemistry*, 53(1):291–318, October 2002. ISSN 0066-426X, 1545-1593. doi: 10.1146/annurev.physchem.53.082301.113146.
- [19] Javier Bonet and Richard D. Wood. *Nonlinear Continuum Mechanics for Finite Element Analysis*. Cambridge University Press, Cambridge, second edition, 2008. doi: 10.1017/CBO9780511755446.
- [20] Freddy Bouchet and Julien Reygner. Generalisation of the eyring–kramers transition rate formula to irreversible diffusion processes. *Annales Henri Poincaré*, 17(12):3499–3532, Dec 2016. ISSN 1424-0661. doi: 10.1007/s00023-016-0507-4. URL <https://doi.org/10.1007/s00023-016-0507-4>.

- [21] John P Boyd. *Chebyshev and Fourier spectral methods*. Courier Corporation, Mineola, 2001.
- [22] F. Boyer, M. Porez, and W. Khalil. Macro-continuous computed torque algorithm for a three-dimensional eel-like robot. *IEEE Transactions on Robotics*, 22(4):763–775, August 2006. ISSN 1941-0468. doi: 10.1109/TRO.2006.875492.
- [23] Frédéric Boyer, Shaukat Ali, and Mathieu Porez. Macrocontinuous Dynamics for Hyperredundant Robots: Application to Kinematic Locomotion Bioinspired by Elongated Body Animals. *IEEE Transactions on Robotics*, 28(2):303–317, April 2012. ISSN 1552-3098, 1941-0468. doi: 10.1109/TRO.2011.2171616.
- [24] Brandon Caasenbrood, Alexander Pogromsky, and Henk Nijmeijer. Energy-Shaping Controllers for Soft Robot Manipulators Through Port-Hamiltonian Cosserat Models. *SN Computer Science*, 3(6):494, September 2022. ISSN 2661-8907. doi: 10.1007/s42979-022-01373-w.
- [25] MK Cameron. Finding the quasipotential for nongradient sdes. *Physica D: Nonlinear Phenomena*, 241(18):1532–1550, 2012.
- [26] D. Q. Cao and Robin W. Tucker. Nonlinear dynamics of elastic rods using the Cosserat theory: Modelling and simulation. *International Journal of Solids and Structures*, 45(2):460–477, January 2008. ISSN 0020-7683. doi: 10.1016/j.ijsolstr.2007.08.016.
- [27] Daniel Carroll, Emek Kose, and Ivan Sterling. Improving Frenet’s Frame Using Bishop’s Frame. *Journal of Mathematics Research*, 5(4):p97, November 2013. ISSN 1916-9795. doi: 10.5539/jmr.v5n4p97.
- [28] Élie Cartan. La theorie des groupes finis et continus et la geometrie differentielle traitees par la methode du repere mobile. *Bulletin of the American Mathematical Society*, 44:598–601, 1938.
- [29] Élie Cartan. *Geometry of Riemannian Spaces: Lie Groups; History, Frontiers and Applications Series*. Math Sci Press, 1983. ISBN 978-0-915692-34-7.
- [30] Elie Cartan and Jean Leray. *La théorie des groupes finis et continus et la géométrie différentielle: traitées par la méthode du repère mobile*. Gauthier-Villars, 1937.
- [31] H. Cendra, D. D. Holm, J. E. Marsden, and T. S. Ratiu. Lagrangian Reduction, the Euler–Poincaré Equations, and Semidirect Products, May 1999.
- [32] Hernán Cendra, Darryl D. Holm, Mark J. W. Hoyle, and Jerrold E. Marsden. The Maxwell–Vlasov equations in Euler–Poincaré form. *Journal of Mathematical Physics*, 39(6):3138–3157, June 1998. ISSN 0022-2488, 1089-7658. doi: 10.1063/1.532244.

- [33] P. M. Chaikin and T. C. Lubensky. *Principles of Condensed Matter Physics*. Cambridge University Press, Cambridge, 1995. ISBN 978-0-521-79450-3. doi: 10.1017/CBO9780511813467.
- [34] Jeanne N. Clelland. *From Frenet to Cartan: The Method of Moving Frames*. American Mathematical Society, 2017. ISBN 978-1-4704-3747-3.
- [35] Giulio Corazza and Matteo Fadel. Normalized Gaussian path integrals. *Physical Review E*, 102(2):022135, August 2020. doi: 10.1103/PhysRevE.102.022135.
- [36] Giulio Corazza and Matteo Fadel. Normalized Gaussian path integrals. *Physical Review E*, 102(2):022135, August 2020. ISSN 2470-0045, 2470-0053. doi: 10.1103/PhysRevE.102.022135. URL <https://link.aps.org/doi/10.1103/PhysRevE.102.022135>.
- [37] Giulio Corazza and Raushan Singh. Unraveling looping efficiency of stochastic Cosserat polymers. *Physical Review Research*, 4(1):013071, January 2022. doi: 10.1103/PhysRevResearch.4.013071.
- [38] Eugene Maurice Pierre Cosserat and F Cosserat. *Theory of Deformable Bodies*. National Aeronautics and Space Administration, 1909.
- [39] S. L. Cotter, G. O. Roberts, A. M. Stuart, and D. White. MCMC Methods for Functions: Modifying Old Algorithms to Make Them Faster. *Statistical Science*, 28(3):424–446, August 2013. ISSN 0883-4237, 2168-8745. doi: 10.1214/13-STS421.
- [40] Daisy Dahiya and Maria Cameron. Ordered line integral methods for computing the quasi-potential. *Journal of Scientific Computing*, 75(3):1351–1384, 2018.
- [41] Christoph Dellago, Peter G. Bolhuis, and David Chandler. Efficient transition path sampling: Application to Lennard-Jones cluster rearrangements. *The Journal of Chemical Physics*, 108(22):9236–9245, June 1998. ISSN 0021-9606, 1089-7690. doi: 10.1063/1.476378.
- [42] Christoph Dellago, Peter G. Bolhuis, Félix S. Csajka, and David Chandler. Transition path sampling and the calculation of rate constants. *The Journal of Chemical Physics*, 108(5):1964–1977, February 1998. ISSN 0021-9606. doi: 10.1063/1.475562.
- [43] Christoph Dellago, Peter G. Bolhuis, and David Chandler. On the calculation of reaction rate constants in the transition path ensemble. *The Journal of Chemical Physics*, 110(14):6617–6625, April 1999. ISSN 0021-9606. doi: 10.1063/1.478569.
- [44] Christopher L DeMarco. A phase transition model for cascading network failure. *IEEE Control Systems Magazine*, 21(6):40–51, 2001.

- [45] C.L. DeMarco. A phase transition model for cascading network failure. *IEEE Control Systems Magazine*, 21(6):40–51, December 2001. ISSN 1941-000X. doi: 10.1109/37.969134.
- [46] Giovanni Dematteis, Tobias Grafke, Miguel Onorato, and Eric Vanden-Eijnden. Experimental Evidence of Hydrodynamic Instantons: The Universal Route to Rogue Waves. *Physical Review X*, 9(4):041057, December 2019. ISSN 2160-3308. doi: 10.1103/PhysRevX.9.041057. URL <https://link.aps.org/doi/10.1103/PhysRevX.9.041057>.
- [47] Cécile Dewitt-Morette and Antoine Folacci. *Functional Integration: Basics and Applications*. Springer Science & Business Media, November 2013. ISBN 978-1-4899-0319-8.
- [48] Gerald V. Dunne. Functional Determinants in Quantum Field Theory. *Journal of Physics A: Mathematical and Theoretical*, 41(30):304006, August 2008. ISSN 1751-8113, 1751-8121. doi: 10.1088/1751-8113/41/30/304006.
- [49] Weinan E, Weiqing Ren, and Eric Vanden-Eijnden. String method for the study of rare events. *Physical Review B*, 66(5):052301, August 2002. ISSN 0163-1829, 1095-3795. doi: 10.1103/PhysRevB.66.052301. URL <https://link.aps.org/doi/10.1103/PhysRevB.66.052301>.
- [50] Weinan E, Weiqing Ren, and Eric Vanden-Eijnden. Minimum action method for the study of rare events. *Communications on Pure and Applied Mathematics*, 57(5): 637–656, May 2004. ISSN 0010-3640. doi: 10.1002/cpa.20005.
- [51] Lasse Ebener, Georgios Margazoglou, Jan Friedrich, Luca Biferale, and Rainer Grauer. Instanton based importance sampling for rare events in stochastic pdes. *Chaos: An Interdisciplinary Journal of Nonlinear Science*, 29(6):063102, 2019.
- [52] Babak Ebrahimian, Ali Noorzad, and Mustafa I. Alsaleh. A numerical study on interface shearing of granular Cosserat materials. *European Journal of Environmental and Civil Engineering*, 25(13):2337–2369, November 2021. ISSN 1964-8189. doi: 10.1080/19648189.2019.1627249.
- [53] J Egger. Stochastically driven large-scale circulations with multiple equilibria. *Journal of the Atmospheric Sciences*, 38(12):2606–2618, 1981.
- [54] Christophe Eloy and Eric Lauga. Kinematics of the Most Efficient Cilium. *Physical Review Letters*, 109(3):038101, July 2012. ISSN 0031-9007, 1079-7114. doi: 10.1103/PhysRevLett.109.038101.

- [55] Lev Ernestovich Elsgolts and George Yankovsky. *Differential equations and the calculus of variations*. Mir Moscow, 1973.
- [56] Eberhard Engel and Reiner M. Dreizler. *Density Functional Theory: An Advanced Course*. Springer Science & Business Media, February 2011. ISBN 978-3-642-14090-7.
- [57] Marcelo Epstein and Manuel de León. Continuous Distributions of Inhomogeneities in Liquid-Crystal-Like Bodies. *Proceedings: Mathematical, Physical and Engineering Sciences*, 457(2014):2507–2520, 2001. ISSN 1364-5021.
- [58] J. L. Ericksen. Conservation Laws for Liquid Crystals. *Transactions of the Society of Rheology*, 5(1):23–34, March 1961. ISSN 0038-0032. doi: 10.1122/1.548883.
- [59] P. Faccioli, M. Sega, F. Pederiva, and H. Orland. Dominant Pathways in Protein Folding. *Physical Review Letters*, 97(10):108101, September 2006. ISSN 0031-9007, 1079-7114. doi: 10.1103/PhysRevLett.97.108101.
- [60] Mark Fels and Peter J. Olver. Moving Coframes: I. A Practical Algorithm. *Acta Applicandae Mathematica*, 51(2):161–213, April 1998. ISSN 1572-9036. doi: 10.1023/A:1005878210297.
- [61] Mark Fels and Peter J. Olver. Moving Coframes: II. Regularization and Theoretical Foundations. *Acta Applicandae Mathematica*, 55(2):127–208, January 1999. ISSN 1572-9036. doi: 10.1023/A:1006195823000.
- [62] Grégoire Ferré and Tobias Grafke. Approximate optimal controls via instanton expansion for low temperature free energy computation. *arXiv:2011.10990 [cond-mat]*, May 2021.
- [63] Samuel Forest, Fabrice Barbe, and Georges Cailletaud. Cosserat modelling of size effects in the mechanical behaviour of polycrystals and multi-phase materials. *International Journal of Solids and Structures*, 37(46):7105–7126, November 2000. ISSN 0020-7683. doi: 10.1016/S0020-7683(99)00330-3.
- [64] F. Frenet. Sur les courbes à double courbure. *Journal de Mathématiques Pures et Appliquées*, pages 437–447, 1852. ISSN 0021-7874.
- [65] Peter K. Friz and Nicolas B. Victoir. *Multidimensional Stochastic Processes as Rough Paths: Theory and Applications*. Cambridge Studies in Advanced Mathematics. Cambridge University Press, Cambridge, 2010. ISBN 978-0-521-87607-0. doi: 10.1017/CBO9780511845079.

- [66] Hiroshi Fujisaki, Motoyuki Shiga, and Akinori Kidera. Onsager–Machlup action-based path sampling and its combination with replica exchange for diffusive and multiple pathways. *The Journal of Chemical Physics*, 132(13):134101, April 2010. ISSN 0021-9606, 1089-7690. doi: 10.1063/1.3372802.
- [67] Hiroshi Fujisaki, Motoyuki Shiga, Kei Moritsugu, and Akinori Kidera. Multiscale enhanced path sampling based on the Onsager-Machlup action: Application to a model polymer. *The Journal of Chemical Physics*, 139(5):054117, August 2013. ISSN 0021-9606. doi: 10.1063/1.4817209.
- [68] Takahiko Fujita and Shin-ichi Kotani. The Onsager-Machlup function for diffusion processes. *Journal of Mathematics of Kyoto University*, 22(1):115–130, January 1982. ISSN 0023-608X. doi: 10.1215/kjm/1250521863.
- [69] Martin J Gander and Gerhard Wanner. From euler, ritz, and galerkin to modern computing. *Siam Review*, 54(4):627–666, 2012.
- [70] Feliks Gantmacher. *Lectures in analytical mechanics.(Translated from the Russian by G. Yankovsky)*. Moscow: Mir Publishers, 1970.
- [71] Crispin Gardiner. *Stochastic Methods: A Handbook for the Natural and Social Sciences*. Springer Berlin Heidelberg, October 2010. ISBN 978-3-642-08962-6.
- [72] Robert B. Gardner. *The Method of Equivalence and Its Applications*. Society for Industrial and Applied Mathematics, 1989. ISBN 978-0-89871-240-7.
- [73] Timothy S Gardner, Charles R Cantor, and James J Collins. Construction of a genetic toggle switch in escherichia coli. *Nature*, 403(6767):339, 2000.
- [74] Timothy S. Gardner, Charles R. Cantor, and James J. Collins. Construction of a genetic toggle switch in Escherichia coli. *Nature*, 403(6767):339–342, January 2000. ISSN 1476-4687. doi: 10.1038/35002131.
- [75] Mohit Garg and Ajeet Kumar. A slender body theory for the motion of special Cosserat filaments in Stokes flow. *Mathematics and Mechanics of Solids*, page 10812865221083323, May 2022. ISSN 1081-2865. doi: 10.1177/10812865221083323.
- [76] Thomas E. III Gartner and Arthi Jayaraman. Modeling and Simulations of Polymers: A Roadmap. *Macromolecules*, 52(3):755–786, February 2019. ISSN 0024-9297. doi: 10.1021/acs.macromol.8b01836.
- [77] M. Gazzola, L. H. Dudte, A. G. McCormick, and L. Mahadevan. Forward and inverse problems in the mechanics of soft filaments. *Royal Society Open Science*, 5(6):171628. doi: 10.1098/rsos.171628.

- [78] I. M. Gelfand and S. V. Fomin. *Calculus of Variations*. Courier Corporation, April 2012. ISBN 978-0-486-13501-4.
- [79] I. M. Gel'fand and A. M. Yaglom. Integration in Functional Spaces and its Applications in Quantum Physics. *Journal of Mathematical Physics*, 1(1):48–69, January 1960. ISSN 0022-2488. doi: 10.1063/1.1703636.
- [80] I.M. Gelfand and S.V. Fomin. *Calculus of Variations*. Dover Books on Mathematics. Dover Publications, 2012. ISBN 9780486135014. URL <https://books.google.co.uk/books?id=CeC7AQAAQBAJ>.
- [81] Andrew Gelman, John B Carlin, Hal S Stern, and Donald B Rubin. *Bayesian Data Analysis*. Chapman and Hall/CRC, 1995.
- [82] G. G. Giusteri, E. Miglio, N. Parolini, M. Penati, and R. Zambetti. Simulation of viscoelastic Cosserat rods based on the geometrically exact dynamics of special Euclidean strands, October 2021.
- [83] Jannes Gladrow, Ulrich F. Keyser, R. Adhikari, and Julian Kappler. Experimental Measurement of Relative Path Probabilities and Stochastic Actions. *Physical Review X*, 11(3):031022, July 2021. doi: 10.1103/PhysRevX.11.031022.
- [84] Raymond E. Goldstein and Stephen A. Langer. Nonlinear Dynamics of Stiff Polymers. *Physical Review Letters*, 75(6):1094–1097, August 1995. ISSN 0031-9007, 1079-7114. doi: 10.1103/PhysRevLett.75.1094.
- [85] Raymond E. Goldstein, Philip Nelson, Thomas Powers, and Udo Seifert. Front Propagation in the Pearling Instability of Tubular Vesicles. *Journal de Physique II*, 6(5):767–796, May 1996. ISSN 1155-4312, 1286-4870. doi: 10.1051/jp2:1996210.
- [86] Raymond E. Goldstein, Thomas R. Powers, and Chris H. Wiggins. Viscous Nonlinear Dynamics of Twist and Writhe. *Physical Review Letters*, 80(23):5232–5235, June 1998. ISSN 0031-9007, 1079-7114. doi: 10.1103/PhysRevLett.80.5232.
- [87] Alain Goriely, Derek E. Moulton, and L. Angela Mihai. A Rod Theory for Liquid Crystalline Elastomers. *Journal of Elasticity*, January 2022. ISSN 0374-3535, 1573-2681. doi: 10.1007/s10659-021-09875-z.
- [88] Tobias Grafke and Eric Vanden-Eijnden. Numerical computation of rare events via large deviation theory. *Chaos: An Interdisciplinary Journal of Nonlinear Science*, 29(6):063118, June 2019. ISSN 1054-1500, 1089-7682. doi: 10.1063/1.5084025. URL <http://aip.scitation.org/doi/10.1063/1.5084025>.

- [89] Tobias Grafke, Rainer Grauer, and Tobias Schäfer. The instanton method and its numerical implementation in fluid mechanics. *Journal of Physics A: Mathematical and Theoretical*, 48(33):333001, August 2015. ISSN 1751-8113, 1751-8121. doi: 10.1088/1751-8113/48/33/333001. URL <https://iopscience.iop.org/article/10.1088/1751-8113/48/33/333001>.
- [90] Tobias Grafke, Tobias Schäfer, and Eric Vanden-Eijnden. *Long Term Effects of Small Random Perturbations on Dynamical Systems: Theoretical and Computational Tools*, pages 17–55. Springer New York, New York, NY, 2017. doi: 10.1007/978-1-4939-6969-2_2. URL https://doi.org/10.1007/978-1-4939-6969-2_2.
- [91] Tobias Grafke, Tobias Schäfer, and Eric Vanden-Eijnden. Sharp Asymptotic Estimates for Expectations, Probabilities, and Mean First Passage Times in Stochastic Systems with Small Noise. *arXiv:2103.04837 [cond-mat, physics:physics]*, March 2021.
- [92] R. Graham. *Statistical Theory of Instabilities in Stationary Nonequilibrium Systems with Applications to Lasers and Nonlinear Optics*, pages 1–97. Springer Berlin Heidelberg, Berlin, Heidelberg, 1973. ISBN 978-3-662-40468-3. doi: 10.1007/978-3-662-40468-3_1. URL https://doi.org/10.1007/978-3-662-40468-3_1.
- [93] R. Graham. *Macroscopic potentials, bifurcations and noise in dissipative systems*, pages 1–34. Springer Berlin Heidelberg, Berlin, Heidelberg, 1987. ISBN 978-3-540-47401-2.
- [94] Robert Graham. Macroscopic potentials, bifurcations and noise in dissipative systems. In Frank Moss and P. V. E. McClintock, editors, *Noise in Nonlinear Dynamical Systems: Volume 1: Theory of Continuous Fokker-Planck Systems*, volume 1, pages 225–278. Cambridge University Press, Cambridge, 1989. ISBN 978-0-521-11850-7. doi: 10.1017/CBO9780511897818.009.
- [95] Stanislao Grazioso, Giuseppe Di Gironimo, and Bruno Siciliano. A Geometrically Exact Model for Soft Continuum Robots: The Finite Element Deformation Space Formulation. *Soft Robotics*, 6(6):790–811, December 2019. ISSN 2169-5180. doi: 10.1089/soro.2018.0047.
- [96] Leonard Gross. Abstract Wiener spaces. In *Proceedings of the Fifth Berkeley Symposium on Mathematical Statistics and Probability, Volume 2: Contributions to Probability Theory, Part 1*, volume 5.2A of *Berkeley Symposium on Mathematical Statistics and Probability*, pages 31–42. University of California Press, California, 1967.

- [97] Hongri Gu, Quentin Boehler, Haoyang Cui, Eleonora Secchi, Giovanni Savorana, Carmela De Marco, Simone Gervasoni, Quentin Peyron, Tian-Yun Huang, Salvador Pane, Ann M. Hirt, Daniel Ahmed, and Bradley J. Nelson. Magnetic cilia carpets with programmable metachronal waves. *Nature Communications*, 11(1):2637, May 2020. ISSN 2041-1723. doi: 10.1038/s41467-020-16458-4.
- [98] M. Hairer, A. M. Stuart, J. Voss, and P. Wiberg. Analysis of SPDEs arising in path sampling. Part I: The Gaussian case. *Communications in Mathematical Sciences*, 3(4):587–603, December 2005. ISSN 1539-6746, 1945-0796.
- [99] M. Hairer, A. M. Stuart, and J. Voss. Analysis of SPDEs arising in path sampling part II: The nonlinear case. *The Annals of Applied Probability*, 17(5-6):1657–1706, October 2007. ISSN 1050-5164, 2168-8737. doi: 10.1214/07-AAP441.
- [100] Martin Hairer, Andrew M. Stuart, and Sebastian J. Vollmer. Spectral gaps for a Metropolis–Hastings algorithm in infinite dimensions. *The Annals of Applied Probability*, 24(6):2455–2490, December 2014. ISSN 1050-5164, 2168-8737. doi: 10.1214/13-AAP982.
- [101] Richard Hamming. *Numerical methods for scientists and engineers*. Courier Corporation, New York, 2012.
- [102] Hidenori Hasimoto. A soliton on a vortex filament. *Journal of Fluid Mechanics*, 51(3):477–485, February 1972. ISSN 1469-7645, 0022-1120. doi: 10.1017/S0022112072002307.
- [103] W. K. Hastings. Monte Carlo Sampling Methods Using Markov Chains and Their Applications. *Biometrika*, 57(1):97–109, 1970. ISSN 0006-3444. doi: 10.2307/2334940.
- [104] Matthias Heymann and Eric Vanden-Eijnden. The geometric minimum action method: A least action principle on the space of curves. *Communications on Pure and Applied Mathematics*, 61(8):1052–1117, 2008.
- [105] Matthias Heymann and Eric Vanden-Eijnden. The geometric minimum action method: A least action principle on the space of curves. *Communications on Pure and Applied Mathematics*, 61(8):1052–1117, 2008. ISSN 1097-0312. doi: 10.1002/cpa.20238.
- [106] Darryl D Holm. Geometric Mechanics, Part II: Rotating, Translating and Rolling. page 304.
- [107] Darryl D. Holm and Rossen I. Ivanov. Matrix G-strands. *Nonlinearity*, 27(6):1445–1469, May 2014. ISSN 0951-7715. doi: 10.1088/0951-7715/27/6/1445.

- [108] Darryl D Holm, Jerrold E Marsden, and Tudor S Ratiu. The Euler–Poincaré Equations and Semidirect Products with Applications to Continuum Theories. *Advances in Mathematics*, 137(1):1–81, July 1998. ISSN 0001-8708. doi: 10.1006/aima.1998.1721.
- [109] Chiao-Peng Hsu, Alfredo Sciortino, Yu Alice de la Trobe, and Andreas R. Bausch. Activity-induced polar patterns of filaments gliding on a sphere. *Nature Communications*, 13(1):2579, May 2022. ISSN 2041-1723. doi: 10.1038/s41467-022-30128-7.
- [110] Sui Huang. The molecular and mathematical basis of waddington’s epigenetic landscape: A framework for post-darwinian biology? *Bioessays*, 34(2):149–157, 2012.
- [111] Sui Huang. The molecular and mathematical basis of Waddington’s epigenetic landscape: A framework for post-Darwinian biology? *BioEssays: News and Reviews in Molecular, Cellular and Developmental Biology*, 34(2):149–157, February 2012. ISSN 1521-1878. doi: 10.1002/bies.201100031.
- [112] D. Iesan. Deformation of porous Cosserat elastic bars. *International Journal of Solids and Structures*, 48(3):573–583, February 2011. ISSN 0020-7683. doi: 10.1016/j.ijsolstr.2010.10.022.
- [113] N. Ikeda and S. Watanabe. *Stochastic Differential Equations and Diffusion Processes*. Elsevier, June 2014. ISBN 978-1-4832-9615-9.
- [114] Hidemi Ito. Probabilistic Construction of Lagrangean of Diffusion Process and Its Application. *Progress of Theoretical Physics*, 59(3):725–741, March 1978. ISSN 0033-068X. doi: 10.1143/PTP.59.725.
- [115] E. A. Ivanova. Modeling of physical fields by means of the Cosserat continuum. *ZAMM - Journal of Applied Mathematics and Mechanics / Zeitschrift für Angewandte Mathematik und Mechanik*, n/a(n/a):e202100333. ISSN 1521-4001. doi: 10.1002/zamm.202100333.
- [116] Elena A. Ivanova. On a New Theory of the Cosserat Continuum with Applications in Electrodynamics. In Holm Altenbach, Svetlana Bauer, Victor A. Eremeyev, Gennadi I. Mikhasev, and Nikita F. Morozov, editors, *Recent Approaches in the Theory of Plates and Plate-Like Structures*, Advanced Structured Materials, pages 75–87. Springer International Publishing, Cham, 2022. ISBN 978-3-030-87185-7. doi: 10.1007/978-3-030-87185-7_7.
- [117] Steven G Johnson. The nlopt nonlinear-optimization package, 2014. URL <http://github.com/stevengj/nlopt>.

- [118] Bartosz Kaczmarski, Derek E. Moulton, Ellen Kuhl, and Alain Goriely. Active filaments I: Curvature and torsion generation. *Journal of the Mechanics and Physics of Solids*, page 104918, May 2022. ISSN 0022-5096. doi: 10.1016/j.jmps.2022.104918.
- [119] N. G. Van Kampen. *Stochastic Processes in Physics and Chemistry*. Elsevier, August 2011. ISBN 978-0-08-047536-3.
- [120] L.V. Kantorovich and V.I. Krylov. *Approximate Methods of Higher Analysis*. P. Noordhoff, Groningen, 1958. URL <https://books.google.co.uk/books?id=M9tCwgEACAAJ>.
- [121] Kari Karhunen. *Über lineare Methoden in der Wahrscheinlichkeitsrechnung*. PhD thesis, Universitat Helsinki, Helsinki, 1947.
- [122] Sergei V. Ketov. *Quantum Non-linear Sigma-Models: From Quantum Field Theory to Supersymmetry, Conformal Field Theory, Black Holes and Strings*. Springer Science & Business Media, March 2013. ISBN 978-3-662-04192-5.
- [123] Lukas Kikuchi, Rajesh Singh, M. E. Cates, and R. Adhikari. Ritz method for transition paths and quasipotentials of rare diffusive events. *Physical Review Research*, 2(3):033208, August 2020. doi: 10.1103/PhysRevResearch.2.033208.
- [124] Félix Klein. *Development of Mathematics in the 19th Century: Appendices, "Kleinian Mathematics from an Advanced Standpoint"*. Math Sci Press, 1979. ISBN 978-0-915692-28-6.
- [125] Kosambi. Statistics in Function Space. *Journal of the Indian Mathematical Society*, 7:76–88, 1943.
- [126] D. D Kosambi. Parallelism and path-spaces. In *Ramaswamy R. (Eds) D.D. Kosambi*, pages 59–70. Springer, New Delhi, 2016. ISBN 978-81-322-3674-0.
- [127] Hidetoshi Kotera, Muneyo Sawada, and Susumu Shima. Cosserat continuum theory to simulate microscopic rotation of magnetic powder in applied magnetic field. *International Journal of Mechanical Sciences*, 42(1):129–145, January 2000. ISSN 0020-7403. doi: 10.1016/S0020-7403(98)00108-8.
- [128] Shankar Krishnaswamy. A cosserat-type model for the red blood cell wall. *International Journal of Engineering Science*, 34(8):873–899, June 1996. ISSN 0020-7225. doi: 10.1016/0020-7225(95)00139-5.
- [129] Shankar Krishnaswamy. A cosserat-type model for the red blood cell wall. *International Journal of Engineering Science*, 34(8):873–899, June 1996. ISSN 0020-7225. doi: 10.1016/0020-7225(95)00139-5.

- [130] L. D. Landau and E. M. Lifshitz. *Mechanics (Third Edition)*. Butterworth-Heinemann, Oxford, 1976. ISBN 978-0-7506-2896-9.
- [131] L. D. Landau, Evgenij M. Lifšic, E. M. Lifshitz, A. M. Kosevich, and L. P. Pitaevskii. *Theory of Elasticity: Volume 7*. Elsevier, January 1986. ISBN 978-0-7506-2633-0.
- [132] Abhrajit Laskar and R. Adhikari. Brownian microhydrodynamics of active filaments. *Soft Matter*, 11(47):9073–9085, November 2015. ISSN 1744-6848. doi: 10.1039/C5SM02021B.
- [133] Abhrajit Laskar and R. Adhikari. Filament actuation by an active colloid at low Reynolds number. *New Journal of Physics*, 19(3):033021, March 2017. ISSN 1367-2630. doi: 10.1088/1367-2630/aa5f80.
- [134] Juyong Lee, In-Ho Lee, InSuk Joung, Jooyoung Lee, and Bernard R. Brooks. Finding multiple reaction pathways via global optimization of action. *Nature Communications*, 8(1):15443, August 2017. ISSN 2041-1723. doi: 10.1038/ncomms15443.
- [135] S. Levit and U. Smilansky. A Theorem on Infinite Products of Eigenvalues of Sturm-Liouville Type Operators. *Proceedings of the American Mathematical Society*, 65(2):299–302, 1977. ISSN 0002-9939. doi: 10.2307/2041911.
- [136] Harry Levy. Review: Elie Cartan, La Méthode de Repère Mobile, La Théorie des Groupes Continus, et Les Espaces Généralisés. *Bulletin of the American Mathematical Society*, 41(11):774–774, November 1935. ISSN 0002-9904, 1936-881X.
- [137] M. Loève. *Probability Theory I*, volume 45 of *Graduate Texts in Mathematics*. Springer-Verlag, New York, fourth edition, 1977. ISBN 978-0-387-90210-4. doi: 10.1007/978-1-4684-9464-8.
- [138] Yulong Lu, Andrew Stuart, and Hendrik Weber. Gaussian Approximations for Transition Paths in Brownian Dynamics. *SIAM Journal on Mathematical Analysis*, 49(4):3005–3047, January 2017. ISSN 0036-1410, 1095-7154. doi: 10.1137/16M1071845. URL <https://pubs.siam.org/doi/10.1137/16M1071845>.
- [139] Donald Ludwig. Persistence of dynamical systems under random perturbations. *Siam Review*, 17(4):605–640, 1975.
- [140] James F. Lutsko. How crystals form: A theory of nucleation pathways. *Science Advances*, April 2019. doi: 10.1126/sciadv.aav7399.
- [141] Robert S Maier and Daniel L Stein. A scaling theory of bifurcations in the symmetric weak-noise escape problem. *Journal of Statistical Physics*, 83(3-4):291–357, 1996.

- [142] M. Mangel. Barrier Transitions Driven by Fluctuations, with Applications to Ecology and Evolution. *Theoretical Population Biology*, 45(1):16–40, February 1994. ISSN 0040-5809. doi: 10.1006/tpbi.1994.1002.
- [143] Marc Mangel. Barrier transitions driven by fluctuations, with applications to ecology and evolution. *Theoretical Population Biology*, 45(1):16–40, 1994.
- [144] Raj Kumar Manna and P. B. Sunil Kumar. Emergent topological phenomena in active polymeric fluids. *Soft Matter*, 15(3):477–486, January 2019. ISSN 1744-6848. doi: 10.1039/C8SM01981A.
- [145] E. L. Mansfield and A. Rojo-Echeburúa. On the use of the rotation minimizing frame for variational systems with Euclidean symmetry. *Studies in Applied Mathematics*, 143(3):244–271, 2019. ISSN 1467-9590. doi: 10.1111/sapm.12275.
- [146] M. C. Marchetti, J. F. Joanny, S. Ramaswamy, T. B. Liverpool, J. Prost, Madan Rao, and R. Aditi Simha. Hydrodynamics of soft active matter. *Reviews of Modern Physics*, 85(3):1143–1189, July 2013. ISSN 0034-6861, 1539-0756. doi: 10.1103/RevModPhys.85.1143.
- [147] Charles-Michel Marle. On Henri Poincaré’s Note “Sur une forme nouvelle des équations de la Mécanique”. *Journal of Geometry and Symmetry in Physics*, 29(none):1–38, January 2013. ISSN 1312-5192, 1314-5673. doi: 10.7546/jgsp-29-2013-1-38.
- [148] Charles-Michel Marle Marle. On Henri Poincaré’s Note ”Sur une forme nouvelle des équations de la Mécanique”. Technical report, Journal of Geometry and Symmetry in Physics, 2013.
- [149] Jerrold E. Marsden and Tudor S. Ratiu. *Introduction to Mechanics and Symmetry: A Basic Exposition of Classical Mechanical Systems*. Springer Science & Business Media, March 2013. ISBN 978-0-387-21792-5.
- [150] Nicholas Metropolis, Arianna W. Rosenbluth, Marshall N. Rosenbluth, Augusta H. Teller, and Edward Teller. Equation of State Calculations by Fast Computing Machines. *The Journal of Chemical Physics*, 21(6):1087–1092, June 1953. ISSN 0021-9606. doi: 10.1063/1.1699114.
- [151] L. Srinivasa Mohan, Prabhu R. Nott, and K. Kesava Rao. A frictional Cosserat model for the flow of granular materials through a vertical channel. *Acta Mechanica*, 138(1):75–96, March 1999. ISSN 1619-6937. doi: 10.1007/BF01179543.
- [152] Klaus Müller and Leo D Brown. Location of saddle points and minimum energy paths by a constrained simplex optimization procedure. *Theoretica chimica acta*, 53(1):75–93, 1979.

- [153] Noel Naughton, Jiarui Sun, Arman Tekinalp, Tejaswin Parthasarathy, Girish Chowdhary, and Mattia Gazzola. Elastica: A Compliant Mechanics Environment for Soft Robotic Control. *IEEE Robotics and Automation Letters*, 6(2):3389–3396, April 2021. ISSN 2377-3766, 2377-3774. doi: 10.1109/LRA.2021.3063698.
- [154] Randolph Nelson. Stochastic catastrophe theory in computer performance modeling. *Journal of the ACM (JACM)*, 34(3):661–685, 1987.
- [155] Daniel Nickelsen and Hugo Touchette. Noise correction of large deviations with anomalous scaling. *Physical Review E*, 105(6):064102, June 2022. ISSN 2470-0045, 2470-0053. doi: 10.1103/PhysRevE.105.064102. URL <https://link.aps.org/doi/10.1103/PhysRevE.105.064102>.
- [156] Ben C Nolting and Karen C Abbott. Balls, cups, and quasi-potentials: quantifying stability in stochastic systems. *Ecology*, 97(4):850–864, 2016.
- [157] Ben C. Nolting and Karen C. Abbott. Balls, cups, and quasi-potentials: Quantifying stability in stochastic systems. *Ecology*, 97(4):850–864, 2016. ISSN 1939-9170. doi: 10.1890/15-1047.1.
- [158] R. P. Nordgren. On Computation of the Motion of Elastic Rods. *Journal of Applied Mechanics*, 41(3):777–780, September 1974. ISSN 0021-8936. doi: 10.1115/1.3423387.
- [159] Roberto Olender and Ron Elber. Yet another look at the steepest descent path. *Journal of Molecular Structure: THEOCHEM*, 398:63–71, 1997.
- [160] Peter J Olver. Modern Developments in the Theory and Applications of Moving Frames. page 37.
- [161] Peter J. Olver. A Survey of Moving Frames. In Hongbo Li, Peter J. Olver, and Gerald Sommer, editors, *Computer Algebra and Geometric Algebra with Applications*, Lecture Notes in Computer Science, pages 105–138, Berlin, Heidelberg, 2005. Springer. ISBN 978-3-540-32119-4. doi: 10.1007/11499251_11.
- [162] Patrick R. Onck. Cosserat modeling of cellular solids. *Comptes Rendus Mécanique*, 330(11):717–722, November 2002. ISSN 1631-0721. doi: 10.1016/S1631-0721(02)01529-2.
- [163] L. Onsager and S. Machlup. Fluctuations and Irreversible Processes. *Physical Review*, 91(6):1505–1512, September 1953. ISSN 0031-899X. doi: 10.1103/PhysRev.91.1505.
- [164] Lars Onsager and Stefan Machlup. Fluctuations and irreversible processes. *Physical Review*, 91(6):1505, 1953.

- [165] Liam Paninski. The most likely voltage path and large deviations approximations for integrate-and-fire neurons. *Journal of Computational Neuroscience*, 21(1):71–87, 2006.
- [166] Liam Paninski. The most likely voltage path and large deviations approximations for integrate-and-fire neurons. *Journal of Computational Neuroscience*, 21(1):71–87, August 2006. ISSN 0929-5313. doi: 10.1007/s10827-006-7200-4.
- [167] Gundhar Paria. A Unified Theory of Mechanics of Ferro-Magnetic Material from Cosserat Point of View. *Bulletin mathématique de la Société des Sciences Mathématiques de la République Socialiste de Roumanie*, 22 (70)(3):303–314, 1978. ISSN 0373-2908.
- [168] H. C. Park and R. S. Lakes. Cosserat micromechanics of human bone: Strain redistribution by a hydration sensitive constituent. *Journal of Biomechanics*, 19(5):385–397, 1986. ISSN 0021-9290. doi: 10.1016/0021-9290(86)90015-1.
- [169] D. F. Parker. On the derivation of nonlinear rod theories from three-dimensional elasticity. *Zeitschrift für angewandte Mathematik und Physik ZAMP*, 35(6):833–847, November 1984. ISSN 1420-9039. doi: 10.1007/BF00945447.
- [170] D. F. Parker. On the derivation of nonlinear rod theories from three-dimensional elasticity. *Zeitschrift für Angewandte Mathematik und Physik (ZAMP)*, 35(6):833–847, November 1984. ISSN 0044-2275. doi: 10.1007/BF00945447.
- [171] Grigoris A Pavliotis. *Stochastic processes and applications: diffusion processes, the Fokker-Planck and Langevin equations*, volume 60. Springer, 2014.
- [172] Henri Poincaré. Sur une forme nouvelle des équations de la mécanique. *CR Acad. Sci*, 132:369–371, 1901.
- [173] M. J. D. Powell. *The NEWUOA software for unconstrained optimization without derivatives*, pages 255–297. Springer US, Boston, MA, 2006. ISBN 978-0-387-30065-8. doi: 10.1007/0-387-30065-1_16. URL https://doi.org/10.1007/0-387-30065-1_16.
- [174] Thomas R. Powers. Dynamics of filaments and membranes in a viscous fluid. *Reviews of Modern Physics*, 82(2):1607–1631, May 2010. ISSN 0034-6861, 1539-0756. doi: 10.1103/RevModPhys.82.1607.
- [175] A. Rajan, R. Pramanik, A. Narayanan, and A. Arockiarajan. Mechanics of viscoelastic buckling in slender hydrogels. *Materials Research Express*, 6(5):055320, February 2019. ISSN 2053-1591. doi: 10.1088/2053-1591/ab0691.

- [176] Padmini Rangamani, Ayelet Benjamini, Ashutosh Agrawal, Berend Smit, David J. Steigmann, and George Oster. Small scale membrane mechanics. *Biomechanics and Modeling in Mechanobiology*, 13(4):697–711, August 2014. ISSN 1617-7940. doi: 10.1007/s10237-013-0528-6.
- [177] Pieter Rein ten Wolde, Maria J. Ruiz-Montero, and Daan Frenkel. Numerical calculation of the rate of crystal nucleation in a Lennard-Jones system at moderate undercooling. *The Journal of Chemical Physics*, 104(24):9932–9947, June 1996. ISSN 0021-9606, 1089-7690. doi: 10.1063/1.471721. URL <http://aip.scitation.org/doi/10.1063/1.471721>.
- [178] Weiqing Ren, Eric Vanden-Eijnden, Paul Maragakis, and Weinan E. Transition pathways in complex systems: Application of the finite-temperature string method to the alanine dipeptide. *The Journal of Chemical Physics*, 123(13):134109, October 2005. ISSN 0021-9606, 1089-7690. doi: 10.1063/1.2013256. URL <http://aip.scitation.org/doi/10.1063/1.2013256>.
- [179] Federico Renda, Michele Giorelli, Marcello Calisti, Matteo Cianchetti, and Cecilia Laschi. Dynamic Model of a Multibending Soft Robot Arm Driven by Cables. *IEEE Transactions on Robotics*, 30(5):1109–1122, October 2014. ISSN 1941-0468. doi: 10.1109/TRO.2014.2325992.
- [180] Federico Renda, Vito Cacucciolo, Jorge Dias, and Lakmal Seneviratne. Discrete Cosserat approach for soft robot dynamics: A new piece-wise constant strain model with torsion and shears. In *2016 IEEE/RSJ International Conference on Intelligent Robots and Systems (IROS)*, pages 5495–5502, October 2016. doi: 10.1109/IROS.2016.7759808.
- [181] Federico Renda, Frederic Boyer, Jorge Dias, and Lakmal Seneviratne. Discrete Cosserat Approach for Multi-Section Soft Robots Dynamics. *IEEE Transactions on Robotics*, 34(6):1518–1533, December 2018. ISSN 1552-3098, 1941-0468. doi: 10.1109/TRO.2018.2868815.
- [182] Wolfgang Rindler. *Relativity: Special, General, and Cosmological*. Oxford University Press, 2001. ISBN 978-0-19-850835-9.
- [183] Hannes Risken and Till Frank. *The Fokker-Planck Equation: Methods of Solution and Applications*. Springer Science & Business Media, December 2012. ISBN 978-3-642-61544-3.
- [184] Walter Ritz. Über eine neue methode zur losung gewisser variationsprobleme der mathematischen physik. *Journal für Mathematik*, 135:1–61, 1909.

- [185] David Marin Roma, Ruadhan A O’Flanagan, Andrei E Ruckenstein, Anirvan M Sengupta, and Ranjan Mukhopadhyay. Optimal path to epigenetic switching. *Physical Review E*, 71(1):011902, 2005.
- [186] M. B. Rubin. Cosserat Rods. In M. B. Rubin, editor, *Cosserat Theories: Shells, Rods and Points*, Solid Mechanics and Its Applications, pages 191–310. Springer Netherlands, Dordrecht, 2000. ISBN 978-94-015-9379-3. doi: 10.1007/978-94-015-9379-3_5.
- [187] K. L. Sack, S. Skatulla, and C. Sansour. Biological tissue mechanics with fibres modelled as one-dimensional Cosserat continua. Applications to cardiac tissue. *International Journal of Solids and Structures*, 81:84–94, March 2016. ISSN 0020-7683. doi: 10.1016/j.ijsolstr.2015.11.009.
- [188] Herbert E Salzer. Lagrangian interpolation at the chebyshev points x_n , $\nu \equiv \cos(\nu\pi/n)$, $\nu = 0 \text{ (1) } n$; some unnoted advantages. *The Computer Journal*, 15(2):156–159, 1972.
- [189] Timo Schorlepp, Tobias Grafke, and Rainer Grauer. Gel’fand-Yaglom type equations for calculating fluctuations around Instantons in stochastic systems. *Journal of Physics A: Mathematical and Theoretical*, April 2021. ISSN 1751-8113, 1751-8121. doi: 10.1088/1751-8121/abfb26.
- [190] J. M. Selig. Characterisation of Frenet–Serret and Bishop motions with applications to needle steering. *Robotica*, 31(6):981–992, September 2013. ISSN 0263-5747, 1469-8668. doi: 10.1017/S026357471300026X.
- [191] J.-A. Serret. Sur quelques formules relatives à la théorie des courbes à double courbure. *Journal de Mathématiques Pures et Appliquées*, pages 193–207, 1851. ISSN 0021-7874.
- [192] James P. Sethna. *Order Parameters, Broken Symmetry, and Topology*, pages 253–286. Oxford University PressOxford, second edition, January 2021. ISBN 978-0-19-886524-7 978-0-19-189761-0. doi: 10.1093/oso/9780198865247.003.0009.
- [193] J. C. Simo and L. Vu-Quoc. A three-dimensional finite-strain rod model. part II: Computational aspects. *Computer Methods in Applied Mechanics and Engineering*, 58(1):79–116, October 1986. ISSN 0045-7825. doi: 10.1016/0045-7825(86)90079-4.
- [194] J.C. Simo and L. Vu-Quoc. A Geometrically-exact rod model incorporating shear and torsion-warping deformation. *International Journal of Solids and Structures*, 27 (3):371–393, 1991. ISSN 00207683. doi: 10.1016/0020-7683(91)90089-X.

- [195] Kunitsugu Soda. Dynamics of Stiff Chains. I. Equation of Motion. *Journal of the Physical Society of Japan*, 35(3):866–870, September 1973. ISSN 0031-9015. doi: 10.1143/JPSJ.35.866.
- [196] I. Stefanou, J. Sulem, and I. Vardoulakis. Three-dimensional Cosserat homogenization of masonry structures: Elasticity. *Acta Geotechnica*, 3(1):71–83, March 2008. ISSN 1861-1133. doi: 10.1007/s11440-007-0051-y.
- [197] Ioannis Stefanou, Jean Sulem, and Hadrien Rattez. Cosserat Approach to Localization in Geomaterials. In George Z. Voyatzis, editor, *Handbook of Nonlocal Continuum Mechanics for Materials and Structures*, pages 1–25. Springer International Publishing, Cham, 2017. ISBN 978-3-319-22977-5. doi: 10.1007/978-3-319-22977-5_10-1.
- [198] R. L. Stratonovich. *Some Markov methods in the theory of stochastic processes in nonlinear dynamical systems*, volume 1, pages 16–71. Cambridge University Press, 1989. doi: 10.1017/CBO9780511897818.004.
- [199] R. L. Stratonovich. Some Markov methods in the theory of stochastic processes in nonlinear dynamical systems. In Frank Moss and P. V. E. McClintock, editors, *Noise in Nonlinear Dynamical Systems: Volume 1: Theory of Continuous Fokker-Planck Systems*, volume 1, pages 16–71. Cambridge University Press, Cambridge, 1989. ISBN 978-0-521-11850-7. doi: 10.1017/CBO9780511897818.004.
- [200] Y. Takahashi and S. Watanabe. The probability functionals (Onsager-machlup functions) of diffusion processes. In David Williams, editor, *Stochastic Integrals*, Lecture Notes in Mathematics, pages 433–463, Berlin, Heidelberg, 1981. Springer. ISBN 978-3-540-38613-1. doi: 10.1007/BFb0088735.
- [201] John Till, Vincent Aloi, and Caleb Rucker. Real-time dynamics of soft and continuum robots based on Cosserat rod models. *The International Journal of Robotics Research*, 38(6):723–746, May 2019. ISSN 0278-3649. doi: 10.1177/0278364919842269.
- [202] Anna-Karin Tornberg and Michael J. Shelley. Simulating the dynamics and interactions of flexible fibers in Stokes flows. *Journal of Computational Physics*, 196(1):8–40, May 2004. ISSN 00219991. doi: 10.1016/j.jcp.2003.10.017.
- [203] Hugo Touchette. The large deviation approach to statistical mechanics. *Physics Reports*, 478(1-3):1–69, 2009.
- [204] Lloyd N Trefethen. *Spectral methods in MATLAB*, volume 10. Siam, 2000.
- [205] Lloyd N Trefethen. *Approximation theory and approximation practice*, volume 128. Siam, 2013.

- [206] Krystyna Twardowska. Wong-Zakai approximations for stochastic differential equations. *Acta Applicandae Mathematica*, 43(3):317–359, June 1996. ISSN 1572-9036. doi: 10.1007/BF00047670.
- [207] Eric Vanden-Eijnden and Matthias Heymann. The geometric minimum action method for computing minimum energy paths. *The Journal of Chemical Physics*, 128(6):061103, February 2008. ISSN 0021-9606. doi: 10.1063/1.2833040.
- [208] Eric Vanden-Eijnden and Matthias Heymann. The geometric minimum action method for computing minimum energy paths, 2008.
- [209] A. D. Ventsel' and M. I. Freidlin. ON SMALL RANDOM PERTURBATIONS OF DYNAMICAL SYSTEMS. *Russian Mathematical Surveys*, 25(1):1, February 1970. ISSN 0036-0279. doi: 10.1070/RM1970v025n01ABEH001254.
- [210] Alexander Verl, Alin Albu-Schäffer, Oliver Brock, and Annika Raatz. *Soft Robotics: Transferring Theory to Application*. Springer, March 2015. ISBN 978-3-662-44506-8.
- [211] Tixian Wang, Udit Halder, Heng-Sheng Chang, Mattia Gazzola, and Prashant G. Mehta. Optimal Control of a Soft CyberOctopus Arm. In *2021 American Control Conference (ACC)*, pages 4757–4764, New Orleans, LA, USA, May 2021. IEEE. ISBN 978-1-66544-197-1. doi: 10.23919/ACC50511.2021.9483284.
- [212] E Weinan, Weiqing Ren, and Eric Vanden-Eijnden. String method for the study of rare events. *Physical Review B*, 66(5):052301, 2002.
- [213] E Weinan, Weiqing Ren, and Eric Vanden-Eijnden. Minimum action method for the study of rare events. *Communications on Pure and Applied Mathematics*, 57(5):637–656, 2004.
- [214] Alexander D Wentzell and Mark Iosifovich Freidlin. On small random perturbations of dynamical systems. *Russian Mathematical Surveys*, 25(1):1–55, feb 1970. doi: 10.1070/rm1970v025n01abeh001254. URL <https://doi.org/10.1070/2Frm1970v025n01abeh001254>.
- [215] E. T. Whittaker. *A Treatise on the Analytical Dynamics of Particles and Rigid Bodies*. Cambridge Mathematical Library. Cambridge University Press, 1988. doi: 10.1017/CBO9780511608797.
- [216] Rafal Wisniewski and Piotr Kulczycki. Euler-Poincaré reduction of externally forced rigid body motion. page 14.
- [217] Peter G. Wolynes, Jose N. Onuchic, and D. Thirumalai. Navigating the Folding Routes. *Science*, March 1995. doi: 10.1126/science.7886447.

- [218] PG Wolynes, JN Onuchic, and D Thirumalai. Navigating the folding routes. *Science*, 267(5204):1619–1620, 1995. ISSN 0036-8075. doi: 10.1126/science.7886447. URL <https://science.scienmag.org/content/267/5204/1619>.
- [219] Eugene Wong and Moshe Zakai. On the Convergence of Ordinary Integrals to Stochastic Integrals. *The Annals of Mathematical Statistics*, 36(5):1560–1564, October 1965. ISSN 0003-4851, 2168-8990. doi: 10.1214/aoms/1177699916.
- [220] Shuo Yang, Samuel F Potter, and Maria K Cameron. Computing the quasipotential for nongradient sdes in 3d. *Journal of Computational Physics*, 379:325–350, 2019.
- [221] Xiaotian Zhang, Fan Kiat Chan, Tejaswin Parthasarathy, and Mattia Gazzola. Modeling and simulation of complex dynamic musculoskeletal architectures. *Nature Communications*, 10(1):4825, December 2019. ISSN 2041-1723. doi: 10.1038/s41467-019-12759-5.

Appendix A

Glossary of notation

A.1 Part I notation

Measure, density, law

Functions $f : A \rightarrow B$

Matrices $\mathbb{R}^{d \times d}$.

$\dot{\mathbf{x}}$.

$C_{\mathbf{x}_0}^0([0, T])$

$\mathbf{a} \cdot \mathbf{b}$.

Let P be the probability density of \mathbb{P} with respect to the Lebesgue measure, and we will henceforth write this relation as $P \sim \mathbb{P}$.

$(Z_i)_j \sim \mathcal{N}(0, 2D)$

$\mathcal{N}(0, \mathbb{1}_d)$

$\langle X \rangle$

A.2 Part II notation

Often we will abbreviate partial derivatives as

$$\begin{aligned}\partial_u f &:= \frac{\partial f}{\partial u} \\ \partial_t f &:= \frac{\partial f}{\partial t}\end{aligned}\tag{A.1}$$

or

$$\begin{aligned}f' &:= \frac{\partial f}{\partial u} \\ \dot{f} &:= \frac{\partial f}{\partial t}\end{aligned}\tag{A.2}$$

This applies to both scalar, vectorial and group-valued functions.

If we have multiple coordinates, derivatives will be denoted by subscripts i.e. f_u , f_t etc. or $\partial_\alpha = \frac{\partial}{\partial u^\alpha}$.

In any dimension d we will assume that \mathbb{R}^d is a vector space equipped with the standard Euclidean metric. Vectors $\mathbf{a} \in \mathbb{R}^d$ will be written as column vectors $\mathbf{a} = (a_1 \ a_2 \ \dots \ a_d)^T$, and their inner product will often be written as

$$\mathbf{a} \cdot \mathbf{b} = \mathbf{a}^T \mathbf{b} \quad (\text{A.3})$$

interchangeably.

which for any two vectors $\mathbf{a}, \mathbf{b} \in \mathbb{R}^d$ can be written in several different ways interchangeably:

$$\mathbf{a} \cdot \mathbf{b} = \mathbf{a}^T \mathbf{b} \quad (\text{A.4})$$

Smooth function C^∞

Norm of vector $|\mathbf{v}|$.

Einstein summation

$f : A \rightarrow B$ is a mapping, or function interchangeably

We will often distinguish \mathbb{E}^d and \mathbb{R}^d .

$\mathbb{R}^{n \times m}$

Introduce the vec notation here as well, and tilde notation \tilde{v} , and do it clearly and in detail.

e is the identity of Lie groups.

introduce the hatmap and give it explicitly (and use the vec notation).

$$\hat{v} = \begin{pmatrix} 0 & -v_3 & v_2 \\ v_3 & 0 & -v_1 \\ -v_2 & v_1 & 0 \end{pmatrix} \quad (\text{A.5})$$

also have that $\vec{\cdot}$ signifies the inverse hatmap for anti-symmetric 3x3 matrices. So $\vec{v} \in \mathbb{R}^3$.

$\hat{v} = v \times$

$x \times y = -y \times x = \hat{y}x$

$\not\propto$ identity matrix

If $f : V \rightarrow W$, then $\Phi(V)$ is the image of V under f .

$X = \{\vec{a}; \vec{b}\}$

Matrix derivatives, and the fact that we only take them with respect to the non-zero values. $A_{ji} = \frac{\partial U}{\partial B_{ij}}$.

$\Lambda_{\beta \neq \alpha}$

closure of sets \bar{U} .

For a map $f : M \rightarrow N$, $f(A)$ is the image of the map under $A \subset M$.

Appendix B

MCMC benchmark models

Here we define the Langevin model systems considered in Ch. 3 and Ch. 4. We begin by defining a non-dimensionalised formulation of the Langevin equation with additive noise

$$d\mathbf{X} = \mu \mathbf{F} dt + \sqrt{2D} d\mathbf{W}. \quad (\text{B.1})$$

where μ is the mobility constant and D the diffusion constant. We write the latter as $D = \mu k_B \theta$, where k_B is the Boltzmann constant θ is the temperature. We assume that the force is the gradient of a potential energy function $U : \mathbb{R}^d \rightarrow \mathbb{R}$ as $\mathbf{F} = -\nabla \cdot U$.

Let $T_0 = \frac{L^2}{k_B \theta_0 \mu}$ be a time-scale, θ_0 a temperature-scale, and L_0 a characteristic length-scale of the potential. We set $t = T_0 \tilde{t}$, $\theta = \theta_0 \tilde{\theta}$, $\mathbf{X} = L_0 \tilde{\mathbf{X}}$, $\mathbf{F} = \frac{\tilde{U}_0}{L_0} \tilde{\mathbf{F}}$ and $\mathbf{W} = \sqrt{T_0} \tilde{\mathbf{W}}$. T_0 is the typical diffusion time-scale at temperature θ_0 . We get

$$d\tilde{\mathbf{X}} = \tilde{U}_0 \tilde{\mathbf{F}} d\tilde{t} + \sqrt{2\tilde{\theta}} d\tilde{\mathbf{W}}. \quad (\text{B.2})$$

where all quantities in the equation are now non-dimensional, and where $\tilde{U}_0 = \frac{U_0}{k_B \theta_0}$ is the ratio of the energetic well-depth U_0 and the thermal energy at temperature θ_0 . We set $\tilde{U}_0 = 1$, such that $\theta = \theta_0$ corresponds to the temperature at which $U_0 = k_B \theta_0$. In other words, the characteristic energy scale of the potential is equal to the thermal energy at temperature θ_0 . Finally, the non-diemsionalised Langevin equation is

$$d\tilde{\mathbf{X}} = \tilde{\mathbf{F}} d\tilde{t} + \sqrt{2\tilde{\theta}} d\tilde{\mathbf{W}}. \quad (\text{B.3})$$

B.1 The asymmetric double-well system

Consider a 1-dimensional Langevin system with a quartic potential

$$U(x) = U_0 \left(1 + a \frac{x}{L_0} + b \left(\frac{x}{L_0} \right)^2 + x \left(\frac{x}{L_0} \right)^3 + d \left(\frac{x}{L_0} \right)^4 \right). \quad (\text{B.4})$$

We impose the following conditions

1. $U'(-L_0) = U'(L_0) = 0$. Extrema at $x = -L_0$ and $x = L_0$.
2. $U(-L_0) = 0$ and $U(L_0) = \Delta U$. The energy cost of moving from the left-most extremum to the right-most extremum is ΔU .

Imposing the conditions on Eq.B.4, we get

$$U(x) = \left(\left(\frac{x}{L_0} - 1 \right)^2 - \frac{1}{4} \frac{\Delta U}{U_0} \left(\frac{x}{L_0} - 2 \right) \right) \left(\frac{x}{L_0} + 1 \right)^2. \quad (\text{B.5})$$

Equation B.6 defines an *asymmetric* variant of a standard quartic double-well system, with minimii at $\frac{x}{L_0} = -1$ and $\frac{x}{L_0} = 1$, and a maximum at $\frac{x}{L_0} = \frac{3\Delta U}{16U_0}$. See Fig. 3.1 for a plot of the potential energy landscape. In non-dimensionalised form, the potential is

$$\tilde{U}(\tilde{x}) = (\tilde{x} - 1)^2 - \frac{1}{4} \frac{\Delta U}{U_0} (\tilde{x} - 2)(\tilde{x} + 1)^2. \quad (\text{B.6})$$

where $\tilde{x} = x/L$. In all numerical simulations, we have set $\frac{\Delta U}{U_0} = 1/2$.

B.2 The switch system

Here we define the *switch* system, and its non-conservative variant used in Ch. 4. We consider a 2-dimensional Langevin system with a Sombrero-type potential $U : \mathbb{R}^2 \rightarrow \mathbb{R}$. Let $\Gamma = \{(x, y) \mid \sqrt{x^2 + y^2} = 1\}$ be the circle centred around the origin, and let Γ^+ and Γ^- signify the upper and lower semi-circle respectively. We will construct the potential such that Γ coincides with a manifold of potential minima, and such that the perpendicular curvature of the potential along Γ^+ is larger than along Γ^- . We start with a radial quartic potential of the form

$$U(x_1, x_2) = U_r(r(x_1, x_2)) \quad (\text{B.7})$$

$$U_r(r) = U_0 \left(\frac{r}{L_0} - 1 \right) \left(1 + a \frac{r}{L_0} + b \left(\frac{r}{L_0} \right)^2 + c \left(\frac{r}{L_0} \right)^3 \right)$$

where L_0 is the length-scale of the system, U_0 will be the value of the potential at the local maximum $r = 0$, and $a, b, c \in \mathbb{R}$ will be specified below. We will henceforth suppress the argument of the radial coordinate function $r(x_1, x_2) = \sqrt{x_1^2 + x_2^2}$. We impose the following conditions on the potential to fix a, b and c :

1. $U'_r(0) = 0$. The origin is an extremum.
2. $U'_r(L_0) = 0$. Γ is an extremum of the potential.

3. $U_r''(L_0) = k$. The curvature along Γ is k .

We get

$$U_r(r) = \frac{1}{2} \left(\frac{r}{L_0} - 1 \right)^2 \left[L_0^2 k \left(\frac{r}{L_0} \right)^2 - 2U_0 \left(\frac{r}{L_0} - 1 \right) \left(3\frac{r}{L_0} + 1 \right) \right] \quad (\text{B.8})$$

which is, in the non-dimensionalised form

$$\tilde{U}_r(\tilde{r}) = \frac{1}{2} (\tilde{r} - 1)^2 \left[L_0^2 \tilde{k} \tilde{r}^2 - 2(\tilde{r} - 1)(3\tilde{r} + 1) \right]. \quad (\text{B.9})$$

where $\tilde{r} = r/L$ and $\tilde{k} = \frac{k}{U_0}$. In order to ensure that the potential has a Sombrero-like form, we must further have that the potential is confining, which is equivalent to $\lim_{r \rightarrow \infty} U_r(r) = \infty$, which implies that $6U_0 \leq L_0^2 k$. We now introduce an angular dependence in the curvature. We set

$$L_0^2 k(\phi) = 6U_0(1 + 2h(\phi)) \quad (\text{B.10})$$

where $\phi = \phi(x_1, x_2)$ is the angle of (x_1, x_2) in polar coordinates so that $x_1 = \cos(\phi)$, $x_2 = \sin(\phi)$, and where

$$h(\phi) = \frac{1}{4} (\xi_2 + \xi_1 + (\xi_2 - \xi_1) \sin \phi) \quad (\text{B.11})$$

where $\xi_2 > \xi_1$, and where $h(\phi) \in [\xi_1, \xi_2]$ satisfies $h(-\pi/2) = \xi_1$ and $h(\pi/2) = \xi_2$. Eq. (B.10) is constructed so that the perpendicular curvature of Γ^+ is larger than that of Γ^- . The drift of the system is now given by $\mathbf{F} = -\nabla U$. This concludes the definition of the switch system.

We now consider a non-conservative variant of the switch system. We introduce an additional non-conservative force $\mathbf{F}^a = -\eta \hat{\phi}$ for which the work done in a displacement $d\mathbf{x} = dr\hat{\mathbf{r}} + rd\phi\hat{\phi}$ is $dW = \mathbf{F}^a \cdot d\mathbf{x} = \eta rd\phi$. This force energetically biases the upper transition channel Γ^+ . The total force is thus $\mathbf{F} = -\nabla U + \mathbf{F}^a$.

In the numerical experiments presented in the main text, we used the Itô Langevin equation

$$d\mathbf{X} = \mu \mathbf{F} dt + \sqrt{2\mu k_B \theta} d\mathbf{W}. \quad (\text{B.12})$$

For the numerical experiments in the main text we use $\tilde{U}_0 = 1$, which means that $\tilde{\theta} = 1$ corresponds to a temperature such that $k_B \theta = U_0$. We also set $\xi_1 = 0$ and $\xi_2 = 2$. To compare the gradient force $-\nabla \cdot U$ with \mathbf{F}^a we also introduce $f_{\text{eq}} = U_0/L$, which is the characteristic force strength of the gradient force.

Appendix C

Nondimensionalisation of the Cosserat rod

Begin with discussion on how to find the dimensions of all kinematic and dynamic quantities.

Appendix D

Numerical algorithms for spatio-temporal reconstruction

D.1 Reconstructing the Cosserat rod from the Maurer-Cartan form

We solve

$$\mathcal{F}' = \mathcal{F}X \quad (\text{D.1a})$$

$$\dot{\mathcal{F}} = \mathcal{F}Y. \quad (\text{D.1b})$$

in order to reconstruct $\mathcal{F}(t, u)$ from its infinitesimal description ξ . Formally, they have solutions

$$\mathcal{F}_{ij}(u, \bar{t}) = \mathcal{F}_{ik}(0, \bar{t}) \mathcal{U} \left\{ e^{\int_0^u X(u, \bar{t}) du} \right\}_{kj} \quad (\text{D.2a})$$

$$\mathcal{F}_{ij}(\bar{u}, t) = \mathcal{F}_{ik}(\bar{u}, 0) \mathcal{T} \left\{ e^{\int_0^t Y(\bar{u}, t) dt} \right\}_{kj} \quad (\text{D.2b})$$

where $\mathcal{U}(\cdot)$ and $\mathcal{T}(\cdot)$ signifies the spatial and temporal time-ordered integral respectively. Numerically, these can be efficiently approximated by discretisation, and incrementally solved using the *Magnus expansion*. Eq. D.1a and Eq. D.1b can therefore be used together to trace out \mathcal{F} from a single initial condition $\mathcal{F}(u_0, t_0)$. Due to the integrability of ξ , the value $\mathcal{F}(t, u)$ at (t, u) is invariant with respect to which particular path in (t, u) -space is taken. In light of this there are theoretically an infinite number of reconstruction schemes. Below we propose what we find to be the most convenient reconstruction scheme.

We discretise time and space as $u_\alpha = \alpha \Delta u$, $\alpha = 0, \dots, N_u$, such that $u_0 = t_0 = 0$ and $t_\beta = \beta \Delta t$, $\beta = 0, \dots, N_t$ and $u_{N_u} = L_0$ and $t_{N_t} = T$. We define $\mathcal{F}^{\alpha, \beta} \approx \mathcal{F}(\alpha \Delta u, \beta \Delta t)$,

$X^{\alpha,\beta} \approx X(\alpha\Delta u, \beta\Delta t)$ and $Y^{\alpha,k} \approx Y(\alpha\Delta u, \beta\Delta t)$.

$$\mathcal{F}_{ij}^{0,\beta+1} = \mathcal{F}_{ik}^{0,\beta} \exp (\Delta t N^{0,\beta})_{kj}, \quad \mathcal{F}^{0,0} = \mathcal{F}^{(i)} \quad (\text{D.3a})$$

$$\mathcal{F}_{ij}^{\alpha+1,\beta} = \mathcal{F}_{ik}^{\alpha,\beta} \exp (\Delta u X^{\alpha,\beta})_{kj} \quad (\text{D.3b})$$

with the initial condition $\mathcal{F}^{0,0} = \mathcal{F}^{(i)}$. The matrix exponential has a closed-form analytical formula given by

$$\exp(H) = \begin{pmatrix} 1 & \vec{0}^T \\ A(\hat{m})\vec{v} & B(\hat{m}) \end{pmatrix} \quad (\text{D.4})$$

for $H = \{\vec{v}; \vec{m}\} \in \mathfrak{se}(3)$ and

$$A(\hat{m}) = \mathbb{1}_3 + \frac{1 - \cos |\vec{m}|}{|\vec{m}|^2} \hat{m} + \frac{|\vec{m}| - \sin |\vec{m}|}{|\vec{m}|^3} \hat{m}^2 \quad (\text{D.5a})$$

$$B(\hat{m}) = \exp(\hat{m}) = \mathbb{1}_3 + \frac{\sin |\vec{m}|}{|\vec{m}|} \hat{m} + \frac{1 - \cos |\vec{m}|}{|\vec{m}|^2} \hat{m}^2 \quad (\text{D.5b})$$

where $B(\hat{m}) \in SO(3)$ is an element of the special orthogonal group in 3 dimensions. As Eq. D.5a and Eq. D.5b are ill-conditioned for small $|\vec{m}|$, in numerics it is often prudent to Taylor expand to at least $O(|\vec{m}|^6)$ when $|\vec{m}| < 0.1$ [82].

One benefit of Eq. D.3 as a numerical solution schema is that it allows for flexibility in terms of when Eq. D.3b is evaluated. For example, in simulations we use a temporal discretisation Δt , but we might only need to reconstruct the Cosserat rod at intervals $n\Delta t$, for some integer n .

D.2 Reconstructing the spatio-temporal configuration from the Maurer-Cartan form